

ERK/MAPK Requirements for the Development of Long-Range Axonal Projections and
Motor Learning in Cortical Glutamatergic Neurons

by

George Reed Bjorklund

A Dissertation Presented in Partial Fulfillment
of the Requirements for the Degree
Doctor of Philosophy

Approved October 2018 by the
Graduate Supervisory Committee:

Jason Newbern, Chair
Janet Neisewander
Brian Smith
Miles Orchinik
Marco Mangone

ARIZONA STATE UNIVERSITY

December 2018

ABSTRACT

The RASopathies are a collection of developmental diseases caused by germline mutations in components of the RAS/MAPK signaling pathway and is one of the world's most common set of genetic diseases. A majority of these mutations result in an upregulation of RAS/MAPK signaling and cause a variety of both physical and neurological symptoms. Neurodevelopmental symptoms of the RASopathies include cognitive and motor delays, learning and intellectual disabilities, and various behavioral problems. Recent noninvasive imaging studies have detected widespread abnormalities within white matter tracts in the brains of RASopathy patients. These abnormalities are believed to be indicative of underlying connectivity deficits and a possible source of the behavioral and cognitive deficits. To evaluate these long-range connectivity and behavioral issues in a cell-autonomous manner, MEK1 loss- and gain-of-function (LoF and GoF) mutations were induced solely in the cortical glutamatergic neurons using a *Nex:Cre* mouse model. Layer autonomous effects of the cortex were also tested in the GoF mouse using a layer 5 specific *Rbp4:Cre* mouse. Immunohistochemical analysis showed that activated ERK1/2 (P-ERK1/2) was expressed in high levels in the axonal compartments and reduced levels in the soma when compared to control mice. Axonal tract tracing using a lipophilic dye and an adeno-associated viral (AAV) tract tracing vector, identified significant corticospinal tract (CST) elongation deficits in the LoF and GoF *Nex:Cre* mouse and in the GoF *Rbp4:Cre* mouse. AAV tract tracing was further used to identify significant deficits in axonal innervation of the contralateral cortex, the dorsal striatum, and the hind brain of the *Nex:Cre* GoF mouse and the contralateral cortex and dorsal striatum of the *Rbp4:Cre* mouse. Behavioral testing of the *Nex:Cre* GoF mouse indicated deficits in motor learning acquisition while the *Rbp4:Cre* GoF mouse showed no failure to acquire motor skills as tested. Analysis of the expression levels

of the immediate early gene ARC in *Nex:Cre* and *Rbp4:Cre* mice showed a specific reduction in a cell- and layer-autonomous manner. These findings suggest that hyperactivation of the RAS/MAPK pathway in cortical glutamatergic neurons, induces changes to the expression patterns of P-ERK1/2, disrupts axonal elongation and innervation patterns, and disrupts motor learning abilities.

ACKNOWLEDGEMENTS

I would like to sincerely thank my mentor and advisor Dr. Jason Newbern for his help, guidance, and patience through my graduate career in neuroscience.

My dissertation committee, Drs. Brian Smith, Miles Orchinik, Janet Neisewander, and Marco Mangone truly deserves my deep appreciation for their patience, feedback, and support. Thank you all.

I am also grateful to Dr. Jeanne Wilson-Rawles for her help and support during my graduate career. I feel it safe to say that without her backing I would not have made it to this point.

Early graduate mentorship from Drs. Hugh Mason and Charles Arntzen has also meant a lot for my academic and scientific development.

I would also like to thank all current and previous lab members and graduate colleagues that have provided help, support, and friendship over these years.

Last but not least, my family. Without their backing and encouragement, I may have never finished. Special thanks to Sticky and all his relatives that made my research possible.

TABLE OF CONTENTS

	Page
LIST OF TABLES	vi
LIST OF FIGURES	vii-ix
LIST OF SYMBOLS / NOMENCLATURE	x-xiv
PREFACE	xv-xvi
CHAPTER	
1 INTRODUCTION	1
The RASopathies.....	1-4
RAS/MAPK Signaling Pathway: Background.....	4-5
RAS/MAPK Signaling Pathway: Core Pathway	6-10
RAS/MAPK Signaling Pathway: Functions	11-17
Connectivity in the RASopathies	18-20
Immediate Early Gene ARC – Memory and Learning	21-21
Summary.....	21-22
2 PROJECTION NEURON DEVELOPMENT IN A LOSS-OF-FUNCTION	
MEK1/MEK2 MOUSE MODEL.....	22
Abstract.....	24
Introduction	25-27
Materials and Methods	28-32
Results	33-56
Discussion.....	57-62
Acknowledgements.....	63

CHAPTER	Page
3 LONG-RANGE AXONAL DEVELOPMENT IN A GAIN-OF-FUNCTION CAMEK	
MOUSE MODEL	64
Abstract.....	65
Introduction	66-69
Materials and Methods	70-76
Results	77-104
Discussion.....	105-112
Acknowledgements.....	113
4 CORTICAL LAYER SPECIFICITY IN A GAIN-OF-FUNCTION CAMEK MOUSE	
MODEL	114
Abstract.....	115
Introduction	116-117
Materials and Methods	118-123
Results	124-137
Discussion.....	138-141
Acknowledgements.....	142
5 CONCLUDING REMARKS	143-149
REFERENCES	150-170
APPENDIX	
A Curriculum Vitae.....	171-177
B Parvalbumin Fast-spiking Interneurons are Selectively Altered by Pediatric Traumatic Brain Injury	178-195
C Animal Subjects	196-197
D Table 2: Nex:Cre/caMEK1 Microarray Profiling	199-198

LIST OF TABLES

Table		Page
1	The RASopathies; Frequencies, Genes, and Mutation Effects.....	2
2	Nex:Cre/caMEK1 Microarray Profiling.	198

LIST OF FIGURES

Figure	Page
1. NTRK2 Recruits Various Adapter Proteins	8
2. RAS Activation by GEFs and Deactivation by GAPs.....	10
3. <i>Mek1/2^{CKO(Nex)}</i> Cortical Excitatory Neurons Specific Recombination.	35
4. Loss of ERK/MAPK Signaling Leads to a Reduction in the Number of CTIP ⁺ Layer 5 Neurons.	37
5. Loss of ERK/MAPK Signaling Leads to a Reduction in the Number of CTIP ⁺ Layer 5 Neurons.	38
6. Corticospinal Tract Defects in the MEK1/2CKO (Nex) Mice.....	41
7. Layer 5 neuron corticospinal axon outgrowth requires ERK/MAPK signaling <i>in vivo</i>	44
8. The Rostrocaudal Elongation of Layer 5 Axons in the Spinal Cord Requires ERK/MAPK.	45
9. Initiation of layer 5 neuron death by P3 in <i>Mek1/2CKO(Nex)</i> mutants.	48
10. Mouse Model for Excitatory Neuron Specific Gain-of-ERK/MAPK Signaling in the Cortex	52
11. No Overt Defects in the Specification or Number of Layer 5 Neurons in <i>caMEK1^(Nex)</i> Mice Detected.....	53
12. Gain-of-Function ERK/MAPK Signaling in <i>caMEK1^(Nex)</i> Mice Decreases Corticospinal Extension into the Spinal Cord.	54
13. Hyperactivation of ERK/MAPK Enhances Axonal Branching in the Hindbrain and Spinal Cord.....	55
14. Hyperactivation of ERK/MAPK Enhances Axonal Branching in the Hindbrain and Spinal Cord.....	56

Figure	Page
15. MEK1 Hyperactivation Results in Increased Levels of P-ERK1/2 in the Axons of Cortical Excitatory Neurons.	80
16. Enhanced MEK1 Expression is Detected in the Somatosensory Cortex of Embryonic <i>NexCre/caMek1</i> Mice.....	81
17. Increased Levels of P-ERK1/2 in the Axons and Reduced Somal Detection of P-ERK1/2 Persists in Adult <i>NexCre/caMek1</i> Mice.....	82
18. Increased Levels of P-ERK1/2 in the Axons and Reduced Somal Detection of P-ERK1/2 Persists in Adult <i>NexCre/caMek1</i> Mice.....	83
19. P-ERK1/2 Localizes to White Matter Tracts in <i>NexCre/caMek1</i> Mice When Compared to Controls.....	84
20. P-ERK1/2 Localizes to white matter tracts in <i>NexCre/caMek1</i> Mice When Compared to Controls.....	85
21. Corticocortical and Corticostriatal Innervation and Branching Patterns are Disrupted by Hyperactivated MEK1	89
22. Corticocortical and Corticostriatal Innervation and Branching Patterns are Disrupted by Hyperactivated MEK1	90
23. ARC Protein Levels are Negatively Affected by MEK1 Hyperactivation.	93
24. ARC Protein Levels are Negatively Affected by MEK1 Hyperactivation.	94
25. Motor Learning and Motor Skill Acquisition is Disrupted by MEK1 Hyperactivation in Cortical Glutamatergic Neurons.	99
26. Motor Learning and Motor Skill Acquisition is Disrupted by MEK1 Hyperactivation in Cortical Glutamatergic Neurons.	100
27. Subcortical Recombination of <i>caMEK1</i> Selectively Affects P-ERK1/2 Detection in the <i>NexCre/caMek1</i> Mice.....	103

Figure	Page
28. Subcortical Recombination of <i>caMEK1</i> Selectively Affects P-ERK1/2 Detection in the <i>NexCre/caMek1</i> Mice.....	104
29. Corticospinal Tract Elongation is Decreased but Corticospinal Axonal Innervation is Increased in Layer V Specific MEK1 Hyperactivation. .	127
30. Corticospinal tract elongation is decreased but Corticospinal Axonal Innervation is Increased in Layer V Specific MEK1 Hyperactivation. ..	128
31. Corticobulbar Tract Axonal Extension and Hindbrain Innervation not Affected in the <i>RBP4Cre/caMek1</i> Mice	129
32. Corticocortical and Corticostriatal Innervation and Branching is Reduced in a Layer V Autonomous Manner.....	131
33. Corticocortical and Corticostriatal Innervation and Branching is Reduced in a Layer V Autonomous Manner.....	132
34. ARC Levels Reduced Specifically in Layer V Glutamatergic Neurons in the <i>RBP4Cre/caMEK1</i> Mice.....	134
35. ARC Levels Reduced Specifically in Layer V Glutamatergic Neurons in the <i>RBP4Cre/caMEK1</i> Mice.....	137

LIST OF SYMBOLS / NOMENCLATURE

AD	Axial diffusivity
ADC	Apparent diffusion coefficient
AKT1	Serine/threonine kinase 1 (λ),
ALPS	Legius syndrome, autoimmune lymphoproliferative syndrome
AMPA	α -amino-3-hydroxy-5-methyl-4-isoxazolepropionic acid receptor
ARC	Activity regulated cytoskeleton associated protein
BAD	BCL2 associated agonist of cell death
BDNF	Brain derived neurotrophic factor
BH3-only	Bcl-2 homology domain 3
BIM	BCL2 like 11
CDK5R1	Cyclin dependent kinase 5 regulatory subunit 1
CFC	Cardio-facio-cutaneous syndrome
CM-AVM	Capillary malformation-arteriovenous malformation syndrome
CNS	Central nervous system
CRK	CRK proto-oncogene, adaptor protein
CS	Costello syndrome
CSK	C-terminal Src kinase
DRG	Dorsal ganglion
DTI	Diffusion tensor imaging
EGF	Epithelial growth factor
EGFR	Epidermal growth factor receptor
ERK1	Extracellular signal-regulated kinase 1
ERK2	Extracellular signal-regulated kinase 2
FA	Fractional anisotropy
FGF	Fibroblast growth factor

FGFR	Fibroblast growth factor receptor
FRS2	Fibroblast growth factor receptor substrate 2
GDP	Guanosine diphosphate
GEF	Guanine exchange factor
GoF	Gain-of-function
GRB2	Growth factor receptor bound protein 2
GRIA1	Glutamate ionotropic receptor AMPA type subunit 1
GRM1	Glutamate metabotropic receptor 1
GTP	Guanosine triphosphate
HGF	Hepatocyte growth factor
HGF1	Hereditary gingival fibromatosis 1
HRAS	Harvey murine sarcoma virus
IDD5	Autosomal dominant intellectual disability type 5
IEG	Immediate early genes
IGFLR1	IGF like family member 1 receptor
KEN	Keratinocytic epidermal nevus
KENS	Keratinocytic epidermal nevus syndrome
KRAS	Kirsten murine sarcoma virus
KSR1	Association with scaffolding proteins kinase suppressor of ras 1
LoF	Loss-of-function
MAP1B	Microtubule associated protein 1B
MAP2K	Mitogen activated kinase kinase
MAP2K1	Mitogen activated protein kinase kinase 1 (MEK1)
MAPK	Mitogen activated kinase
MAPK1	Mitogen activated protein kinase (ERK2)
MAPK14	Mitogen-activated protein kinase 14 (p38)

MAPK2K2	Mitogen activated protein kinase kinase 2 (MEK2)
MAPK3	Mitogen activated protein kinase 3 (ERK1)
MAPK7	Mitogen-activated protein kinase 7 (ERK5)
MAPK8	Mitogen-activated protein kinase 8 (JNK)
MCS	Mosaic Costello syndrome
MD	Mean diffusivity
MEK1	MAPK/ERK kinase 1
MEK2	MAPK/ERK kinase 2
MYLK	Myosin light chain kinase
NF-1	Neurofibromatosis type 1
NF1	Neurofibromin 1
NGF	Nerve growth factor
NMDAR	N-methyl-D-aspartate glutamate receptor
NMDAR	N-methyl-D-aspartate receptor
NS	Noonan syndrome
NSML	Noonan syndrome with multiple lentigines
NTF3	Neurotrophin 3
NTF4	Neurotrophin 4
NTRK1	Neurotrophic receptor tyrosine kinase 1
NTRK2	Neurotrophic receptor tyrosine kinase 2
NTRK3	Neurotrophic receptor tyrosine kinase 3
PEBP1	Phosphatidylethanolamine binding protein 1
PEBP1	Phosphatidylethanolamine binding protein 1
PIK3CA	Phosphatidylinositol-4,5-bisphosphate 3-kinase catalytic subunit alpha
PKC	Protein kinase C
PLC γ 1	Calcium signaling through the phospholipase C gamma 1

PLCG1	Phospholipase C gamma 1
PTK2	Protein tyrosine kinase 2
PTPN11	Protein tyrosine phosphatase, non-receptor type 11
PUMA	BCL2 binding component 3
PXN	Paxillin
RAS/MAPK	RAS-RAF-MEK-ERK cellular signaling cascade
RASA1	RAS p21 protein activator 1
RASA1	RAS p21 protein activator 1
RASGAP	RAS GTPase activating proteins
RASGAPs	RAS GTPase activating proteins
RD	Radial diffusivity
rs-fcMRI	Resting state functional connectivity MRI
SCG	Superior cervical ganglion neurons
SFK	SRC family kinases
SH2B	SH2B type 1, 2, or 3, adaptor proteins
SHC1	SHC adaptor protein 1
SN	Sebaceous nevus
SN1	Segmental neurofibromatosis type I
SOS1	SOS Ras/Rac guanine nucleotide exchange factor
SOS2	SOS Ras/Rho guanine nucleotide exchange factor
SRC	SRC proto-oncogene, non-receptor tyrosine kinase
SS	Schimmelpenning syndrome
SYNGAP1	Synaptic Ras GTPase activating protein 1
SYNGAP1	Synaptic Ras GTPase activating protein 1
TAU	Microtubule associated protein tau
VGCC	Voltage gated calcium channel

PREFACE

The research in this dissertation was performed under the supervision of Dr. J.M. Newbern in the School of Life Sciences at Arizona State University between January 2014 and October 2018. All work herein is to the best of my knowledge original except where acknowledgements or references are made to previous works or the contributions of others.

The work presented in this dissertation is composed of research on both gain- and loss-of-function mutations in the RAS-RAF-MEK-ERK (RAS/MAPK) cellular signaling pathway in the central nervous system (CNS). This work is presented in the context of the RASopathies and the genetic germline mutations within the RAS/MAPK signaling pathway that are responsible for them. Chapter 1 is a literature review that encompasses the individual RASopathies and the germline genetic mutations that cause them. This is accompanied by a brief history of the RAS/MAPK signaling pathway, the core components and mechanism of the RAS/MAPK signaling pathway, and functions of the pathway within the context of the RASopathies and my own research.

Chapter 2 involves a study on the effects of loss-of-function (LoF) of cellular RAS/MAPK signaling primarily in cortical glutamatergic neurons. This chapter primarily consists of materials published in the journal *eLife* (Xing et al. 2016) and has been edited to highlight my own contributions except where referenced. Chapter 3 is comprised of a study on the effects of gain-of-function (GoF) RAS/MAPK signaling primarily in cortical glutamatergic neurons. This work constitutes materials that are currently in revision for publication. Chapter 4 defines the cortical layer specificity of the phenotypes involved in the gain-of-function model of RAS/MAPK cellular signaling. This work constitutes materials that are currently in revision for publication.

Chapter 5 includes concluding remarks as well as future directions and the challenges faced in the field of the RASopathies as well as possible translational implications.

CHAPTER 1
INTRODUCTION

The RASopathies

Germline genetic mutations within the genes that encode components of the RAS-RAF-MEK-ERK (RAS/MAPK) signal transduction pathway cause several human genetic syndromes collectively known as RASopathies. These syndromes include Noonan syndrome (NS), Noonan syndrome with multiple lentigines (NSML) (formerly LEOPARD syndrome), neurofibromatosis type 1 (NF-1), Costello syndrome (CS), capillary malformation-arteriovenous malformation syndrome (CM-AVM), cardio-facio-cutaneous syndrome (CFC), Legius syndrome, autoimmune lymphoproliferative syndrome (ALPS), Hereditary gingival fibromatosis 1 (HGF1), and Autosomal dominant intellectual disability type 5 (IDD5) (Tidyman and Rauen 2009; Katherine A. Rauen 2013). Caused by germline mutations, the RASopathies are classified as developmental disorders that share many overlapping clinical characteristics including craniofacial dysmorphologies, cardiovascular abnormalities, cutaneous, musculoskeletal, and ocular abnormalities, neurocognitive impairment, hypotonia, and an increased risk of cancer (Katherine A. Rauen 2013; Aoki, Niihori, S. Inoue, et al. 2016). Individually, there is a wide range of frequencies in the RASopathies with some syndromes being quite rare. For example, NS occurs in 1:1000 to 1:2500 individuals while NSML and ALPS have approximately 200 reported cases each worldwide (Gelb and Tartaglia 1993; Autoimmune lymphoproliferative syndrome 2018). Regardless of the frequencies of the individual syndromes, as a group, the RASopathies constitute one of the largest groups of developmental syndromes worldwide (Katherine A. Rauen 2013) (Table 1).

Table 1

The RASopathies; frequencies, genes, and mutation effects.

Syndrome	Frequency	Gene Symbol (Synonym)	Gene Name	Chromosome Location	Protein Function	Mutation Effect
Noonan syndrome (NS)	1:1,000 to 1:2,500	<i>PTPN11</i> (<i>SHP2</i>)	Protein tyrosine phosphatase, non-receptor type 11	12q24.1	Phosphatase	Activating Mutation
		<i>SOS1</i>	SOS Ras/Rac guanine nucleotide exchange factor 1	2p22.1	RasGEF	Activating Mutation
		<i>RAF1</i> (<i>CRAF</i>)	Raf-1 proto-oncogene, serine/threonine kinase	3p25.1	Kinase	Activating Mutation
		<i>KRAS</i>	KRAS proto-oncogene, GTPase	12p12.1	GTPase	Activating Mutation
		<i>NRAS</i>	NRAS proto-oncogene, GTPase	1p13.2	GTPase	Activating Mutation
		<i>SHOC2</i>	SHOC2, leucine rich repeat scaffold protein	10q25.2	Scaffolding	Activating Mutation
		<i>CBL</i>	Cbl proto-oncogene	11q23.3	Ubiquitin ligase	Loss of Function
		<i>RRAS</i>	RAS related	19q13.33	GTPase	Activating Mutation
		<i>RTT1</i>	Ras like without CAAX 1	1q22	GTPase	Activating Mutation
		<i>RAS42</i>	RAS p21 protein activator 2	3q23	RasGAP	Activating Mutation
		<i>SOS2</i>	SOS Ras/Rho guanine nucleotide exchange factor 2	14q21.3	RasGEF	Activating Mutation
		<i>MAP3K8</i> (<i>MEK8</i>)	Mitogen-activated protein kinase kinase kinase 8	10p11.23	Kinase	Activating Mutation
		<i>SPRY1</i>	sprouty related EVH1 domain containing 1	4q28.1	Inhibitor	Unknown
		Noonan syndrome with multiple lentiginosis (Prev. LEOPARD syndrome) (NSML)	~200 cases reported worldwide	<i>KAT5B</i>	Lysine acetyltransferase 6B	10q22.2
<i>LZTR1</i>	Leucine zipper like transcription regulator 1			22q11.21	Adaptor	Unknown
<i>A2ML1</i>	Alpha-2-macroglobulin like 1			12p13.31	Protease inhibitor	Unknown
<i>PTPN11</i> (<i>SHP2</i>)	Protein tyrosine phosphatase, non-receptor type 11			12q24.1	Phosphatase	Dysregulation
Neurofibromatosis type 1	1:3,000 to 1:4,000	<i>RAF1</i> (<i>CRAF</i>)	Raf-1 proto-oncogene, serine/threonine kinase	3p25.1	Kinase	Activating Mutation
		<i>BRAF</i>	B-Raf proto-oncogene, serine/threonine kinase	7q34	Kinase	Activating Mutation
Capillary malformation-arteriovenous malformation syndrome (CM-AVM)	1:100,000 ^a	<i>MAP2K1</i> (<i>MEK1</i>)	Mitogen-activated protein kinase kinase 1	15q22.31	Kinase	Activating Mutation (predicted)
		<i>NF1</i>	Neurofibromin 1	17q11.2	RasGAP	Activating Mutation
Costello syndrome (CS)	1:380,000 to 1:1,250,000	<i>RASA1</i>	RAS p21 protein activator 1	5q14.3	RasGAP	Loss of Function
		<i>HRAS</i>	H-Ras proto-oncogene, GTPase	1p15.5	GTPase	Activating Mutation
Autoimmune lymphoproliferative syndrome (ALPS)	Unknown ^b	<i>NRAS</i>	NRAS proto-oncogene, GTPase	1p13.2	GTPase	Activating Mutation
		<i>BRAF</i>	B-Raf proto-oncogene, serine/threonine kinase	7q34	Kinase	Activating Mutation
Cardio-Facio-Cutaneous syndrome (CFC)	1:150,000 to 1:810,000	<i>MAP2K1</i> (<i>MEK1</i>)	Mitogen-activated protein kinase kinase 1	15q22.31	Kinase	Activating Mutation (predicted)
		<i>KRAS</i>	KRAS proto-oncogene, GTPase	12p12.1	GTPase	Activating Mutation
Legus syndrome	Unknown ^c	<i>SPRED1</i>	Sprouty related EVH1 domain containing 1	15q14	Negative Regulator	Loss of Function
		<i>SOS1</i>	SOS Ras/Rac guanine nucleotide exchange factor 1	2p22.1	RasGEF	Activating Mutation
Hereditary gingival fibromatosis 1 (HGF1)	Unknown	<i>SYNGAP1</i>	Synaptic Ras GTPase activating protein 1	6p21.3	RasGAP	Loss of Function
		<i>SYNGAP1</i>	Synaptic Ras GTPase activating protein 1	6p21.3	RasGAP	Loss of Function

a) The prevalence of this condition in populations other than people of northern European origins is unknown.

b) More than 200 affected individuals have been identified worldwide.

c) Many individuals with Legus syndrome may be misdiagnosed because the signs and symptoms are similar to NF1.

(Allanson and Roberts 1993; Friedman 1993; Gelb and Tartaglia 1993; Margaret P Adam et al. 1993; Tidyman and Rauhen 2009; Gripp 2012; Rauhen 2013; Stevenson 2015; Rauhen 2016; Tidyman and Rauhen 2016; Bateman et al. 2017; Bleesing et al. 2017; Yates et al. 2017; Autoimmune lymphoproliferative syndrome 2018)

In addition to germline mutations of the RAS/MAPK pathway, postzygotic genetic mutations cause a mosaic genetic disorder with phenotypes that can be quite distinct from the previously defined RASopathies (Hafner and Groesser 2013). The mosaic RASopathies include Keratinocytic epidermal nevus (KEN), Keratinocytic epidermal nevus syndrome (KENS), Schimmelpenning syndrome (SS), Sebaceous nevus (SN), Mosaic Costello syndrome (MCS), Segmental neurofibromatosis type I (SN1) (Hafner and Groesser 2013). There is a wide range of symptoms for these disorders due to their mosaic nature. Symptoms range from cutaneous nevi in KEN to hemiparesis, ocular abnormalities and skeletal abnormalities including incomplete bone formation, hypertrophy or hypoplasia of bones, bone cysts, kyphoscoliosis, and vitamin-D resistant rickets in KENS and SS. Neurological defects reported in KENS and SS include seizures, intellectual disability, ventricular abnormalities, cortical atrophy, and hemimegalencephaly. Symptoms of MCS and SN1 are largely similar to their germline mutation counterparts with some CS and NF1 patients having been shown to have mosaic mutations with no significant phenotypic differences from those having germline mutations (Colman et al. 1996; Gripp et al. 2006; Hafner and Groesser 2013). Frequencies in individual diseases of mosaic RASopathies also have a large range. KEN ranges from ~1:333 to 1:1000 while MCS has only two known cases reported having been found in the relevant literature (Hafner and Groesser 2013; EN) (Table 2).

Diagnosis of the individual RASopathies is generally performed by clinical findings of key features and confirmed by genetic testing if necessary (Table 3). In some cases, clinical findings may not be sufficient and genetic testing of known genetic variants may need to be performed. Management of each syndrome within the RASopathies largely falls to surveillance and treatment of the individual manifestations (Margaret P Adam et al. 1993-2018). Some syndromes require

preventative treatments to avoid primary and secondary complications. To prevent primary complications in severe cases of ALPS for example, bone marrow transplantation is performed to prevent primary manifestations (Bleesing et al. 2017). To prevent secondary manifestations in CS and CFC cases, antibiotic prophylaxis is used to avoid bacterial endocarditis due to heart valve defects (Gripp 2012; Rauen 2016). In general, syndromes associated with developmental intellectual disabilities and cognitive impairments can be addressed by early intervention and specialized educational programs (Margaret P Adam et al. 1993). Precise and early diagnosis using clinical diagnosis and genetic testing is a critical part in monitoring and treating those afflicted with RASopathies.

RAS/MAPK Signaling Pathway: Background

The discovery of RAS began with the study of oncogenic retroviruses that were the cause of sarcomas infecting mice, rats, cats, monkeys, chickens, and turkeys in the early 1960s. In 1964 the potent oncogenic Harvey murine sarcoma virus (HRAS) was discovered followed by the Kirsten murine sarcoma virus (KRAS) in 1967 (Harvey 1964; Kirsten and Mayer 1967; Cox and Der 2010). These retroviruses, *H-ras* and *K-ras*, contained the potentially oncogenic genetic elements that were later found to comprise the human *HRAS* and *KRAS* oncogenes (Cox and Der 2010). The link between the *H-ras* and *K-ras* retroviruses and human *HRAS* and *KRAS* oncogenes was discovered by several research groups in 1982 and 1983. At this time, it was found that DNA isolated from several different human carcinoma cell lines caused morphologic transformations in NIH/3T3 mouse fibroblasts (Der et al. 1982; Parada et al. 1982; Santos et al. 1982). Researchers discovered that a missense mutation in codon 12 of *HRAS* and *KRAS*, also found in the viral *H-ras* and *K-ras* viral genes, was the molecular basis of RAS activation and the basis of RAS

oncogenicity (Reddy et al. 1982; Taparowsky et al. 1982; O'Toole et al. 1983; Coulier et al. 1989). A third oncogenic *RAS* gene was soon identified in neuroblastoma-derived DNA and labeled *NRAS* (Hall et al. 1983). The detection of mutant *RAS* genes in patient's tumors and not in normal tissues provided additional proof of the role mutant *RAS* has in the formation of carcinomas (Santos et al. 1984; Cox and Der 2010).

It wasn't until about 10 years later that *RAS* would be associated with the EGFR tyrosine kinase (Cox and Der 2010). An important observation was made that the adapter protein growth factor receptor bound protein 2 (GRB2) provided a link between EGFR and *RAS* activation (Lowenstein et al. 1992; Cox and Der 2010). It was speculated that the biochemical function of the *RAS* protein was that of a binary switch involved in signal transduction (Hurley et al. 1984; Cox and Der 2010). This was due to the fact that *RAS* was able to bind both guanosine triphosphate (GTP) and guanosine diphosphate (GDP) which essentially presented *RAS* in either an "on" state or an "off" state respectively (Scolnick et al. 1979; Hurley et al. 1984; Cox and Der 2010). Downstream of *RAS*, it was discovered that the kinase RAF would bind preferentially to activated Ras-GTP hinting to a role in signal transduction from activated *RAS* (Warne et al. 1993; Zhang et al. 1993; Cox and Der 2010). Around a year earlier, it was recognized that there was a Ras- and Raf-dependent activation of mitogen activated protein kinases MAPK3 (ERK1) and MAPK1 (ERK2) and that Raf had the ability to activate the mitogen activated protein kinase kinases MAP2K1 (MEK1) and MAP2K2 (MEK2) (Gallego et al. 1992; Howe et al. 1992; Kyriakis et al. 1992). Together, these observations defined the basis of the *RAS*-RAF-MEK-ERK cellular signaling pathway from extracellular ligand binding to the final protein kinases in the pathway, ERK1 and ERK2.

RAS/MAPK Signalling Pathway: Core Pathway

The RAS/MAPK signaling pathway relays extracellular cues in the form of neurotrophins to affect critical cellular processes. The primary manner of activation for the RAS/MAPK pathway is by ligand binding activation of neurotrophic receptor tyrosine kinase 2 (NTRK2). There are three related yet distinct NTRK receptors, NTRK1, NTRK2, and NTRK3. Each receptor consists of a single transmembrane protein with a tyrosine kinase domain on the cytoplasmic side and each NTRK receptor has a primary affinity for specific neurotrophins. NTRK1 is primarily a receptor for the neurotrophin nerve growth factor (NGF), NTRK2 is primarily a receptor for brain derived neurotrophic factor (BDNF) and neurotrophin 4 (NTF4), and NTRK3 is primarily a receptor for neurotrophin 3 (NTF3). A large amount of structural homology in both the neurotrophins and NTRK receptors can cause cross reactivity between the neurotrophins and the receptors. In addition to the RAS/MAPK pathway, NTRK receptor signaling activates the phosphatidylinositol-4,5-bisphosphate 3-kinase catalytic subunit alpha (PIK3CA)/serine/threonine kinase 1 (AKT1), calcium signaling through the phospholipase C gamma 1 (PLC γ 1) (Kanehisa et al. 2017). Furthermore, within the RAS/MAPK pathway, RAS signals to additional pathways, namely the p38 kinase signaling pathway with additional MAPK signaling via the PIK3CA/AKT1 pathway, and the mitogen-activated protein kinase MAPK7 (ERK5) kinase signaling pathway (Reichardt 2006; Tidyman and Rauen 2016; Kanehisa et al. 2017). In spite of the various signaling and pathway cross-talk dynamics, the common features within pathogenesis of the RASopathies are the genetic mutations within the core components of the RAS/MAPK and pathway activation of ERK1 and ERK2. (Tidyman and Rauen 2009; Katherine A. Rauen 2013; Tidyman and Rauen 2016).

RAS/MAPK signaling through NTRK2 begins with receptor activation and the phosphorylation of tyrosine residues Tyr 516 and Tyr 817 (Leal et al. 2017; The UniProt Consortium 2017). Receptor activation by BDNF/NTF4 binding induces a dimerization of the NTRK2 receptors followed by autophosphorylation of the tyrosine residues at the active sites (Reichardt 2006; Leal et al. 2017). Transactivation of NTRK2 independent of neurotrophin signaling has also been reported to occur through zinc-mediated activation of SRC family kinases (SFK) (Huang et al. 2008; Leal et al. 2017). Once NTRK2 is activated, phosphorylated Tyr 516 recruits and phosphorylates SHC adaptor protein 1 (SHC1) which in turn recruits growth factor receptor bound protein 2 (GRB2) and SOS Ras/Rho guanine nucleotide exchange factor (GEF) 1 and 2 (SOS1, SOS2) (Reichardt 2006; Leal et al. 2017). Additional scaffolding proteins can compete with SHC1 to bind at the phosphorylated Tyr 516 site on the activated NTRK2 receptor. Dimerized SH2B type 1, 2, or 3, adaptor proteins (SH2B1, SH2B2, SH2B3) can bind the phosphorylated Tyr 516 site in place of SHC that can provide a link from the activated NTRK2 receptor to GRB2/SOS (Qian et al. 1998; Reichardt 2006). The adapter molecule fibroblast growth factor receptor substrate 2 (FRS2), also competes for the phosphorylated Tyr 516 site and provides phosphorylation recruitment of adapter protein GRB2 independent of SHC or SH2B recruitment. FRS2 additionally recruits other signaling proteins including C-terminal Src kinase (CSK), SRC proto-oncogene, non-receptor tyrosine kinase (SRC), protein tyrosine phosphatase, non-receptor type 11 (PTPN11), and CRK proto-oncogene, adaptor protein (CRK). This mixture of adapter proteins related to the activation of NTRK2 and the GRB2/SOS complex is believed to be one way to mediate signal strength and duration of signaling through the RAS/MAPK pathway (Reichardt 2006; Minichiello 2009) (Figure 1).

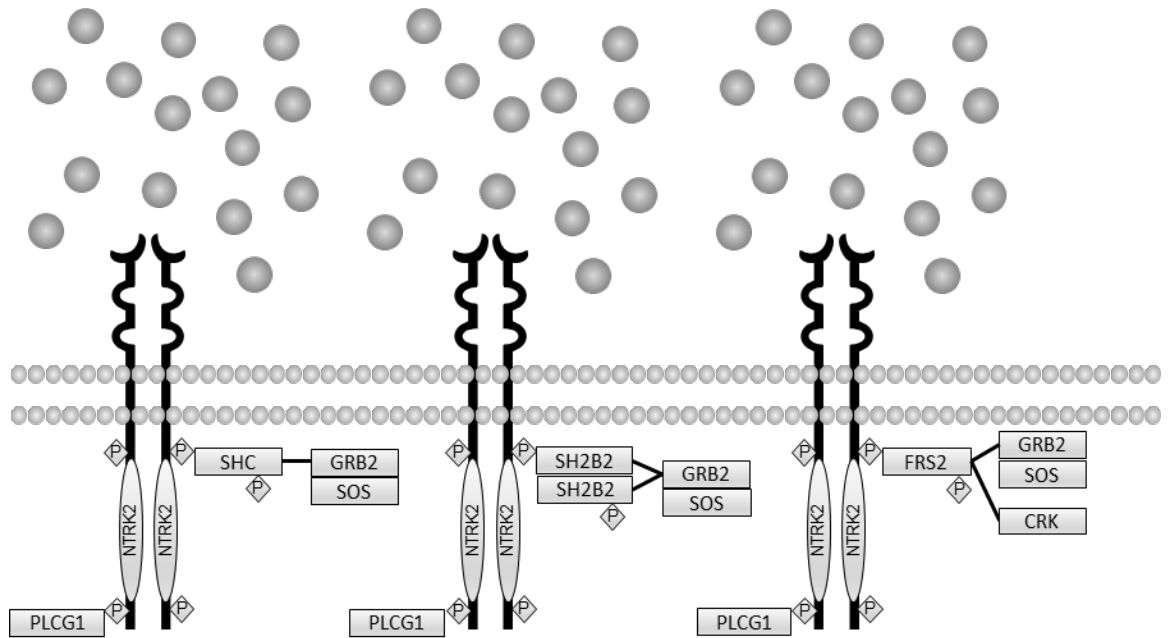


Figure 1.

NTRK2 Recruits Various Adapter Proteins. Several adapter proteins compete for binding at the activated NTRK2 Tyr 516 recruitment site. When bound to active NTRK2, SHC, SH2B2 dimer, and FRS2 become phosphorylated and recruit GRB2 bound to SOS. CRK recruits C3G to activate MAPK alternatively to GRB/SOS recruitment. Phospholipase C gamma 1 (PLCG1) binds to activated NTRK2 Tyr 817 and activates MAPK through an alternative pathway.

Activated SOS1 or SOS2 initiates the exchange of GDP for GTP on the membrane localized RAS protein. The exchange begins with the release of GDP through a quick succession of reactions. Once GDP is released, the series of reactions is reversed by the binding of a nucleotide, usually the RAS activating GTP due to much higher intracellular concentrations (Vetter 2001). When activated, RAS recruits RAF to the cell membrane which begins a series of complex actions to activate RAF. These actions include dimerization of RAF proteins, dephosphorylation and phosphorylation of different domains of RAF, dissociation from phosphatidylethanolamine binding protein 1 (PEBP1), and association with various scaffolding proteins. Several RAS GTPase activating proteins (RASGAPs) engage to exchange the GTP for GDP to inactivate RAS. These RASGAPs include synaptic Ras GTPase activating protein 1 (SYNGAP1), RAS p21 protein activator 1 (RASA1), and neurofibromin 1 (NF1), (Reichardt 2006; McCubrey et al. 2007). When activated, RAS is then capable of activating c-RAF which in turn phosphorylates MEK1 and/or MEK2. ERK1 and/or ERK2 are the specific targets that are then phosphorylated by MEK1 and/or MEK2 thus completing the RAS/MAPK core pathway (Figure 2).

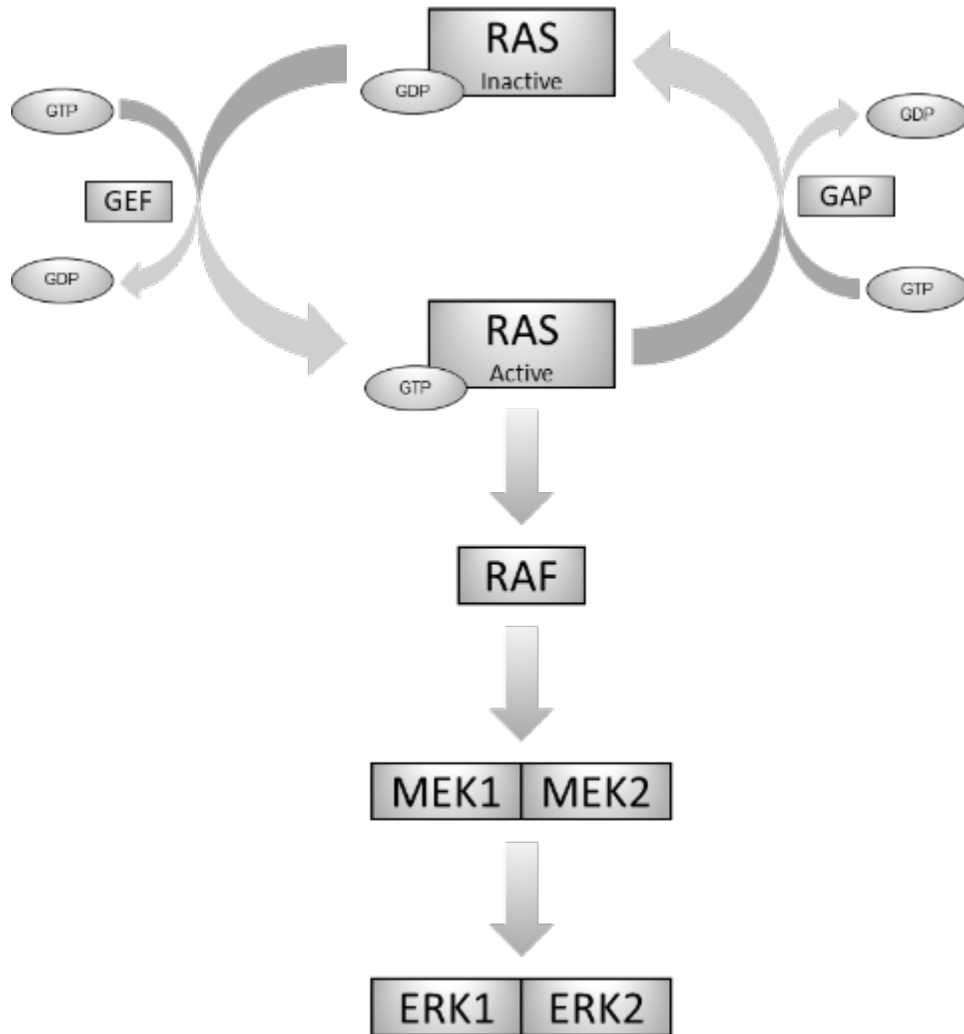


Figure 2.

RAS Activation by GEFs and Deactivation by GAPs. RAS acts as a binary molecular switch that is either in an off or inactive state when bound by GDP, or in an on or active state when bound by GTP. Activation of RAS is performed by the exchange of GDP for GTP by an activated GEF (SOS1 / SOS2). In its active state, RAS can activate several different pathways including the RAS/MAPK pathway implicated in the RASopathies.

RAS/MAPK Pathway: Functions

The well conserved RAS/MAPK signaling pathway is perhaps the most studied cellular signaling pathway to date. The RAS/MAPK signaling pathway functions in many aspects of cellular mechanics including cell survival, differentiation, and proliferation. In the case of neurons, RAS/MAPK signaling pathway functions include axonal outgrowth, synaptic plasticity, synapse stabilization and removal, retrograde transport processes, and actin cytoskeleton regulation. Much of what has been studied and learned about RAS/MAPK signaling comes from cancer research studies performed on specific cell types *in vitro*. Neurons however, consisting of several distinct compartments and operating in a more diverse and complex manner, do not seem to have experienced that same magnitude of research. This is especially true of *in vivo* pathway functions under physiological or diseased conditions as is seen within the RASopathies.

Cell Survival

Early *in vitro* studies using PC12 cells revealed that RAS/MAPK signaling and ERK activation prevents apoptosis suggesting a means of cell survival through ERK activation and the suppression of mitogen-activated protein kinase MAPK8 (JNK) and mitogen-activated protein kinase MAPK14 (p38) signaling (Xia et al. 1995). However, later experiments deleting B-RAF *in vitro* and deleting B-RAF or B-RAF and C-RAF *in vivo* showed conflicting results concerning RAS/MAPK mediated cell survival. Using cultured embryonic sensory dorsal ganglion (DRG) neurons as well as sympathetic and motor neurons, it was demonstrated that B-RAF *in vitro* was needed and sufficient for cell survival (Wiese et al. 2001; Encinas et al. 2008). However, *In vivo* deletion of B-RAF or B-RAF and C-RAF in neurons did not lead to cell death showing that RAF signaling does not significantly mediate survival during embryonic

development (Chen et al. 2006; Zhong et al. 2007; Galabova-Kovacs et al. 2008; Pfeiffer et al. 2013; Zhong 2016). Furthermore, in retinal ganglion cells *in vivo*, RAS/MAPK signaling can be pro-apoptotic upon optic nerve damage or neuroprotective under ocular hypertensive conditions (Zhou et al. 2005; Luo et al. 2007). Interestingly, a prior study found that the deletion of both isoforms of ERK, ERK1 and ERK2, in sensory neurons resulted in a significant amount of cell death *in vivo* (O'Brien et al. 2015). An additional recent *in vivo* study revealed that the conditional deletion of RAS/MAPK signaling in cortical glutamatergic neurons resulted in the significant death of Layer 5 CTIP2⁺ neurons. The reported cell death followed temporally the failure of corticospinal tract axon elongation (Xing et al. 2016). In these cases, it is possible that cell death was primarily due to the loss of axonal connectivity and not due directly to the loss of ERK signaling.

During development and in the presence of NGF, cellular survival functions of the RAS/MAPK signaling pathway work through anti-apoptotic actions. RAS activation occurs upon TRKA receptor binding by NGF and leads to the activation of the PI3K/AKT and RAS/MAPK signaling pathways and inhibition of the JNK - p53 pro-apoptotic pathway (Mazzoni et al. 1999; Kaplan and Miller 2000; Kristiansen and Ham 2014). These actions prevent the release of cytochrome-c from the mitochondria and the subsequent release and cleaving of caspase-3 and have been reported both *in vitro* in sympathetic neurons and *in vivo* in superior cervical ganglion neurons (SCGs) (McCarthy et al. 1997; Martinou et al. 1999; Kristiansen and Ham 2014; Alberts 2015)(Kristiansen and Ham 2014; Alberts 2015). PI3K/AKT signaling inhibits the transcription factor FOXO3a which in turn inhibits the transcription of pro-apoptotic Bcl-2 homology domain 3 (BH3-only) proteins such as BCL2 like 11 (BIM) and BCL2 binding component 3 (PUMA) (Gilley et al. 2003; Zhang et al. 2011; Kristiansen and Ham 2014). PI3K/Akt signaling also inhibits the function

of BCL2 associated agonist of cell death (BAD) by direct phosphorylation which inhibits BAD and prevents the release of BAX from a dimer complex with anti-apoptotic BCL-2 or BCL-XL (Datta et al. 1997; Kristiansen and Ham 2014). Interestingly, phosphorylation of RSK through RAS/MAPK-ERK signaling can also phosphorylate and inhibit BAD (Bonni et al. 1999). Further pro-survival activity by ERK activation of RSK comes via RSK phosphorylation of the transcription factor CREB. Upon activation, CREB initiates transcription of several anti-apoptotic factors including the BCL2 family of apoptosis regulating proteins (Riccio et al. 1999). Activated ERK is also able to directly phosphorylate and inhibit the pro-apoptotic BH3-only protein, BIM, which would otherwise bind to and inactivate pro-survival proteins BCL-2 or BCL-XL (Gilley et al. 2003; Ley et al. 2003; Zhang et al. 2011).

Embryonic Development

Several common or overlapping features of the RASopathies include craniofacial dysmorphologies, cardiac malformations, and CNS defects resulting in neurocognitive deficits (Katherine A. Rauen 2013). The development and morphogenesis of these regions are thought to be highly dependent upon fibroblast growth factor (FGF) induced ERK1/2 signaling during neural crest and neural tube formation in embryonic development (Corson et al. 2003; Samuels et al. 2009; Gilbert and Barresi 2016). Additionally, specific regions of mouse, chick, and zebrafish embryos were found to have spatially restricted areas in which ERK1/2 was detected during transient and prolonged periods of embryonic development. These spatially restricted areas are believed to develop under the influence of FGF as it was seen that ERK1/2 activation could be blocked by inhibiting FGF receptor (FGFR) function (Shinya et al. 2001; Corson et al. 2003; Lunn et al. 2007; Samuels et al. 2009). Additionally, further testing by genetic regulation of FGF8 expression in the

neural tube and neural crest also aided in defining the critical role FGF induced ERK1/2 activation plays in development. It was shown that lowered FGF8 levels was followed by the failure to generate a normal complement of neural crest cells. This led severe cardiac and craniofacial defects whose severity was directly linked to the levels of FGF8 that were shown to be reliant on ERK signaling (Meyers et al. 1998; Kawauchi et al. 2005; Samuels et al. 2009). Normal CNS patterning is also disrupted when FGF8 is disrupted in the developing neural tube causing the failure to develop a cerebellum, olfactory bulb, and a normal cerebral cortex in embryonic mice (Chi et al. 2003). Moreover, inactivation of ERK2 in the developing neural crest also results in cardiac and craniofacial defects similar to the phenotypes seen in the FGF8 mutants and humans that are haploinsufficient for the *MAPK1* gene that encodes the ERK2 protein (Newbern et al. 2008; Samuels et al. 2009). Conditional knockouts of *Braf*, *Raf1*, and *Mek1/2*, upstream elements of ERK1/2, and the transcription factor SRF which is a downstream target of activated ERK1/2, all resulted in similar phenotypes (Newbern et al. 2008). These links of FGF to ERK1/2 activation *in vivo* gave the first evidence of the possibility of a highly selective developmental program within specific sets of progenitors (Samuels et al. 2009).

Neural precursor cells go through mitotic division in the ventricular zone of the newly formed neural tube. The precursor cells are attached to the inner luminal and outer pial surfaces of the ventricular zone. Progression from G₁ to S stages of the cell cycle occurs as they migrate from the luminal surface to the pial surface. The precursor cells then migrate back to the luminal surface during the G₂ stage, lose their attachments to the pial surface, and undergo mitosis. Cell division produces either precursor cells or postmitotic neuroblasts then exit the cell cycle and begin differentiation into neuronal subclasses (Purves 2012; Pillat et al. 2016). The RAS/MAPK signaling pathway is a key source of integrating extracellular cues during

development to influence the actions of the cell cycle. In PC12 cells ERK activation is required for both proliferation and differentiation through stimulation by epithelial growth factor (EGF) or (NGF) respectively (Hallberg et al. 1994; Pouysségur et al. 2002). It has been widely reported that transient ERK activation in the cytoplasm caused by EGF stimulation, results in sustained cell cycle activity and proliferation. However, sustained ERK activation in the cytoplasm created by NGF stimulation causes nuclear re-localization of activated ERK resulting in cell cycle arrest and differentiation (Traverse et al. 1992; Vaudry 2002; von Kriegsheim et al. 2009; Pillat et al. 2016). The sustained activation of ERK is a result of signaling through RAP1-BRAF-MEK as well as RAS-RAF-MEK signaling and may include recruitment of PI3K, PKC, and the second messenger cAMP (Qui and Green 1992; York et al. 2000; Vaudry 2002; Pillat et al. 2016).

Neuron Migration and Axon Growth

Neuronal migration and axon guidance are two crucial processes in development that are highly associated with RAS/MAPK signaling. Involvement in these processes by RAS/MAPK is through not only transcriptional control by ERK phosphorylation of transcription factors, but also by direct interactions with cytoskeletal elements. Cell migration is a crucial and somewhat scheduled event during normal development. For example, during neural crest cell migration, deviation from a specific path of migration or failure to adapt to the target environment leads to elimination (Wakamatsu et al. 1998; Poelmann and Gittenberger-de Groot 1999; Cho and Klemke 2000). Work in identifying substrates of P-ERK1/2 and their roles in migration found several essential elements used in cell motility. Myosin light chain kinase (MYLK) family members involved in cell adhesion dynamics and membrane protrusion (Klemke et al. 1997; Huang et al. 2004), paxillin

(PXN) and protein tyrosine kinase 2 (PTK2) that complex to help regulate cellular adhesion dynamics (Huang et al. 2004; Valiente et al. 2011; Cooper 2013). In cortical neuron migration, it was found that hepatocyte growth factor (HGF) signaling through MET proto-oncogene, receptor tyrosine kinase (MET), Ras/MAPK, Rac1/p38, and PI3K/Akt signaling pathways are all necessary (Segarra et al. 2006). Although this study placed the dependence of Rac1/p38 signaling on the activation of Ras or PI3K, it was shown that Ras/MAPK and PI3K/Akt signaling were parallel pathways and each pathway was required for cell migration (Segarra et al. 2006).

A diverse mixture of extracellular cues, both chemical and mechanical, in the form of neurotrophins, netrins, semaphorins, cell adhesion molecules (CAMs), and ephs and ephrins, for example, work in concert in the execution of axonal outgrowth. These signaling molecules and binding receptors are under the developmental control of transcription factors that are regulated by the RAS/MAPK and protein kinase C (PKC) signaling pathways. Via TRK receptor activation and retrograde signaling, both CREB and NFAT transcription factor families are activated to express the genes necessary to produce the elements needed at the site of axonal extension and pathfinding (Lonze et al. 2002; Graef et al. 2003; Polleux and Snider 2010). In cortical spinal motor neurons, both *in vitro* and *in vivo*, IGF like family member 1 receptor (IGFLR1) activation by IGFL1, specifically activated and enhanced axonal growth through both the PI3K and RAS/MAPK signaling pathways. This study further states that in conjunction with their results and previous studies, that BDNF does not play a role in axonal outgrowth (Ozdinler and Macklis 2006). Early *In vitro* studies however using sympathetic neurons found that TRKB activation induced local axonal outgrowth and that elongation was dependent upon both PI3K and MEK activity (Atwal et al. 2000). The seeming contradiction in these two

conclusions only serves to highlight the cell type specific and spatio-temporal activities of RAS/MAPK signaling.

It was suggested by Atwal et al. that regulation of cytoskeletal stability was induced through PI3K by regulation of cytoskeletal elements, or by the RAS/MAPK and direct interactions of ERK with microtubule and neurofilament proteins (Atwal et al. 2000). It was later found that activated ERK did indeed act in the phosphorylation of microtubule associated protein 1B (MAP1B) and microtubule associated protein tau (TAU). MAP1B is highly enriched and localized in axons during development and has both dendritic and axonal functions in adulthood while non-phosphorylated TAU is predominately detected in the axons (Dehmelt and Halpain 2005; Ramkumar et al. 2018). NGF activation of the RAS/MAPK pathway in PC12 cells and primary neurons activates cyclin dependent kinase 5 regulatory subunit 1 (CDK5R1) that then forms an active complex to phosphorylate MAP1B. Phosphorylated MAP1B has crucial roles in microtubule dynamics that affect axonal elongation and growth cone dynamics (Harada et al. 2001; Hahn et al. 2005; Yang et al. 2012). TAU has been found to have several functions associated with microtubules: Controlling microtubule modifications, altering the mechanical properties of microtubules, spacing of microtubules, and also regulation of microtubule motor transport (Ramkumar et al. 2018). Tau is capable of being phosphorylated on 17 different sites by activated ERK1/2 resulting in Tau losing its affinity for microtubules substantially (Avila 2008; Hanger et al. 2009; Qi et al. 2016). Although ERK mediated phosphorylation of Tau results in microtubule instability, there are several different kinases phosphorylating Tau that have a stabilizing effect. This dynamic effect of stable and unstable phosphorylations could therefore be part of the dynamic assembly / disassembly mechanism that occurs during axonal growth.

Connectivity in the RASopathies

Non-invasive imaging of major white matter tracts within NF1 patients has revealed widespread abnormalities in local and global measurements using diffusion tensor imaging (DTI). DTI has been widely used to measure changes in white matter structure and the relationship to cognitive abilities in different stages of development (Assaf and Pasternak 2008; Qiu et al. 2015). DTI takes advantage of the differences of water diffusion in different directions. By measuring the extent of diffusion in all directions of a three-dimensional space, the anisotropy, or directional dependency, can be measured. In comparing this to isotropic diffusion, distinctions can be made between the elliptical shapes of oligodendrocytic ensheathment of axons and the generally spherical shape of cell bodies. Measurements from the tensor model such as fractional anisotropy (FA), axial diffusivity (AD), radial diffusivity (RD), and mean diffusivity or apparent diffusion coefficient (MD or ADC) are then used to indicate the underlying axonal organization and microstructure of the brain. FA values from DTI are the main measure of white matter microstructural integrity and also indicate increases in overall diffusivity. MD values are an indication of a more diffuse or less organized structure in both adults and children with NF1 (Karlsgodt et al. 2012). DTI does suffer from some drawbacks however, such as only being able to reveal one dominant fiber tract in a given voxel and the inability to distinguish areas between tracts. Even with these limitations, DTI does allow for *in vivo* imaging and is a very useful tool for studying brain architecture both during and after development (Assaf and Pasternak 2008; Qiu et al. 2015).

NF1 patients with megalencephaly and general learning disabilities are thought to have a possible generalized alteration of the microstructure of the brain. DTI studies have defined these significant microstructural changes in the major white matter tracts in NF1 patients in measurements of FA and MD. DTI analysis of the

corpus callosum of children with NF1, aged 3-17, indicated significantly lower FA values compared to control patients. Measurements of whole brain histograms in these children showed an overall significant increase in MD (Filippi, Watts, Lindsay A. N. Duy, et al. 2013). Another study in adolescent NF1 patients, aged 9-18, also detected significantly lower FA values and significantly higher MD values within the cingulate bundle, superior longitudinal fasciculus, and the anterior thalamic radiation compared to controls. This study also reported widespread local and global abnormalities in white matter tracts (Koini et al. 2017). Significant decreases in FA and significant increases in MD of the corpus callosum, caudate nucleus, frontal white matter, parietooccipital white matter, thalamus, pons, and other select areas of adults with NF1 (S. L. Zamboni et al. 2007). In the first brain-wide DTI study of white matter microstructure, significant reductions in FA and overall increases of MD across the brain of adults with NF1. These results were explained that diffusion was not globally increased but was less constrained along the axonal tracts indicating decreased organization of tracts, decrease of myelination, or increased axonal spacing along the tracts (Karlsodt et al. 2012). Regulation of RAS/MAPK as well as Akt and FAK by NF1 has been shown to impact cell adhesion, cell survival, and cellular migration. The findings of these DTI studies have some consistencies with a loss of fasciculation and possibly pathfinding abilities of growing axons during development (Karlsodt et al. 2012). To find a link with these findings, further work is needed.

Resting state functional connectivity MRI (rs-fcMRI) in NF1 adults found significantly reduced anterior-posterior connectivity compared to controls. Comparing edge (link between two nodes that have correlated activity) distribution in NF-1 and control patients, results suggested a pattern of long-range connectivity in the control group that was absent in the NF-1 group. The authors theorized that since these

connectivity differences in network structures were found in the resting state, it may predispose NF-1 patients to additional difficulties when task requirements are presented (Friston 2011; Tomson et al. 2015a). In a task-related fMRI study, key components of working memory circuits were found to be significantly hypo-activated in NF-1 patients versus healthy control subjects. A Variety of additional differential patterns of connectivity were found to be present in the NF-1 patients in direct comparison to the control group. Overall findings of this study could be speculated to show that the NF-1 patients have a less efficient pattern of neural activity (Amira F. A. Ibrahim et al. 2017).

Immediate Early Gene ARC – Memory and Learning

Cognitive, learning, and memory deficits are reported in many cases of RASopathy syndromes and vary widely between disorders. Cognitive impairments are reported in up to 80% of NF1 patients while approximately 25% of Noonan syndrome patients are reported to have learning disabilities (Allanson and Roberts 1993; Plasschaert et al. 2015). Learning and long-term memory formation relies on newly transcribed and translated proteins to stabilize synaptic changes. One of the most defined immediate early genes (IEG) is activity regulated cytoskeleton associated protein (*Arc*). Changes in the expression of ARC in regions associated with memory, learning, and plasticity are used as a widespread readout of activity in these processes (Guzowski et al. 1999; Gallo et al. 2018). The *Arc* gene encodes an mRNA transcript that is translocated from the nucleus to the cytosol then transported to the post-synaptic dendrites (Steward and Worley 2001). Upon synaptic activity, *Arc* mRNA is transported to and stabilized at active synapses indicating local translation of ARC at those sites (Steward et al. 1998; Epstein and Finkbeiner 2018). Shortly after translation, ARC is transported to the nucleus where it accumulates as

seen in neurons of the hippocampus and somatosensory cortex (Korb et al. 2013; Epstein and Finkbeiner 2018). *Arc* is known to play a crucial role in synaptic plasticity leading to learning and memory consolidation that when disrupted can lead to major behavioral abnormalities (Korb and Finkbeiner 2011; Shepherd and Bear 2011; Gallo et al. 2018).

Transcription of *Arc* is induced by a variety of signaling cascades upon neuronal activity. Calcium influx through glutamate binding of the N-methyl-D-aspartate receptor (NMDAR), glutamate metabotropic receptor 1 (GRM1) or α -amino-3-hydroxy-5-methyl-4-isoxazolepropionic acid receptor (AMPA), BDNF stimulation of NTRK2, and voltage gated calcium channels (VGCC) can each stimulate *Arc* transcription through the RAS/MAPK pathway (Epstein and Finkbeiner 2018). Stimulation of the AMPAR also leads to inhibition of *Arc* transcription through a G protein coupled mechanism (Rao et al. 2006; Epstein and Finkbeiner 2018). In turn, ERK itself directly phosphorylates ARC leading to the nuclear localization and the inhibition of glutamate ionotropic receptor AMPA type subunit 1 (GRIA1) (Korb et al. 2013; Nikolaienko et al. 2017; Epstein and Finkbeiner 2018). These inhibitory mechanisms lead to homeostatic scaling of synaptic activity that when dysregulated can lead to a brain that is poorly suited to form memories (Epstein and Finkbeiner 2018).

Summary

The term RASopathies was coined to encapsulate the collection of syndromes caused by germline genetic mutations specifically within the RAS/MAPK signaling pathway. The mechanisms and interactions of this pathway have been exhaustively studied and pieced together from many different cell types mainly in *in vitro* studies. The signaling mechanisms however are extremely specific to various factors

including cell type, environmental, temporal, signal context and duration, and spatial characteristics. The central nervous contains a very heterogenous mixture of cells and numerous brain structures. Recent data has implicated aberrant connectivity issues to be involved in the neurological and behavioral issues within patients with NF1. However, little is known about cell-specific and structural specific contributions within the physiological setting of the RASopathy pathologies.

To address the aberrant RAS/MAPK signaling functions in the context of connectivity, we employed an *in vivo* conditional RAS/MAPK signaling (MEK1) loss- and gain-of-function model to specifically target long-range cortical neurons. This allowed the determination of cell-type autonomous effects on the connectivity issues reported in the RASopathies. This conditional genetics approach was additionally used to determine the presence of any cortical layer autonomous effects in the MEK1 gain-of-function mouse. Behavioral analysis was performed using this approach to address cell-type and layer autonomous effects in motor learning acquisition.

CHAPTER 2
PROJECTION NEURON DEVELOPMENT IN A LOSS-OF-FUNCTION
MEK1/MEK2 MOUSE MODEL

**Layer-specific and general requirements for ERK/MAPK signaling
in the developing neocortex**

Lei Xing, Rylan S. Larsen, George R. Bjorklund, Xiaoyan Li, Yaohong Wu, Benjamin D. Philpot, William D. Snider, Jason M. Newbern

¹University of North Carolina Neuroscience Center, ²Department of Cell Biology and Physiology, ³Carolina Institute for Developmental Disabilities, The University of North Carolina School of Medicine, Chapel Hill, NC, 27599

⁴Allen Institute for Brain Science, Seattle, WA, 98109

⁵School of Life Sciences, Arizona State University, Tempe, AZ, 85287

*Corresponding author

Abstract

Aberrant signaling through the Raf/MEK/ERK (ERK/MAPK) pathway causes pathology in a family of neurodevelopmental disorders known as “RASopathies” and is implicated in autism pathogenesis. Here, we have determined the functions of ERK/MAPK signaling in developing neocortical excitatory neurons. Our data reveal a critical requirement for ERK/MAPK signaling in the morphological development and survival of large Ctip2⁺ neurons in layer 5. Loss of *Mek1/2* led to deficits in corticospinal tract formation and subsequent corticospinal neuron apoptosis. ERK/MAPK hyperactivation also led to reduced corticospinal axon elongation but was associated with enhanced arborization. ERK/MAPK signaling was dispensable for axonal outgrowth of layer 2/3 callosal neurons. However, *Mek1/2* deletion led to reduced expression of *Arc* and enhanced intrinsic excitability in both layers 2/3 and 5, in addition to imbalanced synaptic excitation and inhibition. These data demonstrate selective requirements for ERK/MAPK signaling in layer 5 circuit development and general effects on cortical pyramidal neuron excitability.

Introduction

The canonical Ras/Raf/MEK/ERK (ERK/MAPK) signaling pathway is a key intracellular signaling cascade downstream of cell surface receptors critical for brain development (Samuels et al. 2009). In the developing cortex, the ERK/MAPK pathway is thought to be particularly important for neuronal responses to neurotransmitters and receptor tyrosine kinase (RTK) ligands, such as FGFs and neurotrophins. In the mature brain, it is well established that ERK/MAPK plays a central role in the activity-dependent plasticity of neural circuits (Thomas and Huganir 2004; Shilyansky et al. 2010).

Importantly, a number of human neurodevelopmental syndromes have been linked to aberrant ERK/MAPK activity. This related group of human syndromes, increasingly referred to as RASopathies, are caused by genetic mutations in core components or regulators of the ERK/MAPK signaling cascade (Rauen 2013). Macrocephaly, neurodevelopmental delay, cognitive impairment, and epilepsy are frequently observed in RASopathy patients with clinical manifestations being dependent on the precise causative mutation (Rauen 2013). RASopathies are most often associated with hyperactive ERK/MAPK signaling (e.g. Neurofibromatosis type 1 (NF1), Noonan, Costello, and Cardiofaciocutaneous (CFC) syndromes) (Rauen 2013); however, mutations that lead to diminished ERK/MAPK activation have been identified in a subset of LEOPARD and CFC syndrome patients (Kontaridis et al. 2006; Nowaczyk et al. 2014). Abnormal Ras/MAPK signaling has also been observed in models of other monogenic neurodevelopmental disorders, including Fragile X syndrome and Tuberous Sclerosis (Chévere-Torres et al. 2012; Osterweil et al. 2013; Faridar et al. 2014; Zhang et al. 2014). Recent exciting work has shown that pharmacological normalization of pathological Ras/MAPK activity is sufficient for correcting select cellular and behavioral abnormalities in Fragile X, Tuberous

Sclerosis, NF1, Noonan, and Costello syndrome mutant mice (Li et al. 2005; Cui et al. 2008; Wang et al. 2012; Osterweil et al. 2013; Lee et al. 2014; Zhang et al. 2014). However, our understanding of these disorders remains rudimentary as there is limited information on brain cell type-specific consequences of either loss- or gain-of-function through this pathway.

Accumulating evidence also suggests that pathological ERK/MAPK signaling contributes to certain forms of autism. Altered Ras/MAPK signaling has been identified as a common downstream mediator of divergent genetic mutations linked to autism, and *Erk1/MAPK3* is present in a region of 16p11.2 mutated in ~1% of cases of autism (Kumar et al. 2007; Eichler and Zimmerman 2008; Weiss et al. 2008; Pinto et al. 2010; Gilman et al. 2011; Gilman et al. 2012; Pucilowska et al. 2015). Little is known about how ERK/MAPK signaling might relate to the pathogenesis of autism. An important current research theme is that the behavioral manifestations of autism spectrum disorders (ASDs) may be linked to both functional hypo- and hyper-connectivity between distinct brain regions (Geschwind and Levitt 2007; Just et al. 2007; Keown et al. 2013; Supekar et al. 2013). Furthermore, recent work in postmortem brains of autistic patients suggests that local patches of disorganization, in which cortical layers 4-5 are particularly affected, play an important role in disease pathogenesis (Stoner et al. 2014). In one study, co-expression network analyses of autism-linked genetic mutations suggested that layer 5 in prefrontal and sensorimotor cortex is a key site of convergence for pathogenesis (Willsey et al. 2013). Whether aberrant ERK/MAPK signaling might result in cortical layer disorganization and defective long-range connectivity is unknown.

To address questions of cell type specificity and consequences for circuit formation, we have defined the effects of ERK/MAPK loss- and gain-of-function on the development of cortical pyramidal neurons. Pyramidal neuron-specific functions

of ERK/MAPK signaling were assessed by deleting the upstream kinases *Mek1/MAP2K1* and *Mek2/MAP2K2* (*Mek1/2*) or overexpressing hyperactive *Mek1*. Conditional deletion of *Mek1/2* led to major disruption of layer 5 with noticeably fewer *Ctip2*-expressing large neurons compared to controls. Further, long range axon extension of layer 5 corticospinal projection neurons during early development was markedly impaired. Subsequent to delayed entry of axons into the cervical spinal cord, many layer 5 projection neurons in sensorimotor cortices underwent apoptosis. Gain-of-function ERK/MAPK signaling also affected layer 5 CST neurons with a resultant decrease in axon elongation and associated increase in axon branching. The morphological requirement for ERK/MAPK signaling was specific for layer 5, as layer 2/3 was not disrupted and callosal projection neurons in upper cortical layers do not exhibit overt changes in axon extension or targeting following *Mek1/2* deletion. In contrast to the layer-specific functions of ERK/MAPK on axonal development, we found that ERK/MAPK was required for the expression of *ARC* and other plasticity-associated genes across all cortical lamina. Further, loss of ERK/MAPK signaling in pyramidal neurons disrupted excitatory and inhibitory neurotransmission and altered intrinsic excitability in both layers 2/3 and 5. Our data reveal unexpectedly specific requirements for ERK/MAPK signaling in layer 5 circuit development and general effects on the excitability of cortical pyramidal neurons in multiple layers.

Materials and Methods

Transgenic Mice

Animal experiments were performed in accordance with established protocols approved by the Institutional Animal Care and Use Committee at the University of North Carolina–Chapel Hill and Arizona State University and NIH guidelines for the use and care of laboratory animals. All mice were housed in standard conditions with food and water provided ad libitum and maintained on a 12-hr. dark/light cycle. Experiments were replicated a minimum of three times with mice derived from independent litters. *Nes:Cre* expression alone did not have a detectable effect on the phenotypes described in this manuscript. Thus, Cre-expressing or Cre-negative littermates were utilized as controls unless indicated otherwise. *Mek1^{loxp/loxp}* mice possess a loxp flanked exon 3 while *Mek2^{-/-}* mice contain a neo insertion in exons 4-6, which encodes the kinase domain (Bélanger et al. 2003; Bissonauth et al. 2006). *Mek2^{-/-}* mice are viable and breed normally. *Loxp-STOP-loxp-caMEK1* mice were kindly provided by Dr. Maïke Krenz and Dr. Jeffrey Robbins (Krenz et al. 2008); the *IGF1R^{loxp/loxp}* were kindly provided by Dr. Ping Ye (Liu et al. 2009); the *Nes:Cre* mice were kindly provided by Dr. Klaus Nave and Dr. Sandra Goebbels (Goebbels et al. 2006); and the *Emx1:Cre* mice were kindly provided by Dr. Franck Polleux (Gorski et al. 2002). “*Ai3*” mice were purchased from Jackson laboratories (Madisen et al. 2010). All mice in this study were of mixed genetic background.

Genomic DNA extracted from tail or toe samples was utilized for mouse genotyping by PCR using standard techniques. Primers for gene amplification are as follows (listed 5’-3’): Cre - TTCGCAAGAACCTGATGGAC and CATTGCTGTCACCTGGTCGT amplify a 266 bp Cre allele; *Mek1* – CAGAAGTTCCCACGACACTA, CTGAAGAGGAGTTTACGTCC, and GTCTGTCACCTGTCTTCTGG amplifies a 372 bp wild type and a 682 bp floxed allele;

Mek2 – CTGACCTTCCTGTAGGTG, ACTCACGGACATGTAGGA, and AGTCATAGCCGAATAGCCTC amplify a 293 bp wild-type allele and a 450 bp knockout allele; *caMEK1* -GTACCAGCTCGGCGGAGACCAA and TTGATCACAGCAATGCTAACTTTC amplify a 600 bp mutant allele; *Ai3* – AAGGGAGCTGCAGTGGAGTA, CCGAAAATCTGTGGGAAGTC, ACATGGTCCTGCTGGAGTTC, and GGCATTAAAGCAGCGTATCC amplify a 297 bp wild-type allele and a 212 bp *Ai3* allele; IGF1R-CTTCCCAGCTTGCTACTCTAGG and CAGGCTTGCAATGAGACATGGG amplify a 124 and a 220 bp band for wild-type and floxed alleles.

Viral and Dil Injections

P0-P5 litters were removed as a group, cryo-anesthetized on wet-ice for 3-5 min, and immediately injected with 50-500nl of solution using a 5 uL Hamilton syringe fitted with a 32-gauge beveled needle mounted to a stereotaxic arm. For viral labeling, the AAV5-CAG-FLEX-tdTomato vector was prepared by the UNC Viral Vector Core and diluted in sterile PBS, 5% sorbitol, and 0.1% Fast Green to allow for visualization prior to injection. For Dil tracing, a 10% Dil solution (Life Technologies) was prepared in DMSO and injected into the primary motor cortex or the cervical spinal cord. Upon completion of the injection, pups recovered on a heating pad and were returned as a group to the home cage.

Tissue Preparation

Mice of the appropriate age were anesthetized and perfused transcardially with 4% paraformaldehyde/PBS. For cryoprotection, sub dissected samples were incubated in a graded series of 10%, 20%, and 30% sucrose/PBS at 4 °C before embedding in O.C.T. compound and freezing. Cryostat sections were collected on Fisherbrand Superfrost/Plus slides (Fisher Scientific) and air-dried prior to staining.

For some experiments, brains were dissected, post fixed, and mounted in agarose prior to vibratome sectioning.

Immunolabeling

For immunofluorescent staining, sections were rinsed in PBS and blocked with 5% normal serum/0.1% Triton X-100/PBS at room temperature. Primary antibodies were diluted in blocking solution and incubated 1-2 days at 4°C with gentle agitation. The antibodies utilized were; rabbit anti-Parvalbumin (Swant), chicken anti-GFP (Aves Labs), rat anti-Ctip2 (Abcam), rabbit anti-Satb2 (Abcam), rabbit anti-Cux1 (Santa Cruz), mouse anti-NeuN (Chemicon), rabbit anti-Cleaved Caspase-3 (Cell Signaling Technology), rabbit anti-Iba1 (Wako), goat anti-IGF1 (R&D Research), rabbit anti-PKC γ (Santa Cruz), rabbit anti-MEK1/2 (Abcam), rabbit anti-P-ERK1/2 (Cell Signaling Technology) and rabbit anti-IGF1R β (Cell signaling Technology). After rinsing in PBS/T, the secondary antibody was diluted in blocking solution and added overnight at 4°C. Secondary antibodies included Alexa Fluor 488, 546 or 568, and 647 conjugated anti-rabbit, anti-mouse, anti-rat, or anti-goat IgG (Invitrogen). For some experiments, slides were then incubated in Hoechst or DAPI for nuclear labeling, rinsed, and mounted. Images were collected with a Zeiss LSM 710, 780, or Leica SP5 laser scanning confocal microscope.

Image Analysis and Quantitation

Confocal images of regions of interest were collected from individual brain sections for each animal. For assessment of relative neocortical volume, cortical area was measured in five anatomically matched coronal sections along the rostro-caudal axis, averaged, and normalized against the control brain. For assessment of Ctip2, Cux1, Satb2, and NeuN expressing cells, regions of primary sensory, motor, and

visual cortex from at least three anatomically matched sections of mutant and control cortices were defined using morphological and anatomical features described in Paxinos and Franklin 2001 (Franklin and Paxinos 2013). Radial columns were outlined within the cortical region of interest and measured. The total sampled area from a specific region of cortex of a single brain ranged from 1-3 mm². Individual layer boundaries were determined by the changes in density and appearance of NeuN labeling. Images were then transferred into ImageJ, a pixel intensity threshold was set manually by an observer blind to the genotype, and watershed segmentation was performed. The binary image mask was then analyzed using the particle analysis tool to count the number of events with a min-max size cutoff of 50-600 μm² for NeuN labeling and 30-300 μm² for Ctip2⁺, Cux1⁺, or Satb2⁺ labeled nuclei. For NeuN density determination, the total number of NeuN⁺ cells within a radial column was divided by the area of the column and averaged across at least three separate columns within the cortical region of interest. For determination of the relative proportion of Ctip2⁺ or Satb2⁺ cells in layer 5 or Cux1⁺ cells in layers 2-4, the number of each labeled cell within specific laminar boundaries was divided by the total NeuN count within the entire radial column to determine the proportion of each neuronal subtype per radial column. Results from this analysis were averaged across three individual radial columns per cortical region and normalized against the littermate control analyzed in parallel for each mutant. These images were also utilized for determination of the cross-sectional area of neuronal soma. Randomly selected, well-labeled NeuN expressing neurons that included a DAPI labeled nucleus were outlined manually in Photoshop and measured.

For analysis of axonal innervation, a modification of the cell counting procedure described above was utilized where images of the region of axonal innervation from at least three anatomically matched sections were collected,

manually thresholded in ImageJ, and the number of labeled pixels was measured.

Representative images have been cropped and adjusted for brightness and contrast in Photoshop for presentation. Student's t-test was used for statistical analysis.

Western Blotting

Sensorimotor cortices were dissected from both mutant and litter mate control mice and lysed in RIPA buffer (0.05M Tris-HCl, pH 7.4, 0.5M NaCl, 0.25% deoxycholic acid, 1% NP-40, and 1mM EDTA, Millipore) supplemented with 0.1% SDS, protease inhibitor cocktail (Sigma) and phosphatase inhibitor cocktail II and III (Sigma). Lysates were cleared by centrifugation and protein concentration was determined using the Bio-Rad protein assay (Bio-Rad) using BSA as a standard. Equal amounts of protein were denatured in reducing sample buffer, separated by SDS-PAGE gels, and blotted to PVDF membranes (Bio-Rad). Blots were blocked with 5% BSA in TBS containing 0.5% Tween 20 (TBS-T) for 1 h at room temperature, then incubated overnight at 4°C with primary antibodies. The primary antibodies used were rabbit anti-phospho Erk1/2 (Thr202/Tyr204) (Cell Signaling Technology, Inc), rabbit anti-Erk1/2 (CST), rabbit anti-phospho-p90RSK (Thr573) (Cell Signaling Technology, Inc.), rabbit anti-RSK (Cell Signaling Technology, Inc.), rabbit anti-MSK1(Ser360) (Abcam), rabbit anti-MSK1 (Cell Signaling Technology, Inc.), rabbit anti-Mek1/2 (Cell Signaling Technology, Inc.), rabbit anti-Arc (Synaptic System) and anti-GAPDH (Cell Signaling Technology, Inc.). After washing with TBS-T, membranes were incubated with HRP-conjugated secondary antibodies in 5% milk in TBS-T for 2 h at room temperature. Blots were washed with TBS-T and detection was performed with SuperSignal West Pico chemiluminescent substrate (Thermo Scientific).

Results

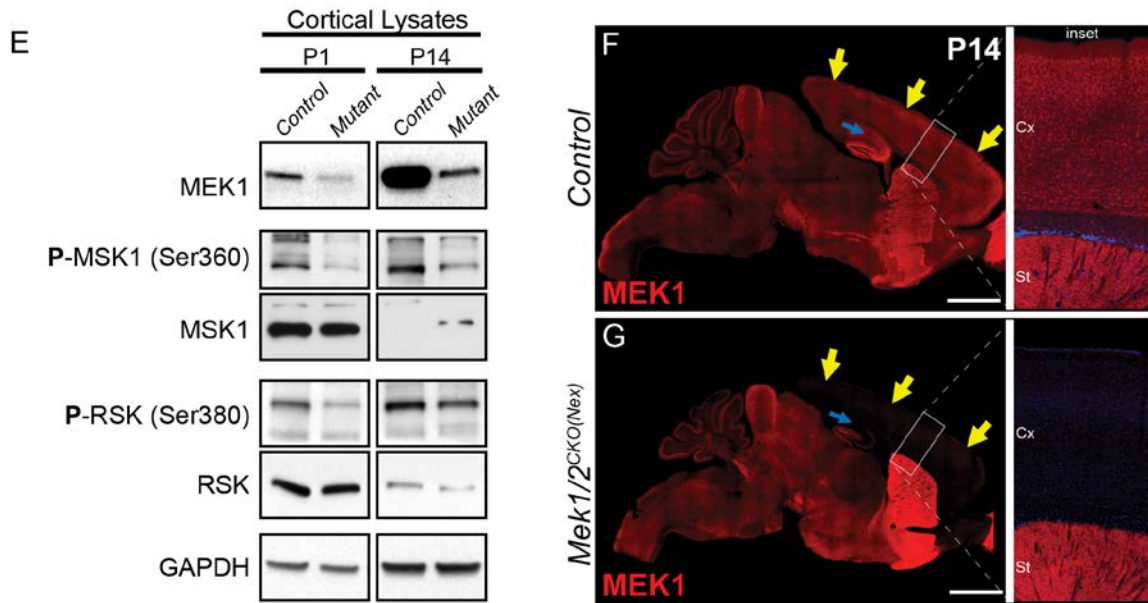
Excitatory neuron-specific modification of ERK/MAPK activity

Previous work has shown that ERK1/2 is activated in embryonic cortical neurons, albeit at much lower levels than in the ventricular zone (Faedo et al. 2010; Toyoda et al. 2010; Pucilowska et al. 2012; Li et al. 2014). In western blots of sensorimotor cortical lysates from P1, 2, 7, 14, and 21-day old mice, it was shown that levels of pan-ERK1/2 and pan-MEK1/2 exhibit a steady but evident increase from a relatively lower level at birth. Phosphorylated-ERK1/2 and phosphorylated-MEK1/2 levels were also relatively low at birth but increased noticeably by P7 and peaked at P14 (Oliveira et al. 2008). The expression of phosphorylated ERK1/2 at P3 did not exhibit any clear-cut laminar specificity. These findings indicate that ERK/MAPK signaling is activated in the developing cortex, peaking during the second postnatal week (Xing et al. 2016).

We generated a mouse model to test the direct, neuron-autonomous role of ERK/MAPK signaling by inactivating *Mek1/2* specifically in immature mouse cortical excitatory neurons. We conditionally deleted *Mek1/2* with a Cre-dependent *Mek1* allele, a germ-line *Mek2* deletion allele, and Cre-recombinase under the control of the *Nex/NeuroD6* promoter (*Mek1^{loxp/loxp} Mek2^{-/-} Nex:Cre*, referred to hereafter as *Mek1/2^{CKO(Nex)}*) (Goebbels et al.). As expected, *Nex:Cre* activated reporter-gene expression in the Cre-dependent EYFP mouse line, *Ai3*, in excitatory, but not inhibitory, neurons in the neocortex (Figure 3B-C) (Madisen et al. 2010). Cre-mediated reporter gene expression was apparent by mid-embryogenesis (data not shown). Western blotting of neocortical lysates and immunolabeling show that *Mek1/2^{CKO(Nex)}* mice exhibit significantly reduced MEK1 levels by birth and reduced phosphorylation of ERK/MAPK substrates, RSK, and MSK (Figure 3A). Complete loss

of MEK1 protein would not be expected in whole cortical lysates due to MEK1 expression in inhibitory interneurons and non-neuronal cell types. These data show that the *Nex:Cre*-mediated genetic targeting strategy is effective at inducing loss of ERK/MAPK signaling in developing cortical excitatory neurons. *Mek1/2^{CKO(Nex)}* pups were born at normal Mendelian ratios without overt differences from littermate controls. However, a delay in overall growth could be detected by the end of the first postnatal week. At P14 *Mek1/2^{CKO(Nex)}* mice exhibited an average reduction in body weight of $37.1 \pm 11.3\%$ and neocortical volume was reduced by $23.2 \pm 6.4\%$ (mean \pm SEM, n=7, p<0.0001). Behaviorally, P14 *Mek1/2^{CKO(Nex)}* mice exhibited spontaneous and persistent hindlimb clasping when lifted by the tail (data not shown), an indicator of neurological impairment. Lethality was invariably observed in the third to fourth postnatal week. A qualitatively similar effect on growth, neurological function, and viability was also observed in *Erk1^{-/-} Erk2^{loxp/loxp} Nex:Cre* mice (data not shown), demonstrating that phenotypes are conserved following deletion of different core components of the ERK/MAPK cascade (Xing et al. 2016).

Figure 3



***Mek1/2^{CKO(Nex)}* Cortical Excitatory Neurons Specific Recombination.** (E) P1 and P14 *Map2k1/2*; *Neurod6-Cre* cortices show pronounced loss of MAP2K1 expression and reduced phosphorylation of ERK/MAPK pathway substrates, RSK and MSK (n=5). (F-G) Representative confocal images of P14 control mouse brains show that cortical excitatory neurons in the cortex and hippocampus exhibit a high level of MAP2K1 immunolabeling (E). MAP2K1 levels are profoundly reduced in the cortex (yellow arrows) and hippocampal subfields CA1-CA3 (blue arrow) in P14 *Map2k1/2*; *Neurod6-Cre* mice (G) (n=6, scale bar=2 mm).

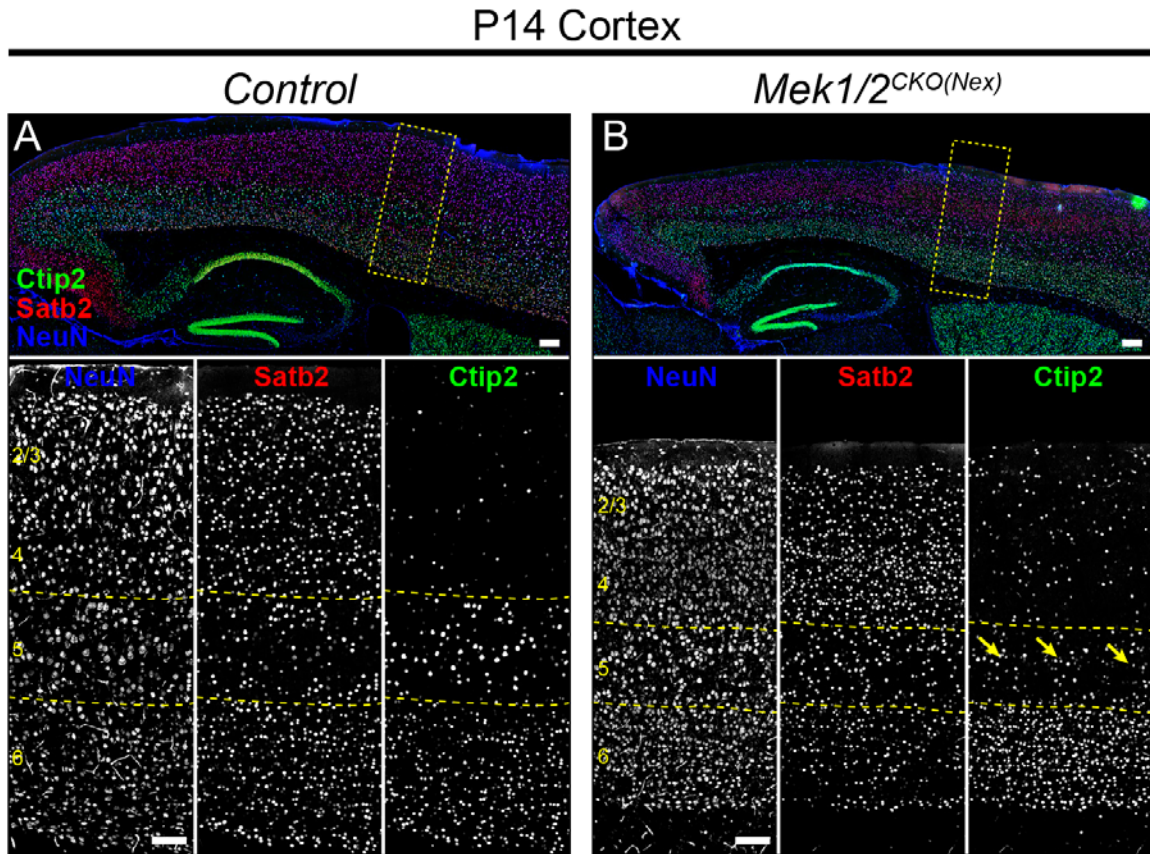
Disruption of layer 5 and reduced number of Ctip2⁺ neurons after ERK/MAPK inactivation

Comprehensive analyses of layer 5 neurons have identified specific gene expression patterns, morphologies, and electrophysiological characteristics for this neuronal subtype (Leone et al. 2008; Kwan et al. 2012; Custo Greig et al. 2013). We analyzed the expression pattern of a critical transcription factor for layer 5 development, Ctip2, in control and mutant cortices (Figure 4A-B) (Arlotta et al. 2005). The appearance of co-labeled Ctip2⁺/NeuN⁺ neurons in layer 5 appeared disrupted in rostral P14 *Mek1/2^{CKO(Nex)}* cortices compared to controls (Figure 4B, yellow arrows).

Ctip2⁺ layer 5 neurons are a small percentage of the total cortical neuron population. In the sensory cortex of control mice, we found that Ctip2⁺ layer 5 neurons represent only 9.61 ±0.84% (mean ±SEM, n=5) of all NeuN⁺ neurons within a radial column. Thus, our previous global NeuN estimates across an entire cortical column were not sensitive enough for detecting changes confined to sparse neuronal subtypes. To quantify the number of Ctip2⁺ neurons, we determined the relative proportion of cells in layer 5 that express Ctip2⁺ as a percentage of NeuN⁺ cells across all lamina in a radial cortical column. This measurement was performed in motor, sensory, and visual cortices. Indeed, we found that P14 *Mek1/2^{CKO(Nex)}* primary motor and sensory cortices exhibit a clear decrease in the relative proportion of Ctip2⁺ neurons in layer 5 (Figure 5A-F, G). Qualitatively similar results were observed in P14 *Mek1/2^{CKO(Emx1)}* cortices (Data not shown). The relative proportion of Ctip2⁺ neurons in visual cortices (Figure 5E-F, G) was not significantly diminished in *Mek1/2^{CKO(Nex)}* mutants, suggesting the effect in sensory and motor cortex was due to loss of the cell type and not a result of ERK/MAPK regulation of global Ctip2

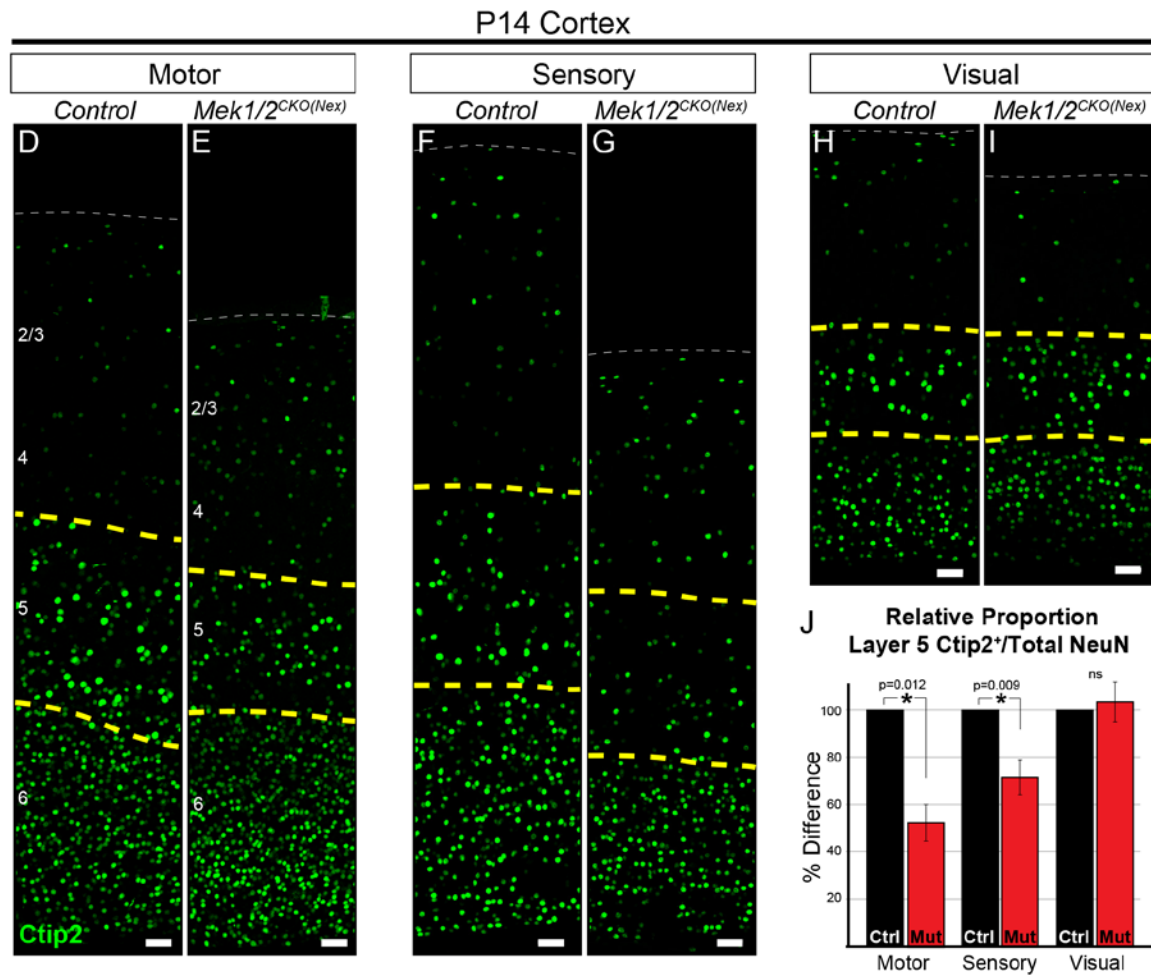
expression levels (Xing et al. 2016).

Figure 4.



Loss of ERK/MAPK signaling leads to a reduction in the number of Ctip⁺ layer 5 neurons. Immunostaining of P14 control (A) and *Mek1/2^{CKO(Nex)}* (B) sagittal forebrain sections for all neurons, callosal projection neurons, and subcortical projection neurons with NeuN, Satb2, and Ctip2, respectively, revealed an aberrant pattern of Ctip2 expression in layer 5 of mutant sensorimotor cortices (yellow arrows) (n=6, scale bar = 100 μ m).

Figure 5.



Loss of ERK/MAPK signaling leads to a reduction in the number of Ctip⁺ layer 5 neurons. Representative confocal images of Ctip2 immunolabeling in radial columns of primary motor (D-E), sensory (F-G), and visual (H-I) cortex from P14 control (D, F, H) and *Mek1/2^{CKO(Nex)}* (E, G, I) brains (scale bar = 30 μ m). Quantification of the relative number of layer 5 Ctip2⁺ neurons as a proportion of the total number of NeuN⁺ neurons in a cortical column revealed a substantial decrease in motor and sensory, but not visual, cortices in P14 mutant mice (J) (n=4, mean \pm SEM, * = p < 0.05).

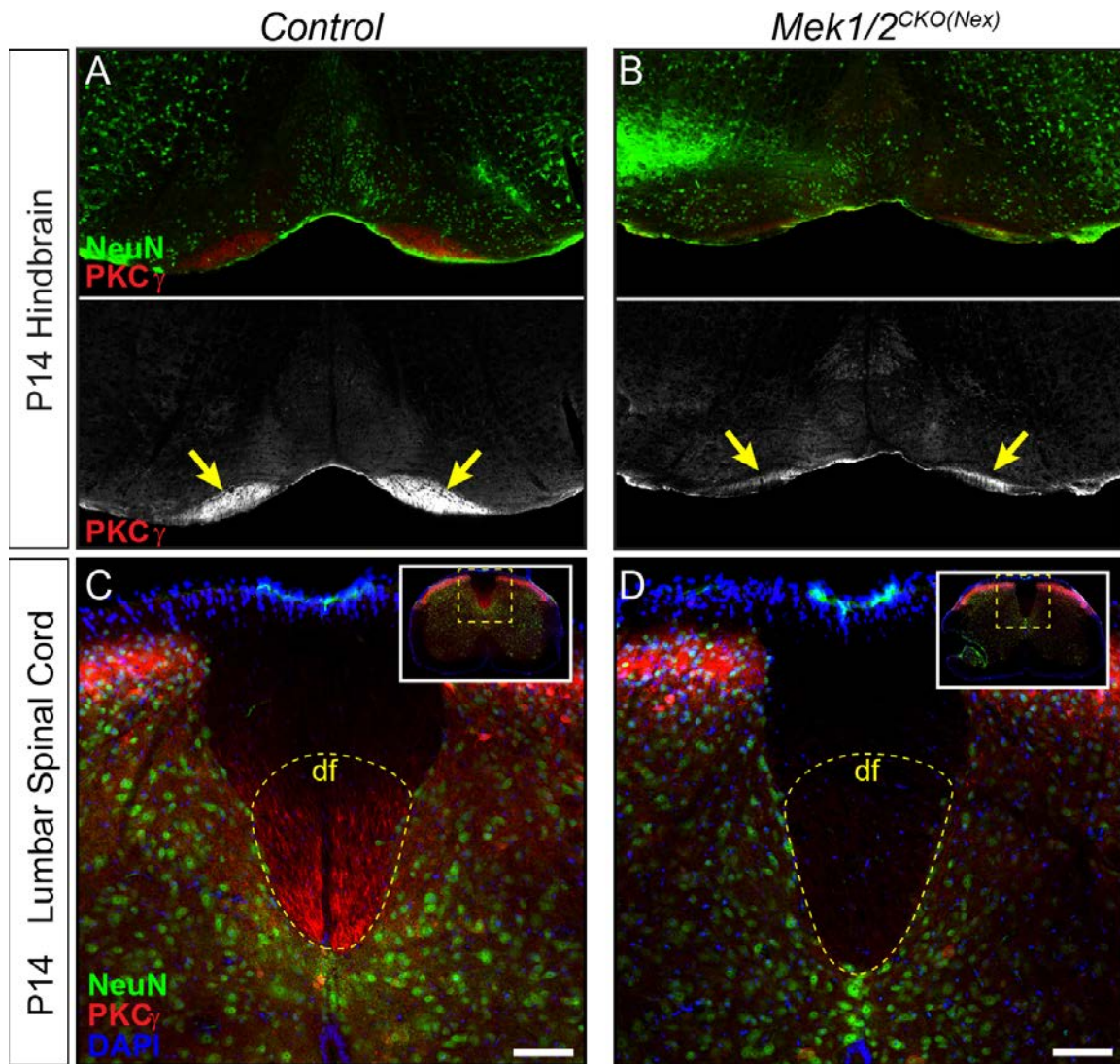
Failure of CST development neurons in layer 5

Layer 5 neurons are morphologically heterogeneous with distinct subpopulations that can be differentiated by cortico-cortical or subcortical axonal projections. We examined layer 5 projections in the hindbrain corticobulbar tract (CBT) and spinal cord corticospinal tract (CST) of P14 *Mek1/2* mutant mice. Immunostaining for a well-established marker of corticospinal projections, PKC γ , and genetic labeling with *Ai3* revealed a profound decrease in the size of the CBT in P14 *Mek1/2*^{CKO(Nex)} hindbrains (Figure 6A-B). CST labeling was also strikingly reduced in the cervical spinal cord (data not shown) and essentially absent in the lumbar spinal cord in both *Mek1/2*^{CKO(Nex)} (Figure 6C-D) and *Mek1/2*^{CKO(Emx1)} mutants (Figure 6E-F). Analysis of rare *Mek1/2* mutants that survived as late as P24 revealed that no CST axons were present in lumbar spinal cords (data not shown). These data provide further evidence of an overt loss of corticospinal neurons by the second postnatal week (Xing et al. 2016).

Corticospinal neurons represent a subset of the entire Ctip2⁺ population in sensorimotor layer 5 (Arlotta et al. 2005). The lack of layer 5 neuron loss in the *Mek1/2*^{CKO(Nex)} visual cortex suggests that ERK/MAPK signaling is dispensable for the development of projection neurons targeting structures other than the spinal cord. Past work has shown that callosally projecting layer 5 neurons have significantly shorter and less complex apical dendritic arbors than subcortical projection neurons (Molnár and Cheung 2006; Larsen et al. 2007). To determine which of these classes was affected by *Mek1/2* deletion, a Thy1-based reporter, *YFP-16*, that fluorescently labels a small proportion of layer 5 neurons in sensorimotor cortex, was bred with *Mek1/2*^{CKO(Nex)} mice (Feng et al. 2000).

These mutants clearly show that the fluorescently labeled layer 5 neurons in P14-P21 *Mek1/2^{CKO(Nex)}* *YFP-16* sensorimotor cortices have substantially shorter apical dendrites than in controls (Data not shown). The reduction in large, tufted neurons in layer 5 of mutant mice provide further evidence for a deficit in the development of corticospinal projection neurons (Xing et al. 2016).

Figure 6.



Corticospinal tract defects in the *Mek1/2CKO (Nex)* mice. To further evaluate the loss of layer 5 projection neurons, we examined the expression of a well-established corticospinal tract marker, PKC γ . Compared to control hindbrains (A) and spinal cords (C), a profound decrease in corticospinal tract labeling was observed in the *Mek1/2CKO (Nex)* hindbrain (B-yellow arrows, scale bar = 200 μ m) and spinal cord (D), consistent with the reduced number of Ctip2+ layer 5 neurons (df=dorsal funiculus, n=3, scale bar = 50 μ m).

ERK/MAPK signaling is necessary for corticospinal axon extension

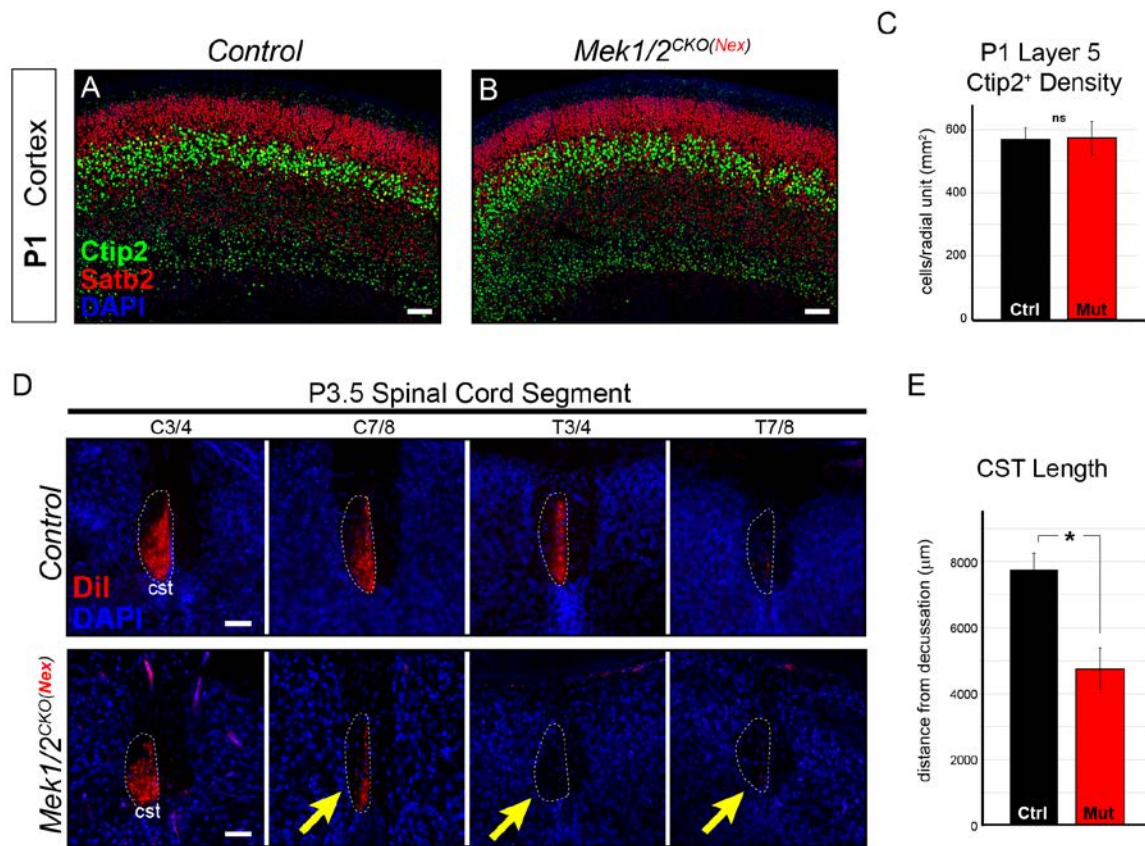
The loss of layer 5 neurons following deletion of *Mek1/2* could be due to an early disruption in the initial specification of this neuronal subtype. During layer 5 neuron development, *Nex:Cre* is not expressed until neurons are post-mitotic (Wu et al. 2005; Goebbels et al.). However, it remained possible that post-mitotic stages of embryonic layer 5 neuron specification were altered during embryogenesis. In newborn mutant pups, we found that the expression and number of Ctip2⁺ neurons in presumptive layer 5 was not diminished following *Mek1/2* deletion (Figure 7A-C). Thus, ERK/MAPK signaling is not required for the initial establishment of the correct numbers of the Ctip2⁺ deep-layer neuron population.

By P3 in wild-type neonates, corticospinal axons have projected through the ventral hindbrain, crossed the midline at the medullary/spinal cord boundary, and are extending into cervical spinal cord through the dorsal funiculus (Schreyer and Jones 1982). We asked whether ERK/MAPK signaling was required for the initial outgrowth of corticospinal projections *in vivo*. *In vivo* Dil injections into the motor cortex of P0.5 neonates were performed to assess subcortical axon growth, especially into the spinal cord (Figure 8A). Strikingly, analysis of anterogradely labeled axonal projections at P3-4 revealed a highly significant decrease in the extension of corticospinal axons into the lower cervical/upper thoracic segments of spinal cord (Figure 7D-E). Moreover, a profound decrease in the caudal extension of descending corticospinal axons into the spinal cord of P2 *Mek1/2^{CKO(Emx1)} Ai3* mice was also observed (Data not shown). Dil labeling of subcortical projections in *Mek1/2^{CKO(Nex)}* mice revealed that layer 5 neuron growth into the tectum and pons/medulla was not significantly decreased (Figure 8B). These data demonstrate that the initial growth of corticospinal axons to the level of the hindbrain is not significantly disrupted in *Mek1/2* mutants, however, ERK/MAPK signaling is clearly

necessary for corticospinal axon elongation into the spinal cord.

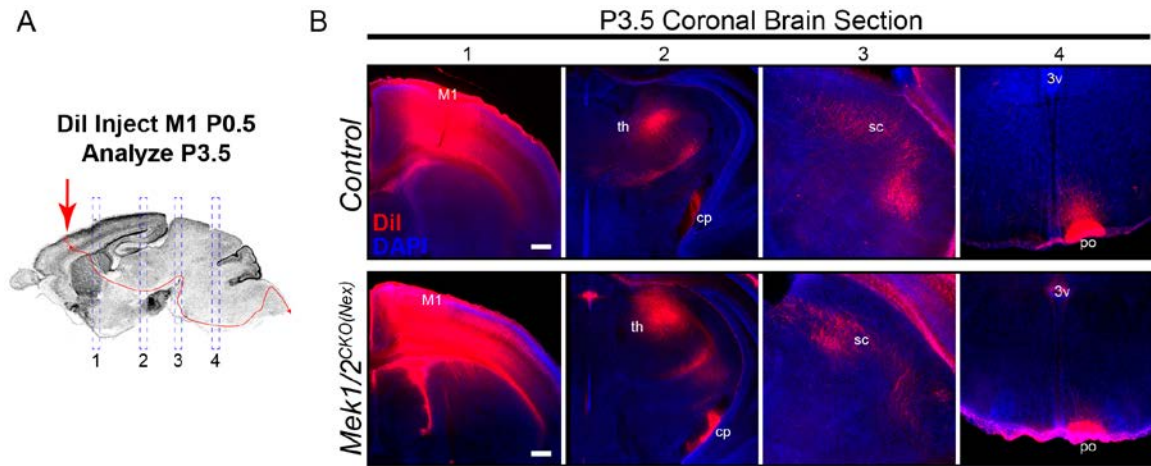
In vitro studies have demonstrated that IGF1 signaling acting via PI3K and ERK/MAPK promotes corticospinal axon outgrowth *in vitro* (Ozdinler and Macklis 2006). IGF1 is also focally and intensely expressed in the medulla in the presumptive inferior olivary nucleus during the precise developmental time frame (P1 – P2) that CST axons normally enter the spinal cord (Data not shown). IGF-1 expression is temporally regulated, being present by E18 and much diminished by P14 (data not shown). *Mek1/2* deletion in CST axons does not affect IGF1 expression by these cells (Data not shown). Thus, IGF-1 may act via ERK/MAPK within corticospinal neurons to regulate corticospinal outgrowth (Xing et al. 2016).

Figure 7.



Layer 5 neuron corticospinal axon outgrowth requires ERK/MAPK signaling *in vivo*. Expression of a well-known master transcription factor for layer 5 neurons, Ctip2, was intact in cortical layer 5 as shown in representative confocal images of newborn control (A) and *Mek1/2^{CKO(Nex)}* (B) sensorimotor cortices (scale bar = 50 μm). Quantitation of the number of Ctip2-expressing nuclei in cortical layer 5 did not reveal a significant difference in Ctip2⁺ neuron density between control and mutant neonates (C) (n=3, mean ± SEM, p = 0.89). *In vivo* Dil injections into the sensorimotor cortex of P0.5 control and *Mek1/2^{CKO(Nex)}* neonates were performed and mice were collected three days after injection. The extent of anterograde Dil labeling was analyzed in coronal sections through the spinal cord (D). We observed a significant decrease in the extent of corticospinal (cst) elongation in mutant mice, especially in the lower cervical/thoracic spinal cord segments (yellow arrows in D) (n=3, scale bar = 100 μm). Quantitation of CST length relative to the medullary decussation revealed a significant decrease in corticospinal axon growth in mutant spinal cords (E) (n=3, mean ± SEM, * p = 0.02).

Figure 8.



The rostro caudal elongation of layer 5 axons in the spinal cord requires ERK/MAPK. A-B. *In vivo* Dil injections into the sensorimotor cortex were performed in P0.5 control and *Mek1/2^{CKO(Nex)}* neonates to label subcortical projection neuron afferents (A). Mice were collected three days after injection and the extent of Dil labeling in multiple subcortical targets was analyzed in coronal sections through the brain (B). A substantial difference in the innervation of the thalamus (th), cerebral peduncle (cp), superior colliculus (sc), or pons (po) was not detected in mutants (B) (n=3, scale bar=100 μ m).

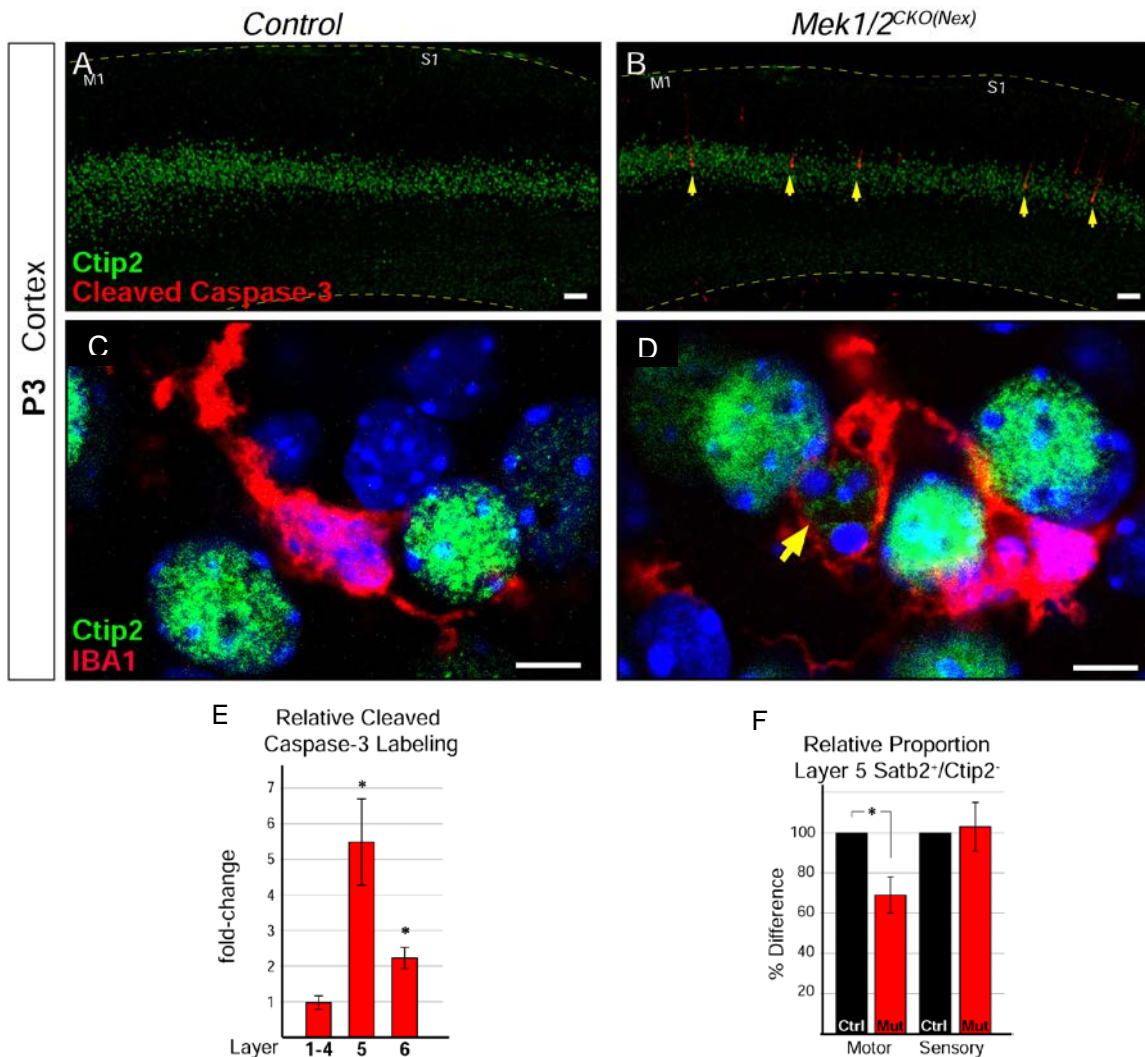
Caspase-3 activation in Layer 5 neurons after ERK/MAPK deletion

By P3 we noted a dramatic increase in the number of activated caspase-3 labeled neurons in layer 5 in *Mek1/2^{CKO(Nex)}* mutants when compared to controls (Figure 9A-B, E). Modest caspase-3 activation was also observed in layer 6, but not in upper layers 1-4 (Figure 9E). In line with the elevation of caspase-3 activity, we observed Iba1⁺ microglia in P3 *Mek1/2^{CKO(Nex)}* cortices with a ramified morphology that appeared to be engulfing Ctip2⁺ neurons (Figure 9C-D). To further confirm the absence of corticospinal neurons, we retrogradely labeled corticospinal projection neurons by injecting Dil into the cervical spinal cord in *Mek1/2^{CKO(Nex)}* neonates at P3, the time point when dying cells could initially be detected in the cortex. Analysis of retrogradely labeled corticospinal neurons in the primary motor cortex at P7 revealed a significantly reduced number of Dil labeled cells consistent with the death of these neurons during this time period (Data not shown). Interestingly, retrograde Dil labeling of P5 layer 5 neurons that project into the contralateral hemisphere did not reveal a substantial decrease in P9 mutants relative to controls (Data not shown). These data indicate that loss of *Mek1/2* results in overt caspase-3 activation and corticospinal neuron death that can be first detected at P3-4.

We examined the possibility that transformation of Ctip2⁺ corticospinal neurons into an alternative phenotype during the neonatal period contributes to the reduction in Ctip2⁺ layer 5 neuron number observed at P14. We tested whether Ctip2⁺ layer 5 neurons might be transforming into a callosal phenotype by quantifying the proportion of cortical neurons that express *Satb2*, an important transcription factor for the differentiation of callosal neurons (Alcamo et al. 2008; Britanova et al. 2008). Since *Satb2* is co-expressed by a minority of Ctip2⁺ neurons and *Satb2* plays a transient role in corticospinal differentiation, we only assayed *Satb2*⁺ layer 5 neurons that were Ctip2⁻ (Leone et al. 2015; McKenna et al. 2015). A

significant decrease in the proportion of Satb2⁺/Ctip2⁻ neurons in layer 5 could be detected in motor cortex, but not sensory cortex, in P14 *Mek1/2*^{CKO(Nex)} mice when compared to controls (Figure 9F). These findings demonstrate that the reduced number of Ctip2⁺ neurons in layer 5 does not coincide with a compensatory increase in the proportion of Satb2⁺/Ctip2⁻, presumably callosal, layer 5 neurons.

Figure 9.



Initiation of layer 5 neuron death by P3 in *Mek1/2CKO(Nex)* mutants.

Representative confocal images of immunolabeling for cleaved activated caspase-3, a well-known marker of neuronal apoptosis in P3 control (A) and *Mek1/2CKO(Nex)* (B) sensorimotor cortices. Note the extensive increase in the number of activated caspase-3+ cells co-labeled with Ctip2 in layer 5 of mutant cortices (B, yellow arrows) (n=4, scale bar = 50 μ m). Quantification of activated caspase-3+ cells in upper layers (layer 1-4), layer 5 (Ctip2+) and layer 6 revealed a pronounced elevation in the number of apoptotic cells in layer 5 in P3 *Mek1/2CKO(Nex)* mice relative to controls (E). The numbers of activated caspase-3+ cells are comparable in upper layers and doubled in layer 6 relative to controls (E) (n=4, mean \pm SEM, * p<0.05). Quantification of the relative number of layer 5 Satb2⁺/Ctip2⁻ neurons as a proportion of the total number of NeuN⁺ neurons in a cortical column revealed a substantial decrease in motor, but not sensory, cortices in mutant mice (F) (n=3, mean \pm SEM, * p=0.003). Relative to controls many microglia (Iba1+) were observed with processes surrounding Ctip2 labeled neurons in Layer 5 of mutant cortices (C-D) (n=3, scale bar=5 μ m).

Gain-of-function ERK/MAPK signaling reduces CST elongation, but enhances branching

Many neurodevelopmental syndromes that involve mutations in canonical members of the ERK/MAPK cascade exhibit enhanced ERK/MAPK activity (Rauen 2013). Thus, we assessed effects of hyper-activation of the ERK/MAPK pathway on developing cortical excitatory circuits. A Cre-dependent constitutively-active *Mek1^{S217/222Q}* (*caMEK1*) overexpressing line was crossed with *Nex:Cre* (*caMEK1^(Nex)*) and *Emx1:Cre* (*caMEK1^(Emx1)*) mice to induce gain-of-function ERK/MAPK signaling (Krenz et al. 2008). Immunolabeling for MEK1 confirmed overexpression of the *caMEK1* allele in the *caMEK1^(Nex)* cortex (Figure 10). In contrast to the loss-of-function mutants, *caMEK1^(Nex)* mice are viable and able to breed but are reduced in weight. Adult male control mice weighed 41.01 ± 1.17 g while mutants were 27.68 ± 0.67 g (mean \pm SEM, n=14 controls, 11 mutants). *CaMEK1^(Emx1)* are viable and grossly normal, but exhibit lethality between 6 and 10 weeks of age.

We first asked whether ERK/MAPK hyperactivation led to defects in lamination, particularly in layer 5. Ctip2 labeling of mature sensorimotor cortices showed no overt defects in the specification or number of layer 5 neurons in *caMEK1^(Nex)* mice (Figure 11 A-C). Based on our previous results, we hypothesized that hyperactivation of ERK/MAPK would lead to enhanced corticospinal axon growth into the spinal cord. *In vivo* Dil injections of P0.5 motor cortices were performed to assess the extent and pattern of layer 5 subcortical axon outgrowth. Innervation of the thalamus and medulla appeared normal in P3.5 gain of function mutants (Data not shown). Surprisingly, we detected a marked decrease in the initial extension of Dil labeled corticospinal afferents into the spinal cord in P3-4 *caMEK1^(Nex)* mutants (Figure 12 A-B). Further, genetic labeling of corticospinal projections revealed a significantly diminished CST size in the spinal cord dorsal funiculus of both

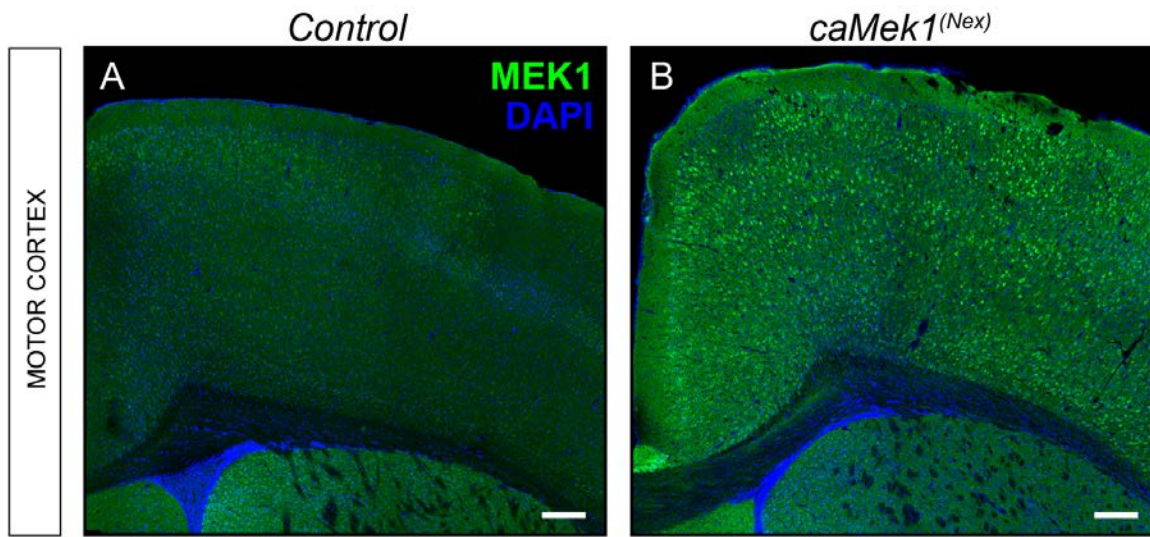
caMEK1^(Emx1) and *caMEK1^(Nex)* mutants (Data not shown). These data show that enhanced ERK/MAPK signaling results in a decrease in the elongation of corticospinal axons into the spinal cord that persists into adulthood.

We tested whether the final pattern of axonal elongation and arborization was altered in *caMEK1^(Nex)* mutants using a Cre-dependent, *tdTomato*-expressing viral vector (AAV5-CAG-FLEX-tdTomato). Following unilateral injection of AAV into primary motor cortex at P1, the extent of axonal labeling was assessed in the white matter tract and grey matter in hindbrain (Figure 13, A-F) and spinal cord (Figure 14, G-J) sections. To determine the amount of axonal elongation that occurred between the hindbrain and the spinal cord, high resolution confocal imaging and measurement of axonal RFP labeling in the white matter of the hindbrain corticobulbar tract (CBT) (Figure 13, C-D) and cervical spinal cord CST (Figure 14, I-J) was performed. We then calculated the amount of RFP labeling in the spinal cord white matter tract relative to the amount of labeling in the hindbrain white matter tract within individual mice to provide a measure of axonal elongation. While control mice showed little reduction in the extent of labeling in the spinal cord white matter tract relative to the hindbrain, *caMEK1^(Nex)* mutant mice exhibited a significant $60.14 \pm 8.3\%$ reduction in labeling in the spinal cord CST relative to the hindbrain (Figure 14, M). These findings provide further support for a substantial and persistent decrease in the elongation of corticospinal axons following hyperactivation of ERK/MAPK.

In striking contrast to the decreased axonal elongation into the spinal cord, we noted a significant increase in the density of axonal labeling in the hindbrain grey matter of *caMEK1^(Nex)* mutants (Figure 13, A-B, E-F). The hindbrain reticular nucleus is known to receive input from the primary motor cortex (Esposito et al. 2014). The ratio of axonal labeling in the hindbrain grey matter relative to labeling in the

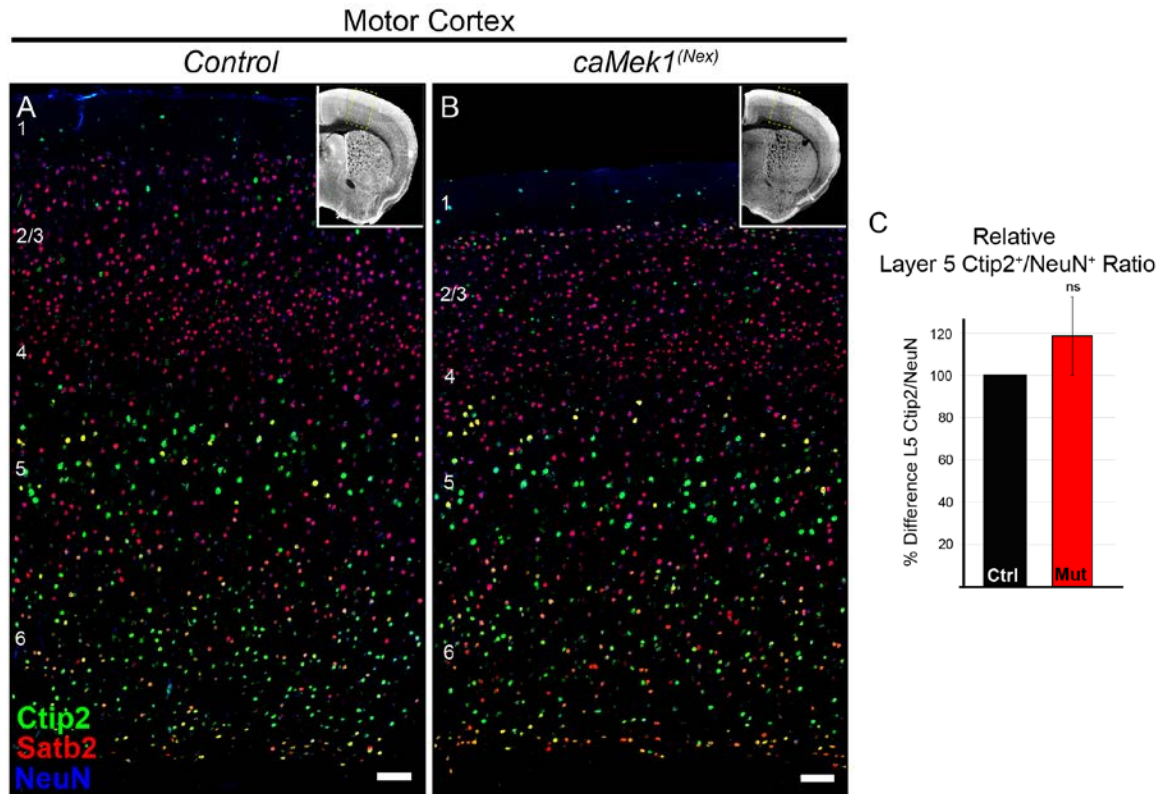
hindbrain white matter (CBT) provided quantitative evidence of enhanced axonal arborization in the *caMEK1^(Nex)* mutants (Figure 14, N). We also tested whether increased arborization could be detected in the spinal cord. The absolute level of axonal labeling density in the spinal cord grey matter was reduced in mutant mice (Figure 14, I and K, J and L). However, a comparison of the ratio of axonal labeling in the spinal cord grey matter relative to axonal labeling in the spinal cord white matter tract suggests that CST axon arborization is increased per axon (Figure 14, N). A similar result was also observed in the spinal cord of *showncaMEK1^(Emx1) Ai3* mutants (Data not shown). In sum, our findings show that ERK/MAPK hyperactivation reduces the number of axons that extend longitudinally down the spinal cord, but the extent of arborizing axonal outgrowth into the hindbrain and spinal cord grey matter is enhanced.

Figure 10.



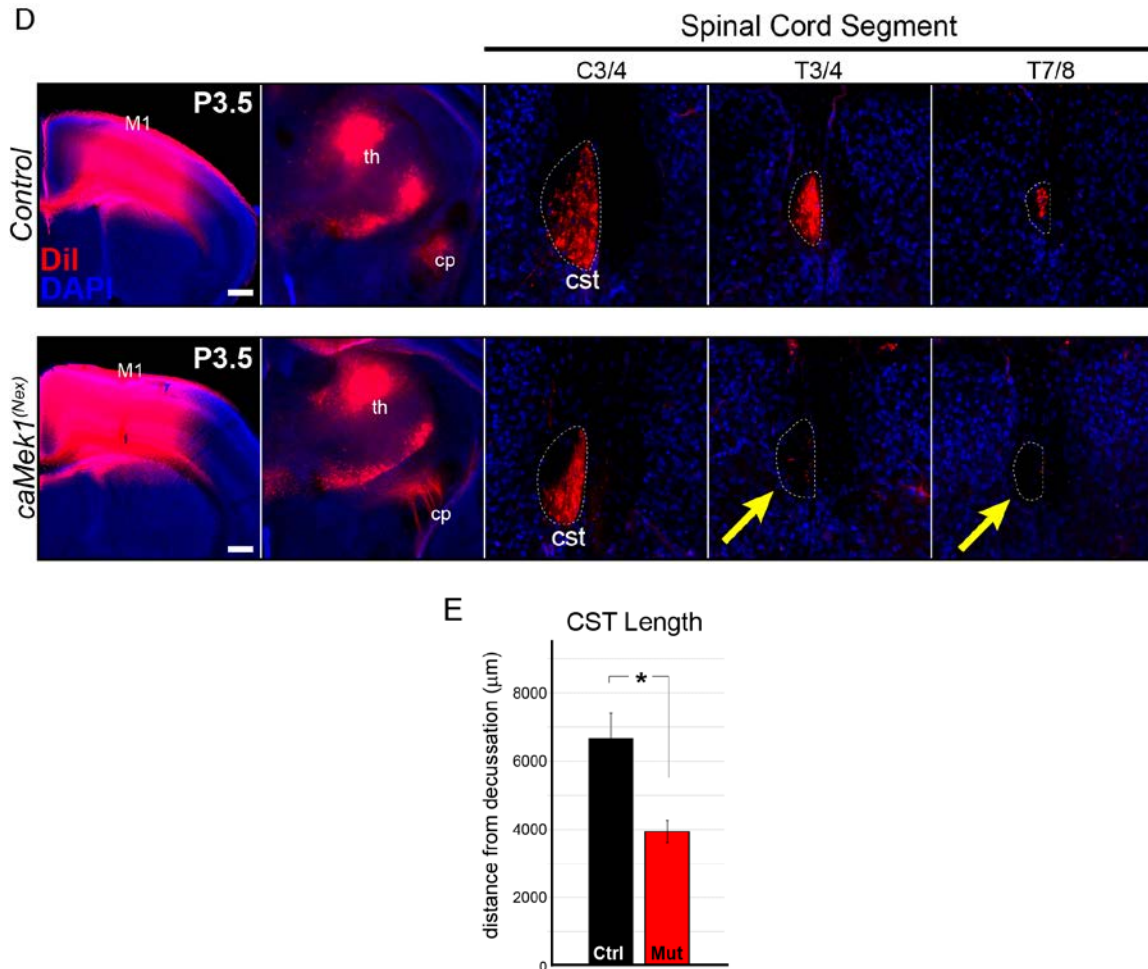
Mouse model for excitatory neuron specific gain-of-ERK/MAPK signaling in the cortex. Representative confocal images of forebrain sections from controls (A) and *caMEK1*^(Nex) mutants (B) demonstrate that the expression of MEK1 is substantially higher in excitatory neurons across all layers of the cortex, but not in the striatum (n=4, scale bar = 100 μ m).

Figure 11.



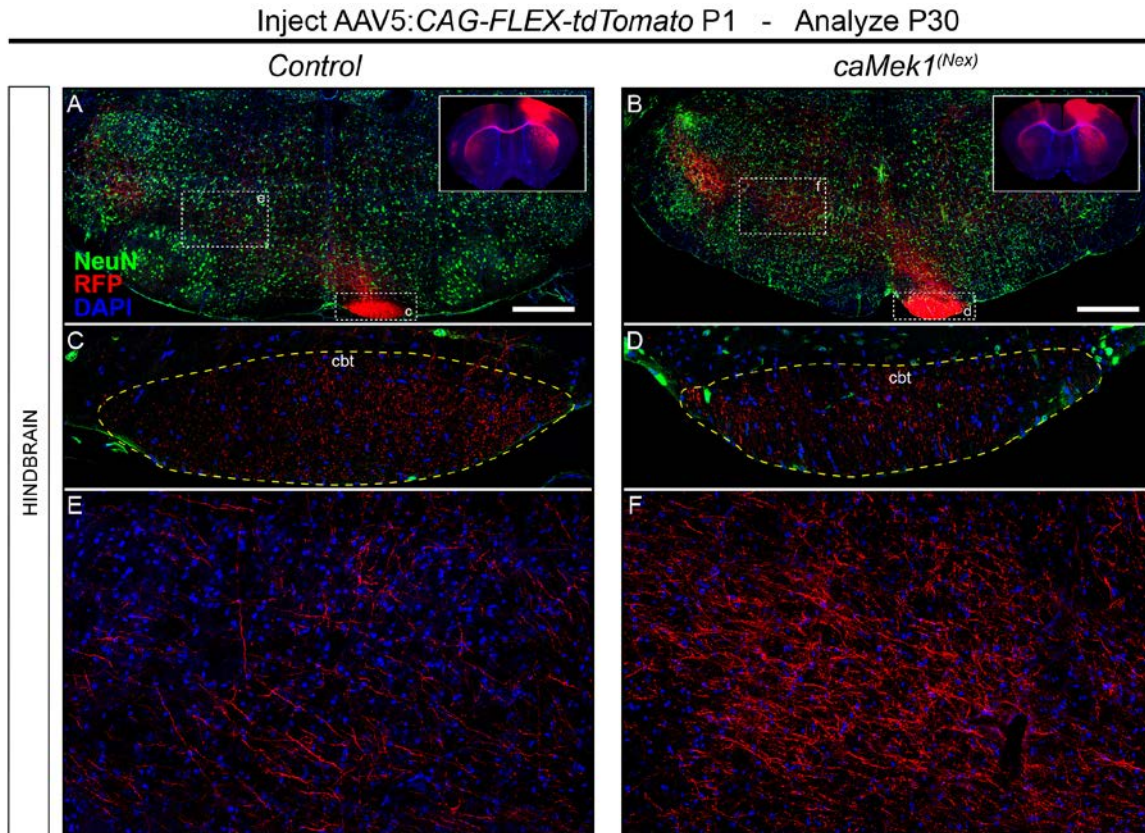
No overt defects in the specification or number of layer 5 neurons in *caMEK1^(Nex)* mice detected. Representative confocal images of sensory cortices show that the expression and distribution of the callosal projection neuron marker, *Satb2*, and subcerebral projection neuron marker, *Ctip2*, in *caMEK1^(Nex)* forebrains (B) appears normal when compared to littermate controls (A) (n=4, scale bar=100 μ m). The relative proportion of *Ctip2⁺* layer 5 neurons as a percentage of *NeuN⁺* neurons within a radial unit did not show a significant difference between adult mutant and control motor cortices (C) (n=3, mean \pm SEM, p=0.2).

Figure 12.



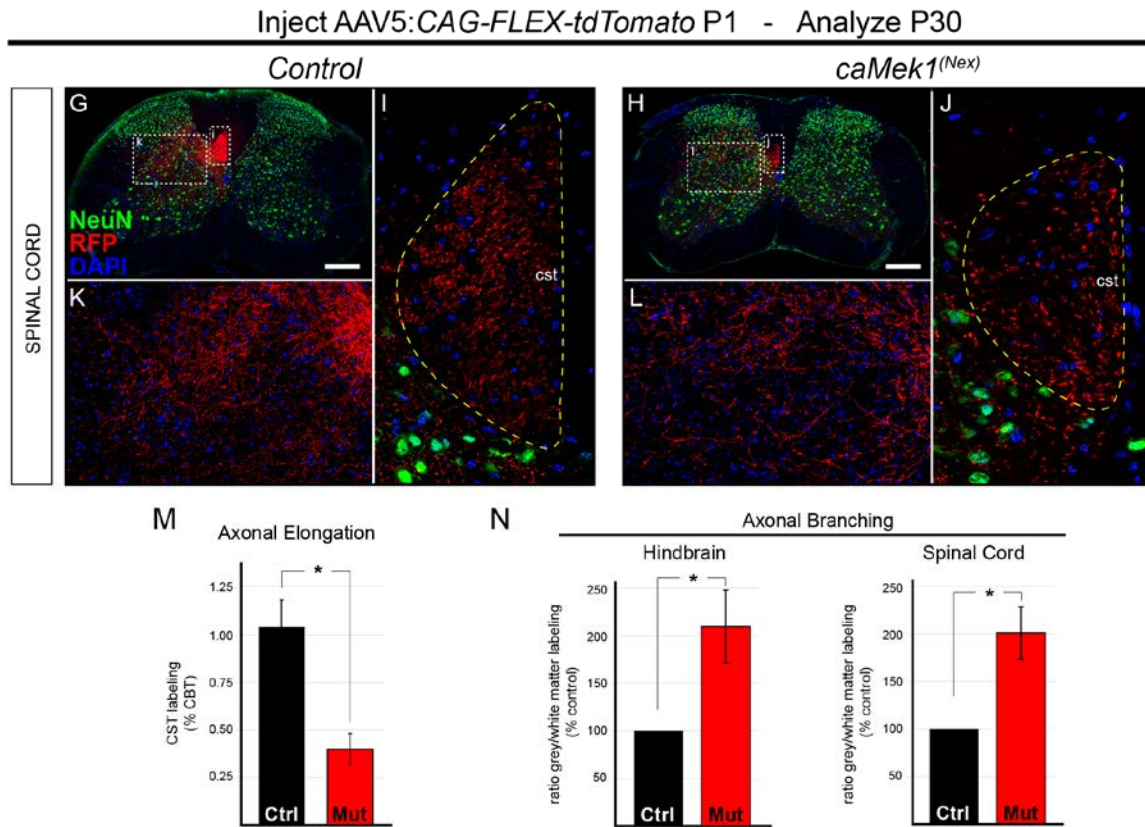
Gain of function ERK/MAPK signaling in *caMEK1^(Nex)* mice decreases corticospinal extension into the spinal cord. In vivo DiI injections into P0 neonates were performed to label corticospinal axons during initial stages of elongation into the spinal cord (D). Analysis of DiI labeling in the spinal cord dorsal funiculus at P3 revealed a significant decrease in the extent of axonal elongation in mutant spinal cords relative to controls (E) ($n=3$, mean \pm SEM, * $p = 0.033$, scale bar = 100 μm).

Figure 13.



Hyperactivation of ERK/MAPK enhances axonal branching in the hindbrain and spinal cord. AAV5-FLEX-tdTomato injections into control (*Nex:Cre*) and *caMEK1^(Nex)* motor cortices at P1 (inset in A-B) results in labeling of subcerebral axon projections in P30 hindbrains (A-F). The extent of axonal branching was measured by comparing the amount of axonal labeling in the hindbrain (A-B, zoom in E-F), to the amount of axonal labeling in the corresponding white matter tract, the CBT (C-D), respectively. We observed a significant increase in the relative ratio of grey/white matter labeling in *caMEK1^(Nex)* mutant hindbrains (n=4, mean \pm SEM, * p < 0.05) when compared to controls (Figure 10b, N).

Figure 14.



Hyperactivation of ERK/MAPK enhances axonal branching in the hindbrain and spinal cord. AAV5-FLEX-tdTomato injections into control (*Nex:Cre*) and *caMEK1^(Nex)* motor cortices at P1 (inset in Figure 10a, A-B) spinal cords (G-L). To measure axonal elongation from the hindbrain to spinal cord, high resolution confocal images of the extent of axonal labeling in sections of the hindbrain corticobulbar tract (cbt, C-D) and brachial spinal cord corticospinal tract (cst, I-J) were collected and compared. The ratio of corticospinal to corticobulbar tract axonal labeling was significantly decreased in *caMEK1^(Nex)* mutants (M), providing further evidence for a reduction in corticospinal axon elongation at P30 (n=3, mean \pm SEM, * p < 0.01, scale bar = 500 μ m).

The extent of axonal branching was measured by comparing the amount of axonal labeling in the spinal cord grey matter (zoom in K-L), to the amount of axonal labeling in the corresponding white matter tract, CST (I-J). We observed a significant increase in the relative ratio of grey/white matter labeling in *caMEK1^(Nex)* mutant spinal cords (n=3, mean \pm SEM, * p < 0.05) when compared to controls (N).

Discussion

The pathogenesis of neurological deficits in neurodevelopmental syndromes associated with altered ERK/MAPK signaling is poorly understood, due to the lack of knowledge regarding cell-type specific effects of loss and gain of function through the ERK/MAPK pathway. Here, we have identified a striking dependence on levels of ERK/MAPK signaling for the development of large Ctip2⁺ neurons in layer 5. Both high and low levels of ERK/MAPK signaling disrupted corticospinal axon projections. Interestingly, ERK/MAPK signaling does not appear to be a key regulator of projections for all excitatory neuron subtypes as axons of callosally projecting layer 2/3 neurons extend and target normally in the absence of ERK/MAPK signaling. In contrast to the neuronal subtype-specific effects on axonal outgrowth, the expression of plasticity associated proteins and neuronal intrinsic excitability were dependent on ERK/MAPK signaling in multiple cortical layers.

Specific regulation of layer 5 CST neuron morphology

In vitro analyses have suggested that ERK/MAPK signaling acts as an important regulator of cortical neuron dendritic and axonal morphogenesis (Dijkhuizen and Ghosh 2005; Kumar et al. 2005; Wu et al. 2005). However, our *in vivo* data reveal a remarkably specific requirement for the ERK/MAPK pathway in the morphological development of layer 5 long range projection neurons. ERK/MAPK signaling is dispensable for the early phases of CST neuronal differentiation, axon growth all the way to the medulla, and even responsiveness to midline guidance cues. However, a drastic delay in corticospinal axon growth was observed in *Mek1/2* mutants between P2-4 when CST axons in control mice start to invade the spinal cord. By P14 in controls, CST axons have reached the lumbar spinal cord. In P14 mutant mice, only a few corticospinal axons were present in the cervical spinal cord

and no axons reached lumbar segments.

Trophic cues linked to ERK/MAPK activation, specifically, BDNF, IGF1, IGF2, GDNF, and pleiotrophin, have been shown to regulate developing corticospinal neuron growth (Giehl et al. 1998; Ozdinler and Macklis 2006; Dugas et al. 2008; Ueno et al. 2013). IGF1 has been described as a particularly potent growth factor for CST development both *in vitro* and *in vivo* (Ozdinler and Macklis 2006). IGF1 protein levels are higher in the spinal cord than the brain in the early postnatal stage (Rotwein et al. 1988) and we identified a focal pattern of IGF1 protein expression in the ventral medulla near the location where developing corticospinal axons enter the cervical spinal cord. However, we quite surprisingly found that deletion of IGF1R in long-range projection neurons did not lead to the predicted failure of CST development. Our results suggest that CST axon growth in the spinal cord may be orchestrated by multiple growth factors or via non-neuronal actions of IGF1. For example, vascular endothelial cells also express IGF1R and endothelial cell-derived trophic cues are potent regulators of corticospinal neuron survival and outgrowth *in vitro* (Dugas et al. 2008). Overall our data support the view that multiple cues converge upon ERK/MAPK to regulate transcriptional and cell biological processes required for extension of long axons.

Following the delayed entry of axons into the spinal cord in *Mek1/2* mutants, we detected layer 5 neurons undergoing apoptosis in a restricted time frame during the first postnatal week. Counts revealed loss of roughly half of the *Ctip2*-expressing layer 5 neurons, which reflects a substantial proportion of the CST population. The reduced number of CST neurons in ERK/MAPK mutants is reminiscent of the loss of CST neurons after lesions to developing corticospinal projections in the neonatal period (Tolbert and Der 1987; Merline and Kalil 1990). Loss of trophic support from the spinal cord could plausibly account for these findings; an effect that might be

exacerbated by known consequences of ERK/MAPK disruption on retrograde transport of growth factor signaling components including signaling endosomes (Mitchell et al. 2012). We cannot completely exclude that the reduced number of Ctip2⁺ neurons in layer 5 results, in part, from conversion into an alternative neuronal type. For example, loss of *Fezf2* results in conversion of corticospinal neurons into a callosal fate (B. Chen et al. 2005; J.-G. Chen et al. 2005; Molyneaux et al. 2007). Our assessment of Satb2⁺/Ctip2⁻ layer 5 neurons did not reveal a coincident increase in the number of presumed callosally fated layer 5 neurons in *Mek1/2^{CKO(Nex)}* mice. Interestingly we did not find similar layer 5 apoptosis occurring in conditional IGF1R mutants, placing our results at odds with a recent study suggesting that microglia-derived IGF1 is required for the survival of layer 5 long range projection neurons (Ueno et al. 2013). Whatever the mechanism, our data show that layer 5 corticospinal neurons are remarkably vulnerable to loss of ERK/MAPK signaling during the neonatal period and our results may be relevant to motor system dysfunction in RASopathy patients and layer 5 disorganization observed in ASDs.

Perhaps surprisingly, rostro caudal corticospinal axon extension was also highly diminished in the setting of enhanced ERK/MAPK signaling. At every stage examined from P3 onward, the number of CST axons in the dorsal funiculus in response to gain of ERK/MAPK signaling was reduced. A distinct feature of axon growth in gain of function mutants was enhanced axonal branching in the hindbrain. Normally, over the first two postnatal weeks, ERK/MAPK activation is upregulated, coincident with increased BDNF/TrkB expression (Maisonpierre et al. 1990; Timmusk et al. 1994). BDNF/TrkB signaling has been shown to promote corticospinal axon branching *in vitro* (Ozdinler and Macklis 2006). We suggest that hyperactivation of ERK/MAPK triggers mechanisms normally associated with BDNF induced corticospinal

branching, possibly resulting in premature closure of the period of rostral caudal axon elongation. Reduced axon extension of layer 5 projection neurons in the setting of ERK/MAPK hyperactivation would likely have major implications for cortical circuit development in the human brain where distances are vastly longer than in rodents.

Global regulation of neuronal excitability

In addition to effects on axonal connectivity, dysregulated ERK/MAPK signaling is likely to disrupt glutamatergic signaling (Di Cristo et al. 2001; Thomas and Huganir 2004). Studies have demonstrated that mature RASopathy mouse models exhibit reduced hippocampal LTP and spatial memory impairment (Costa et al. 2002; Cui et al. 2008; Lee et al. 2014). Our findings provide genetic confirmation for prior work using pharmacological inhibitors demonstrating ERK/MAPK regulation of plasticity-associated genes induced by excitatory activity, including *Arc*, *Egr2*, and *Fos* (Waltereit et al. 2001; Majdan and Shatz 2006; Tropea et al. 2006; Panja et al. 2009). Further, we establish a link between ERK/MAPK and expression of *Npas4*, *Nrn1/Cpg16*, and *Nptx2/Narp* *in vivo* (Coba et al. 2008). Unexpectedly, hyper-activation of ERK/MAPK signaling with the *caMEK1^{S217/221Q}* mutation had little effect on the expression of these same plasticity associated genes. These findings are in line with a past study of hippocampal gene expression in a different *caMEK1* mouse mutant (Nateri et al. 2007). The severity of effects on expression of plasticity associated genes is likely correlated with the magnitude of ERK/MAPK hypo- or hyper-activity in response to specific mutations.

Since ERK/MAPK dependent changes in plasticity associated gene expression were widespread, we asked whether ERK/MAPK has general or layer-specific effects on developing projection neuron excitability and synaptic transmission. Our work demonstrates that complete loss of ERK/MAPK signaling leads to increased intrinsic

excitability of both layer 2/3 and layer 5 pyramidal neurons. Further, we show that *Mek1/2* deleted layer 2/3 neurons exhibited increased excitatory synaptic strength. We conclude that ERK/MAPK signaling contributes to excitatory/inhibitory balance during the early postnatal period by reducing the excitability of cortical excitatory neurons. Changes in excitatory drive in a subset of layer 2/3 neurons have been shown to trigger a compensatory homeostatic increase in inhibitory drive, thus maintaining a stable synaptic excitatory/inhibitory ratio (Xue et al. 2014).

Remarkably, layer 2/3 pyramidal neurons lacking *Mek1/2* exhibit reduced inhibitory synaptic input in the absence of a fully compensatory change in excitation. Loss of ERK/MAPK activity in cortical pyramidal neurons may disrupt the homeostatic balance between synaptic excitation and inhibition, a mechanism hypothesized to form the neurological basis of autism (Rubenstein and Merzenich 2003). ERK/MAPK may also regulate the release of BDNF from excitatory neurons, a well-known regulator of inhibitory synapse formation (Huang et al. 1999; Kohara et al. 2007; Porcher et al. 2011).

During postnatal cortical pyramidal neuron development, input resistance decreases and the frequency of GABAergic and amplitude of glutamatergic spontaneous neurotransmission increase (Desai et al. 2002; Morales et al. 2002). Our findings are consistent with pyramidal neurons lacking *Mek1/2* failing to undergo these developmental alterations and further suggest that loss of ERK/MAPK signaling may arrest normal physiological development. Importantly, the alterations in action potential threshold in neurons lacking *Mek1/2* may secondarily result from increased sodium channel density due to the smaller neuronal size or the observed increase in membrane resistance, which may also influence quantal amplitude measurements. Our observations that disruption of ERK/MAPK signaling alters excitatory/inhibitory balance and the expression of select plasticity associated genes, coupled with known

effects on Hebbian forms of synaptic plasticity (Thomas and Huganir 2004), suggest that alterations in ERK/MAPK signaling are likely to dramatically disrupt network activity and cortical re-wiring.

Circuit abnormalities in RASopathies

Hypotonia, muscle weakness, and delay in motor milestones are often observed in RASopathy patients (Dileone et al. 2010; Mejias et al. 2011; Tidyman et al. 2011; Oberman et al. 2012; Stevenson et al. 2012). Although some of these symptoms may be due to alterations in muscle development, we have shown here that upper motor neuron and corticospinal tract development are especially sensitive to both gain and loss of ERK/MAPK activity. Thus, deficits in motor function or motor learning in Ras/MAPK Syndromes may be explained, in part, by altered corticospinal connectivity. Importantly, our data point to distinct effects in gain vs loss of function mutants. Our results therefore argue for a mutation-specific approach to correct neurological dysfunction within the RASopathy spectrum. Aberrant long-range circuit development has also been proposed as a defining feature of ASD pathogenesis and that layer 5 may be a focal point (Stoner et al. 2014; Willsey et al. 2013). An interesting possibility is that altered activation of ERK/MAPK at early developmental stages in response to certain ASD linked mutations (*Fmr1*, *Mecp2*, *Tsc1/2*) and environmental insults (hypoxia, inflammation, etc.) might contribute to select cortical circuit abnormalities, especially for neurons projecting over long distances.

Acknowledgements

We are grateful to E. Anton, F. Polleux, and the members of the Snider and Philpot labs for many helpful discussions and providing transgenic mice. We thank Vladimir Ghukasyan, Colin Parker, Becca Reinking-Herd, Sam Lusk, Anna Krueger, Julia Pringle, Meghan Morgan-Smith, and Cyril Justin Dizon for technical assistance and Ping Ye (UNC-Chapel Hill) for generously sharing the IGF1R conditional knockout mice.

Contributions

Viral and Dil injections:

George Reed Bjorklund and Lei Xing.

Tissue prep and Immunolabeling:

George Reed Bjorklund, Xiaoyan Li, and Yaohong Wu.

Image analysis and quantitation:

George Reed Bjorklund, Lei Xing, and Jason M Newbern

Western Blotting:

George Reed Bjorklund and Lei Xing

Experimental conception and design:

George Reed Bjorklund, Lei Xing, and Jason M Newbern

Drafting or revising the article:

Lei Xing, Rylan S. Larsen, George R. Bjorklund, Xiaoyan Li, Yaohong Wu, Benjamin D. Philpot, William D. Snider, and Jason M. Newbern.

CHAPTER 3
LONG-RANGE AXONAL DEVELOPMENT IN A GAIN-OF-FUNCTION
CAMEK MOUSE MODEL

**Hyperactivation of MEK1 in cortical glutamatergic neurons results
in projection axon deficits and aberrant motor
learning in a layer autonomous manner**

Abstract

Germline mutations within the components of the RAS-RAF-MEK-ERK (RAS/MAPK) pathway form a group of neurodevelopmental disorders collectively known as RASopathies. A large portion of these mutations result in an upregulation of signaling. Here, we used cre-loxp technologies to hyperactivate the RAS/MAPK pathway in cortical glutamatergic neurons to determine developmental effects on long-range axonal projections by inserting a constitutively active MEK1 construct. In hyperactive mutants, cortical glutamatergic neurons displayed an increased level of activated ERK1/2 in axons, but a surprising reduction in the cell body. The expression of RAS/MAPK substrates in the soma important for plasticity, such as ARC, were also reduced in the neurons. We further identified significant deficits in corticocortical and corticostriatal axonal innervation and branching and a significant reduction of corticospinal tract elongation. In addition to the connectivity issues, hyperactivation of RAS/MAPK signaling also led to motor learning acquisition deficits in an accelerating rotarod test and a fine reaching and grasping task. These data suggest that the pathogenesis of cognitive deficits in RASopathies involves changes in the development of neuronal connectivity and the expression of plasticity associated genes at an early stage of cortical formation and subsequent developmental stages.

Introduction

The RAS-RAF-MEK-ERK (RAS/MAPK) signaling pathway plays a crucial role in the development and maintenance of the central nervous system. Extracellular cues in the form of neurotrophins are transmitted through the pathway to activate a variety of transcription factors and influence cellular processes in the cytoplasm (Mebratu and Tesfaigzi 2009). Several cellular processes that rely on the RAS/MAPK pathway include; cellular proliferation and differentiation, cell growth and survival, axon growth and pathfinding, neurite arborization, and dendritic spine formation (Jeanneteau et al., 2010; Kalil and Dent, 2014; Mebratu and Tesfaigzi, 2009; Nowaczyk et al., 2013; Polleux and Snider, 2010). Additionally, RAS/MAPK signaling in the mature brain is essential for activity-dependent plasticity and associative learning and consolidation (Atkins et al., 1998; Thomas and Huganir, 2004; Gómez-Palacio-Schjetnan and Escobar, 2013).

Several germline mutations found in the RAS/MAPK signaling pathway are the source of many well-defined genetic syndromes collectively referred to as RASopathies (Rauen, 2012). Many of these syndromes such as Noonan Syndrome (NS), Legius Syndrome (formally known as NF1-like syndrome), Costello Syndrome (CS), Neurofibromatosis type 1 (NF1), Capillary Malformation-Arteriovenous Malformation (CM_AVM), and Cardio-facio-cutaneous (CFC), result in hyperactivity of the RAS/MAPK signaling pathway (Rauen, 2012). Mutations that lead to downregulation of the RAS/MAPK pathway include subsets of Noonan Syndrome with Multiple Lentigines (formerly referred to as LEOPARD syndrome) (NSML), and CFC syndrome (Nowaczyk et al., 2013; Rauen, 2012). While some of these syndromes such as CS and CFC are quite rare, up to 1:810,000 and 1:380,000 respectively (Allanson and Roberts, 1993; Gripp and Lin, 2012), others, such as NS and NF1, are more prevalent and affect ~1:1000 - 1:2500 and ~1:2500 - 1:3000 individuals

worldwide respectively (Rauen, 2012; Williams et al., 2009). Specific genetic mutations in the individual components of the signaling pathway are found in upstream elements of MAPK3/MAPK1 (ERK1/2) (Rauen, 2012). Additional monogenic neurodevelopmental disorders that ultimately lead to activation of MAPK signaling includes Fragile X syndrome, Tuberous Sclerosis and 16p11.2 deletion syndrome (Subramanian et al., 2015). The result of these syndromic genetic mutations are several neurodevelopmental disorders that include macrocephaly, neurodevelopmental and intellectual disabilities, neurocognitive impairment and delay, motor delay, seizures, learning disabilities and an increasing association with Autism spectrum disorders (ASD) (Axelrad et al., 2011; Jozwiak et al., 2008; Rauen, 2012; Subramanian et al., 2015).

Current evidence indicates widespread abnormal structural changes in the white matter tracts of NF1 patients. Diffusion tensor imaging (DTI) studies in children with NF1, have detected these abnormal structural changes in the corpus callosum and in the brains microstructures (S L Zamboni et al. 2007; Filippi, Watts, Lindsay A.N. Duy, et al. 2013; Aydin et al. 2016). DTI analysis of select brain regions in mature NF1 patients, indicate basic and diffuse changes in cerebral microstructure in the caudate and lentiform nuclei, thalamus, pons, frontal and parietooccipital white matter, and the corpus callosum (S L Zamboni et al. 2007). Functional magnetic resonance imaging (fMRI) and functional connectivity magnetic resonance imaging (fcMRI) studies in subjects with NF1 indicated altered neural activity and network connectivity (Tomson et al. 2015b; Amira F.A. Ibrahim et al. 2017). DTI analysis in mouse models of NF1, revealed significant differences in three main structures of interest, prefrontal cortex, caudate putamen, and the hippocampus. Additionally, widespread cortical and subcortical changes in white matter diffusivity patterns with no major disruption or disorganization of axons is also reported in the

DTI study of this mouse model (Fame et al. 2011). These imaging techniques have provided a wide view of global differences in major white and gray matter areas. However, very little is known of the specific effects of RAS/MAPK signaling misregulation on system wide connectivity and long-range axonal circuit formation during and after development. Furthermore, DTI imaging gives a broad view of structural anomalies in relation to white matter tracts (oligodendrocytes/myelination) but does not directly address any underlying axonal contribution to these anomalies. This is especially true of cell and circuit specific effects during and after development.

Previously, we reported a critical requirement for RAS/MAPK signaling in loss- and gain-of-function as it applies specifically to cortical pyramidal neurons (Xing et al., 2016). Deletion of *Map2k1/2* (*Mek1/2*) in cortical glutamatergic neurons resulted in the absence of large CTIP2⁺ neurons in cortical layer 5 and the impairment of corticospinal tract (CST) axonal extension in the dorsal funiculus of the cervical and lumbar spinal cord (Xing et al., 2016). Up-regulation of ERK/MAPK signaling in cortical glutamatergic neurons also decreased CST axonal elongation but markedly increased axonal branching in the gray matter of the spinal cord and the gray matter of the hind brain (Xing et al., 2016). Nonetheless, further research is needed to assess aberrant RAS/MAPK signaling on cortical glutamatergic neuronal projections in the forebrain and sub-cortical projections, cortical layer specific effects, activated ERK1/2 levels and localization patterns, or behavior and learning phenotypes.

To address these issues, we created mouse models with a constitutively active *Mek1* (*caMek1*) gene construct driven by CRE to hyperactivate MEK1 in cortical glutamatergic neurons. Our connectivity and innervation analysis focused on all cortical layers of the primary motor cortex to address the learning disabilities associated with motor function and motor delay. Furthermore, we were able to

analyze subcortical projections to lower motor and CST extension that could further lead to the neurodevelopmental phenotypes seen in human RASopathy patients.

We first analyzed the developmental and mature levels of activated ERK1/2 (P-ERK1/2) and localization pattern. MEK1 hyperactivation led to a succinct localization of P-ERK1/2 in the axonal projections of post-mitotic glutamatergic neurons in embryonic tissue that persisted in adult mice. Analysis of contralateral cortical projections and cortico-striatal projections revealed a significant decrease in axonal innervation and branching. Behavioral testing in the open-field, rotarod, and reaching and grasping task revealed no overt motor control deficiencies but did show a significant impairment in motor control learning. Analysis of activity dependent gene expression showed a surprisingly low level of expression of gene products that are highly dependent on the activation the RAS/MAPK pathway. The use of these conditional genetic tools allowed the analysis of cell specific effects and contributions to the pathologies reported in RASopathy patients.

Materials and Methods

Transgenic Mice

All animal experiments were performed in accordance with established procedures approved by the Institutional Animal Care and Use Committee of Arizona State University and NIH guidelines for the use and care of laboratory animals. Mice used in this work were of a mixed genetic background and housed in standard conditions. The mice were kept on a 12-hour light/dark cycle with food and water provided ad libitum. Each experiment was replicated a minimum of three times using littermates or mice from independent litters. No detectable effects on the phenotypes described in this manuscript were observed from Cre expression alone. Therefore, Cre-expressing or Cre-negative mice were used as controls. *Map2k1*^{s217/222} mice were furnished by Dr. Maïke Krenz and Dr. Jeffrey Robbins (Krenz et al., 2008). *NeuroD6-Cre* mice were provided by Dr. Klaus Nave and Dr. Sandra Goebbels (Goebbels et al., 2006). *Rbp4:Cre* mice were purchased from the Mutant Mouse Resource & Research Centers (RRID:MMRRC_036400-UCD).

Tissue Preparation

Transcardial perfusions were performed on mice using a 4% paraformaldehyde/PBS solution with dissected brains being post-fixed in the same solution overnight at 4°C. Dissected brains were then serially incubated in 15% and 30% sucrose/PBS solutions prior to embedding in Tissue-Tek O.C.T. (Tissue-Tek 4583) and freezing. Cryostat sectioning was performed with sections being collected on Fisherbrand Superfrost/Plus slides (Fisher Scientific 12-550-15) and air-dried prior to staining. Alternatively, cryostat sections were collected in well plates with cold PBS for free-floating staining as appropriate. For some experiments, brains were mounted in agarose after post-fixation in preparation for vibratome sectioning.

Viral Injections

P1 pups were removed from their home cage as a group and were individually cryo-anesthetized on ice for 4-6 minutes. Viral injections were then performed immediately with 50-80nl of solution using a 32-gauge beveled needle fitted to a Hamilton 5µl neuros syringe mounted on a stereotaxic arm. After injections, pups were placed on a 37°C heated surface for recovery and returned to their home cage as a group. Adeno Associated Viral vectors, RAAV9/AAV-Flex-tdTomato and RAAV8/CAG-Flex-tdTomato were purchased from the UNC Viral Vector Core and used for all viral tracing experiments.

Behavioral Assays

A single-pellet reaching and grasping task test was performed using both male and female *Nex:Cre/caMek1* mice and male *RBP4:Cre/caMek1* mice. Mice were mildly food restricted throughout training to maintain at least 90% of their baseline weight which amounted to free feeding between 2 and 6 hours daily. Sucrose pellets (TestDiet 1811555) were used for this test and the mice were acclimated to the pellets in their home cages. After pellet acclimation, mice were then placed in the testing chamber, an acrylic chamber 15cm X 10cm X 20cm, with pellets either singly or in pairs depending on their housing for further acclimation. After acclimation, forelimb dominance was determined by placing a single pellet on the food platform (10cm high) outside a single slit (5cm wide) in one end of the test chamber. Once a mouse has conducted at least 20 reaching attempts within 20 mins with at least 70% of those reaches made with one hand, that mouse was moved on to testing. Testing consisted of placing a single pellet on the food platform in front of the slit, right or left, corresponding with the preferred paw. Testing was performed for 10 minutes

daily for 5 days. Scoring was performed as follows; Success: if the mouse reached with its preferred paw, retrieved the pellet, and fed the pellet into its mouth. Drop: If the mouse grasped the pellet but drops it before reaching its mouth. Fail: If the mouse reached for the pellet but failed to grasp it or knocked it out of position. Mice were scored on the rate (metric/attempts) for each of these metrics.

Open field testing was performed in an open top opaque plexiglass box measuring 38cm X 38cm X 30cm. The area within the box is illuminated by a single 40-watt spotlight approximately 2 meters overhead and centered within the area. Recording of mouse movements is done using a Microsoft LifeCam or Logitech HD Webcam and VirtualDub video capture software. Open field quantitation was performed using the MouseMove (Samson et al. 2015) plugin for ImageJ (Schindelin et al. 2012).

Rotarod analysis for the *NexCre/caMek1* mice was performed on a Ugo Basile (Stoelting Co.) accelerating rotarod. Animals were given three trials in the first test session, with 45 seconds between each trial. Two additional trials (Test 2) were given 48 hours later. RPMs (revolutions per minute) increased from 3 to 30 RPMS over the 5-minute trial period. Measures were taken for latency to fall from the top of the rotating barrel. Nine to ten weeks following the first two tests, a subset of mice were given an additional two trials (Test 3). In the last test (Test 4), mice were given 2 trials using a reversed-rotation procedure, in which the direction of the barrel rotation was periodically altered.

In the elevated plus maze task, mice were given one five-minute trial on the plus maze which had two walled arms (the closed arms, 20 cm in height) and two open arms. The maze was elevated 50 cm from the floor, and the arms were 30 cm long. Animals were placed on the center section (8 cm x 8 cm) and allowed to freely

explore the maze. Measures were taken of time on, and number of entries into, the open arms of the maze.

The Morris water maze task consisted of a large circular pool (diameter = 122 cm) partially filled with water (45 cm deep, 24-26°C), located in a room with numerous visual cues. The procedure involved three different phases: a visual cue test with a visible platform, acquisition in the hidden platform task, and a test for reversal learning. Only mice that performed well in the visual cue test were further evaluated in the acquisition and reversal tests. Three to four days following the visible platform task, mice were tested for their ability to find a submerged, hidden escape platform (diameter = 12 cm). Each animal was given 4 trials per day, with 1 minute per trial, to swim to the hidden platform. Mice were tested until the group reached learning criterion, with a maximum of 9 days of testing. When criterion was reached, mice were given a one-minute probe trial in the pool with the platform removed. Selective quadrant search was evaluated by measuring the percent of time spent in the target (platform quadrant) and opposite quadrants. Following the acquisition phase, mice were tested for reversal learning, using the same procedure as described above except the hidden platform was re-located to the opposite quadrant in the pool. As before, measures were taken of swim distance to find the platform. Once the criterion for learning was met, the platform was removed from the pool, and the group was given a probe trial to evaluate reversal learning as previously described.

Immunohistochemistry

Tissue sections were rinsed with PBS/0.1% Triton X-100 (PBST) and blocked with 5% normal donkey serum in PBST at room temperature for ~1 hour. Primary antibodies were diluted in PBST/5%NDS and incubated overnight at 4°C with gentle

shaking. Primary antibodies used were; rabbit anti-MEK1 (Abcam ab32091), rabbit anti-phosph-p44/42 MAPK (ERK1/2) (Thr202/Tyr204) (Cell Signalling 4370), rabbit anti-ERK2 (Abcam ab32081), rabbit anti-ARC (Synaptic Systems 156 003), mouse anti- β 3 Tubulin (TUBB3) (Biolegend 801202), rabbit anti-RFP (Rockland 600-901-379), chicken anti-RFP (Rockland 600-401-379), mouse anti-neun (Millipore Sigma MAB377), and DAPI (Sigma Aldrich 10236276001). After rinsing in PBST 3X, secondary antibodies diluted in PBST/5%NDS were added and incubated overnight at 4°C with gentle shaking. Secondary antibodies included Alexa Fluor 488, 546 or 568, and 647 conjugated anti-rabbit, anti-mouse, or anti-goat IgG (Invitrogen). Imaging was performed using a Zeiss LSM 800 laser scanning confocal microscope (LSCM), or a Leica SP5 LSCM.

Western Blotting

Cortices were collected from mutant and control mice and lysed in a buffer containing 50mM Tris-CL, 150mM NaCl, 0.1%triton x-100, Protease Inhibitor (Sigma-Aldrich P2714), and Phosphatase Inhibitor (Sigma-Aldrich P5726) either by sonication or with a syringe. Lysates were then cleared by centrifugation and total soluble protein concentrations determined by Bradford Assay using a Peirce Protein Assay Kit (Thermo Scientific 23200). Proteins were denatured in equal amounts of 2X Laemmli sample buffer (BioRad 161-0737), separated by SDS-PAGE using either 10% or 4-20% Mini-PROTEAN TGX precast gels (BioRad 456-1035 and 456-8095), then transferred to PVDF membranes (BioRad 162-0177). Membranes were blocked with 5% non-fat dry milk (NFDM) in TBS with 0.5% Tween (TBST) for 1 hour at room temperature followed by overnight incubation at 4°C with primary antibodies in 5% bovine serum albumin. Primary antibodies used were; rabbit anti-MEK1 (Abcam ab32091), rabbit anti-phosph-p44/42 MAPK (ERK1/2) (Thr202/Tyr204) (Cell

Signalling 4370), rabbit anti-ERK2 (Abcam ab32081), rabbit anti-ARC (Synaptic Systems 156 003), rabbit anti-GAPDH (Cell Signalling 2118), goat anti β -Actin (Cell Signaling 8457), and rabbit anti- β actin (Cell Signalling 8457). Secondary antibodies used were anti-rabbit HRP and anti-goat HRP (Jackson Immunoresearch 711-035-152 and 705-035-147). Membranes were then washed in TBST and incubated with HRP-conjugated secondary antibodies in 5% NFDM/PBST for 1 hour at room temperature. Membranes were washed in TBST, developed with Pierce ECL Western Blotting Substrate (Thermo Scientific 32106), and exposed to radiographic film (Thermo Scientific 34089).

Quantification of Western Blots was performed using a high-resolution scanned image of the exposed radiographic film in a grayscale TIFF file format. The file was then transferred to Imagej where a region of interest was created to encompass individual bands for all mutant, control and loading control samples. The mean gray value of each band was then recorded along with a background measurement for each band. All values were inverted (subtracted from 255) and the background values were subtracted from the band values. The net band values were then reported as a ratio of net band value over net loading control value.

Image Analysis and Quantitation

For quantitation of axonal innervation and branching in the cortex and striatum, a radial section of the cortex encompassing all layers within the primary motor cortex was used. A minimum of 4 sections from each mutant and control animal centered about the rostral-caudal area of the injection site was analyzed. The area in μm^2 of this region was measured in Photoshop and the image was then transferred to Imagej. Once in Imagej, pixel intensities were adjusted using the Otsu Auto Threshold component, total pixels counted, and multiplied by the images pixel

size to obtain the total μm^2 of pixels in the ROI. The total μm^2 was then divided by the number of transfected cells that were manually counted in an identical ROI in the ipsilateral (RFP injected) cortical hemisphere to obtain the axonal labeling per transduced cell. Spinal cord arborization was measured in the same manner except the μm^2 of pixels was normalized to the CST to obtain a spinal cord arborization ratio.

The CBT was measured using at least three anatomically matched hind brain sections from each mutant and control animal. The CBT was outlined using the difference of appearance in NEUN or DAPI and the image was transferred to Imagej. A pixel intensity threshold was manually set by an observer blinded to the genotype. The number of labeled pixels was then measured and multiplied by the images pixel size to obtain the μm^2 of pixels in the CBT. The μm^2 of pixels was then normalized to the number of transfected cells in the injection site ROI to obtain the CBT axonal labeling per transduced cell. The CST in the dorsal funiculus was measured in the same manner except the μm^2 of pixels was normalized to the CBT to obtain the CST elongation ratio.

Representative images have been cropped and adjusted for brightness and contrast in Photoshop for presentation. All images used for comparison analysis were collected using the same microscope settings and all adjustments made were done equally between images.

Statistical Analysis

Data analysis was performed using SPSS software (IBM Analytics). Statistical methods used included Student's t-test (unpaired, two-tailed), ANOVA, repeated measures ANOVA, and multivariate ANOVA. F-test results, p-values, and tests used are reported where appropriate.

Results

MEK1 hyperactivation results in increased levels of P-ERK in the axons of cortical excitatory neurons

To evaluate the effects of up-regulation of the RAS/MAPK pathway in cortical excitatory neurons and long-range axonal projections, we generated an ERK/MAPK gain-of-function mouse by crossing a *Map2k1*^{S217/222} (*caMek1*) (Krenz et al., 2008) mouse with a *NeuroD6-Cre* (*NexCre*) (Goebbels et al., 2006) mouse. The resulting mouse line, *NexCre/caMek1*, is designed to express a constitutively active MEK1 construct primarily in cortical glutamatergic neurons. *Nex* promoter activity is detected as early as E11.5 in the telencephalon with prominent levels of CRE recombinase being produced at around E13.5 (Goebbels et al., 2006). Western Blot analysis of cortical lysates from E 14.5 *NexCre/caMek1* embryos confirmed highly elevated levels of MEK1 with a fold change of $+14.99 \pm 2.00$ when compared to controls (Mean \pm SEM, GAPDH normalized, $p=0.002$, $n=5$, Student's t-test) (Figure 15A). Immunohistochemical (IHC) analysis of MEK1 expression in cortical samples of E14.5 embryos confirmed a robust level of MEK1 in cortical glutamatergic neurons in the cortical plate and axonal processes in the intermediate zone (Figures 16A-F) ($n=5$).

Having verified a strong presence of MEK1 in E14.5 embryos, we next examined the *NexCre/caMek1* embryos at E14.5 for activated ERK1/2 (P-ERK1/2). At this time-point in development, layer VI corticothalamic projection neurons (CThPN) and layer V subcerebral projection neurons (SCPN) will have been generated in the cortex along with a portion of layer II/III callosal projection neurons (Greig et al., 2013). Western Blot analysis confirmed significantly elevated levels of P-ERK1/2 with a fold change of $+1.47 \pm 0.20$ over controls (Mean \pm SEM, ERK2 normalized, $p=0.043$, $n=5$, Student's t-test) (Figures 15C-D). ERK2 Western Blotting showed no

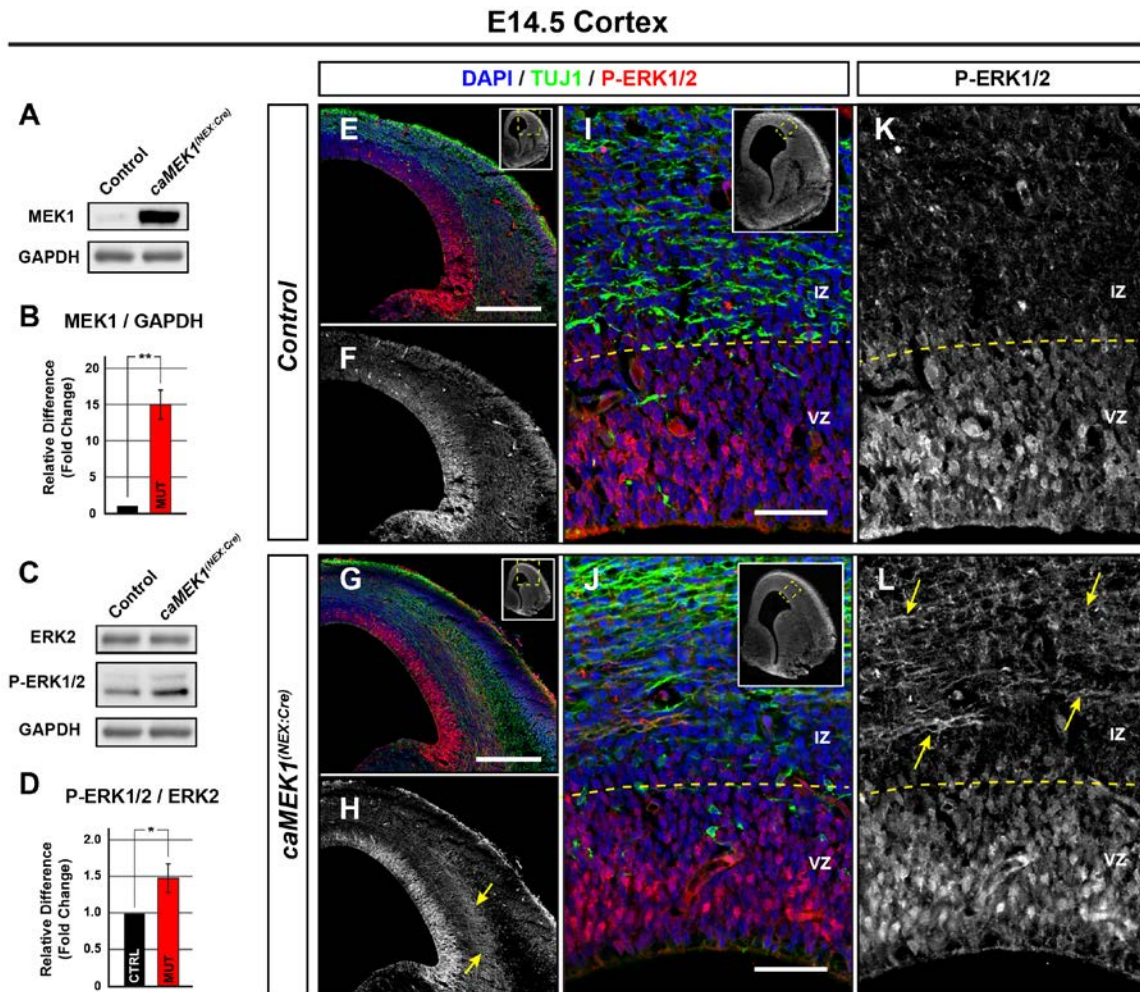
significant difference between the *NexCre/caMek1* and control mice (controls = 1.00 ± 0.00 SEM, mutants = 1.06 ± 0.05 SEM, $p=0.245$, $n=5$) (Figure 15C).

Histochemical analysis revealed a pattern of P-ERK1/2 localized to the intermediate zone, a region in the embryonic cortex that contains the axonal processes of cortical glutamatergic neurons ($n=5$) (Figures 15E-L).

Adult *NexCre/caMek1* cortical lysate Western Blotting revealed a significant fold change of $+1.61 \pm 0.20$ of MEK1 detection over controls (Mean \pm SEM, GAPDH normalized, $p=0.041$, $n=3$, Student's t-test) (Figures 17A-B). IHC analysis confirmed the specificity and increased levels of MEK1 expression in *NexCre/caMek1* cortical glutamatergic neurons (Figures 17E-H) ($n=3$). No significant difference was found in P-ERK1/2 levels between adult *NexCre/caMek1* and control mice (controls = 1.00 ± 0.00 SEM, mutants = 0.95 ± 0.21 SEM, $p=0.832$, $n=3$, Student's t-test) when normalized to ERK2 levels (controls = 1.00 ± 0.00 SEM, mutants = 1.07 ± 0.08 SEM, β -actin normalized, $p=0.389$, $n=3$, Student's t-test) (Figures 17C-D). IHC analysis of the adult *NexCre/caMek1* however revealed distinctly lower levels of P-ERK1/2 in the neuronal cell bodies through all layers of the cortex when compared to controls ($n=3$) (Figures 17I-L and 18Q, R). Importantly, white matter tracts in the adults showed the same P-ERK1/2 localization that was seen in the E14.5 samples ($n=3$) (Figures 17I-L and 2b, M-P). High resolution confocal imaging of white matter tracts showed a pattern of P-ERK1/2 co-localizing with the neuron specific class III β -tubulin, TUJ1 ($n=3$) (Figures 18M-P).

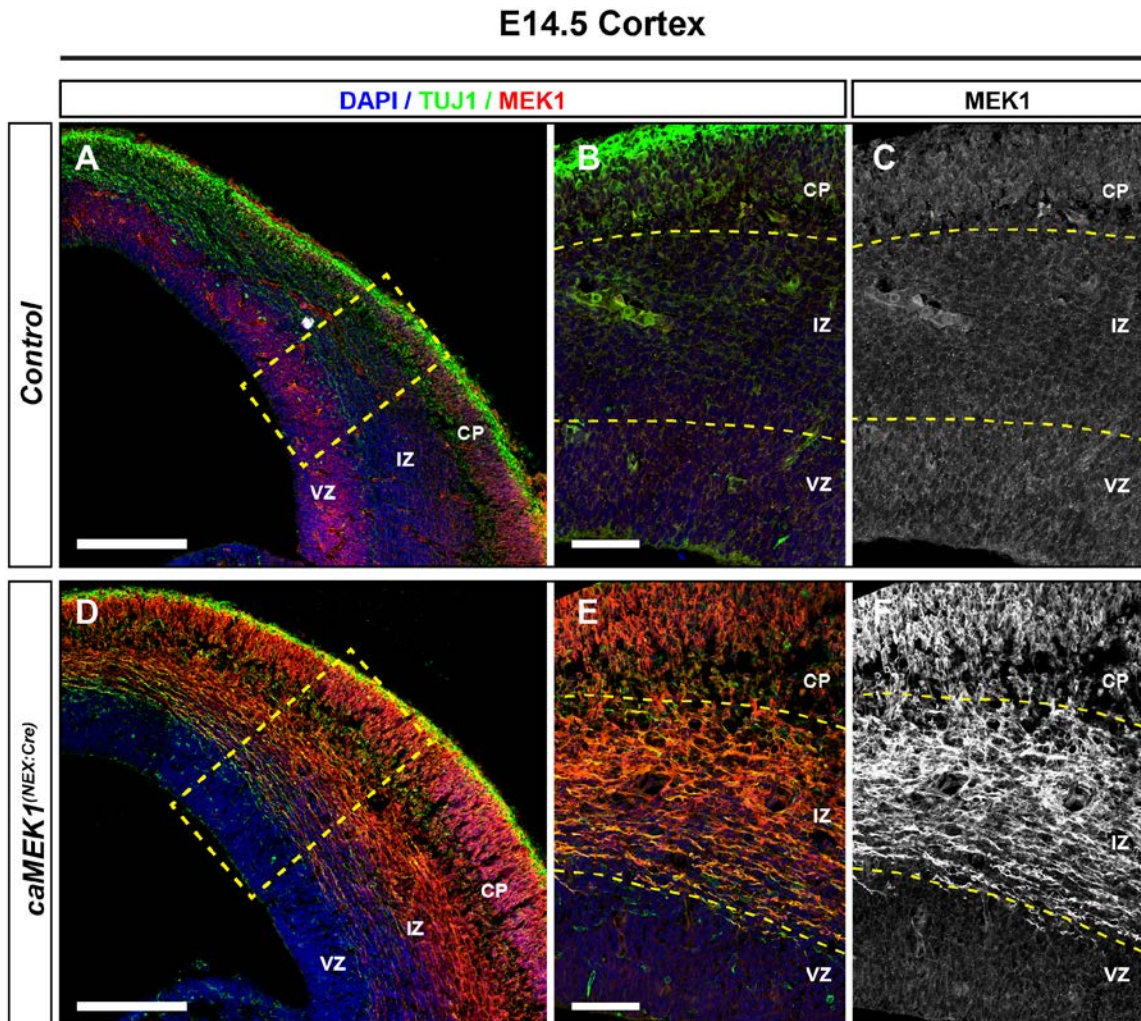
Additional white matter tracts that showed comparable localization of P-ERK1/2 included the anterior commissure and hippocampal commissure tracts, and the cerebral peduncle and corticospinal tracts in the midbrain (n=3) (Figure 19A-D and 20E-H). These data indicate that hyperactivation of MEK1 in cortical glutamatergic neurons results in a significant change in the compartmental localization of P-ERK1/2 that is evident in both embryonic and adult mice.

Figure 15.



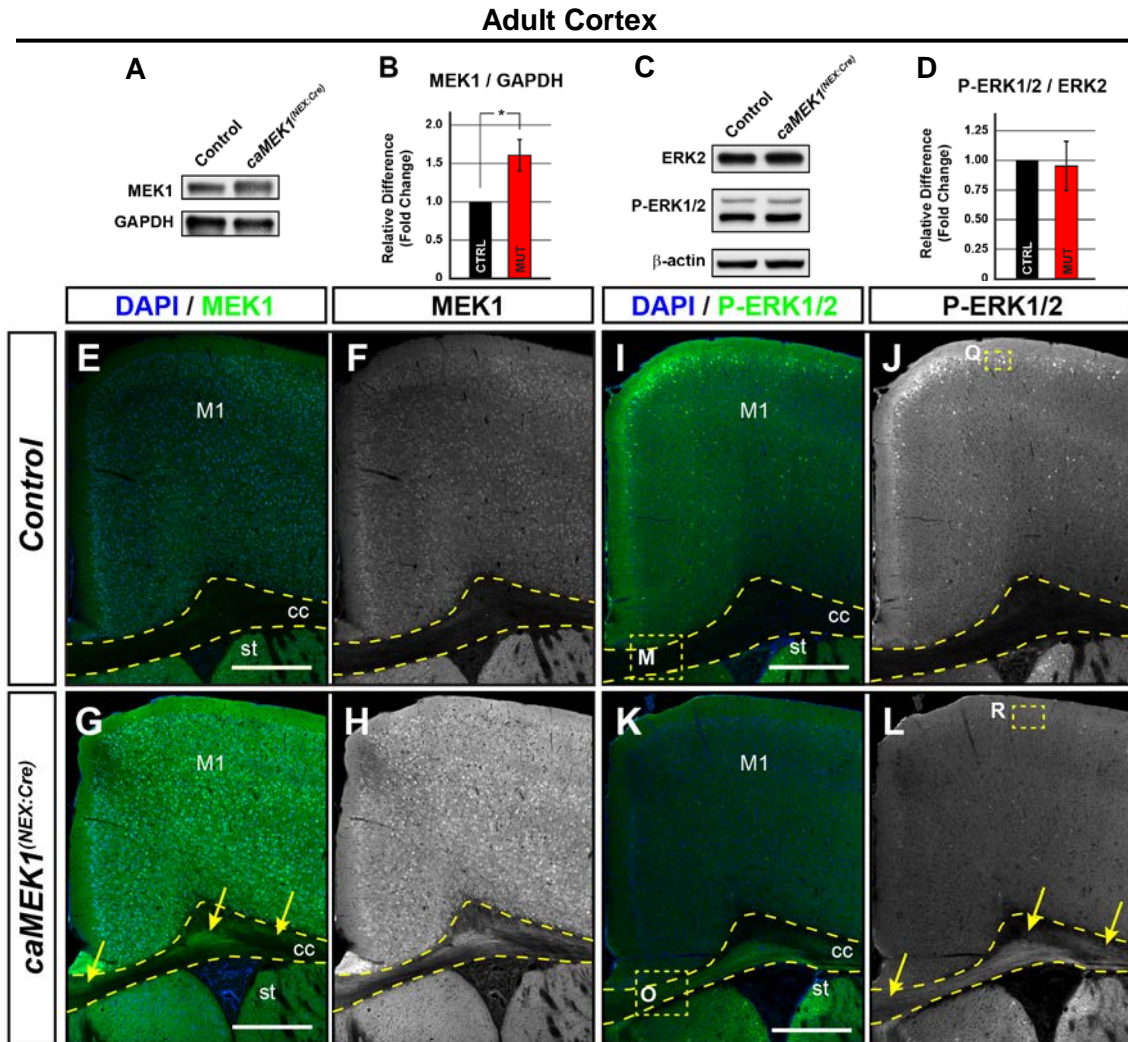
MEK1 hyperactivation results in increased levels of P-ERK1/2 in the axons of cortical excitatory neurons. Western Blot analysis of E14.5 cortical lysates showed a MEK1 fold increase in the *NexCre/caMek1* mice when compared to controls of $+14.99 \pm 2.00$ (Mean \pm SEM, GAPDH normalized, $p=0.002$, $n=5$, Student's t-test) (A-B). P-ERK1/2 levels in the E14.5 cortical lysates revealed a MEK1 fold change in the *NexCre/caMek1* mice when compared to controls of $+1.47 \pm 0.20$ (Mean \pm SEM, $p=0.043$, $n=5$, Student's t-test). No significant change in protein expression levels of ERK2 was detected (controls = 1.00 ± 0.00 SEM, mutants = 1.06 ± 0.05 SEM, $p=0.245$, $n=5$, Student's t-test) (C-D). Immunohistochemical (IHC) analysis of E14.5 *NexCre/caMek1* cortical samples (G-L, H, L yellow arrows) exhibits a P-ERK1/2 localization in the region of the embryonic cortex that contains axonal projections of cortical glutamatergic neurons that was not detected in control mice (E-K) (IZ = Intermediate zone, VZ = ventricular zone, $n=5$, scale bars: 1E through 1H = $200\mu\text{m}$, 1I through 1L = $50\mu\text{m}$).

Figure 16.



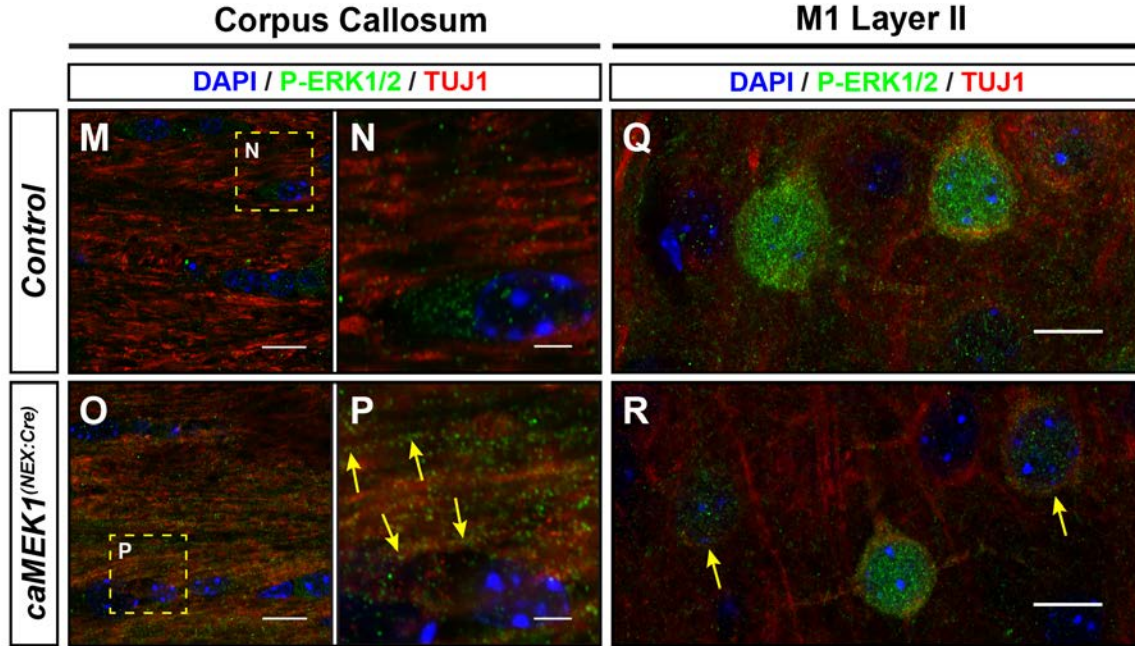
Enhanced MEK1 expression is detected in the somatosensory cortex of embryonic *NexCre/caMek1* mice. Immunostaining of E14.5 somatosensory cortex reveals a substantial up-regulation of MEK1 expression in the intermediate zone (white matter tracts) and the cortical plate (glutamatergic neuronal bodies) of the *NexCre/caMek1* (D-F) when compared to controls (A-C) (IZ = Intermediate zone, VZ = ventricular zone, cp = cortical plate, n=5, scale bars: A, D = 200 μ m, B,C,E,F = 50 μ m).

Figure 17.



Increased levels of P-ERK1/2 in the axons and reduced somal detection of P-ERK1/2 persists in adult *NexCre/caMek1* mice. Western Blots of adult cortical lysates revealed a MEK1 fold increase in the *NexCre/caMek1* when compared to control mice of $+1.61 \pm 0.20$ (Mean \pm SEM, GAPDH normalized, $p=0.041$, $n=3$, Student's t-test) (A-B). No significant differences in P-ERK1/2 expression levels between the *NexCre/caMek1* and control mice were detected (controls = 1.00 ± 0.00 SEM, mutants = 0.95 ± 0.21 SEM, $p=0.832$, $n=3$, Student's t-test) when normalized to ERK2 levels (controls = 1.00 ± 0.00 SEM, mutants = 1.07 ± 0.08 SEM, β -actin normalized, $p=0.389$, $n=3$, Student's t-test) (C-D). IHC analysis of MEK1 shows the increased expression in the targeted cortical glutamatergic neurons of the *NexCre/caMek1* mice (G-H) when compared to controls (E-F) (M1 = primary motor cortex, cc = corpus callosum, st = striatum, $n=3$, scale bars = 500 μ m). P-ERK1/2 localization to white matter tracts as described in the embryonic *NexCre/caMek1* (Fig. 1) persists in the adult *NexCre/caMek1* (K-L) when compared to control mice (I-J). Additionally, a reduction of somal P-ERK1/2 was detected throughout all cortical layers of the *NexCre/caMek1* when compared to controls (I-L) (M1 = primary motor cortex, cc = corpus callosum, st = striatum, $n=3$, scale bars = 500 μ m).

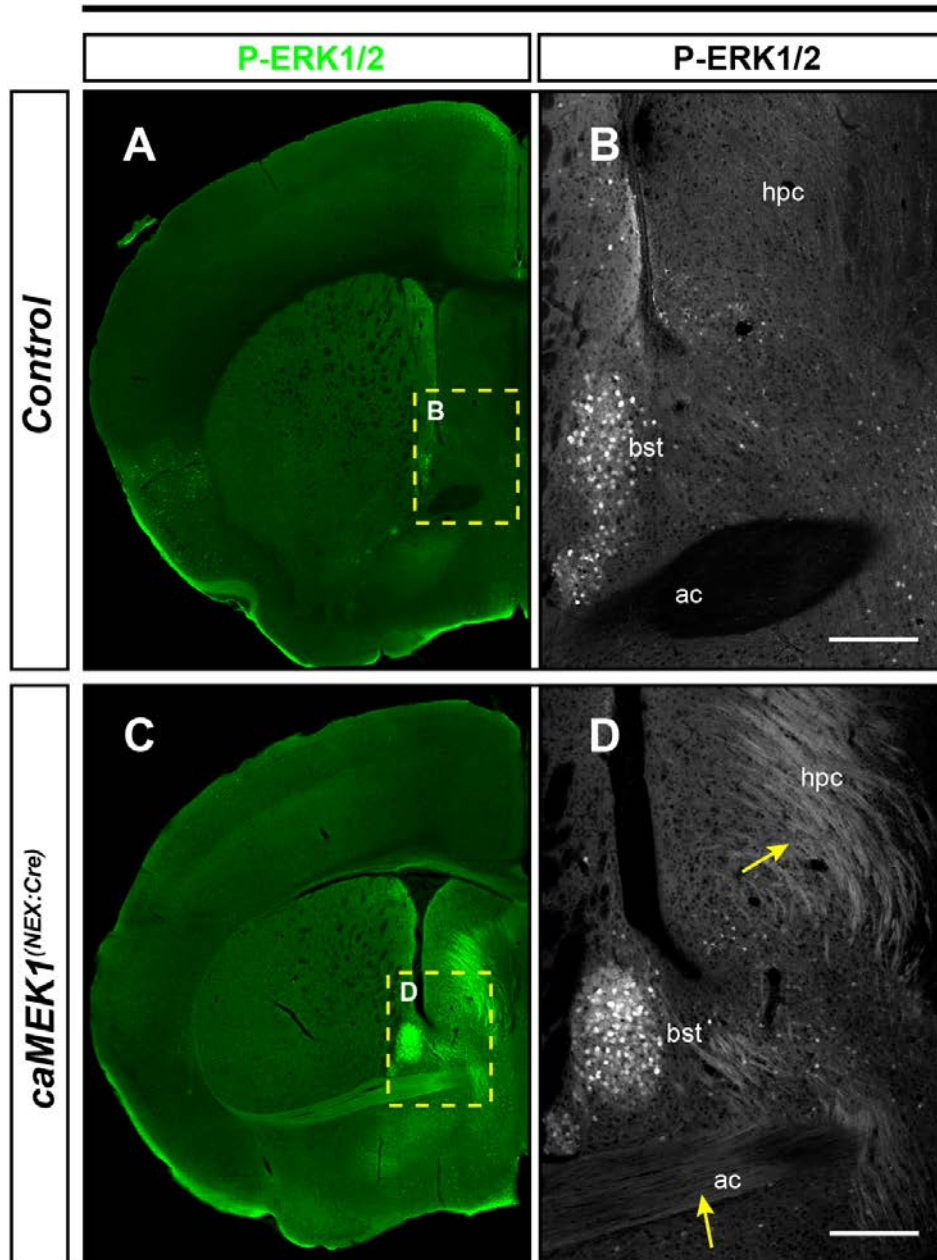
Figure 18.



Increased levels of P-ERK1/2 in the axons and reduced somal detection of P-ERK1/2 persists in adult NexCre/caMek1 mice. High resolution confocal imaging of the corpus callosum revealed an increased level of punctate patterned P-ERK1/2 co-localizing with axonal TUJ1 in the *NexCre/caMek1* (O-P, yellow arrows) when compared to controls (M-N) (Scale bars, M, O = 10 μ m, N, P = 2.5 μ m, n = 3). High resolution confocal images of neuronal bodies in the cortex showed the punctate pattern of P-ERK1/2 immunolabeling in the soma with a marked reduction of the number of somas expressing P-ERK1/2 in the *NexCre/caMek1* mice (R, yellow arrows) when compared to controls (Q) (Scale bars = 10 μ m, n = 3).

Figure 19.

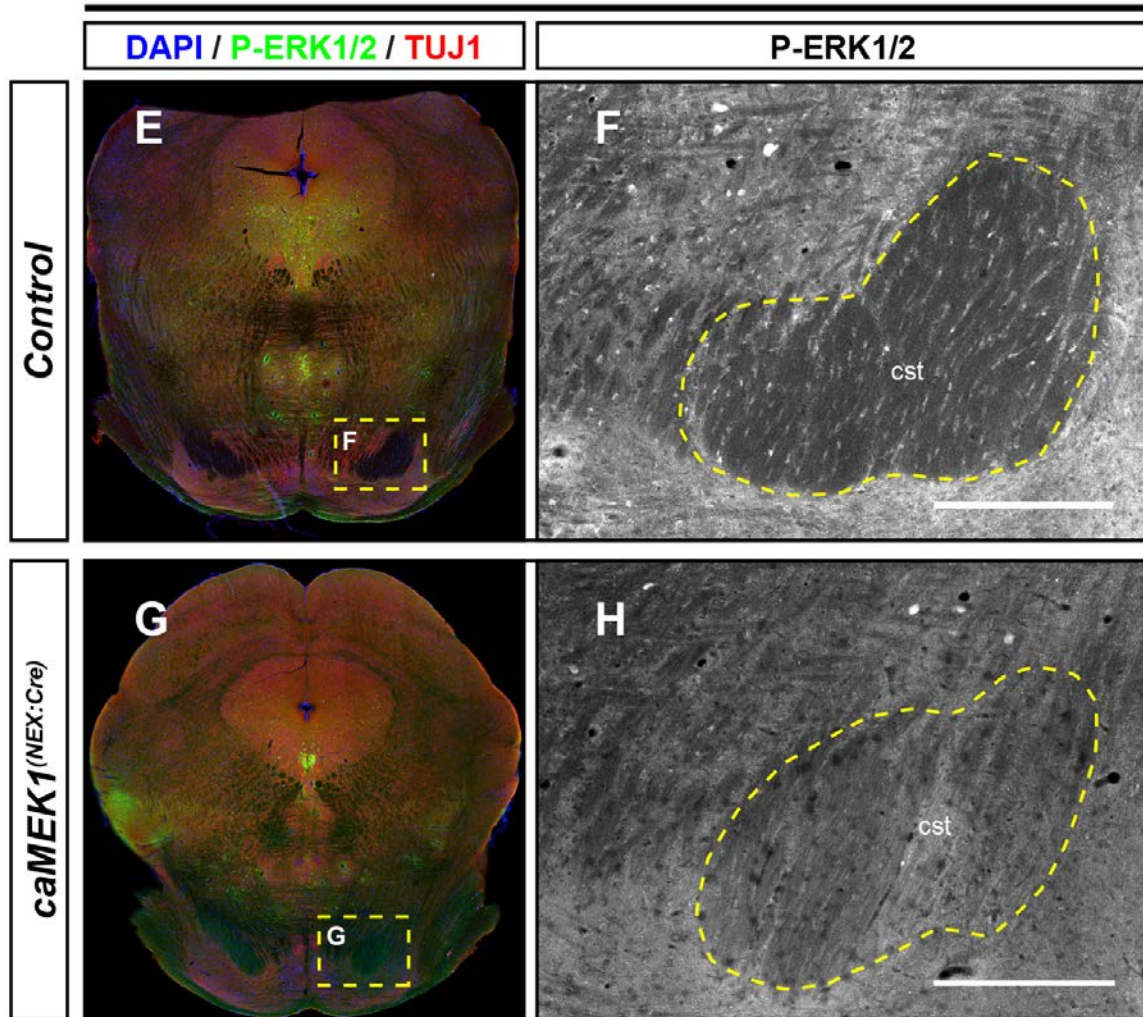
Adult Forebrain



P-ERK1/2 localizes to white matter tracts in *NexCre/caMek1* mice when compared to controls. Additional white matter tracts in the forebrain of the *NexCre/caMek1* (C-D) that exhibit increased levels of P-ERK1/2 when compared to controls (A-B) include the anterior commissure and the hippocampal commissure (scale bars = 100 μ m, n=3, ac = anterior commissure, bst = bed nuclei of the stria terminalis, hpc = hippocampal commissure).

Figure 20.

Adult Midbrain



P-ERK1/2 localizes to white matter tracts in *NexCre/caMek1* mice when compared to controls. Subcortical CST projections of the *NexCre/caMek1* (G-H) mice in the cerebral peduncle also exhibit increased levels P-ERK1/2 when compared to control mice (E-F) (scale bars=250µm, n=3, cst = corticospinal tract).

Corticocortical and corticostriatal innervation and branching patterns are disrupted by constitutively active MEK1

The current findings regarding the localization patterns of P-ERK1/2, led us to question what effect MEK1 glutamatergic hyperactivation has on corticocortical and corticostriatal axonal branching and innervation. We had previously reported a reduction of corticospinal tract (CST) elongation in the *NexCre/caMek1* mice. Additionally, we also found enhanced branching and innervation of CST axons in the gray matter of the spinal cord and the hind brain when compared to control mice (Xing et al., 2016). Axonal targets of the projection neurons of the mouse cortex have been established to be primarily layer specific. The deficits found in the CST, spinal cord, and hind brain in our previous study, predominately originate from cortical layer V (Fame et al. 2011). A smaller number of layer V neurons, ~20%, also project to the contralateral cortex (Sohur et al. 2014). Corticostriatal projection neurons (CStrPNs) that innervate the contralateral dorsolateral striatum, mainly originate from layers II/III and V with a smaller portion occupying layer VI (Sohur et al. 2014). Due to the detected abnormalities in long-range cortical projection axons in the spinal cord and hind-brain, and the increased levels of P-ERK1/2 detected in the axonal compartments, we hypothesized that there would also be an increased or hyperactivated branching pattern in the contralateral cortex and contralateral dorsal striatum.

To investigate this hypothesis, we utilized an anterograde tracing approach to transfect the glutamatergic neurons of the primary motor cortex of one cortical hemisphere, with an Adeno Associated Virus that expresses a CRE dependent td-Tomato vector (*AAV: CAG-FLEX-tdTomato*). Then, using high resolution confocal images, we measured the axonal innervation of the contralateral cortical hemisphere and the contralateral dorsal striatum. Corticocortical axonal projections of the

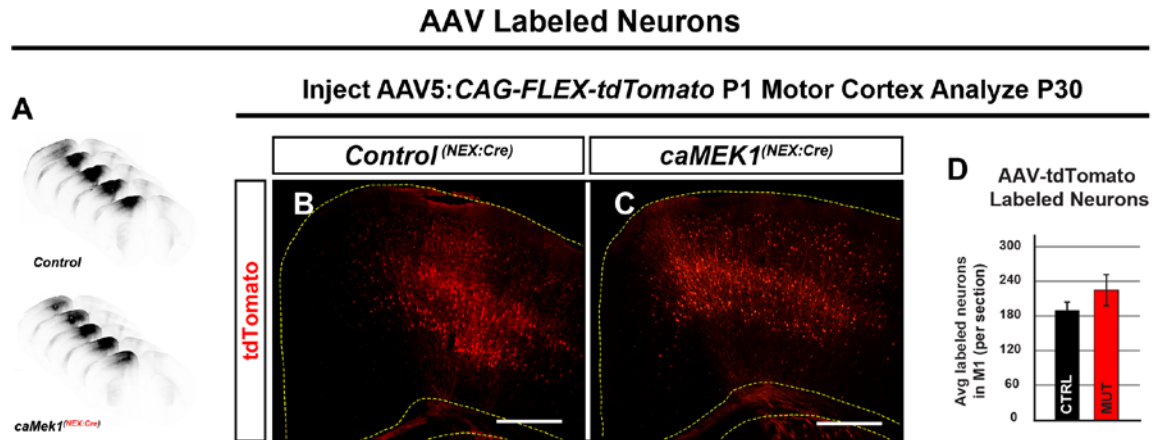
glutamatergic neurons in motor and somatosensory cortices are homotopic and therefore innervate corresponding areas in the contralateral cortical hemisphere (Lee et al. 2005; Katherine A Rauen 2013; Aoki, Niihori, S.I. Inoue, et al. 2016). Additionally, corticostriatal axonal projections from these neurons innervate the dorsal medial-lateral striatum both contralaterally and ipsilaterally (Jindal et al. 2015). Accordingly, we used similar areas in the primary motor cortex and the dorsal medial to dorsal lateral striatum to measure specific differences in the amount of axonal innervation in the *NexCre/caMek1* and control mice. The raw axonal pixelation was then normalized to the number of transfected cells in the comparable site from the injection hemisphere for each of the serial slices measured.

The AAV: *CAG-FLEX-tdTomato* injections were done in the primary motor cortex of P1 *NexCre/caMek1* and control mice. Analysis of contralateral cortical and dorsal striatum axonal innervation was performed at P30 in serial sections of mouse cortex (Figure 21A). Cell counts in the injection hemispheres revealed no significant difference between the *NexCre/caMek1* and control mice (*NexCre/caMek1* = 224.73 ± 26.73 SEM, control = 189.96 ± 14.20 SEM, n=5, p=0.284, Student's t-test) (Figure 21B-D). Measurements of axonal density in the contralateral cortex revealed a significant reduction in axonal branching and innervation. Axonal innervation and branching measured 631.68 ± 27.51 SEM pixels²/transfected cell in the *NexCre/caMek1* mice and 791.79 ± 42.88 SEM pixels²/transfected cell in the control mice. This translated to a $19.57\% \pm 4.30$ reduction in the *NexCre/caMek1* mice when compared to the controls (Mean \pm SEM, p=0.014, n=5, Student's t-test) (Figures 22E, F, H, I, K). Contralateral dorsal striatal innervation was also significantly reduced in the *NexCre/caMek1* mice measuring 155.44 ± 21.18 SEM pixels²/transfected cell (n=5) and controls measuring 255.67 ± 23.64 SEM pixels²/transfected. This translated to a $37.50\% \pm 9.14$ reduction in axonal

innervation in the *NexCre/caMek1* mice when compared to controls (Mean \pm SEM, $p=0.013$, $n=5$, Student's t-test) (Figure 3b, E, G, H, J, L).

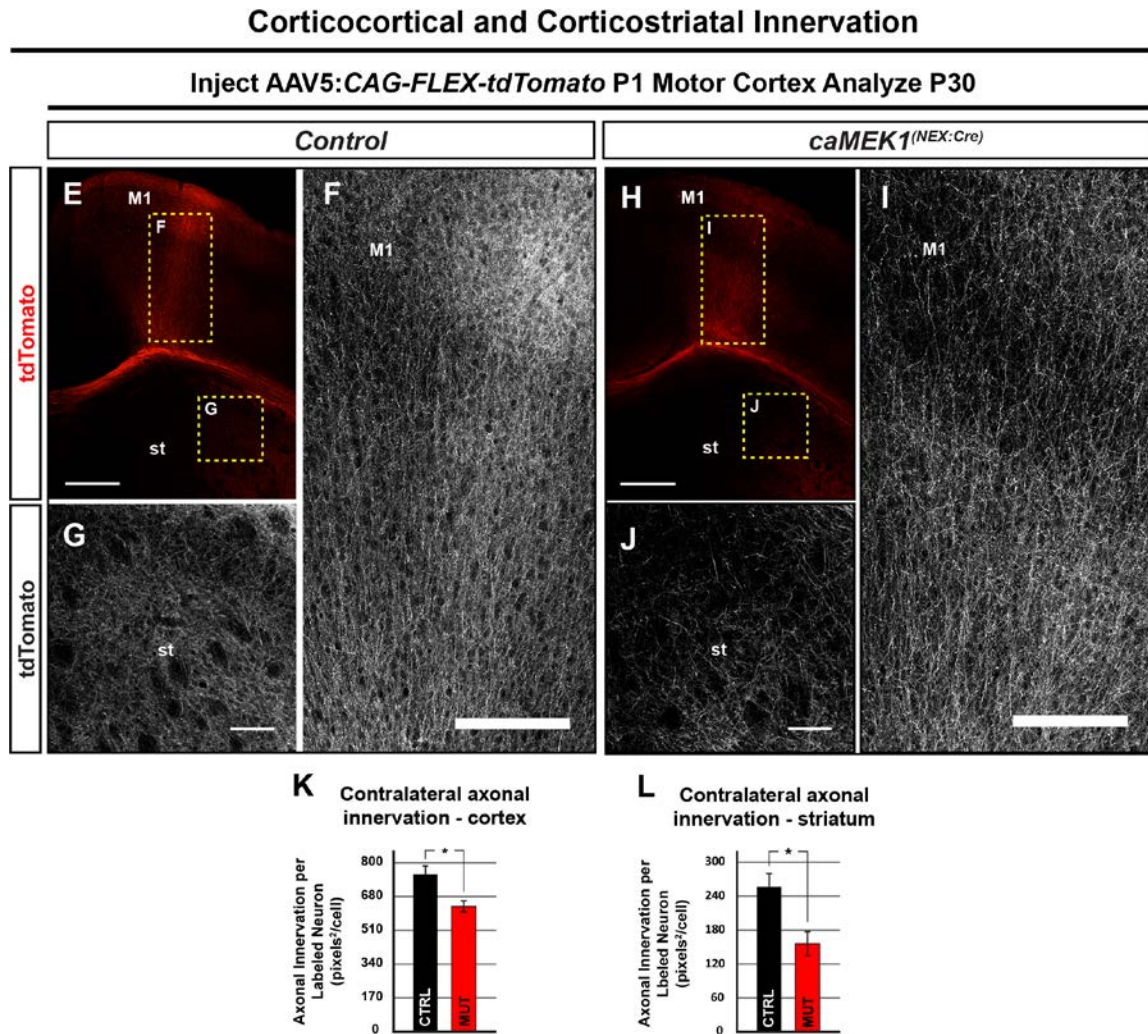
These results indicate that MEK1 hyperactivation not only affects extreme long-range cortical axonal projections in the hindbrain and CST, as found in our previous study, but also affects the innervation of relatively close targets innervated by corticocortical and corticostriatal projections. Additionally, these deficits in axonal projections coupled with the results indicating the localization of P-ERK1/2 in the axonal compartments, provides evidence that excess P-ERK1/2 disrupts the normal development of axonal innervation and branching.

Figure 21.



Corticocortical and corticostriatal innervation and branching patterns are disrupted by hyperactivated MEK1. Adeno associated viral vector AAV: *CAG-Flex-tdTomato* was injected in the primary motor cortex of P1 mice followed by analysis of contralateral cortical and dorsal striatum axonal innervation and branching at P30. Axonal innervation and branching in the contralateral primary motor cortex and dorsal striatum was measured and normalized to the number of transfected cells in the injection site. Serial section images of the AAV: *CAG-Flex-tdTomato* injection site showing both rostral-caudal and medial-lateral positions of the AAV-tdTomato labeled cells (A). Representative images of the AAV injection site in the primary motor cortex of the *NexCre/caMek1* (C) and control (B) contralateral to cortical hemispheres used for the axonal innervation analysis. Viral-labeled cells were counted in the primary motor region of each section used for contralateral innervation analysis. No significant differences in labeled cell counts between *NexCre/caMek1* and control mice were detected (*NexCre/caMek1* = 224.73 ± 26.73 SEM, control = 189.96 ± 14.20 SEM, n=5, p-value ≤ 0.2839, Student's t-test) (D).

Figure 22.



Corticocortical and corticostriatal innervation and branching patterns are disrupted by hyperactivated MEK1. Representative images of contralateral axonal innervation and branching in the cortex and dorsal striatum of the *NexCre/caMek1* (H-I) and control mice (E-F). Contralateral cortical axonal innervation measured 631.68 ± 27.51 SEM pixels²/labeled neuron in the *NexCre/caMek1* mice (n=5) and 791.79 ± 42.88 SEM pixels²/labeled neuron in the control mice (n=5). This translated to a $19.57\% \pm 4.30$ reduction in axonal innervation in the *NexCre/caMek1* contralateral primary motor cortex when compared to control mice (Mean \pm SEM, $p=0.014$, n=5, Student's t-test) (K). Contralateral axonal innervation of the dorsal striatum measured 155.44 ± 21.18 SEM pixels²/labeled neuron in the *NexCre/caMek1* mice (n=5) and 255.67 ± 23.64 SEM pixels²/labeled neuron in the control mice (n=5). This translated to a $37.50\% \pm 9.14$ reduction in axonal innervation in the *NexCre/caMek1* contralateral dorsal striatum when compared to control mice (Mean \pm SEM, $p=0.013$, n=5, Student's t-test) (L). (M1 = primary motor cortex, st = striatum, scale bars: A, B-D, G = 500 μ m, E, F-H, I = 100 μ m). *ARC* protein levels are negatively affected by MEK1 hyperactivation

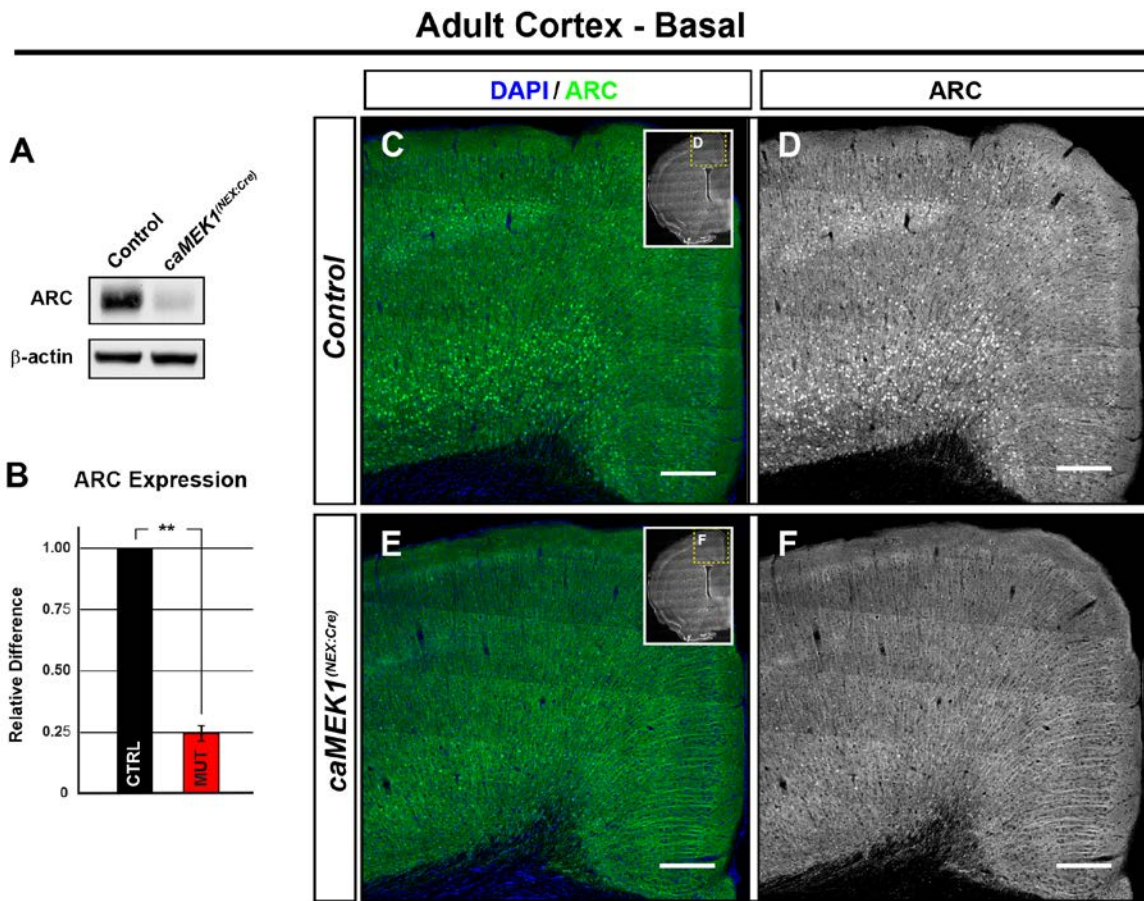
It is well established that ERK/MAPK is a major factor in regulating neuronal activity and synaptic plasticity (Impey et al., 1999; Thomas and Huganir, 2004), and that the transcriptional activity of these processes are regulated or targeted by the ERK/MAPK pathway and other pathways (Bramham et al. 2010). ARC is an immediate early gene (IEG) whose transcription is controlled by ERK/MAPK and the activation of the glutamate receptor *N*-methyl-D aspartate following LTP induction (NMDAR) (Cao et al. 2015). ARC is also identified as a crucial part of learning consolidation in motor cortex required learning paradigms, specifically, secondary motor cortex (M2) requirements for motor learning in the rotarod task (Petrella et al. 2016). Motor and learning delays and cognitive impairments reported in RASopathy patients in conjunction with our findings on the axonal localization of P-ERK1/2, led us to hypothesize that there would be a disruption in the amount of ARC protein being produced.

When measured in the basal state, Western Blots of whole cortical lysates revealed a significant decrease of ARC expression in the *NexCre/caMek1* mice (control = 1.00 ± 0.00 SEM, n=3, *NexCre/caMek1* = 0.22 ± 0.02 SEM, n=3, $p < 0.005$, Student's t-test) (Figure 23A-B). Immunostaining of cortical samples confirmed the substantial decrease of cortical ARC expression (n=4) (Figures 23C-F).

Having detected these significantly reduced amounts of ARC protein levels in the basal state, we tested to determine if expression and translation levels of ARC would be detected at a normal or hyperactivated level in stimulated mice. To test this, we examined cortical samples of *NexCre/caMek1* and control mice by IHC in the stimulated state 2 hours after performance on the rotarod. These samples also revealed a marked reduction of ARC expression in the *NexCre/caMek1* mice when compared to control mice (Figure 24G-4J).

These findings revealed that hyperactivation of the ERK/MAPK pathway may disrupt an internal pathway equilibrium that results in the downregulation of transcription or translation of ARC mRNA or ARC protein in both the basal and stimulated states.

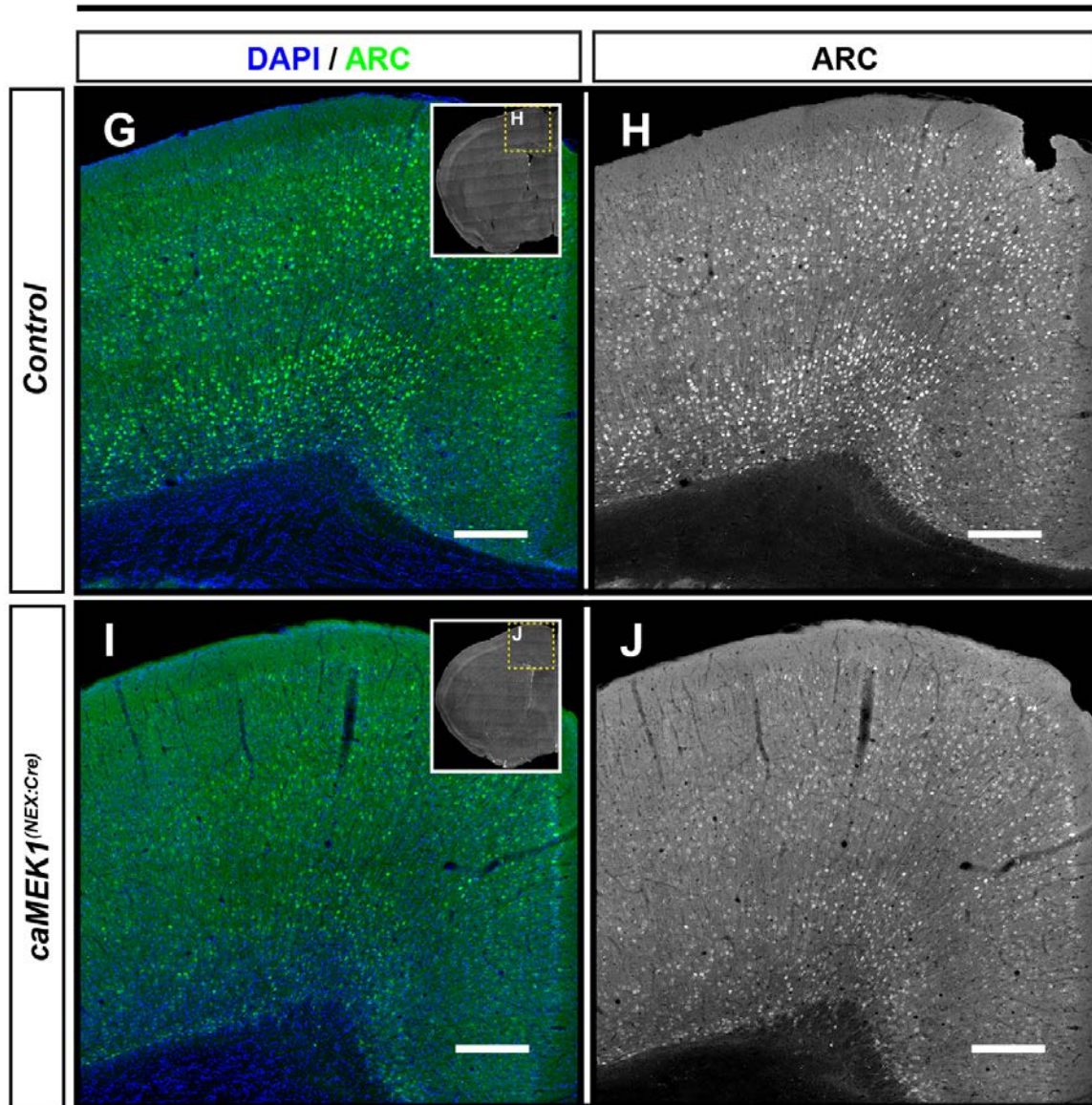
Figure 23.



ARC protein levels are negatively affected by MEK1 hyperactivation. Western Blot analysis of whole cortical lysates showed a significant reduction in *NexCre/caMek1* ARC levels when compared to control mice (control = 1.00 ± 0.00 SEM, $n=3$, *NexCre/caMek1* = 0.22 ± 0.02 SEM, $p<0.005$, $n=3$, Student's t-test) (A-B). Immunolabeling showed substantial reduction of ARC throughout all layers of the *NexCre/caMek1* cortex (E-F) in the basal state when compared to controls (C-D) ($n=4$, scale bars = $250\mu\text{m}$).

Figure 24.

Adult Cortex - Stimulated



ARC protein levels are negatively affected by MEK1 hyperactivation.

Immunolabeling of ARC expression after rotarod stimulation also showed a marked reduction in the *NexCre/caMek1* cortices (I-J) when compared to controls (G-H) (n=5, scale bars = 250μm).

Motor learning and motor skill acquisition is disrupted by MEK1 hyperactivation in cortical glutamatergic neurons

Having identified deficiencies in long range axonal projections originating in cortical glutamatergic neurons and the decrease of ARC detection in the cortex, we next questioned if these findings would impair motor function or motor learning acquisition. Impairments in motor coordination and motor learning, motor delays, and learning disabilities are common elements in the RASopathies (Davis et al. 2000; Monje et al. 2005; Blüthgen et al. 2017). These issues have also been identified in mouse models created to study the effects of disease subsets within the RASopathies (Greig et al. 2013). Therefore, we hypothesized that the *NexCre/caMek1* mice would show significant deficits in these areas. To analyze this, we employed the open field test for gross locomotor function and movement, the accelerating rotarod test for locomotor function and motor learning acquisition, and a fine reaching and grasping task for fine locomotor function and motor learning acquisition. Additionally, to test the for anxiolytic phenotypes, we used the open arm maze and measure of center time in the open field test.

The *NexCre/caMek1* mice display no obvious physical defects other than a slightly smaller size and ~28% less weight. Our first step however was to assess the gross locomotor functions of the mutant mice visually and in an open field test (Crawley, 1999). Open field testing revealed no significant difference in total distance traveled between the *NexCre/caMek1* and control mice (controls = 1834.88cms \pm 172.29cms SEM n=12, *NexCre/caMek1* = 2162.80cms \pm 218.72cms SEM n=12, p=0.252, Student's t-test) (Figure 25A). Measurements of percent center time also showed no significant differences between the *NexCre/caMek1* and control mice (% center time, controls = 32.40% \pm 3.75% SEM, n=12, *NexCre/caMek1* = 26.50% \pm 2.56% SEM, p=0.208, n=12, Student's t-test) (Figure 25A). Results of the open field

test and visual observation of the *NexCre/caMek1* mice indicated no gross motor or locomotion defects that would hinder their physical performance in subsequent testing.

NexCre/caMek1 and control mice were then tested for motor coordination and learning on an accelerating rotarod. During Test 1, the *NexCre/caMek1* mice showed significantly better motor coordination than the control mice (main effect of genotype, $[F(1,22)=5.85, p=0.0243]$, $n=12$) (Figure 25B).

To test for any anxiety-like effects, we used an elevated plus maze to test the *NexCre/caMek1* and control mice. In the elevated plus maze, the *NexCre/caMek1* had similar levels of activity to the control but showed a decrease in anxiety-like behavior for both percent of open arm time (genotype, $[F(1,23)=8.57, p=0.008]$ $n=13$ controls, $n=11$ mutants) and percent open arm entries $[F(1,23)=5.91, p=0.023]$ $n=13$ controls, $n=11$ mutants) (Figure 25C).

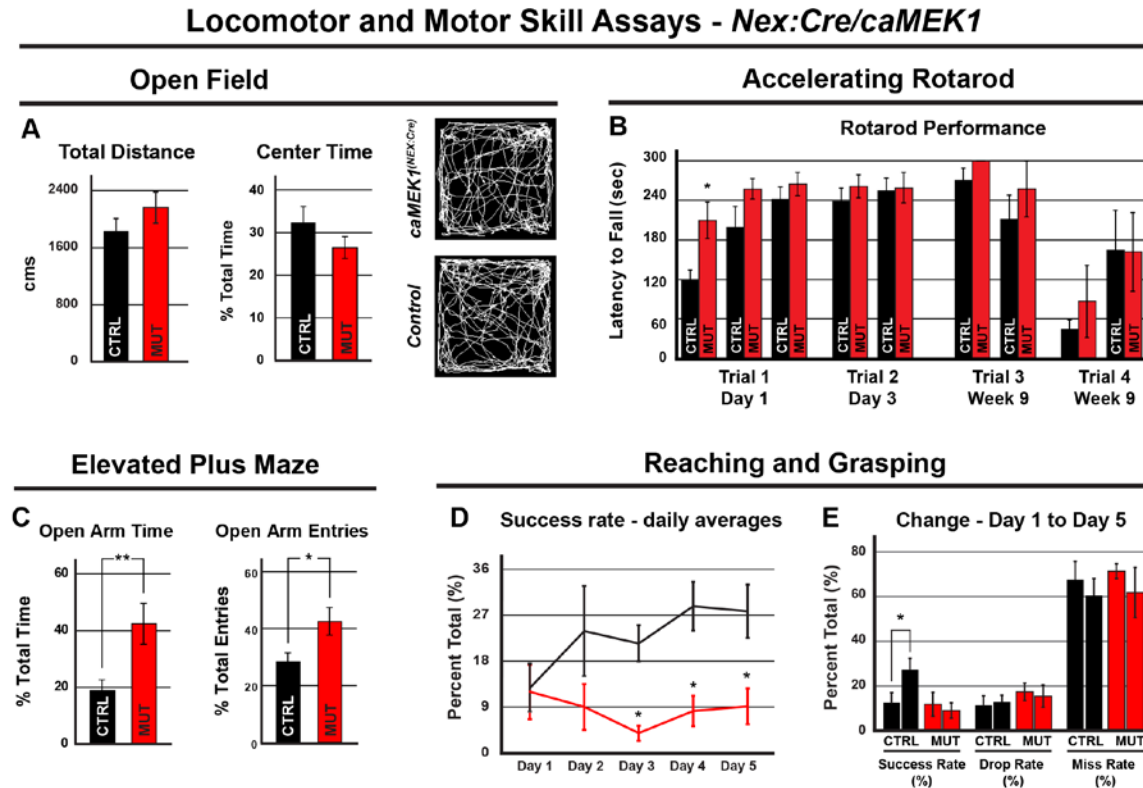
Additional testing of motor skill learning acquisition was performed using a skilled reaching and grasping task. This test was designed and used to assay fine motor skills and motor learning acquisition of the *NexCre/caMek1* and control mice. Additionally, the use of this test will serve to assess learning acquisition independent of the size differences in the mice. The first days testing showed that both the mutants and controls had approximately the same level of skill and ability in base performance of this test (Figure 25D). Over the course of the five-day trial however, the control mice showed significant improvements in their ability to successfully grasp and retrieve the pellet starting with 12.39 ± 4.50 successful attempts on day one and increasing to 27.06 ± 5.11 successes on day five (mean, \pm SEM, $[F(1,10)=5.531, p=0.041$ Wilks' $\Lambda=0.644$, partial $\eta^2=0.644]$, $n=11$) (Figures 25D - E). The *NexCre/caMek1* mice made no improvements over the trial period starting with 11.70 ± 5.32 successful grabs on day one and ending with 8.88 ± 3.44 on day

five (mean, \pm SEM, [F(1,7)=0.450, p=0.524 Wilks' Λ =0.940, partial η^2 =0.060], n=8) (Figures 25D - E). A significant effect of genotype was also detected between the *NexCre/caMek1* and control mice (genotype, [F(5,12)=3.165, p=0.047, Wilks' Λ =0.431, partial η^2 =0.569], n=11 controls, n=7 mutants). These results indicate that the *NexCre/caMek1* mice exhibit an impairment in motor learning acquisition when compared to control mice.

To test the question of motor coordination and motor learning acquisition effects due to hyperactivation of MEK1 in lower motor neurons (LMNs), we used a *ChAT-IRES-Cre* mouse bred with a *caMEK1* mouse (*ChAT:Cre*) to express the constitutively active MEK1 construct in the cholinergic LMNs of the hind brain spinal cord (Rossi et al., 2100, Krenz et al., 2008). The *ChAT:Cre* and control mice were then subjected to open field and accelerating rotarod testing. When compared to control mice, the *ChAT:Cre* mice showed a significantly lowered difference in total distance traveled (control = 2262.4cms \pm 143.96cms SEM, n=9, *ChAT:Cre* = 1779.32cms \pm 93.31cms SEM, n=14, p=0.008, Student's t-test) and no difference in percent center time (control = 40.79% \pm 2.21% SEM, n=9, *ChAT:Cre* = 41.06% \pm 5.45% SEM, n=14, p=0.969 Student's t-test) (Figure 26F). The Results of rotarod testing showed that both the *ChAT:Cre* and control mice groups were able to significantly improve in performance over the five-day testing period. The *ChAT:Cre* mice improved their latency to fall from 65.67secs \pm 3.96 to 136.95secs \pm 4.18 (latency to fall, [F(4,52)=15.238, p<0.005, repeated measures ANOVA], n=42) (Figure 26G) and the control group improved their latency to fall from 78.15secs \pm 6.01 to 130.18secs \pm 6.02 (latency to fall, [F(4,36)=11.208, p<0.005, repeated measures ANOVA], n=30) (Figure 26G).

No significant effect of genotype between the *ChAT:Cre* and control group was detected (genotype x latency to fall, $[F(4,88)=0.673, p=0.613, \text{repeated measures ANOVA}]$). The data from these tests demonstrate that hyperactivation of MEK1 in the LMNs had some effect on voluntary locomotor activity but no direct effect on motor coordination or motor skill learning.

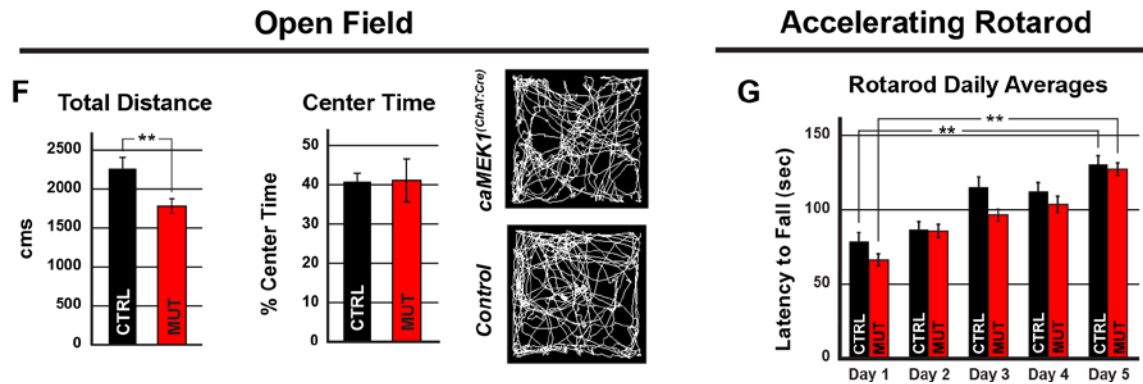
Figure 25.



Motor learning and motor skill acquisition is disrupted by MEK1 hyperactivation in cortical glutamatergic neurons. Open field testing of the *NexCre/caMEK1* and control mice revealed no significant difference in distance traveled over the testing period indicating an intact motor system in the *NexCre/caMEK1* mice (controls = 1834.88cm \pm 172.29 SEM, n=12, *NexCre/caMEK1* = 2162.80cm \pm 218.72 SEM, p=0.252, n=12, Student's t-test) (A). Center time measurements also revealed no significant differences between *NexCre/caMEK1* and control mice (% center time, controls = 32.40% \pm 3.75% SEM, n=12, *NexCre/caMEK1* = 26.50% \pm 2.56% SEM, p=0.208, n=12, Student's t-test). Accelerating rotarod testing revealed inconsistent results possibly due to size differences in the mutant and control mice. (B). In the elevated plus maze, the *NexCre/caMEK1* had similar levels of activity to the control but showed a decrease in anxiety-like behavior for both percent of open arm time (genotype, [F(1,23)]=8.57, p=0.008] n=13 controls, n=11 mutants) and percent open arm entries [F(1,23)=5.91, p=0.023] n=13 controls, n=11 mutants). C). In a single pellet reaching and grasping task, the control group significantly improved over the course of the trial increasing from 12.39 \pm 4.50 to 27.06 \pm 5.11 successful attempts (mean, \pm SEM, [F(1,10)]=5.531, p=0.041 Wilks' Λ =0.644, partial η^2 =0.644], n=11). The *NexCre/caMEK1* however made no improvements over the trial period starting with 11.70 \pm 5.32 and ending with 8.88 \pm 3.44 successful attempts (mean, \pm SEM, [F(1,7)]=0.450, p=0.524 Wilks' Λ =0.940, partial η^2 =0.060], n=7) (D-E). A significant effect of genotype was also detected between the *NexCre/caMEK1* and control mice (genotype, [F(5,12)]=3.165, p=0.047, Wilks' Λ =0.431, partial η^2 =0.569], n=11 controls, n=7 mutants) (D-E).

Figure 26.

Locomotor and Motor Skill Assays - *ChAT:Cre/caMEK1*



Motor learning and motor skill acquisition is disrupted by MEK1

hyperactivation in cortical glutamatergic neurons. Open field testing of *ChAT:Cre* and control mice groups showed a significant difference in total distance traveled (control = 2262.4cms \pm 143.96cms SEM, n=9, *ChAT:Cre* = 1779.32cms \pm 93.31cms SEM, n=14, p=0.008, Student's t-test) and no difference in percent center time (control = 40.79% \pm 2.21% SEM, n=9, *ChAT:Cre* = 41.06% \pm 5.45% SEM, n=14, p=0.969 Student's t-test) (F). Rotarod testing showed that both the *ChAT:Cre* and control mice groups were able to significantly improve in performance over the five-day testing period. The *ChAT:Cre* mice improved their latency to fall from 65.67secs \pm 3.96secs to 136.95secs \pm 4.18secs ([F(4,52)=15.238, p<0.005, repeated measures ANOVA], n=42) and the control group improved from 78.15secs \pm 6.01secs to 130.18secs \pm 6.02secs ([F(4,36)=11.208, p<0.005, repeated measures ANOVA], n=30) (G). No significant effect of genotype between the *ChAT:Cre* and control group was detected (genotype x latency to fall, [F(4,88)=0.673, p=0.613, repeated measures ANOVA]) (G).

Hippocampal MEK1 gain-of-function downregulates P-ERK1/2 expression levels in the dentate gyrus and CA3 regions but upregulates in hippocampal associated white matter tracts

In addition to cortical glutamatergic neurons, NEX promoter activity is detected in dentate gyrus granule cells and mossy fibers that extend to the CA3 region (Goebbels et al. 2006). Immunostaining for P-ERK1/2 showed a distinct downregulation in the cell bodies and the processes associated with them in the *NexCre/caMek1* when compared to controls (N=3) (Figure 27A - D). However, the fimbria of the hippocampus and the stria terminalis show a substantial amount of P-ERK1/2 labeling (Figure 27A - D). Due to the P-ERK1/2 localization detected here, we wanted to determine if there would be any effects on spatial learning associated with the hippocampus. For this analysis we used the Morris water maze tests.

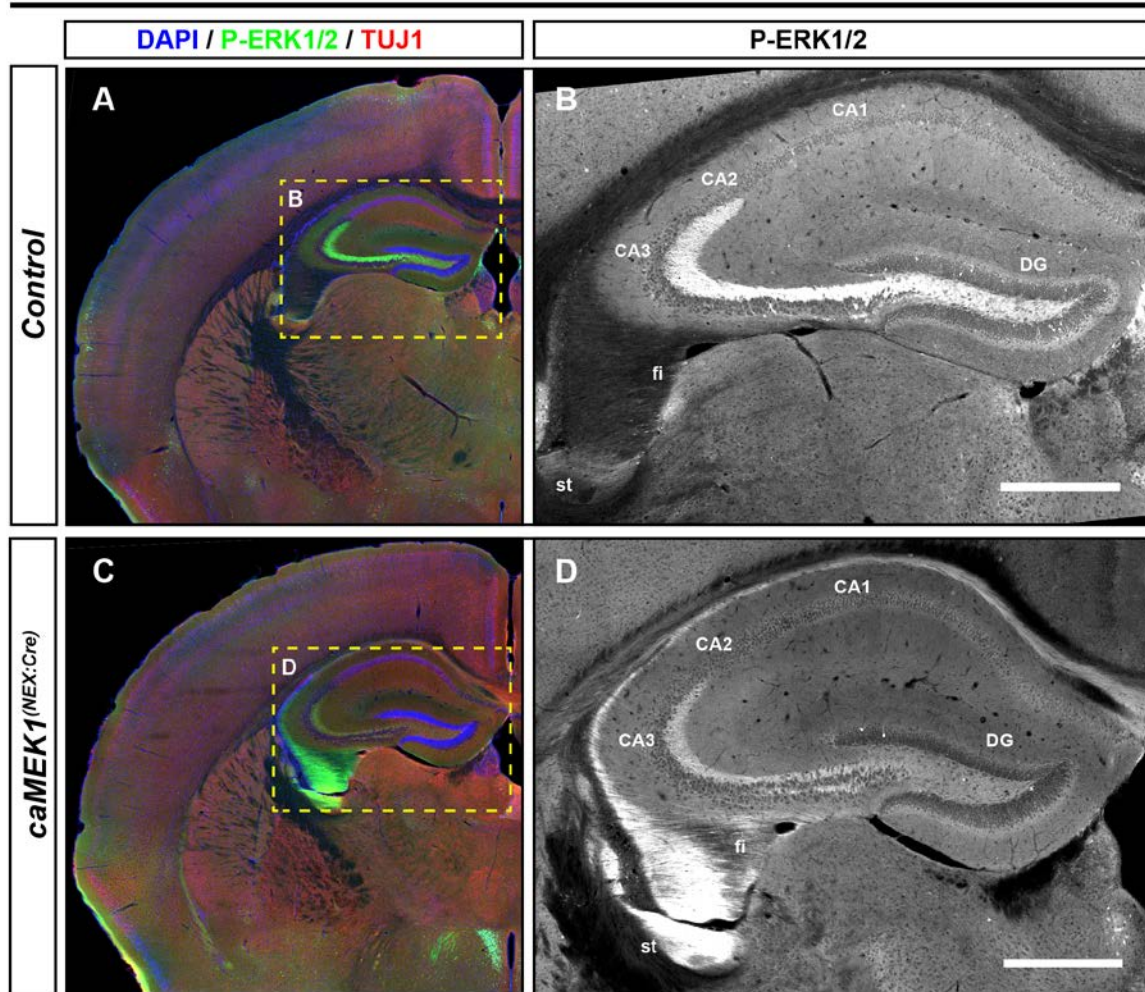
NexCre/caMek1 and control mice were first subjected to a visual cue test with a visible platform. No effects of genotype were found between the *NexCre/caMek1* and control mice. A total of 5 mice (3 *NexCre/caMek1* and 2 controls) had poor performance in finding the visible platform and were excluded from the acquisition and reversal phases of the water maze. In the acquisition phase, the *NexCre/caMek1* and control mice showed similar spatial learning in the hidden platform test (Figure 28E). In the reversal phase, no effect of genotype was detected between the *NexCre/caMek1* and control mice (Figure 28G). Although no effect of genotype was detected between the two groups, the *NexCre/caMek1* mice failed to reach the criteria for learning while the control group reached that criteria from days 3 to 5 (Figure 28G). Furthermore, the *NexCre/caMek1* mice had significantly longer swim paths than the control mice (main effect of genotype, $[F(1,16)=5.31]$, $p=0.0349$) (Figure 28G). This indicated a decreased ability to locate the new position of the hidden platform in the reversal phase.

In the probe trial following acquisition, a significant effect of quadrant was detected between *NexCre/caMek1* and control mice (effect of quadrant, [F(1,16)=8.91], p=0.0088] repeated measures ANOVA) (Figure 28F). No effect of genotype was detected (Figure 28F). Significant quadrant preference was observed in the control mice (quadrant preference, [F(1,9)=8.83], p=0.0156) but not in the *NexCre/caMek1* mice (Figure 28F). During the reversal probe trial, the control mice showed a shift in quadrant preference to the new location (quadrant preference, [F(1,9)=14.39], p=0.0043) (Figure 28H). In contrast, *NexCre/caMek1* mice failed to show quadrant selectivity (Figure 28H). A significant effect of genotype was detected between the *NexCre/caMek1* and control mice in quadrant selectivity (genotype x quadrant interaction, [F(1,16)=4.63], p=0.047, repeated measures ANOVA) (Figure 28H).

Swimming distance to the escape platform is dependent upon swimming velocity during the timed water maze test. Both the *NexCre/caMek1* and control mice performed comparably in the visual cue test, for the acquisition, reversal and acquisition probe trial, the *NexCre/caMek1* mice displayed significantly increased swim speeds (overall effect of genotype, [F(1,15)=4.56], p=0.0497, post-hoc tests following repeated measures ANOVA) (effect of phase of testing, [F(4,60)=21.06], p<0.0001, post-hoc tests following repeated measures ANOVA) (Figure 28I).

Figure 27.

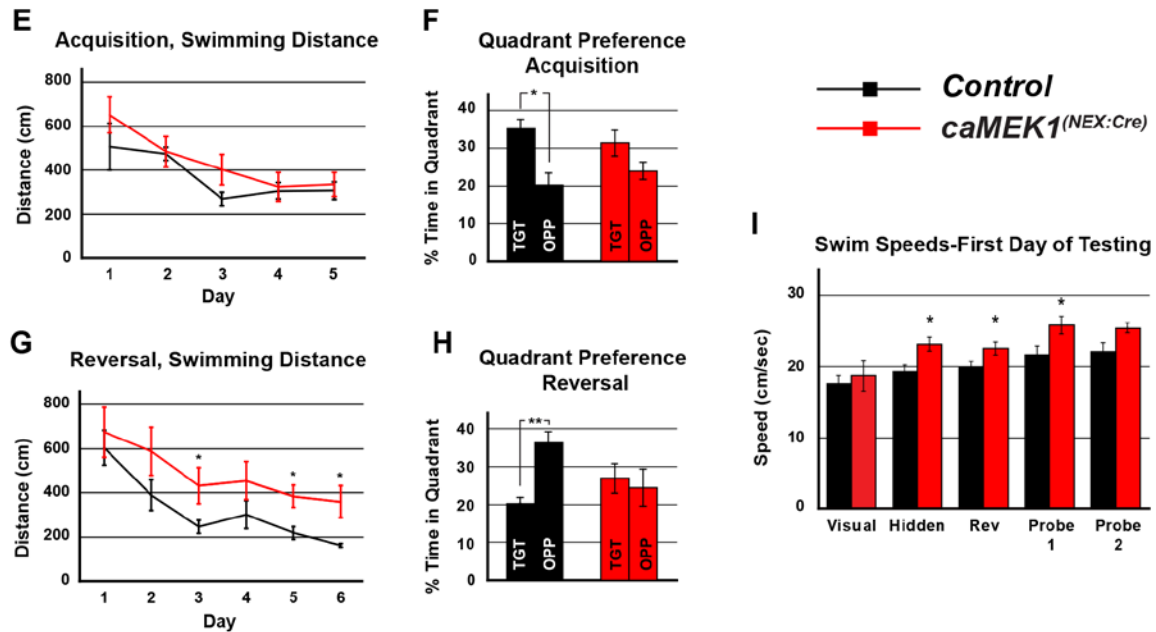
Adult Forebrain - Hippocampus



Subcortical recombination of *caMEK1* selectively affects P-ERK1/2 detection in the *NexCre/caMek1* mice. Immunostaining of *NexCre/caMek1* and control mice revealed a lack of P-ERK detection in the granule layer of the dentate gyrus and axonal extension into the CA3 region of the hippocampus (n=3) (A-D). Additionally, a substantial increase in P-ERK1/2 detection was noted in the fimbria and the stria terminalis that contain white matter tracts originating in MEK1 hyperactivating regions (n=3) (A-D). (scale bars = 500 μ m, DG = dentate gyrus, fi = fimbria, st=stria terminalis).

Figure 28.

Morris Water Maze Performance



Subcortical recombination of *caMEK1* selectively affects P-ERK1/2 detection in the *NexCre/caMek1* mice. Hidden platform test in the Morris water maze indicated similar spatial learning in the *NexCre/caMek1* and control mice with no genotype differences detected (controls $n=10$, *NexCre/caMek1* $n=8$) (E). In the probe trial following acquisition, no effect of genotype was found controls $n=10$, *NexCre/caMek1* $n=8$). However, only the control mice showed a higher percent of time in the target quadrant (within genotype analysis [$F(1,9)=8.83$, $p=0.016$], $n=10$) while the *NexCre/caMek1* mice showed no significant preference, $n=8$) (F). In the reversal phase, only the control mice reached the criterion for learning (controls $n=10$, *NexCre/caMek1* $n=8$). During this phase, the *NexCre/caMek1* mice had significantly longer swim paths than the control mice (controls $n=10$, *NexCre/caMek1* $n=8$) (G). In the probe trial following reversal, the control mice displayed a shift in quadrant preference to the new location (within genotype analysis [$F(1,9)=14.39$, $p=0.004$], repeated measures ANOVA, $n=10$). The *NexCre/caMek1* mice however failed to show any quadrant preference (H). *NexCre/caMek1* mice displayed significantly increased swim speeds on the first days of acquisition and reversal training, and during the acquisition probe trial (main effect of genotype, $F(1,15)=4.56$, $p=0.0497$, and phase of testing, $F(4,60)=21.06$, $p<0.0001$], post-hoc tests following repeated measures ANOVA, controls $n=10$, *NexCre/caMek1* $n=8$) (I).

Discussion

The ERK/MAPK signaling pathway is perhaps the most studied cellular signaling pathway to date. The majority of this research however has been performed in the context of cancers and specific cell types in culture. In the field of neurodevelopment and neurodevelopmental syndromes however, there is a lack of knowledge regarding the effects of aberrant ERK/MAPK signaling within a biological system. This absence is particularly noticeable concerning the formation and maintenance of cell-type specific connectivity under normal and syndromic conditions. In this study, we have identified the effects of hyperactivating MEK1 in the ERK/MAPK signaling pathway on the development of cortical glutamatergic axonal outgrowth and plasticity associated genes and its effect on motor learning acquisition.

caMEK1 hyper-phosphorylates axonal but not somal ERK

The classic RAS/MAPK signaling pathway ends with the dual phosphorylation of ERK1/2 at tyrosine and threonine residues. Phosphorylated ERK (P-ERK1/2) then acts upon several substrates within the cytosol, the nuclear membrane, and in the case of neurons, axons, dendrites and synaptic boutons. Substrates that are affected by P-ERK1/2 include cytoskeletal elements, cytoplasmic kinases, nuclear substrates, membrane proteins, and even upstream components of its own signaling chain. In the cytosol and nucleus, P-ERK1/2 is dephosphorylated or sequestered by dual specificity phosphatases (DUSPs). It is currently unclear whether this same method of deactivation is present in the axonal or dendritic compartments of the neuron.

This current investigation involves the use of Cre-Loxp recombination to conditionally activate a constitutively active MEK1 construct (caMEK1) to hyper phosphorylate ERK1/2 specifically in cortical glutamatergic neurons. Transcription of

caMEK1 is controlled by the NEUROD6 promoter which initially begins being transcribed in post-mitotic glutamatergic neurons at approximately E11.5. We began by testing for production of the caMEK1 construct at E14.5 by immunohistochemical (IHC) analysis of the cortex and Western Blotting of whole cortical lysates. Western Blot results indicated a robust production of caMEK1 accompanied by a significant upregulation of P-ERK1/2 at this embryonic stage. IHC analysis of the embryonic cortices showed a high level of P-ERK1/2 localized to the trailing processes of the nascent glutamatergic neurons but no clear evidence of enrichment in the somal bodies. In Western Blots of adult mouse whole cortical lysates however, caMEK1 detection remained at significantly increased levels and P-ERK1/2 surprisingly showed no differences in detected levels. IHC examination of the adult caMEK1 mice however revealed an extremely high level of P-ERK1/2 detection in the axonal compartments coupled with very little P-ERK1/2 detection in the somas. This finding was surprising and contrary to our expectations of hyper-phosphorylation of ERK1/2 being detectable in all areas of the affected glutamatergic neurons. At this point we speculated that the early hyper-phosphorylation of ERK may have led to an upregulation of DUSP6 which is a P-ERK1/2 specific phosphatase. Western Blots and immunostaining however showed no evidence of upregulated DUSP6. There are several more phosphatases, pathway feedback mechanisms, and cellular transport systems specific to the regulation of P-ERK1/2 to investigate in future investigations.

In our previous investigations, we found that the loss of MEK1/2 signaling in cortical glutamatergic neurons led to early cell death in the mutated neurons and the mice were not viable past approximately P21. The MEK1/2 loss-of-function (LoF) cell death was most notably evident in layer V CTIP2⁺ sub-cerebral projection neurons (SCPNS) and temporally followed disruption of cortico-spinal tract axonal extension. Here, in comparison, we found that the hyperactivation of MEK1 disrupts the

phosphorylation of ERK1/2 in the somas, greatly enhances P-ERK1/2 detection in axons, disrupts the elongation of the cortico-spinal tract, but does not lead to cell death. Most importantly though, these mice are viable long term thus allowing for further connectivity analysis and behavioral testing as adults. The comparison between our previous LoF MEK mice and the apparent down-regulation of somal expression of P-ERK1/2 in the caMEK1 mice leads to some interesting questions. Is there a basal level of P-ERK1/2 operating or necessary in the glutamatergic neuron necessary to support cell survival? Does the upregulation of P-ERK1/2 in the axon regulate or conduct survival cues independent of the RAS/MAPK pathway to the soma and nucleus? Further work with the Nex:CRE/caMEK1 model will be necessary to elucidate the specific nuances in this surprising compartmentalization effect of P-ERK1/2.

Key synaptic plasticity and immediate early gene ARC is downregulated

In addition to the somal down-regulation of P-ERK1/2 in the caMEK1 mice, Western Blots of whole cortical lysates also revealed a significant reduction in activity-regulated cytoskeleton-associated protein (ARC). IHC analysis of basal state adult mouse cortices showed that this reduction is primarily detected in the soma with the dendritic compartment showing robust levels in both the control and caMEK1 mice. When stimulated with physical activity on the rotarod, ARC detection by IHC in the cortex becomes more pronounced in the caMEK1 mice yet still does not reach the level of ARC expression in activity stimulated control mice or even the basal state control mice. IHC detection of P-ERK1/2 in the activity induced mice revealed no changes in expression levels over basal caMEK1 mice.

The amount of ARC detected in the soma and dendrites of the glutamatergic neurons in the caMEK1 mice reveals that a basal level of *Arc* is both transcribed and

translated. However, it is unknown what level of either *Arc* mRNA or ARC protein in our mutants can be attributed to P-ERK1/2 in either the somal or dendritic compartment. Several reports of the transcriptional dependence of *Arc* transcription on P-ERK1/2 in cultures and in hippocampal *in vivo* studies suggest that P-ERK1/2 is required for *Arc* transcription in general or *Arc* transcription above a basal level. Due to extensive pathway convergence and cross-talk, it is unclear if our data would suggest that *Arc* is transcribed at a basal level or that the caMEK1 affected neurons contain a basal level of P-ERK1/2 to activate transcription of *Arc*. Further detailed studies would need to be performed to describe fully ARCs dependence on this caMEK1 mutation.

Long range axonal connectivity is disrupted

We previously found deficits in axonal elongation of the cortico-spinal tract and arborization in the gray matter of the spinal cord and the hindbrain in the *Nex:CRE/caMEK1* mice (Xing et al. 2016). In this current study, we describe a surprising change in the levels of P-ERK1/2 in the soma and the axons of the cortical glutamatergic neurons of the *Nex:CRE/caMEK1* mice as well as reduced expression of select immediate early genes. Additionally, in this current study, we further analyzed axonal innervation deficits by analyzing corticocortical and corticostriatal axonal innervation and branching patterns.

The analysis of corticocortical and corticostriatal innervation was performed by injecting an AAV virus that expresses a CRE dependent tdTomato construct in a single hemisphere of the primary motor cortex. The AAV injections were performed at P1 and all analysis was performed at P30. Analysis of the contralateral cortex and dorsal striatum allowed the precise quantitation of axonal innervation and branching in the *Nex:CRE/caMEK1* mice. Our analysis found a significant reduction of axonal

innervation in both the contralateral motor cortex and the dorsal striatum. A significant reduction of tubulin beta 3 class III (TUBB3) in Western Blots of whole cortical lysates in the adult *Nex:CRE/caMEK1* mice was also detected which supports the finding of reduced axonal innervation. Unlike the loss-of-function mice in our previous paper, we detected no loss of cortical glutamatergic neurons in the *Nex:CRE/caMEK1* mice (Xing et al. 2016). While we can attribute the axonal deficits to the mis-regulation of P-ERK1/2 in general, it is unclear at this point whether it is the apparent low levels of P-ERK1/2 in the soma, or the high levels of P-ERK1/2 within the axons that is the main element of these deficits. Considering the high complexity of ERKs involvement in the axonal growth program; neurotrophin induced axon assembly (Atwal et al. 2000), ERKs links to microtubule associated proteins 1 and 2 (MAP1 and MAP2) (Ray and Sturgill 1987; Goold and Gordon-Weeks 2005), ERK regulation of actin filaments (Atwal et al. 2003), growth cone local protein regulation by ERK (Campbell and Holt 2003), and not least of all ERKs influence on gene transcription, further work will be needed to elucidate the exact cause or causes of these findings.

Motor learning acquisition is disrupted

With the discovery of these specific axonal extension, innervation, and branching deficits and the findings of the IEG ARC disruptions, we next subjected the mutant and control mice to motor learning acquisition testing. We began with the open field test to determine if overall motor function was impaired. The *Nex:CRE/caMEK1* mice showed no difference from control mice for voluntary motor function in total distance traveled or in center time in the open field. This finding indicated that the *Nex:CRE/caMEK1* mice did not have any physical impediments to voluntary motor function.

The *Nex:CRE/caMEK1* mice were also subjected to an elevated plus maze test to test for any anxiolytic-like phenotypes. In general, it is reported that individuals with a RASopathy, especially NF1 and CS patients, are at a higher risk for anxiety disorders. This anxiety type may not be due to a personality shift or driven by neuroticism, but is suggested that it may be a distinct subtype of anxiety (Bizaoui et al. 2018). Our results indicated that the *Nex:CRE/caMEK1* showed no anxiolytic-type behavior and actually made significantly more entries into the open arms and spent significantly more time on the open arms of the maze. To make any determination concerning an anxiety-like phenotype of any kind in this mouse model, much more specific behavioral tests should be performed.

Accelerating rotarod testing for motor testing acquisition showed a surprising set of results for the *Nex:CRE/caMEK1* mice. The mice were significantly better at performing on the rotarod than the control mice in initial performance. We theorized that this result was caused by the smaller size of the *Nex:CRE/caMEK1* mice allowing them to better balance on the rotating rod than the larger control mice. In order to negate any effects of size differences between the mutant and control mice, we subjected the mice to a skilled reaching and grasping task. In this task, the *Nex:CRE/caMEK1* mice showed no ability to improve over the course of the trial. In fact, their ability to succeed in this task actually dropped over the course of the trial. These results for the *Nex:CRE/caMEK1* mice indicate deficits in motor learning acquisition such as seen in the RASopathies.

ChAT:Cre/caMEK1 mice (Rossi et al. 2011) were also subjected to the open field and accelerating rotarod. This allowed for the analysis of motor learning acquisition due to the hyperactivating mutation on lower motor neurons. Within some of the RASopathies, common neurological issues include motor development delays and deficits and motor skill deficits associated with learning and cognition.

Open field analysis of the *ChAT:Cre/caMEK1* mice revealed a significant deficit in total distance traveled when compared to control mice with no difference in center time. However, testing on the accelerating rotarod revealed no difference between mutant and control mice indicating the open field results to be a voluntary motor issue. Both the mutants and controls significantly improved their performance over the course of the test indicating no impairments in motor skill acquisition. These tests indicated that *caMEK1* mutations in cholinergic lower motor neurons have little to no effect on motor behaviors.

Recombination of the *caMEK1* construct in the *Nex:CRE/caMEK1* mice also affected regions of the hippocampus. This allowed us to test the *Nex:CRE/caMEK1* mice for associative and spatial learning in the Morris water maze. No significant differences were found between the mutants and controls in the acquisition phase as measured by swimming distance. However, in the probe trial following acquisition, the *Nex:CRE/caMEK1* mice failed to establish a quadrant preference with the platform removed. In the reversal phase, there was also a significant difference between the *Nex:CRE/caMEK1* and control mice in learning the new placement of the hidden platform. In the probe trial following reversal learning, the *Nex:CRE/caMEK1* mice again failed to establish a quadrant preference. It is interesting to note that again the *Nex:CRE/caMEK1* mice outperformed the control mice in swimming speed. These results indicate a deficit in associative and spatial learning in the *Nex:CRE/caMEK1* mice due to the *caMEK1* mutation.

Conclusion

Our results here are the first to detect a compartmentalization effect of P-ERK1/2 by a hyperactivating MEK1 mutation in a mammalian system. This work further defines that the axonal extension aberrations as well as the learning phenotypes described here, stem from within a single cell type indicating a cell-autonomous effect.

These results provide a basis for further examination of current clinical treatments of RAS/MAPK activating mutations. Furthermore, the down-regulating effect on detectable P-ERK1/2 within the somas questions a crucial aspect of clinical treatment of RASopathic genetic mutations. Is the treatment of an activating RAS/MAPK mutation by administering MEK inhibitors to ameliorate physical symptoms of the disease worsening the symptoms of the neurodevelopmental aspects of the disease? Can the neurodevelopmental symptoms be treated separately or even shielded in some way from the physiological treatments available? Is it possible or feasible to treat separate compartments of a single cell (i.e. cell body versus the axon versus the dendrite)? Further *in vivo* testing is needed to address these issues and to help develop effective strategies in treatment for the ongoing neurological symptoms of the RASopathies.

Acknowledgments

We wish to thank Noah Fry, Becca Reinking-Herd, and Sarah Bjorklund for their technical assistance.

Contributions

Viral and Dil injections:

George Reed Bjorklund.

Tissue prep and Immunolabeling:

George Reed Bjorklund, Sarah Bjorklund and Becca Reinking-Herd.

Image analysis and quantitation:

George Reed Bjorklund and Jason M Newbern.

Western Blotting:

George Reed Bjorklund.

Experimental conception and design:

George Reed Bjorklund and Jason M Newbern.

Behavioral analysis:

George Reed Bjorklund, Sheryl Moy, Lauren Hewitt, and Kenji Nishimura

Drafting or revising the article:

George Reed Bjorklund.

CHAPTER 4

CORTICAL LAYER SPECIFICITY IN A GAIN-OF-FUNCTION

CAMEK MOUSE MODEL

**Hyperactivation of MEK1 in cortical glutamatergic neurons results in
projection axon deficits and aberrant motor learning
in a layer autonomous manner**

Abstract

Germline mutations within the components of the RAS-RAF-MEK-ERK (RAS/MAPK) pathway form a group of neurodevelopmental disorders collectively known as RASopathies. A large portion of these mutations result in an upregulation of signaling. Previously we have described that a cell-type specific MEK1 hyperactivating mutation leads to significant axonal connectivity issues and deficits in motor learning acquisition in a biological system. Here, we used cre-loxp technologies to hyperactivate the RAS/MAPK pathway in cortical glutamatergic neurons in a layer specific manner to affect only cortical layer 5. We have identified significant deficits in corticocortical, and corticostriatal axonal innervation and branching and a significant reduction in the expression of the immediate early gene ARC in a cell and layer autonomous manner. Unlike MEK1 hyperactivation of glutamatergic neurons across all cortical layers, layer 5 specific hyperactivation does not lead to motor learning deficits. These data reveal specific cortical layer requirements for RAS/MAPK signaling during development for axonal innervation and connectivity and further indicate that behavioral plasticity depends upon RAS/MAPK expression in cortical projection neurons other than layer 5.

Introduction

Previously, we reported a critical requirement for RAS/MAPK signaling in loss- and gain-of-function as it applies specifically to cortical pyramidal neurons (Xing et al., 2016). Deletion of *Map2k1/2* (*Mek1/2*) in cortical glutamatergic neurons resulted in the absence of large CTIP2⁺ neurons in cortical layer 5 and the impairment of corticospinal tract (CST) axonal extension in the dorsal funiculus of the cervical and lumbar spinal cord (Xing et al., 2016). Up-regulation of ERK/MAPK signaling in cortical glutamatergic neurons also decreased CST axonal elongation but markedly increased axonal branching in the gray matter of the spinal cord and the gray matter of the hind brain (Xing et al., 2016). The hyperactivating mutations also created a paradoxical change in the expression patterns of cellular P-ERK1/2. In the axonal compartment of the cortical glutamatergic neurons we detected a high level of P-ERK1/2 while the somas contained a highly reduced expression level. Furthermore, corticocortical and corticostriatal axonal innervation was significantly reduced and indications of motor learning acquisition deficits were found upon hyperactivation of MEK1.

In this study we have employed an *Rbp4:Cre* mouse crossed with the *caMek1* mouse to restrict *Mek1* over-expression to layer 5 glutamatergic neurons. The layer 5 specific hyperactivation will address specifically any layer autonomous effects with CST extension and further delineate the previous cell-type autonomous effect that was detected in the *Nex:CRE/caMEK1* mice. An *NF1* conditional knock-out mouse model was also used to further assess CST elongation phenotypes. The *NF1* conditional knock-out mouse is thought to more closely replicate the human condition in a cell-specific manner (Gutmann and Giovannini 2002). The use of these conditional genetic tools will allow the analysis of cell specific effects and contributions to the pathologies reported in RASopathy patients.

Analysis of contralateral cortical projections and cortico-striatal projections revealed a significant decrease in axonal innervation and branching while corticobulbar projections showed little change in the hindbrain. Much like the *Nex:Cre/caMek1* mouse however, there was a significant decrease in CST elongation in the cervical and lumbar spinal cord and a significant increase in axonal branching in the spinal cord gray matter. Behavioral testing of the *Rbp4:Cre/caMEK1* mice showed no gross motor defects but did display an apparent deficit in voluntary locomotor function. However, unlike the *Nex:Cre/caMek1* mice, the *Rbp4:Cre/caMEK1* mice showed no deficits in motor learning and acquisition. Furthermore, reduction of activity regulated gene expression appeared localized to layer V with no apparent effect on other regions. These results indicate that layer V hyperactivation of MEK1 is sufficient to cause the deficits detected in long range glutamatergic axonal projections. However, layer V hyperactivation is not sufficient to cause the motor learning acquisition disruptions as detected in the *Nex:Cre/caMek1* mice indicating behavioral plasticity depends upon RAS/MAPK expression in cortical projection neurons other than layer 5.

Materials and Methods

Transgenic Mice

All animal experiments were performed in accordance with established procedures approved by the Institutional Animal Care and Use Committee of Arizona State University and NIH guidelines for the use and care of laboratory animals. Mice used in this work were of a mixed genetic background and housed in standard conditions. The mice were kept on a 12-hour light/dark cycle with food and water provided ad libitum. Each experiment was replicated a minimum of three times using littermates or mice from independent litters. No detectable effects on the phenotypes described in this manuscript were observed from Cre expression alone. Therefore, Cre-expressing or Cre-negative mice were used as controls. *Map2k1*^{s217/222} mice were furnished by Dr. Maïke Krenz and Dr. Jeffrey Robbins (Krenz et al., 2008). *Rbp4:Cre* mice were purchased from the Mutant Mouse Resource & Research Centers (RRID:MMRRC_036400-UCD).

Tissue Preparation

Transcardial perfusions were performed on mice using a 4% paraformaldehyde/PBS solution with dissected brains being post-fixed in the same solution overnight at 4°C. Dissected brains were then serially incubated in 15% and 30% sucrose/PBS solutions prior to embedding in Tissue-Tek O.C.T. (Tissue-Tek 4583) and freezing. Cryostat sectioning was performed with sections being collected on Fisherbrand Superfrost/Plus slides (Fisher Scientific 12-550-15) and air-dried prior to staining. Alternatively, cryostat sections were collected in well plates with cold PBS for free-floating staining as appropriate. For some experiments, brains were mounted in agarose after post-fixation in preparation for vibratome sectioning.

Viral Injections

P1 pups were removed from their home cage as a group and were individually cryo-anesthetized on ice for 4-6 minutes. Viral injections were then performed immediately with 50-80nl of solution using a 32-gauge beveled needle fitted to a Hamilton 5µl neuro syringe mounted on a stereotaxic arm. After injections, pups were placed on a 37°C heated surface for recovery and returned to their home cage as a group. Adeno Associated Viral vectors, RAAV9/AAV-Flex-tdTomato and RAAV8/CAG-Flex-tdTomato were purchased from the UNC Viral Vector Core and used for all viral tracing experiments.

Behavioral Assays

A single-pellet reaching and grasping task test was performed using male *RBP4:Cre/caMek1* mice. Mice were mildly food restricted throughout training to maintain at least 90% of their baseline weight which amounted to free feeding between 2 and 6 hours daily. Sucrose pellets (TestDiet 1811555) were used for this test and the mice were acclimated to the pellets in their home cages. After pellet acclimation, mice were then placed in an acrylic chamber 15cm X 10cm X 20cm, with pellets either singly or in pairs depending on their housing for further acclimation. After acclimation, forelimb dominance was determined by placing a single pellet on the food platform (10cm high) outside a single slit (5cm wide) in one end of the test chamber. Once a mouse has conducted at least 20 reaching attempts within 20 mins with at least 70% of those reaches made with one hand, that mouse was moved on to testing. Testing consisted of placing a single pellet on the food platform in front of the slit, right or left, corresponding with the preferred paw. Testing was performed for 10 minutes daily for 5 days. Scoring was performed as follows; Success: if the mouse reached with its preferred paw, retrieved the pellet, and fed the pellet into its

mouth. Drop: If the mouse grasped the pellet but drops it before reaching its mouth. Fail: If the mouse reached for the pellet but failed to grasp it or knocked it out of position. Mice were scored on the rate (metric/attempts) for each of these metrics.

Open field testing was performed in an open top opaque plexiglass box measuring 38cm X 38cm X 30cm. The area within the box is illuminated by a single 40-watt spotlight approximately 2 meters overhead and centered within the area. Recording of mouse movements is done using a Microsoft LifeCam or Logitech HD Webcam and VirtualDub video capture software. Open field quantitation was performed using the MouseMove (Samson et al. 2015) plugin for ImageJ (Schindelin et al. 2012).

Rotarod analysis for the *RBP4:Cre/caMEK1* mice was performed using a San Diego Instruments Rotor-Rod. Prior to testing, mice were habituated by being placed on an approximately 5.0cm diameter foam roller followed by the standard 3.175cm diameter knurled plastic rollers. The mice were allowed three attempts on each rod to reach 180 seconds on the foam rollers and 90 seconds on the plastic rollers. All habituation is performed at a constant 4 RPMs. Rotarod testing is performed starting the first day following habituation. The mice are placed on the plastic rollers and the machine measures the latency to fall under accelerating conditions from 4 RPMs to 40 RPMs for a maximum of 5 minutes. The testing period consisted of three trials per day for 5 consecutive days. Mice were allowed 5-10 minutes between trials for rest.

Immunohistochemistry

Tissue sections were rinsed with PBS/0.1% Triton X-100 (PBST) and blocked with 5% normal donkey serum in PBST at room temperature for ~1 hour. Primary antibodies were diluted in PBST/5%NDS and incubated overnight at 4°C with gentle shaking. Primary antibodies used were; rabbit anti-MEK1 (Abcam ab32091), rabbit

anti-phosph-p44/42 MAPK (ERK1/2) (Thr202/Tyr204) (Cell Signalling 4370), rabbit anti-ERK2 (Abcam ab32081), rabbit anti-ARC (Synaptic Systems 156 003), mouse anti- β 3 Tubulin (TUBB3) (Biolegend 801202), rabbit anti-RFP (Rockland 600-901-379), chicken anti-RFP (Rockland 600-401-379), mouse anti-neun (Millipore Sigma MAB377), and DAPI (Sigma Aldrich 10236276001). After rinsing in PBST 3X, secondary antibodies diluted in PBST/5%NDS were added and incubated overnight at 4°C with gentle shaking. Secondary antibodies included Alexa Fluor 488, 546 or 568, and 647 conjugated anti-rabbit, anti-mouse, or anti-goat IgG (Invitrogen). Imaging was performed using a Zeiss LSM 800 laser scanning confocal microscope (LSCM), or a Leica SP5 LSCM.

Western Blotting

Cortices were collected from mutant and control mice and lysed in a buffer containing 50mM Tris-CL, 150mM NaCl, 0.1%triton x-100, Protease Inhibitor (Sigma-Aldrich P2714), and Phosphatase Inhibitor (Sigma-Aldrich P5726) either by sonication or with a syringe. Lysates were then cleared by centrifugation and total soluble protein concentrations determined by Bradford Assay using a Peirce Protein Assay Kit (Thermo Scientific 23200). Proteins were denatured in equal amounts of 2X Laemmli sample buffer (BioRad 161-0737), separated by SDS-PAGE using either 10% or 4-20% Mini-PROTEAN TGX precast gels (BioRad 456-1035 and 456-8095), then transferred to PVDF membranes (BioRad 162-0177). Membranes were blocked with 5% non-fat dry milk (NFDM) in TBS with 0.5% Tween (TBST) for 1 hour at room temperature followed by overnight incubation at 4°C with primary antibodies in 5% bovine serum albumin. Primary antibodies used were; rabbit anti-MEK1 (Abcam ab32091), rabbit anti-phosph-p44/42 MAPK (ERK1/2) (Thr202/Tyr204) (Cell Signalling 4370), rabbit anti-ERK2 (Abcam ab32081), rabbit anti-ARC (Synaptic

Systems 156 003), rabbit anti-GAPDH (Cell Signalling 2118), goat anti β -Actin (Cell Signaling 8457), and rabbit anti- β actin (Cell Signalling 8457). Secondary antibodies used were anti-rabbit HRP and anti-goat HRP (Jackson Immunoresearch 711-035-152 and 705-035-147). Membranes were then washed in TBST and incubated with HRP-conjugated secondary antibodies in 5% NFDM/PBST for 1 hour at room temperature. Membranes were washed in TBST, developed with Pierce ECL Western Blotting Substrate (Thermo Scientific 32106), and exposed to radiographic film (Thermo Scientific 34089).

Quantification of Western Blots was performed using a high-resolution scanned image of the exposed radiographic film in a grayscale TIFF file format. The file was then transferred to Imagej where a region of interest was created to encompass individual bands for all mutant, control and loading control samples. The mean gray value of each band was then recorded along with a background measurement for each band. All values were inverted (subtracted from 255) and the background values were subtracted from the band values. The net band values were then reported as a ratio of net band value over net loading control value.

Image Analysis and Quantitation

For quantitation of axonal innervation and branching in the cortex and striatum, a radial section of the cortex encompassing all layers within the primary motor cortex was used. A minimum of 4 sections from each mutant and control animal centered about the rostral-caudal area of the injection site was analyzed. The area in μm^2 of this region was measured in Photoshop and the image was then transferred to Imagej. Once in Imagej, pixel intensities were adjusted using the Otsu Auto Threshold component, total pixels counted, and multiplied by the images pixel size to obtain the total μm^2 of pixels in the ROI. The total μm^2 was then divided by

the number of transfected cells that were manually counted in an identical ROI in the ipsilateral (RFP injected) cortical hemisphere to obtain the axonal labeling per transduced cell. Spinal cord arborization was measured in the same manner except the μm^2 of pixels was normalized to the CST to obtain a spinal cord arborization ratio.

The CBT was measured using at least three anatomically matched hind brain sections from each mutant and control animal. The CBT was outlined using the difference of appearance in NEUN or DAPI and the image was transferred to Imagej. A pixel intensity threshold was manually set by an observer blinded to the genotype. The number of labeled pixels was then measured and multiplied by the images pixel size to obtain the μm^2 of pixels in the CBT. The μm^2 of pixels was then normalized to the number of transfected cells in the injection site ROI to obtain the CBT axonal labeling per transduced cell. The CST in the dorsal funiculus was measured in the same manner except the μm^2 of pixels was normalized to the CBT to obtain the CST elongation ratio.

Representative images have been cropped and adjusted for brightness and contrast in Photoshop for presentation. All images used for comparison analysis were collected using the same microscope settings and all adjustments made were done equally between images.

Statistical Analysis

Data analysis was performed using SPSS software (IBM Analytics). Statistical methods used included Student's t-test (unpaired, two-tailed), ANOVA, repeated measures ANOVA, and multivariate ANOVA. F-test results, p-values, and tests used are reported where appropriate.

Results

ERK/MAPK gain-of-function in layer V excitatory neurons reduces CST elongation and increases spinal cord axonal innervation but does not affect CBT elongation or hind brain axonal innervation

In our previous study, we found that both MEK1 loss-of function mice, *Map2k1;Neurod6-Cre*, and MEK1 gain-of-function mice, *NexCre/caMek1*, exhibited CST elongation deficiencies. The MEK1 loss-of-function mutation was lethal at ~P21 and prevented further characterization. However, the the gain-of-function *NexCre/caMek1* mouse was viable and exhibited additional deficiencies in CBT elongation and enhanced innervation and branching of the spinal cord and hindbrain (Xing et al. 2016). Our current work further defines deficits in corticocortical and corticostriatal axonal innervation and branching in the *NexCre/caMek1* mouse. At this point we wanted to further explore layer specific contributions to the abnormalities that we have documented.

Generally, callosal projection neurons (CPNs) residing in cortical layers II/III, and to a lesser extent in layers V and VI, project to mirrored areas in the contralateral cortex. Subcerebral projection neurons (SCP) from M1 project to the brainstem motor nuclei and spinal cord motor neurons (Greig et al. 2013). With our *NexCre/caMek1* deficits in mind, we wanted to test the possibility of a layer autonomous role when MEK1 is hyperactivated in layer V glutamatergic neurons only. A loss-of-function mouse designed by crossing an *Erk1^{-/-},Erk2^{fl/fl}* mouse with an *Erk1^{-/-},Erk2^{wt/fl};RBP:Cre* mouse that would specifically knock-out *Erk1/2* function in cortical layer V. Unfortunately, this appeared to be an embryonic lethal mutation even though we restricted the knock-out of *ERK1/2* function to layer V glutamatergic neurons only. Over the course of ~85 live births, no mice were born with *Erk1^{-/-},Erk2^{fl/fl};RBP:Cre* genotype when we should have expected

~21 by Mendelian ratios (1 in 4). For the gain-of-function mouse we used an *RBP4:Cre* mouse crossed with the *caMEK1* mouse (*RBP4:Cre/caMEK1*), to produce a mouse that will hyperactivate ERK/MAPK primarily in cortical layer V glutamatergic neurons. With this mouse, we employed the previously described method of using the AAV:*CAG-FLEX-tdTomato* viral vector to trace and quantify the developed axons. As previously performed on the *NexCre/caMek1* mice, the *RBP4:Cre/caMEK1* mice were injected in the primary motor cortex at P1 with a CRE dependent AAV-tdTomato with axonal extension and innervation analyzed at P30.

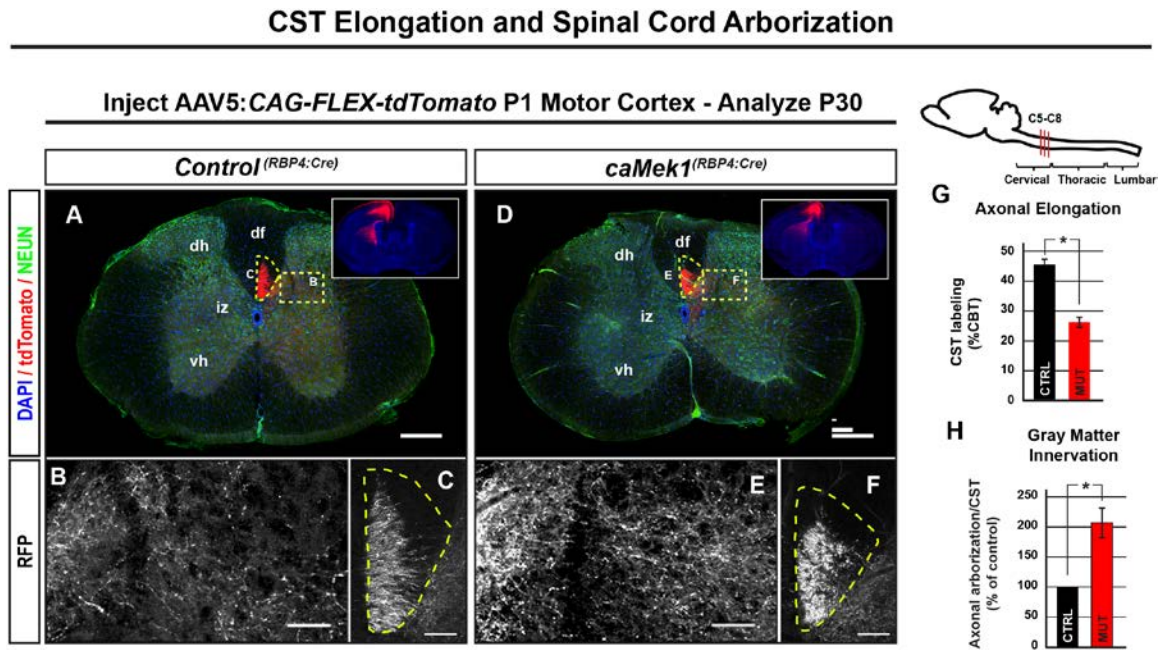
Analysis of the CBT in the *RBP4:Cre/caMEK1* mice was performed by measuring the amount of RFP labeling in the tract and normalizing to the number of tdTomato labeled glutamatergic neurons in the primary motor cortex injection site. Cell counts between the *RBP4:Cre/caMEK1* and control mice revealed no significant differences (labeled cells, *RBP4Cre/caMEK1* = 96.30 ± 10.38 SEM, n=5, control = 85.60 ± 6.12 SEM, n=5, p=0.400, Student's t-test) (Figures 32A-C). In contrast to our previous findings when hyperactivating all cortical glutamatergic neurons in the *NexCre/caMek1* mice, layer V specific hyperactivation in the *RBP4:Cre/caMEK1* mice showed no significant differences in CBT elongation when compared to control mice (CBT labeling per tdTomato labeled neuron, *RBP4Cre/caMek1* = 319.38 ± 77.74 SEM, n=4, control = 298.46 ± 38.95 SEM, n=4, p=0.818, Student's t-test) (Supplemental Figure 31D - E, H). Additionally, analysis of axonal innervation in the contralateral side of matched sections of the hindbrain in *RBP4:Cre/caMEK1* and control mice also revealed no significant differences (innervation factor, *RBP4Cre/caMek1* = 4366.57 ± 742.36 SEM, n=4, control = 5061.28 ± 1103.85 SEM, n=4, p=0.620, Student's t-test) (Supplemental Figures 31C - D, F, I).

CST elongation was determined by measuring the area and extent of labeling of the CST in the dorsal funiculus between C5 and T1 (Figures 29A, C - D, F). The

RBP4:Cre/caMEK1 mice were found to have a significantly lower amount of labeling in the CST as a percentage of labeling in the CBT (Figures 29I, L) (labeling/%CBT, *RBP4:Cre/caMEK1* 26.23 +/- 1.69 SEM, n=4, controls = 45.62 +/- 7.01 SEM, n=4, p=0.036, Student's t-test) (Figure 29G). We next measured the amount of axonal labeling in the spinal cord gray matter in relation to the white matter of the CST in the *RBP4:Cre/caMEK1* mice (Figures 29A - C, E). We found that the *RBP4:Cre/caMEK1* mice had a significant increase in the amount of axonal innervation in the ipsilateral grey matter in relation to CST elongation (arborization/CST, control = 100.00% +/- 0.00 SEM, n=4, *RBP4:Cre/caMEK1* = 206.83 +/- 24.59 SEM, n=4, p=0.015, Student's t-test) (Figure 29H). These findings show that layer 5 specific hyperactivation of MEK1 leads to a reduction in the number of axons extending down the CST yet enhances the extent of innervation (per axon) in the grey matter of the spinal cord.

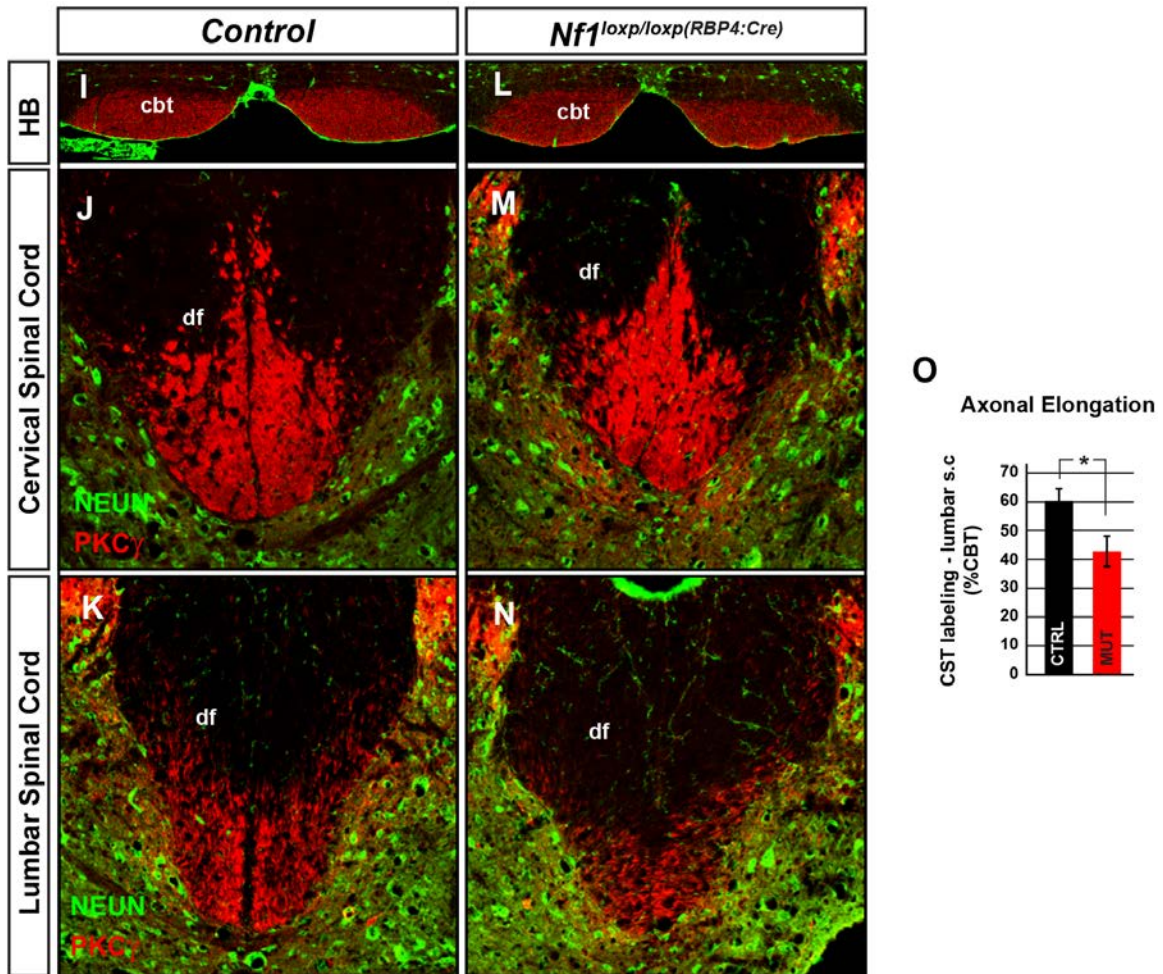
Having determined a layer V specific effect on CST elongation in the *RBP4:Cre/caMEK1* mice, we next wanted to determine if a direct mutation in the RAS/MAPK pathway would phenocopy those results. For this we used the layer V glutamatergic specific *RBP4:Cre* mouse crossed with an *NF1* mouse. The *NF1* mouse produces a mutation in the *NF1* gene that encodes neurofibromin which is a RasGAP upstream of MEK and ERK in the RAS/MAPK pathway. Neurofibromin is a GTPase-activating protein that is a negative regulator of Ras ultimately causing an upregulation in ERK/MAPK signaling. CST elongation in the *RBP4:Cre/NF1* mouse was also significantly reduced as measured in the lumbar spinal cord (Figures 30J - K, M - O). These results indicate a substantial reduction in the elongation of the CST due to the hyperactivation of MEK1 or the knock-out of *NF1* selectively in cortical layer V glutamatergic neurons.

Figure 29.



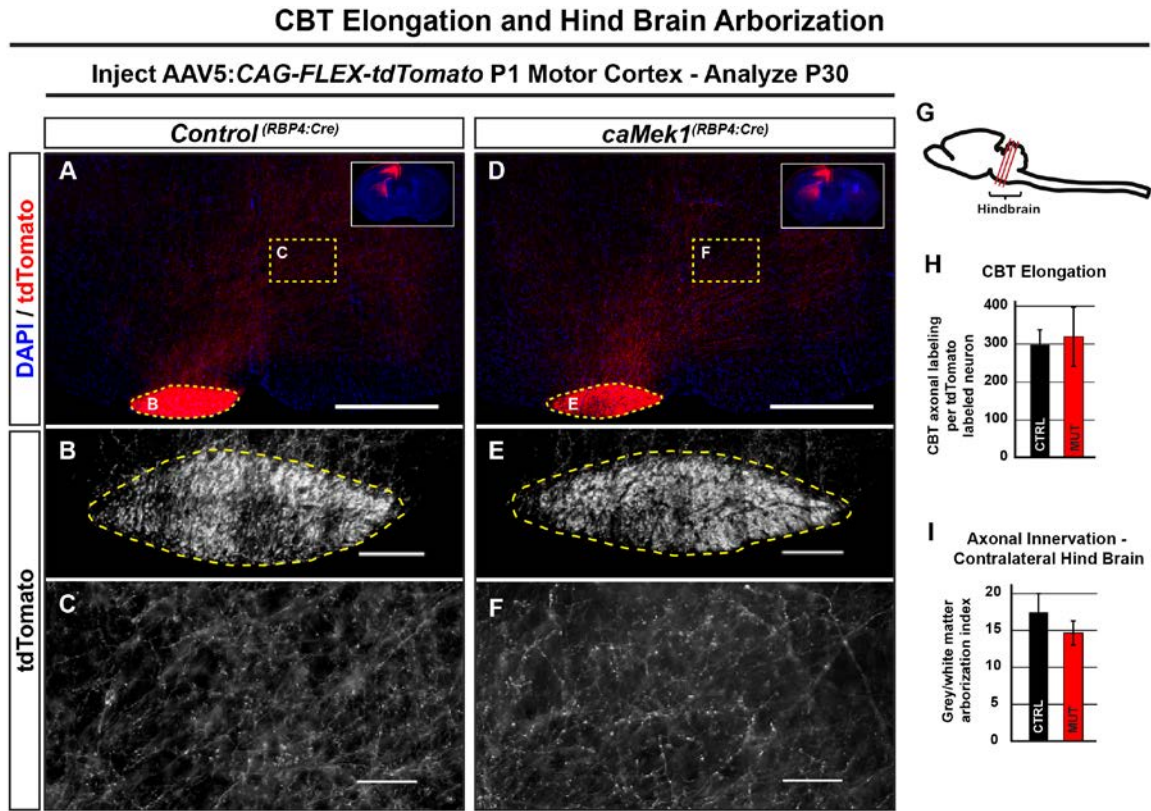
Corticospinal tract elongation is decreased but corticospinal axonal innervation is increased in layer V specific MEK1 hyperactivation. Axonal innervation of corticospinal tract elongation and innervation analysis was performed on cross sections of *RBP4Cre/caMEK1* (D-F) and control mice (A-C) cervical spinal cords. High resolution confocal microscopy shows a reduction of corticospinal axonal elongation in the dorsal funiculus of the *RBP4Cre/caMEK1* (F) when compared to control mice (C). Increased axonal innervation of spinal cord gray matter was detected *RBP4Cre/caMEK1* mice when compared control mice (B, E) (scale bars = A,D=200µm, B,E=50µm, D,F=20µm n=4, dh = dorsal horn, df = dorsal funiculus, iz = intermediate zone, vh = ventral horn). Quantification of corticospinal tract elongation revealed a significant reduction in the *RBP4Cre/caMEK1* mice when compared to control mice (labeling/%CBT, *RBP4:Cre/caMEK1* 26.23% +/- 1.69% SEM, n=4, controls = 45.62% +/- 7.01% SEM, n=4, p=0.036, Student's t-test) (G).

Figure 30.



Corticospinal tract elongation is decreased but corticospinal axonal innervation is increased in layer V specific MEK1 hyperactivation. Axonal innervation of spinal cord gray matter revealed an increase in the *RBP4Cre/caMEK1* mice when compared to control mice (axonal arborization/CST, % of control, *RBP4Cre/caMEK1* = 206.83% +/- 24.59% SEM, n=4, control = 100.00% +/- 0.00% SEM, n=4, p-value ≤ 0.0148) (H). Axonal innervation of *RBP4:Cre/NF1^{loxp/loxp}* revealed a similar reduction in CST innervation in the CBT in the hind brain (I and L), and the dorsal funiculus of the cervical spinal cord (J and M). Additionally, the dorsal funiculus of the lumbar spinal cord also showed a reduction of elongation (K and N) (LEI - n=?). CST labeling of the lumbar spinal cord was significantly reduced when measured as a % of the CBT (O).

Figure 31.



Corticobulbar tract axonal extension and hindbrain innervation not affected in the *RBP4Cre/caMek1* mice. Confocal imaging of the corticobulbar tract and axonal innervation of the hind brain revealed little to no differences between the *RBP4Cre/caMek1* (D-F) and control mice (A-C) (scale bars, A,D=500 μ m, B,E=100 μ m, C,F=50 μ m). Quantification of tdTomato labeled axons in the corticobulbar tract revealed no significant differences between the *RBP4Cre/caMek1* and control mice (CBT labeling/tdTomato labeled neuron, *RBP4Cre/caMek1* = 319.38 \pm 77.74 SEM, n=4, control = 298.46 \pm 38.95 SEM, n=4, p=0.818, Student's t-test) (H). Axonal innervation of the hind brain also revealed no significant differences between the *RBP4Cre/caMek1* and control mice (innervation factor, *RBP4Cre/caMek1* = 4366.57 \pm 742.36 SEM, control = 5061.28 \pm 1103.85 SEM, n=4, p=0.620, Student's t-test) (I).

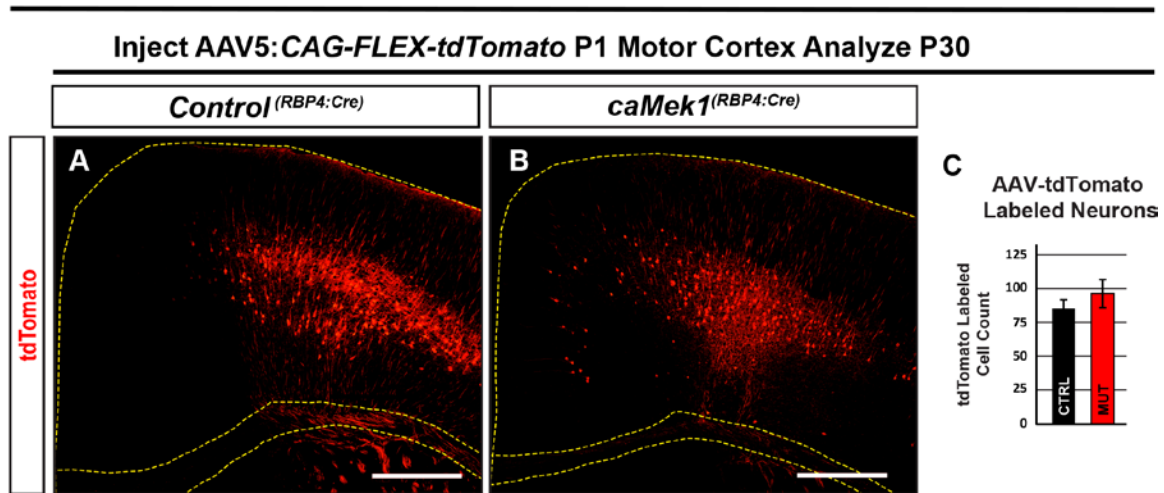
Hyper-activation of ERK/MAPK in layer V excitatory neurons significantly reduces contralateral axonal innervation and contralateral striatal innervation

By using a layer V specific mouse model to hyperactivate MEK1, we expected to find little to no change in the axonal projections and branching patterns in the contralateral primary motor cortex and contralateral dorsal striatum. To test this, we analyzed high resolution confocal images of serial sections of the forebrains of the *AAV:CAG-Flex-tdTomato* injected P30 *RBP4:Cre/caMEK1* and control mice. Axonal labeling was measured in the primary motor cortex and the dorsal ventral to medial ventral area of the striatum. These measurements were normalized to the area measured and the number of transfected cells in the contralateral injection site.

As in the *NexCre/caMek1* mice, we controlled the injection area in both the rostral-caudal and medial-lateral position (Figure 32A-B). Labeled cell counts in the primary motor cortex of the injected hemisphere showed no significant differences between the *RBP4Cre/caMEK1* and control mice (labeled cells, *RBP4Cre/caMEK1* = 96.30 ± 10.38 SEM, n=5, control = 85.60 ± 6.12 SEM, n=5, p=0.400, Student's t-test) (scale bars = 500 μ m) (Figure 32C). Contralateral cortical innervation labeling in the *RBP4:Cre/caMEK1* mice was significantly reduced when compared to control mice (axonal labeling/transduced cell, *RBP4Cre/caMEK1* = 173.21 ± 15.20 SEM, n=5, control = 234.83 ± 14.69 SEM, n=5, p=0.019, Student's t-test) (Figures 33D, G, H, K, M). Contralateral dorsal striatum labeling was also significantly reduced in the *RBP4:Cre/caMEK1* mice when compared to controls (axonal labeling/transduced cell, *RBP4Cre/caMEK1* = 89.54 ± 18.69 SEM, n=5, control = 189.82 ± 20.67 SEM, n=5, p=0.007, Student's t-test) (Figures 33 - F, I, J, N). These results indicate that ERK/MAPK is necessary for corticocortical and corticostriatal innervation by cortical layer V glutamatergic axonal extensions irrespective of all other cortical layers.

Figure 32.

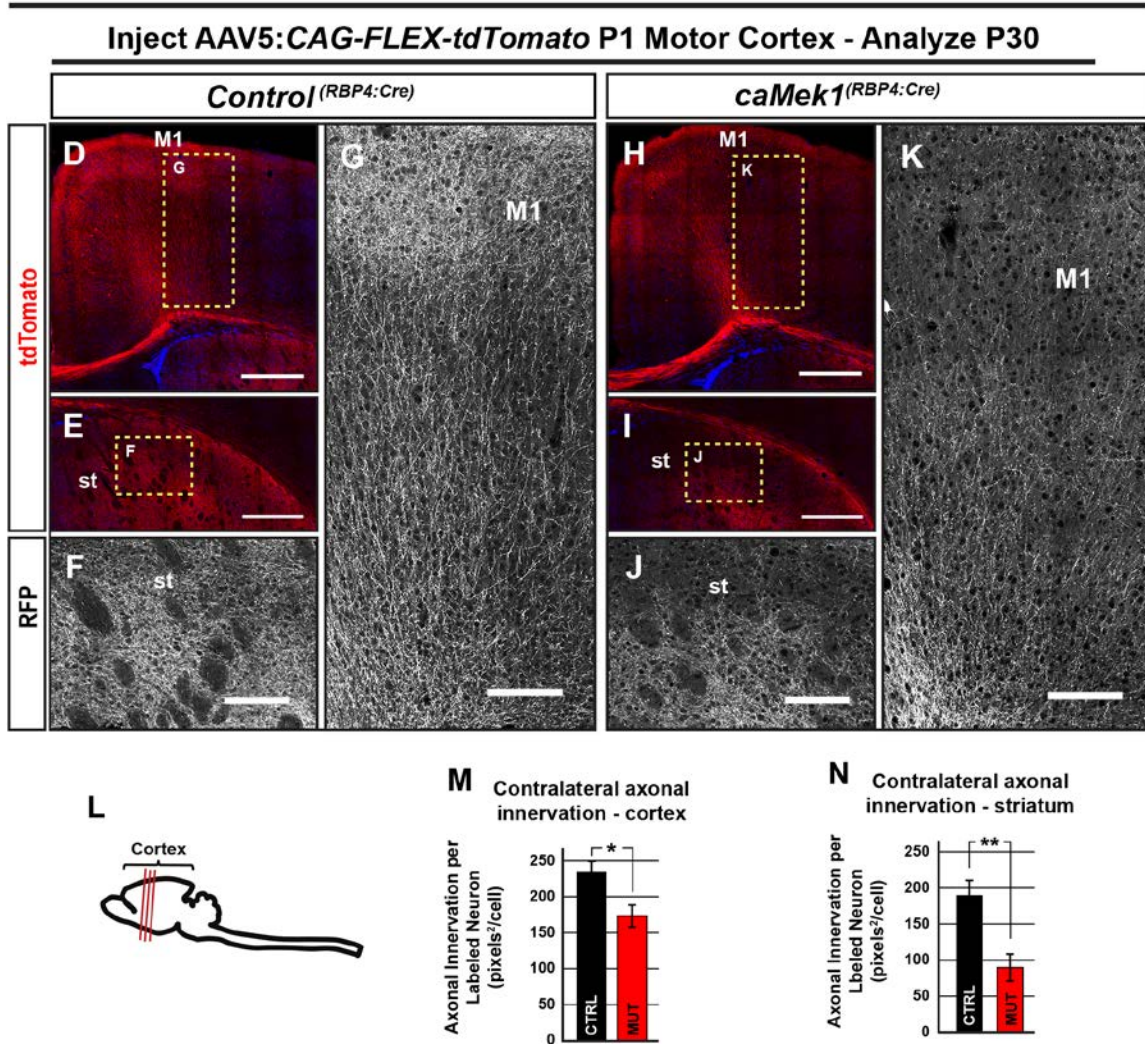
AAV Labeled Neurons



Corticocortical and corticostriatal innervation and branching is reduced in a layer V autonomous manner. To analyze corticocortical and corticostriatal innervation and branching, *RBP4Cre/caMEK1* and control mice were injected at P1 in the primary motor cortex with an AAV: *CAG-Flex-tdTomato*. Contralateral primary motor cortex and dorsal striatum were analyzed at P30 to determine the amount of labeling in axonal innervation and branching. Injection locations were controlled in both the medial-lateral and rostral-caudal positions (A-B) (scale bars = 500 μ m). Labeled cell counts in the primary cortex region showed no significant differences between the *RBP4Cre/caMEK1* and control mice (labeled cells, *RBP4Cre/caMEK1* = 96.30 ± 10.38 SEM, n=5, control = 85.60 ± 6.12 SEM, n=5, p=0.400, Student's t-test) (scale bars = 500 μ m) (C).

Figure 33.

Corticocortical and Corticostriatal Innervation



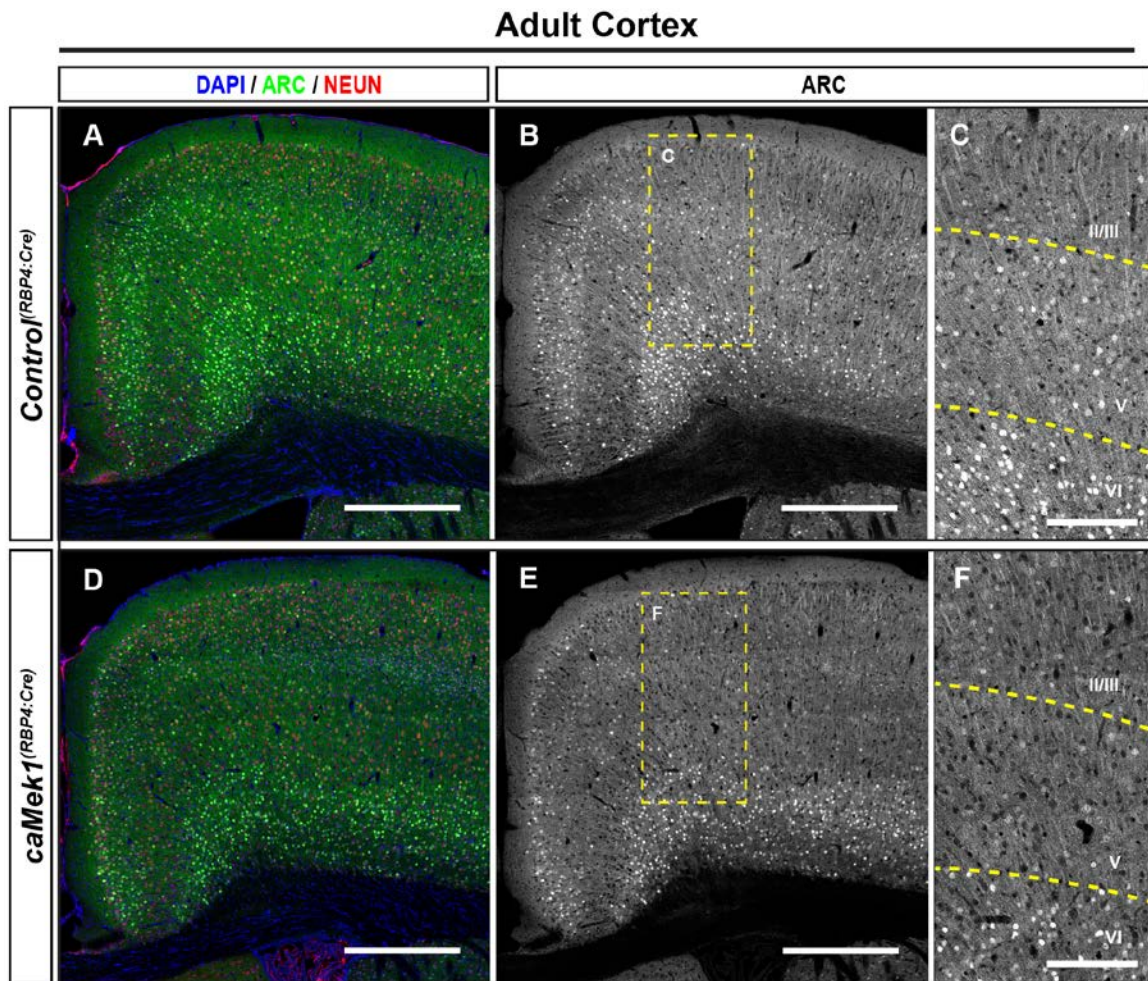
Corticocortical and corticostriatal innervation and branching is reduced in a layer V autonomous manner. Representative samples of diminished tdTomato labeling in the contralateral cortex and dorsal striatum of the *RBP4Cre/caMEK1* mice (H-K) compared to control mice (D-G) (scale bars = D,E,H,I = 500µm, F,G,J,K=150µm, n=5, M1 = primary motor cortex, st = striatum). A significant reduction of tdTomato labeled axons from contralateral layer V glutamatergic neurons was detected in the cortex of the *RBP4Cre/caMEK1* mice when compared to controls (axonal labeling/transduced cell, *RBP4Cre/caMEK1* = 173 ± 15.20 SEM, control = 235.00 ± 14.69 SEM, n=5, p=0.019, Student's t-test) (M). A significant reduction was also detected in the dorsal striatum of the *RBP4Cre/caMEK1* (axonal labeling/transduced cell, *RBP4Cre/caMEK1* = 90.00 ± 18.69 SEM, control = 190.00 ± 20.67 SEM, n=5, p=0.007, Student's t-test) (N).

ARC protein levels are selectively affected by MEK1 hyperactivation in layer V cortical glutamatergic neurons

Having detected reduced levels of ARC in all glutamatergic neurons in the *NexCre/caMek1* mice cortices, we wanted to see if the effects of hyperactivating MEK1 solely in layer V or if there is an effect on other layers also.

IHC analysis of basal state *RBP4:Cre/caMEK1* mice revealed a localized down-regulation of ARC protein detected in layer V when compared to control mice (Figure 34A-F). These data show that hyperactivating MEK1 solely in layer V glutamatergic neurons has little to no effect on ARC detection in other layers.

Figure 34.



ARC levels reduced specifically in layer V glutamatergic neurons in the *RBP4Cre/caMEK1* mice. Immunostaining of adult cortex revealed a specific and marked reduction of ARC levels in layer V glutamatergic neurons in the *RBP4Cre/caMEK1* mice (D-F) when compared to controls (A-C) (scale bars = 200 μ m).

MEK1 hyperactivation in layer V cortical glutamatergic neurons is not sufficient to disrupt skilled motor learning

In the behavioral analysis of the *NesCre/caMek1* mice, we found that hyperactivation of MEK1 in all glutamatergic neurons of the cortex led to disruption of motor skill learning and acquisition. Here we wished to determine if the *RBP4:Cre/caMEK1* mice would exhibit the same deficits in motor learning acquisition as the *NesCre/caMek1* mice did.

Like the *NesCre/caMek1* mice, the *RBP4:Cre/caMEK1* mice also displayed no overt physical defects other than a smaller size than wild-type mice. However, since the RBP4 Cre recombinase is active in liver hepatocytes and adipose tissue (Thompson et al. 2017), the *RBP4:Cre/caMEK1* mice were in some cases much more sensitive to the standard food restriction paradigm. In the case of the *RBP4:Cre/caMEK1* and their control mice, food restriction was changed to allow free-feeding for 6 hours per day approximately 3-4 hours after behavioral testing. This allowed the mice to maintain a healthy body weight and helped prevent any health issues arising.

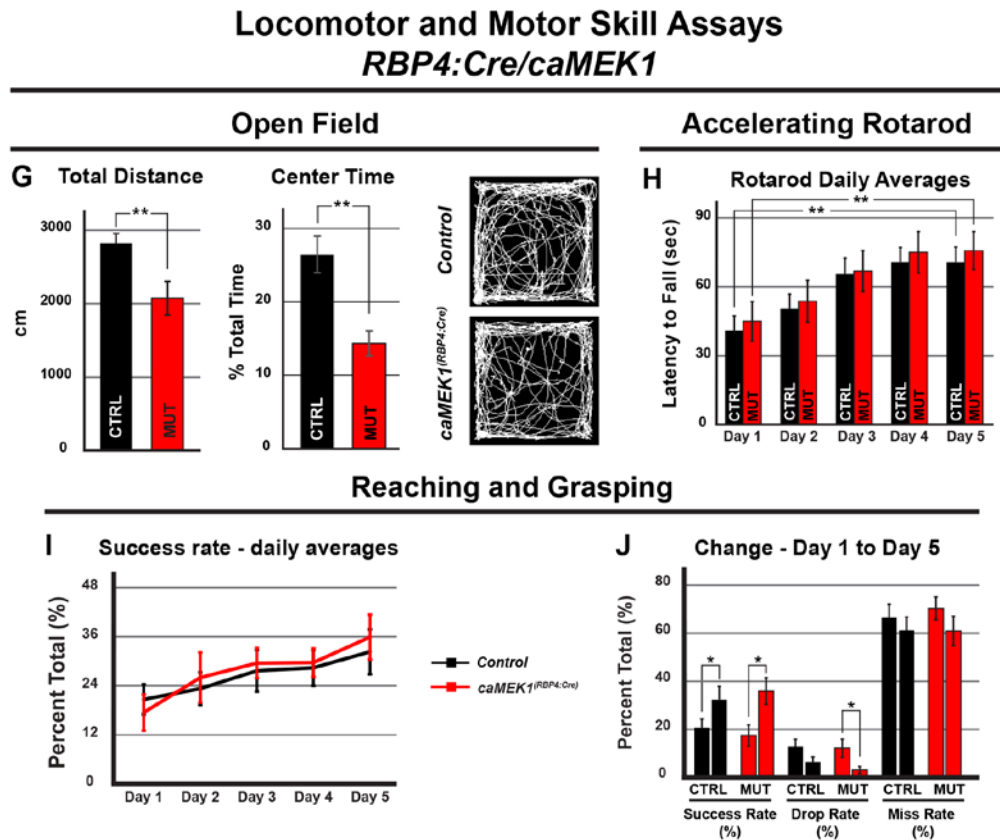
Open field testing of the *RBP4:Cre/caMEK1* mice showed a significant decrease in overall distance traveled when compared to control mice (cm traveled, controls = 2818.77cm +/- 132.28 SEM, n=19, *RBP4:Cre/caMEK1* = 2069.23cm +/- 228.61 SEM, n=12, p=0.005, Student's t-test) and a significant difference in percent center time (control = 26.46% ± 22.50% SEM, n=19, *RBP4Cre/caMEK1* = 14.36% ± 1.68% SEM, n=, p=0.001 Student's t-test) (Figure 35G). In the accelerating rotarod test however, the *RBP4:Cre/caMEK1* mice displayed no significant difference from the control mice in either overall performance or motor skill acquisition and learning in the five-day trial (genotype x latency to fall, [F(1,38)=0.237, p=0.629], repeated measures ANOVA) (Figure 35H). Over the course of the trial, both the

BP4Cre/caMek1 and control groups made significant improvements (*RBP4Cre/caMek1* 45.02secs \pm 8.58 SEM to 75.80secs \pm 8.29 SEM, [F(1,11)=12.501, p=0.005, n=12, controls = 40.85secs \pm 6.51 SEM to 70.59secs \pm 6.73 SEM, [F(1,27)=19.943, p<0.005, n=18, repeated measures ANOVA) (Figure 35H).

In the skilled reaching and grasping task, the *RBP4:Cre/caMEK1* mice also performed as well as the control mice as measured by the increase in successful attempts over the course of the trial (retrievals/overall attempts, *RBP4Cre/caMek1* = 17.44% \pm 4.43 SEM to 35.94% \pm 5.50 SEM, [F(1,11)=5.275, p=0.042], n=12, controls = 20.67% \pm 3.69 SEM to 32.33% \pm 5.51 SEM, [F(1,13)=8.641, p=0.011], n=14, ANOVA) (Figure 35I). In measurements of drop rate and miss rate however, only the *RBP4Cre/caMek1* made a significant improvement in reducing the rate of dropped pellets (drop/overall attempts, *RBP4Cre/caMek1* = 12.21% \pm 3.79 SEM to 3.13% \pm 1.43 SEM, [F(1,11)=9.607, p=0.010], n=12, ANOVA) (Figure 35J).

These results indicate that layer V specific hyperactivation of MEK1 in glutamatergic neurons is insufficient to disrupt motor skill learning and acquisition. However, open field testing alone indicates a deficit in voluntary locomotor activity and the possibility of an anxiety-like phenotype.

Figure 35.



ARC levels reduced specifically in layer V glutamatergic neurons in the *RBP4Cre/caMEK1* mice. Open field testing revealed a significant difference in total distance traveled between *RBP4Cre/caMEK1* and control (controls = 2818.77cms \pm 132.28 SEM, n=19, *RBP4Cre/caMek1* = 2069.23cm \pm 228.61 SEM, n=12, p=0.005, Student's t-test) and a significant difference in percent center time (control = 26.46% \pm 22.50% SEM, n=19, *RBP4Cre/caMEK1* = 14.36% \pm 1.68% SEM, n=, p=0.001 Student's t-test) (G). Rotarod performance revealed no significant differences between the *RBP4Cre/caMek1* and control groups (genotype x latency to fall, [F(1,38)=0.237, p=0.629], repeated measures ANOVA). Both the *RBP4Cre/caMek1* and control groups made significant improvements over the course of the trial (latency to fall, *RBP4Cre/caMek1* 45.02secs \pm 8.58 SEM to 75.80secs \pm 8.29 SEM, [F(1,11)=12.501, p=0.005, n=12, control = 40.85secs \pm 6.51 SEM to 70.59secs \pm 6.73 SEM, [F(1,27)=19.943, p<0.005, n=18, ANOVA) (H). In the skilled reaching and grasping task, no significant differences were found between the *RBP4Cre/caMek1* and control groups (genotype X success rate, [F(1,24)=0.050, p=0.825]) (I). Both the *RBP4Cre/caMek1* and control groups made significant improvements in their success rates over the course of the trial (success rate, *RBP4Cre/caMek1* = 17.44% \pm 4.43 SEM to 35.94% \pm 5.50 SEM, [F(1,11)=5.275, p=0.042], n=12, controls = 20.67% \pm 3.69 SEM to 32.33% \pm 5.51 SEM, [F(1,13)=8.641, p=0.011], n=14, ANOVA) (I – J). In measurements of drop rate and miss rate, only the *RBP4Cre/caMek1* made a significant improvement in reducing the rate of dropped pellets (*RBP4Cre/caMek1* = 12.21% \pm 3.79 SEM to 3.13% \pm 1.43 SEM, [F(1,11)=9.607, p=0.010], n=12, ANOVA) (J).

Discussion

The ERK/MAPK signaling pathway is perhaps the most studied cellular signaling pathway to date. The majority of this research however has been performed in the context of cancers and specific cell types in culture. In the field of neurodevelopment and neurodevelopmental syndromes however, there is a lack of knowledge regarding the effects of aberrant ERK/MAPK signaling. This absence is particularly noticeable concerning the formation and maintenance of cell-type specific connectivity under normal and syndromic conditions. In this study, we have identified the effects of hyperactivating MEK1 in the ERK/MAPK signaling pathway on the development of cortical glutamatergic axonal outgrowth and plasticity associated genes and its effect on motor learning. Furthermore, we have also identified a cortical layer autonomous effect on cortical axonal projections and innervation patterns, ARC expression, and motor learning acquisition. Interestingly, when MEK1 is hyperactivated in glutamatergic neurons across all layers of the cortex, we detect similar deficits with corticocortical, corticostriatal, and corticospinal axonal projections and innervation as when MEK1 hyperactivation is restricted to only layer V cortical glutamatergic neurons. In contrast to these projection deficits, we find a deficit in motor learning acquisition with cortex wide MEK1 glutamatergic hyperactivation whereas no motor learning deficit was detected in layer V specific MEK1 hyperactivation.

Key synaptic plasticity and immediate early gene ARC is downregulated

Interestingly, when MEK1 was hyperactivated in layer V glutamatergic neurons in the *RBP4:CRE/caMEK1* mice, the reduction of ARC expression was isolated to only those glutamatergic neurons located in cortical layer V. This cell and layer autonomous effect shows that the reduction of ARC levels is a direct

consequence of the reduction of P-ERK1/2 levels and the *RBP4:CRE/caMEK1* cell specific mutation.

Long range axonal connectivity is disrupted

We previously found deficits in axonal elongation of the cortico-spinal tract and arborization in the gray matter of the spinal cord and the hindbrain in the *Nex:CRE/caMEK1* mice (Xing et al. 2016). Additionally, we found significant deficits with corticocortical and corticostriatal innervation, deficits in motor learning acquisition, and a cell-autonomous effect in the down-regulation of ARC. Due to this cell-autonomous effect, we began address a layer specific hyperactivating mutation on axonal projections of cortical layer 5 glutamatergic neurons independent of any other cortical layers excitatory or inhibitory effects. The *RBP4:CRE/caMEK1* mice were subjected to the same AAV injection scheme and analysis controls as the *Nex:CRE/caMEK1* with the CRE-dependent tdTomato expressing AAV injected at P1 in one hemisphere of the primary motor cortex and analysis performed at P30. Analysis of CST extension and innervation of the cervical spinal cord showed a very similar and significant deficit in axonal elongation coupled with an increased amount of innervation in the spinal cord gray matter. Interestingly, a mouse model of NF1 also expressed a significant deficit in CST axonal extension as measured in the lumbar spinal cord. As NF1 is an activating mutation resulting in an overall increase in GTP bound RAS (Katherine A. Rauen 2013), this finding served to reinforce the results of both the *Nex:CRE/caMEK1* and *RBP4:CRE/caMEK1* mouse models.

We next investigated the contralateral axonal innervation of the contralateral cortex and dorsal striatum and the gray matter axonal innervation in the hind brain of the *RBP4:CRE/caMEK1* mice. Unlike the *Nex:CRE/caMEK1*, the *RBP4:CRE/caMEK1* mice displayed no changes in either cortico-bulbar tract extension or axonal gray

matter innervation when compared to control mice as had been previously found. Axonal innervation of the contralateral cortex though revealed a significant reduction of axonal innervation and branching as did the dorsal striatum. These results again showed that the *caMEK1* mutation expressed in a single layer, layer 5 in this instance, acts in an autonomous fashion in regard to axonal extension, innervation, and branching. Nevertheless, in order to determine a probable cause of the hind brain innervation differences between the *Nex:CRE/caMEK1* and the *RBP4:CRE/caMEK1* mice, more work will be necessary.

Motor learning acquisition is disrupted

Unlike the *Nex:CRE/caMEK1* mice, the *RBP4:CRE/caMEK1* showed a significant deficit in voluntary movement over the course of the test as measured by total distance traveled. While the *Nex:CRE/caMEK1* appeared unhindered in locomotor function, the *RBP4:CRE/caMEK1* appeared to lack either motivation or perhaps had an unknown impairment. However, much unlike the *Nex:CRE/caMEK1* mice, the *RBP4:CRE/caMEK1* revealed no differences from control mice over the course of the accelerating rotarod test. This indicated that the performance of the *RBP4:CRE/caMEK1* mice in the open field test was not due to a motor or physical impairment. Both groups, the *RBP4:CRE/caMEK1* and control mice, also showed a significant level of improvement over the course of the test indicating the ability to acquire the motor skills needed to perform this task.

In the skilled reaching and grasping task, the *RBP4:CRE/caMEK1* mice again revealed no differences from control mice. The *RBP4:CRE/caMEK1* and control mice both showed significant increases in their success rates and the *RBP4:CRE/caMEK1* mice also significantly decreased their drop rate. These results indicated that a layer 5 specific MEK1 hyperactivation had no effect on motor learning acquisition.

The combined results from the *Nex:CRE/caMEK1* and the *RBP4:CRE/caMEK1* shows that RAS/MAPK signaling plays an important bi-directional and cortical projection neuron autonomous role in axonal outgrowth and motor learning *in vivo*. Furthermore, cortical layer 5 specific RAS/MAPK mutants exhibit no change in motor learning, indicating behavioral plasticity depends upon RAS/MAPK expression in cortical projection neurons other than layer 5. Overall, our research suggests that the pathogenesis of cognitive deficits in RASopathies involves changes in the development of neuronal connectivity and the expression of plasticity associated genes at an early stage of cortical formation and subsequent developmental stages.

Acknowledgments

We wish to thank Noah Fry, Becca Reinking-Herd, and Sarah Bjorklund, for their technical assistance.

Contributions

Viral and DiI injections:

George Reed Bjorklund.

Tissue prep and Immunolabeling:

George Reed Bjorklund, Sarah Bjorklund, and Becca Reinking-Herd.

Image analysis and quantitation:

George Reed Bjorklund and Jason M Newbern.

Western Blotting:

George Reed Bjorklund.

Experimental conception and design:

George Reed Bjorklund and Jason M Newbern.

Behavioral analysis:

George Reed Bjorklund, Colton Smith, and Kenji Nishimura

Drafting or revising the article:

George Reed Bjorklund.

CHAPTER 5

CONCLUSION

Recent findings of diffusion tensor imaging (DTI) of major white matter (WM) tracts as well as functional magnetic resonance imaging (fMRI) in neurofibromatosis (NF-1) patients has highlighted connectivity issues within the RASopathies. These studies have allowed a non-invasive look into the composition, construction, and integrity of connectivity in normal and diseased brains. While these studies have shown major areas of connectivity disorganization in the brains of NF1 patients, they have not addressed the molecular causes at the root of these problems. Birchmeier and colleagues studied the effects of a constitutively active form of MEK1 in the myelinating cells of the peripheral nervous system, Schwann cells. They found that continuous MEK1 signaling was able to overcome the termination of myelin growth during development by protein synthesis stimulation (Sheean et al. 2014). The failure to terminate myelin growth in turn created a significantly increased amount of WM. Bansal and colleagues found similar results in the oligodendrocytes of the central nervous system by hyperactivation of MEK1 (Ishii et al. 2016). While this may explain the WM aberrations in DTI studies of NF-1 patients, either in part or in whole, it does not address connectivity issues or pathologies associated with the underlying axons themselves. In our studies, we have sought to address the cell-type specific contributions to the reported connectivity issues as well as the pathophysiology of the axons themselves within the WM tracts.

The RASopathies contain both loss- and gain-of function (LoF and GoF) mutations within the Ras/MAPK intracellular signaling pathway. In these *in vivo* mouse studies, we used both a MEK1/2 conditional knockout or a constitutively active MEK1 (caMEK1) construct activated in cortical glutamatergic neurons. As these

neurons provide long-range connectivity both within the cortex and sub-cortically, we were able to determine the effects of both LoF and GoF RAS/MAPK signaling in a cell-autonomous manner. In addition to cell-autonomous effects, we also analyzed cortical layer autonomous effects by inducing the GoF caMEK1 mutation solely in layer 5 glutamatergic neurons. We further moved to address behavioral and cognitive issues, particularly motor learning acquisition, as reported within the RASopathies with these mouse models.

Much like the referenced DTI and fMRI studies in NF1 patients, we found widespread aberrations in cortical and subcortical connectivity in addition to cell survival and behavioral deficits. In the LoF model, we found a significant cell-death phenotype most notably in cortical layer 5 CTIP2⁺ neurons as well as significant deficits in corticospinal tract (CST) elongation. In the cortex wide GoF in cortical glutamatergic neurons model, we found a surprising down-regulation of phosphorylated ERK1/2 (P-ERK1/2) in the soma and a high amount of P-ERK1/2 in the axons compared to controls. We additionally found significant deficits in corticocortical and corticostriatal axonal innervation, a significant deficit in CST elongation with hyperactivated innervation in spinal cord and hind brain gray matter, a reduction in the expression of immediate early gene (IEG) ARC, and a deficit in motor learning acquisition. When the GoF mutation was restricted to layer 5 glutamatergic neurons we also found significant deficits in corticocortical and corticostriatal axonal innervation, and a significant deficit in CST elongation with hyperactivated innervation in the spinal cord. However, we did not detect any changes in hind brain gray matter and the reduction in the expression of immediate early gene (IEG) ARC was restricted to layer 5 glutamatergic neurons. Furthermore, we detected no deficits in motor learning acquisition of the layer 5 specific GoF mutation mice.

Overall, this research shows that RAS/MAPK signaling plays an important bi-directional and cortical projection neuron autonomous role in axonal outgrowth and motor learning in vivo. These data suggest that the pathogenesis of cognitive deficits in RASopathies involves changes in the development of neuronal connectivity, but not neuronal number, at an early stage of cortical formation and the expression of plasticity associated genes during subsequent developmental stages.

Our LoF model used a CRE activated conditional knockout of MEK1/2 that was activated in post-mitotic neurons at approximately E11.5 due to embryonic lethality of germline mutations. In our study, we found that the initial complement of cortical glutamatergic neurons was fully intact at P1. At P3 we found a significant deficit in CST elongation. By P14 we found a significant amount of cell death most notably in layer 5 glutamatergic neurons. Analyzing the cell death at earlier time points we found a peak at approximately P5. This mutation however was lethal at about P21 so we were unable to further investigate connectivity, behavioral, or the cell death phenotypes in this model.

Our early discovery concerning deficits in CST elongation addressed partially the involvement of RAS/MAPK in axonal extension during this early developmental period. However, we were unable to observe RAS/MAPK signaling requirements or consequences in the period after development. To address this issue, we have designed experiments that creates a MEK1/2 LoF mutation in the primary motor cortex (M1) of one cortical hemisphere. With this model, we will be able to analyze axonal elongation of the CST as well as corticocortical and corticostriatal axonal projections and innervation. IEG expression will also be analyzed in dual expression labeling experiments of the affected neurons. Motor learning acquisition may not be able to be addressed due to the mono-hemisphere and single structure mutation, however, motor function will be assessed by analyzing the lateralization of motor

skills. Insights gained from these experiments will further add to our knowledge of RAS/MAPK LoF beyond early development.

Our GoF mouse model relied on the same post-mitotic activation of CRE to transcribe the caMEK1 construct. Unlike the LoF mice however, the GoF mice were viable and vital with the exception of a smaller size. This model allowed not only the identification of CST elongation deficits early in development but also the post-developmental P-ERK1/2 localization/expression phenotype, corticocortical and corticostriatal innervation deficits, and motor learning deficits.

One of the most surprising findings of the GoF analysis proved to be the apparent down-regulation of P-ERK1/2 in the bodies of the caMEK1 mutated neurons accompanied by an accumulation in the axons. This phenotype has not appeared in the known literature and the cause of it is a very interesting area for further research and possible therapeutic targets in the RASopathies. Two areas that would be of immediate promise to focus on for this phenotype would be axonal transportation mechanisms and P-ERK1/2 regulation. Retrograde transport of P-ERK1/2 from the distal axon to the nucleus is critical to evoke transcriptional programs and changes in development. Several phosphatases have been identified to deactivate P-ERK1/2 and their activities are thought to be compartment specific. We tested for one of the most commonly reported neuronal phosphatases but found no evidence of changes. This leaves the question of additional phosphatases that may be active and their compartmental specificity as well as transcriptional programs that control their expression.

Our *in vivo* connectivity analysis also confirmed the widespread WM aberrations and functional disorganization detected in DTI and fMRI studies in NF1 patients. Furthermore, these deficits were detected in a cell-autonomous manner within a biological system and may solely be a function of axonal dynamics. Much

further analysis however is needed to pinpoint the cause or causes of these connectivity issues. Due the many functions and cross-talk characteristics of the RAS/MAPK signaling pathway, there are many areas to be analyzed. A major area to address would be transcription programs affected by the apparent loss of somal P-ERK1/2. It is thought that the disorganization seen in the DTI studies may be a function of loosely packed or non-fasciculated axons. This may indicate the loss of cellular adhesion and-or pathfinding molecules needed by the axons during elongation and growth. Additionally, the build-up of P-ERK1/2 in the axonal compartment is also a major consideration in axonal elongation and innervation during development. P-ERK1/2 interactions with MAP1B and TAU serve to stabilize microtubules and neurofilaments. However, axonal elongation and branching rely on the dynamic actions of de-stabilization and stabilization. Therefore, the accumulation of P-ERK1/2 in the axons may in fact be causing a scenario of over stabilization interfering with growth cone and axonal branching dynamics. There are several different aspects within these identified phenotypes that need further investigation to identify.

The cortex-wide expression of the caMEK1 mutation in glutamatergic neurons also affected motor learning acquisition. We also detected a significant down-regulation of ARC which is known to play an important role in synaptic plasticity. Whether the deficits in motor learning are a consequence of ARC down-regulation or due to a loss in axonal innervation is unknown at this point. Western Blot results of whole cortical lysates show a significant reduction of ARC in the *Nex:Cre/caMEK1*. Immunostaining for ARC confirms this reduction and it appears that the majority of ARC loss is in the neuronal bodies of glutamatergic neurons. Additionally, while ARC expression is still detected in the dendritic compartments, it is unclear at this point if those are the dendrites of the mutated glutamatergic neurons. Glutamate activation

of NMDA and AMPA receptors in the post-synaptic density are required for *Arc* induction and *Arc* regulation respectively. NMDAR activation leads to *Arc* transcription through several signaling pathways including the RAS/MAPK pathway. *Arc* transcription can be further accelerated through BDNF/TRKB activation. Nuclear transportation of ERK-phosphorylated ARC however acts in the down-regulation of *Arc* transcription by inhibiting GluA1 transcription and in turn AMPAR activation. This NMDAR activating and AMPAR inhibition is required to mediate changes in synaptic competence and regulate homeostatic scaling required for learning and memory (Epstein and Finkbeiner 2018). Here we have detected a decreased level of both P-ERK1/2 and the IEG ARC in the soma and nuclear spaces. The lack of both these of these proteins could lead to a drastic down-regulation not only of *Arc* induction, but all other immediate early genes that rely on the same transcriptional program. Our previous study analyzed differential gene expression of the *Nex:Cre/caMEK1* and control mice (Xing et al. 2016). In that study, we found no evidence of differential RNA expression (greater than +/-1.5 fold change in mutants vs controls) in neurotrophins or their receptors (Appendix D, Table 2) (Xing et al. 2016). This however does account for post-translation modifications or actual protein levels for each transcript. Further work is necessary to determine the cellular mechanisms responsible for the lack of nuclear and cytosolic ARC as well as neurotrophins and their receptors.

In addition to the cell-autonomous deficits that we identified in the GoF model, we also identified a cortical layer autonomous effect. When the caMEK1 mutation was applied solely to layer 5 glutamatergic neurons we found similar deficits in long-range connectivity. Significant deficits were identified in corticocortical and corticostriatal axonal innervation, CST elongation deficits, and hyperinnervation of the spinal cord gray matter but no changes of axonal innervation

in the hind brain. ARC expression levels were also reduced but the reduction was isolated to solely glutamatergic neurons in cortical layer 5. No deficits in motor learning acquisition in the layer 5 GoF mice were detected indicating behavioral plasticity depends upon RAS/MAPK signaling in cortical projection neurons other than layer 5.

These combined data show the cell-type specific and layer specific phenotypes associated with the RASopathies. Future studies to analyze cell-cell interactions would also help to identify the effects of RAS/MAPK signaling in connectivity and system communications. This would entail adding the GoF MEK1 mutation to additional cell types. For example, introducing the hyperactivating MEK1 mutation in inhibitory neurons would affect the excitatory-inhibitory balance of the cortex. However, how this would affect connectivity or plasticity is unknown. The same could be said of oligodendrocytes. Would the hyperactivating mutation in glutamatergic cells and oligodendrocytes change the conclusions of these current studies? Would these interactions afford the opportunity for RASopathy targeted interventions?

A major question that arises in the RASopathies is: What are the differences in RAS/MAPK signaling requirements in and after development? To take that even further: What points in development are more or are less dependent on RAS/MAPK signaling functions? Currently the spatial and temporal dynamics of the consequences of RAS/MAPK signaling are not fully understood in the development of a biological system. Another very important question for the RASopathies is not only at what point in development should we intervene, but at what point can we intervene? The developmental trajectory of the mouse models we use and that of a human are very different. These problems that we have identified in post-natal mouse development are mostly completed in human development during the second trimester of pregnancy. This leads to a very important question of how to treat the

disease after development. As we have identified an apparent down-regulation effect of P-ERK1/2 in neuronal cell bodies, is it still wise to treat a heart condition with MEK inhibitors in a RASopathy patient? While there is much further work to do to pinpoint causes of the molecular phenotypes we have shown here, there is also that many more areas of intervention to explore. For example, instead of a MEK1 inhibitor for a GoF mutation, is there a target that can be manipulated to fix axonal transport to release P-ERK1/2 to the soma? Or can MAP1B and TAU be intermittently destabilized to promote axonal branching or improve synaptic plasticity? Currently, management of the RASopathy diseases are to treat their manifestations. These studies have presented on the cellular level several possible manifestations to treat.

REFERENCES

- Alberts B. 2015. *Molecular biology of the cell*. Sixth edition. New York, NY: Garland Science, Taylor and Francis Group.
- Alcamo EA, Chirivella L, Dautzenberg M, Dobрева G, Fariñas I, Grosschedl R, McConnell SK. 2008. *Satb2* regulates callosal projection neuron identity in the developing cerebral cortex. *Neuron*. 57(3):364–377. doi: 10.1016/j.neuron.2007.12.012.
- Allanson JE, Roberts AE. 1993. Noonan Syndrome. In: Adam MP, Ardinger HH, Pagon RA, Wallace SE, Bean LJ, Stephens K, Amemiya A, editors. *GeneReviews®*. Seattle (WA): University of Washington, Seattle. [accessed 2018 Jun 14]. <http://www.ncbi.nlm.nih.gov/books/NBK1124/>.
- Aoki Y, Niihori T, Inoue S, Matsubara Y. 2016. Recent advances in RASopathies. *Journal of Human Genetics*. 61(1):33–39. doi:10.1038/jhg.2015.114.
- Aoki Y, Niihori T, Inoue SI, Matsubara Y. 2016. Recent advances in RASopathies. *Journal of Human Genetics*. 61(1):33–39. doi:10.1038/jhg.2015.114.
- Arlotta P, Molyneaux BJ, Chen J, Inoue J, Kominami R, Macklis JD. 2005. Neuronal subtype-specific genes that control corticospinal motor neuron development in vivo. *Neuron*. 45(2):207–221. doi:10.1016/j.neuron.2004.12.036.
- Assaf Y, Pasternak O. 2008. Diffusion tensor imaging (DTI)-based white matter mapping in brain research: a review. *J Mol Neurosci*. 34(1):51–61. doi: 10.1007/s12031-007-0029-0.
- Atwal JK, Massie B, Miller FD, Kaplan DR. 2000. The TrkB-Shc Site Signals Neuronal Survival and Local Axon Growth via MEK and PI3-Kinase. *Neuron*. 27(2):265–277. doi: 10.1016/S0896-6273(00)00035-0.
- Atwal JK, Singh KK, Tessier-Lavigne M, Miller FD, Kaplan DR. 2003. Semaphorin 3F Antagonizes Neurotrophin-Induced Phosphatidylinositol 3-Kinase and Mitogen-Activated Protein Kinase Kinase Signaling: A Mechanism for Growth Cone Collapse. *The Journal of Neuroscience*. 23(20):7602–7609. doi: 10.1523/JNEUROSCI.23-20-07602.2003.
- Autoimmune lymphoproliferative syndrome. 2018. National Library of Medicine (US). Genetics Home Reference. [accessed 2018 Jun 14]. <https://ghr.nlm.nih.gov/condition/autoimmune-lymphoproliferative-syndrome>.
- Avila J. 2008. Tau kinases and phosphatases. *Journal of Cellular and Molecular Medicine*. 12(1):258–259. doi: 10.1111/j.1582-4934.2007.00214.x.
- Aydin S, Kurtcan S, Alkan A, Guler S, Filiz M, Yilmaz TF, Sahin TU, Aralasmak A. 2016. Relationship between the corpus callosum and neurocognitive disabilities in children with NF-1: diffusion tensor imaging features. *Clinical Imaging*. 40(6):1092–1095. doi: 10.1016/j.clinimag.2016.06.013.

Bateman A, Martin MJ, O'Donovan C, Magrane M, Alpi E, Antunes R, Bely B, Bingley M, Bonilla C, Britto R, et al. 2017. UniProt: the universal protein knowledgebase. *Nucleic Acids Res.* 45(D1):D158–D169. doi:10.1093/nar/gkw1099.

Bélanger L-F, Roy S, Tremblay M, Brott B, Steff A-M, Mourad W, Hugo P, Erikson R, Charron J. 2003. Mek2 is dispensable for mouse growth and development. *Mol Cell Biol.* 23(14):4778–4787.

Bissonauth V, Roy S, Gravel M, Guillemette S, Charron J. 2006. Requirement for Map2k1 (Mek1) in extra-embryonic ectoderm during placentogenesis. *Development.* 133(17):3429–3440. doi:10.1242/dev.02526.

Bizaoui V, Gage J, Brar R, Rauen KA, Weiss LA. 2018. RASopathies are associated with a distinct personality profile. *American Journal of Medical Genetics Part B: Neuropsychiatric Genetics.* 177(4):434–446. doi:10.1002/ajmg.b.32632.

Bleesing JJ, Nagaraj CB, Zhang K. 2017. Autoimmune Lymphoproliferative Syndrome. p. 36.

Blüthgen N, Van Bentum M, Merz B, Kuhl Di, Hermey G. 2017. Profiling the MAPK/ERK dependent and independent activity regulated transcriptional programs in the murine hippocampus in vivo. *Scientific Reports.* 7(November 2016):1–14. doi:10.1038/srep45101.

Bonni A, Brunet A, West AE, Datta SR, Takasu MA, Greenberg ME. 1999. Cell survival promoted by the Ras-MAPK signaling pathway by transcription-dependent and -independent mechanisms. *Science.* 286(5443):1358–1362.

Bramham CR, Alme MN, Bittins M, Kuipers SD, Nair RR, Pai B, Panja D, Schubert M, Soule J, Tiron A, et al. 2010. The Arc of synaptic memory. *Experimental Brain Research.* 200(2):125–140. doi:10.1007/s00221-009-1959-2.

Britanova O, de Juan Romero C, Cheung A, Kwan KY, Schwark M, Gyorgy A, Vogel T, Akopov S, Mitkovski M, Agoston D, et al. 2008. Satb2 is a postmitotic determinant for upper-layer neuron specification in the neocortex. *Neuron.* 57(3):378–392. doi:10.1016/j.neuron.2007.12.028.

Campbell DS, Holt CE. 2003. Apoptotic Pathway and MAPKs Differentially Regulate Chemotropic Responses of Retinal Growth Cones. *Neuron.* 37(6):939–952. doi:10.1016/S0896-6273(03)00158-2.

Cao VY, Ye Y, Mastwal S, Ren M, Coon M, Liu Q, Costa RM, Wang KH. 2015. Motor Learning Consolidates Arc-Expressing Neuronal Ensembles in Secondary Motor Cortex. *Neuron.* 86(6):1385–1392. doi:10.1016/j.neuron.2015.05.022.

Chen AP, Ohno M, Giese KP, Kühn R, Chen RL, Silva AJ. 2006. Forebrain-specific knockout of B-raf kinase leads to deficits in hippocampal long-term potentiation, learning, and memory. *J Neurosci Res.* 83(1):28–38. doi:10.1002/jnr.20703.

Chen B, Schaevitz LR, McConnell SK. 2005. Fezl regulates the differentiation and axon targeting of layer 5 subcortical projection neurons in cerebral cortex. *Proc Natl Acad Sci USA.* 102(47):17184–17189. doi:10.1073/pnas.0508732102.

Chen J-G, Rasin M-R, Kwan KY, Sestan N. 2005. Zfp312 is required for subcortical axonal projections and dendritic morphology of deep-layer pyramidal neurons of the cerebral cortex. *Proc Natl Acad Sci USA*. 102(49):17792–17797. doi: 10.1073/pnas.0509032102.

Chévere-Torres I, Kaphzan H, Bhattacharya A, Kang A, Maki JM, Gambello MJ, Arbiser JL, Santini E, Klann E. 2012. Metabotropic glutamate receptor-dependent long-term depression is impaired due to elevated ERK signaling in the Δ RG mouse model of tuberous sclerosis complex. *Neurobiology of Disease*. 45(3):1101–1110. doi: 10.1016/j.nbd.2011.12.028.

Chi CL, Martinez S, Wurst W, Martin GR. 2003. The isthmic organizer signal FGF8 is required for cell survival in the prospective midbrain and cerebellum. *Development*. 130(12):2633–2644. doi: 10.1242/dev.00487.

Cho SY, Klemke RL. 2000. Extracellular-Regulated Kinase Activation and Cas/Crk Coupling Regulate Cell Migration and Suppress Apoptosis during Invasion of the Extracellular Matrix. *The Journal of Cell Biology*. 149(1):223–236. doi: 10.1083/jcb.149.1.223.

Coba MP, Valor LM, Kopanitsa MV, Afinowi NO, Grant SGN. 2008. Kinase networks integrate profiles of N-methyl-D-aspartate receptor-mediated gene expression in hippocampus. *J Biol Chem*. 283(49):34101–34107. doi: 10.1074/jbc.M804951200.

Colman SD, Rasmussen SA, Ho VT, Abernathy CR, Wallace MR. 1996. Somatic Mosaicism in a Patient with Neurofibromatosis Type. *Am J Hum Genet*.:7.

Cooper JA. 2013. Mechanisms of cell migration in the nervous system. *J Cell Biol*. 202(5):725–734. doi: 10.1083/jcb.201305021.

Corson LB, Yamanaka Y, Lai K-MV, Rossant J. 2003. Spatial and temporal patterns of ERK signaling during mouse embryogenesis. *Development*. 130(19):4527–4537. doi: 10.1242/dev.00669.

Costa RM, Federov NB, Kogan JH, Murphy GG, Stern J, Ohno M, Kucherlapati R, Jacks T, Silva AJ. 2002. Mechanism for the learning deficits in a mouse model of neurofibromatosis type 1. *Nature*. 415(6871):526–530. doi: 10.1038/nature711.

Coulier F, Martin-Zanca D, Ernst M, Barbacid M. 1989. Mechanism of activation of the human trk oncogene. *Mol Cell Biol*. 9(1):15–23.

Cox AD, Der CJ. 2010. Ras history: The saga continues. *Small GTPases*. 1(1):2–27. doi: 10.4161/sgtp.1.1.12178.

Cui Y, Costa RM, Murphy GG, Elgersma Y, Zhu Y, Gutmann DH, Parada LF, Mody I, Silva AJ. 2008. Neurofibromin Regulation of ERK Signaling Modulates GABA Release and Learning. *Cell*. 135(3):549–560. doi: 10.1016/j.cell.2008.09.060.

Custo Greig LF, Woodworth MB, Galazo MJ, Padmanabhan H, Macklis JD. 2013. Molecular logic of neocortical projection neuron specification, development and diversity. *Nat Rev Neurosci*. 14(11):755–769. doi: 10.1038/nrn3586.

- Datta SR, Dudek H, Tao X, Masters S, Fu H, Gotoh Y, Greenberg ME. 1997. Akt Phosphorylation of BAD Couples Survival Signals to the Cell-Intrinsic Death Machinery. *Cell*. 91(2):231–241. doi:10.1016/S0092-8674(00)80405-5.
- Davis S, Vanhoutte P, Pages C, Caboche J, Laroche S. 2000. The MAPK/ERK cascade targets both Elk-1 and cAMP response element-binding protein to control long-term potentiation-dependent gene expression in the dentate gyrus in vivo. *The Journal of neuroscience : the official journal of the Society for Neuroscience*. 20(12):4563–4572. doi:20/12/4563 [pii].
- Dehmelt L, Halpain S. 2005. The MAP2/Tau family of microtubule-associated proteins. *Genome Biol*. 6(1):204. doi:10.1186/gb-2004-6-1-204.
- Der CJ, Krontiris TG, Cooper GM. 1982. Transforming genes of human bladder and lung carcinoma cell lines are homologous to the ras genes of Harvey and Kirsten sarcoma viruses. *Proc Natl Acad Sci USA*. 79(11):3637–3640.
- Desai NS, Cudmore RH, Nelson SB, Turrigiano GG. 2002. Critical periods for experience-dependent synaptic scaling in visual cortex. *Nat Neurosci*. 5(8):783–789. doi:10.1038/nn878.
- Dijkhuizen PA, Ghosh A. 2005. BDNF regulates primary dendrite formation in cortical neurons via the PI3-kinase and MAP kinase signaling pathways. *J Neurobiol*. 62(2):278–288. doi:10.1002/neu.20100.
- Dileone M, Profice P, Pilato F, Alfieri P, Cesarini L, Mercuri E, Leoni C, Tartaglia M, Di Iorio R, Zampino G, et al. 2010. Enhanced human brain associative plasticity in Costello syndrome. *J Physiol (Lond)*. 588(Pt 18):3445–3456. doi:10.1113/jphysiol.2010.191072.
- Dugas JC, Mandemakers W, Rogers M, Ibrahim A, Daneman R, Barres BA. 2008. A novel purification method for CNS projection neurons leads to the identification of brain vascular cells as a source of trophic support for corticospinal motor neurons. *J Neurosci*. 28(33):8294–8305. doi:10.1523/JNEUROSCI.2010-08.2008.
- Eichler EE, Zimmerman AW. 2008. A Hot Spot of Genetic Instability in Autism. *New England Journal of Medicine*. 358(7):737–739. doi:10.1056/NEJMe0708756.
- EN. Epidermal nevus. Genetics Home Reference [Internet]. [accessed 2018 Jun 13]. <https://ghr.nlm.nih.gov/condition/epidermal-nevus>.
- Encinas M, Rozen EJ, Dolcet X, Jain S, Comella JX, Milbrandt J, Johnson EM. 2008. Analysis of Ret knockin mice reveals a critical role for IKKs, but not PI 3-K, in neurotrophic factor-induced survival of sympathetic neurons. *Cell Death Differ*. 15(9):1510–1521. doi:10.1038/cdd.2008.76.
- Epstein I, Finkbeiner S. 2018. The Arc of cognition: Signaling cascades regulating Arc and implications for cognitive function and disease. *Semin Cell Dev Biol*. 77:63–72. doi:10.1016/j.semcdb.2017.09.023.

- Esposito MS, Capelli P, Arber S. 2014. Brainstem nucleus MdV mediates skilled forelimb motor tasks. *Nature*. 508(7496): 351–356. doi:10.1038/nature13023.
- Faedo A, Borello U, Rubenstein JLR. 2010. Repression of Fgf Signaling by Sprouty1-2 Regulates Cortical Patterning in Two Distinct Regions and Times. *Journal of Neuroscience*. 30(11): 4015–4023. doi: 10.1523/JNEUROSCI.0307-10.2010.
- Fame RM, MacDonald JL, Macklis JD. 2011. Development, specification, and diversity of callosal projection neurons. *Trends in Neurosciences*. 34(1): 41–50. doi: 10.1016/j.tins.2010.10.002.
- Faridar A, Jones-Davis D, Rider E, Li J, Gobius I, Morcom L, Richards LJ, Sen S, Sherr EH. 2014. Mapk/Erk activation in an animal model of social deficits shows a possible link to autism. *Molecular Autism*. 5(1):57. doi:10.1186/2040-2392-5-57.
- Feng G, Mellor RH, Bernstein M, Keller-Peck C, Nguyen QT, Wallace M, Nerbonne JM, Lichtman JW, Sanes JR. 2000. Imaging neuronal subsets in transgenic mice expressing multiple spectral variants of GFP. *Neuron*. 28(1): 41–51.
- Filippi CG, Watts R, Duy Lindsay A. N., Cauley KA. 2013. Diffusion-tensor imaging derived metrics of the corpus callosum in children with neurofibromatosis type I. *AJR Am J Roentgenol*. 200(1): 44–49. doi: 10.2214/AJR.12.9590.
- Filippi CG, Watts R, Duy Lindsay A.N., Cauley KA. 2013. Diffusion-tensor imaging derived metrics of the corpus callosum in children with neurofibromatosis type I. *American Journal of Roentgenology*. 200(1): 44–49. doi: 10.2214/AJR.12.9590.
- Franklin KBJ, Paxinos G. 2013. Paxinos and Franklin's The mouse brain in stereotaxic coordinates. Fourth edition. Amsterdam: Academic Press, an imprint of Elsevier.
- Friedman J. 1993. Neurofibromatosis 1. In: Adam MP, Ardinger HH, Pagon RA, Wallace SE, Bean LJ, Stephens K, Amemiya A, editors. *GeneReviews®*. Seattle (WA): University of Washington, Seattle.
- Friston KJ. 2011. Functional and effective connectivity: a review. *Brain Connect*. 1(1): 13–36. doi:10.1089/brain.2011.0008.
- Galabova-Kovacs G, Catalanotti F, Matzen D, Reyes GX, Zezula J, Herbst R, Silva A, Walter I, Baccarini M. 2008. Essential role of B-Raf in oligodendrocyte maturation and myelination during postnatal central nervous system development. *J Cell Biol*. 180(5): 947–955. doi: 10.1083/jcb.200709069.
- Gallego C, Gupta SK, Heasley LE, Qian NX, Johnson GL. 1992. Mitogen-activated protein kinase activation resulting from selective oncogene expression in NIH 3T3 and rat 1a cells. *Proc Natl Acad Sci USA*. 89(16): 7355–7359.
- Gallo FT, Katche C, Morici JF, Medina JH, Weisstaub NV. 2018. Immediate Early Genes, Memory and Psychiatric Disorders: Focus on c-Fos, Egr1 and Arc. *Front Behav Neurosci*. 12. doi: 10.3389/fnbeh.2018.00079. [accessed 2018 Nov 5]. <https://www.frontiersin.org/articles/10.3389/fnbeh.2018.00079/full>.

Gelb BD, Tartaglia M. 1993. Noonan Syndrome with Multiple Lentigines. In: Adam MP, Ardinger HH, Pagon RA, Wallace SE, Bean LJ, Stephens K, Amemiya A, editors. GeneReviews®. Seattle (WA): University of Washington, Seattle. [accessed 2018 Jun 14]. <http://www.ncbi.nlm.nih.gov/books/NBK1383/>.

Geschwind DH, Levitt P. 2007. Autism spectrum disorders: developmental disconnection syndromes. *Current Opinion in Neurobiology*. 17(1):103–111. doi: 10.1016/j.conb.2007.01.009.

Giehl KM, Schütte A, Mestres P, Yan Q. 1998. The survival-promoting effect of glial cell line-derived neurotrophic factor on axotomized corticospinal neurons in vivo is mediated by an endogenous brain-derived neurotrophic factor mechanism. *J Neurosci*. 18(18):7351–7360.

Gilbert SF, Barresi MJF. 2016. *Developmental biology*. Eleventh edition. Sunderland, Massachusetts: Sinauer Associates, Inc.

Gilley J, Coffey PJ, Ham J. 2003. FOXO transcription factors directly activate bim gene expression and promote apoptosis in sympathetic neurons. *J Cell Biol*. 162(4):613–622. doi: 10.1083/jcb.200303026.

Gilman SR, Chang J, Xu B, Bawa TS, Gogos JA, Karayiorgou M, Vitkup D. 2012. Diverse types of genetic variation converge on functional gene networks involved in schizophrenia. *Nature Neuroscience*. 15(12):1723–1728. doi: 10.1038/nn.3261.

Gilman SR, Iossifov I, Levy D, Ronemus M, Wigler M, Vitkup D. 2011. Rare De Novo Variants Associated with Autism Implicate a Large Functional Network of Genes Involved in Formation and Function of Synapses. *Neuron*. 70(5):898–907. doi: 10.1016/j.neuron.2011.05.021.

Goebbels S, Bormuth I, Bode U, Hermanson O, Schwab MH, Nave K-A. Genetic targeting of principal neurons in neocortex and hippocampus of NEX-Cre mice. *genesis*. 44(12):611–621. doi: 10.1002/dvg.20256.

Goold RG, Gordon-Weeks PR. 2005. The MAP kinase pathway is upstream of the activation of GSK3 β that enables it to phosphorylate MAP1B and contributes to the stimulation of axon growth. *Molecular and Cellular Neuroscience*. 28(3):524–534. doi: 10.1016/j.mcn.2004.11.005.

Gorski JA, Talley T, Qiu M, Puelles L, Rubenstein JLR, Jones KR. 2002. Cortical excitatory neurons and glia, but not GABAergic neurons, are produced in the Emx1-expressing lineage. *J Neurosci*. 22(15):6309–6314. doi: 20026564.

Graef IA, Wang F, Charron F, Chen L, Neilson J, Tessier-Lavigne M, Crabtree GR. 2003. Neurotrophins and Netrins Require Calcineurin/NFAT Signaling to Stimulate Outgrowth of Embryonic Axons. *Cell*. 113(5):657–670. doi: 10.1016/S0092-8674(03)00390-8.

- Greig LC, Woodworth MB, Galazo MJ, Padmanabhan H, Macklis JD. 2013. Molecular logic of neocortical projection neuron specification, development and diversity. *Nature Reviews Neuroscience*. 14(11):755–769. doi:10.1038/nrn3586.
- Gripp KW. 2012. Costello Syndrome. In: *Gene Reviews*.
- Gripp KW, Stabley DL, Nicholson L, Hoffman JD, Sol-Church K. 2006. Somatic mosaicism for anHRAS mutation causes Costello syndrome. *American Journal of Medical Genetics Part A*. 140A(20):2163–2169. doi:10.1002/ajmg.a.31456.
- Guzowski JF, McNaughton BL, Barnes CA, Worley PF. 1999. Environment-specific expression of the immediate-early gene Arc in hippocampal neuronal ensembles. *Nat Neurosci*. 2(12):1120–1124. doi:10.1038/16046.
- Hafner C, Groesser L. 2013. Mosaic RASopathies. *Cell Cycle*. 12(1):43–50. doi:10.4161/cc.23108.
- Hahn CM, Kleinholz H, Koester MP, Grieser S, Thelen K, Pollerberg GE. 2005. Role of cyclin-dependent kinase 5 and its activator P35 in local axon and growth cone stabilization. *Neuroscience*. 134(2):449–465. doi:10.1016/j.neuroscience.2005.04.020.
- Hall A, Marshall CJ, Spurr NK, Weiss RA. 1983. Identification of transforming gene in two human sarcoma cell lines as a new member of the ras gene family located on chromosome 1. *Nature*. 303(5916):396–400.
- Hallberg B, Rayter SI, Downward J. 1994. Interaction of Ras and Raf in intact mammalian cells upon extracellular stimulation. *J Biol Chem*. 269(6):3913–3916.
- Hanger DP, Seereeram A, Noble W. 2009. Mediators of tau phosphorylation in the pathogenesis of Alzheimer's disease. *Expert Rev Neurother*. 9(11):1647–1666. doi:10.1586/ern.09.104.
- Harada T, Morooka T, Ogawa S, Nishida E. 2001. ERK induces p35, a neuron-specific activator of Cdk5, through induction of Egr1. *Nature Cell Biology*. 3(5):453–459. doi:10.1038/35074516.
- Harvey JJ. 1964. AN UNIDENTIFIED VIRUS WHICH CAUSES THE RAPID PRODUCTION OF TUMOURS IN MICE. *Nature*. 204:1104–1105.
- Howe LR, Leever SJ, Gómez N, Nakielnny S, Cohen P, Marshall CJ. 1992. Activation of the MAP kinase pathway by the protein kinase raf. *Cell*. 71(2):335–342.
- Huang C, Jacobson K, Schaller MD. 2004. MAP kinases and cell migration. *Journal of Cell Science*. 117(20):4619–4628. doi:10.1242/jcs.01481.
- Huang YZ, Pan E, Xiong Z-Q, McNamara JO. 2008. Zinc-Mediated Transactivation of TrkB Potentiates the Hippocampal Mossy Fiber-CA3 Pyramid Synapse. *Neuron*. 57(4):546–558. doi:10.1016/j.neuron.2007.11.026.

- Huang ZJ, Kirkwood A, Pizzorusso T, Porciatti V, Morales B, Bear MF, Maffei L, Tonegawa S. 1999. BDNF regulates the maturation of inhibition and the critical period of plasticity in mouse visual cortex. *Cell*. 98(6):739–755.
- Hurley JB, Simon MI, Teplow DB, Robishaw JD, Gilman AG. 1984. Homologies between signal transducing G proteins and ras gene products. *Science*. 226(4676):860–862.
- Ibrahim Amira F. A., Montojo CA, Haut KM, Karlsgodt KH, Hansen L, Congdon E, Rosser T, Bilder RM, Silva AJ, Bearden CE. 2017. Spatial working memory in neurofibromatosis 1: Altered neural activity and functional connectivity. *Neuroimage Clin*. 15:801–811. doi:10.1016/j.nicl.2017.06.032.
- Ibrahim Amira F.A., Montojo CA, Haut KM, Karlsgodt KH, Hansen L, Congdon E, Rosser T, Bilder RM, Silva AJ, Bearden CE. 2017. Spatial working memory in neurofibromatosis 1: Altered neural activity and functional connectivity. *NeuroImage: Clinical*. 15(February):801–811. doi:10.1016/j.nicl.2017.06.032.
- Ishii A, Furusho M, Dupree JL, Bansal R. 2016. Strength of ERK1/2 MAPK Activation Determines Its Effect on Myelin and Axonal Integrity in the Adult CNS. *The Journal of Neuroscience*. 36(24):6471–6487. doi:10.1523/JNEUROSCI.0299-16.2016.
- Jindal GA, Goyal Y, Burdine RD, Rauen KA, Shvartsman SY. 2015. RASopathies: unraveling mechanisms with animal models. *Disease Models & Mechanisms*. 8(9):1167–1167. doi:10.1242/dmm.022442.
- Just MA, Cherkassky VL, Keller TA, Kana RK, Minshew NJ. 2007. Functional and Anatomical Cortical Underconnectivity in Autism: Evidence from an fMRI Study of an Executive Function Task and Corpus Callosum Morphometry. *Cerebral Cortex*. 17(4):951–961. doi:10.1093/cercor/bh1006.
- Kanehisa M, Furumichi M, Tanabe M, Sato Y, Morishima K. 2017. KEGG: new perspectives on genomes, pathways, diseases and drugs. *Nucleic Acids Research*. 45(D1):D353–D361. doi:10.1093/nar/gkw1092.
- Kaplan DR, Miller FD. 2000. Neurotrophin signal transduction in the nervous system. *Curr Opin Neurobiol*. 10(3):381–391.
- Karlsgodt KH, Rosser T, Lutkenhoff ES, Cannon TD, Silva A, Bearden CE. 2012. Alterations in white matter microstructure in neurofibromatosis-1. *PLoS ONE*. 7(10):e47854. doi:10.1371/journal.pone.0047854.
- Kawauchi S, Shou J, Santos R, Hébert JM, McConnell SK, Mason I, Calof AL. 2005. Fgf8 expression defines a morphogenetic center required for olfactory neurogenesis and nasal cavity development in the mouse. *Development*. 132(23):5211–5223. doi:10.1242/dev.02143.
- Keown CL, Shih P, Nair A, Peterson N, Mulvey ME, Müller R-A. 2013. Local Functional Overconnectivity in Posterior Brain Regions Is Associated with Symptom Severity in Autism Spectrum Disorders. *Cell Reports*. 5(3):567–572. doi:10.1016/j.celrep.2013.10.003.

- Kirsten WH, Mayer LA. 1967. Morphologic responses to a murine erythroblastosis virus. *J Natl Cancer Inst.* 39(2): 311–335.
- Klemke RL, Cai S, Giannini AL, Gallagher PJ, Lanerolle P de, Cheresh DA. 1997. Regulation of Cell Motility by Mitogen-activated Protein Kinase. *The Journal of Cell Biology.* 137(2): 481–492. doi:10.1083/jcb.137.2.481.
- Kohara K, Yasuda H, Huang Y, Adachi N, Sohya K, Tsumoto T. 2007. A local reduction in cortical GABAergic synapses after a loss of endogenous brain-derived neurotrophic factor, as revealed by single-cell gene knock-out method. *J Neurosci.* 27(27):7234–7244. doi:10.1523/JNEUROSCI.1943-07.2007.
- Koini M, Rombouts SARB, Veer IM, Van Buchem MA, Huijbregts SCJ. 2017. White matter microstructure of patients with neurofibromatosis type 1 and its relation to inhibitory control. *Brain Imaging Behav.* 11(6):1731–1740. doi:10.1007/s11682-016-9641-3.
- Kontaridis MI, Swanson KD, David FS, Barford D, Neel BG. 2006. *PTPN11* (Shp2) Mutations in LEOPARD Syndrome Have Dominant Negative, Not Activating, Effects. *Journal of Biological Chemistry.* 281(10):6785–6792. doi:10.1074/jbc.M513068200.
- Korb E, Finkbeiner S. 2011. Arc in synaptic plasticity: from gene to behavior. *Trends Neurosci.* 34(11):591–598. doi:10.1016/j.tins.2011.08.007.
- Korb E, Wilkinson CL, Delgado RN, Lovero KL, Finkbeiner S. 2013. Arc in the nucleus regulates PML-dependent GluA1 transcription and homeostatic plasticity. *Nature Neuroscience.* 16(7):874–883. doi:10.1038/nn.3429.
- Krenz M, Gulick J, Osinska HE, Colbert MC, Molkentin JD, Robbins J. 2008. Role of ERK1/2 signaling in congenital valve malformations in Noonan syndrome. *Proc Natl Acad Sci USA.* 105(48):18930–18935. doi:10.1073/pnas.0806556105.
- von Kriegsheim A, Baiocchi D, Birtwistle M, Sumpton D, Bienvenut W, Morrice N, Yamada K, Lamond A, Kalna G, Orton R, et al. 2009. Cell fate decisions are specified by the dynamic ERK interactome. *Nat Cell Biol.* 11(12):1458–1464. doi:10.1038/ncb1994.
- Kristiansen M, Ham J. 2014. Programmed cell death during neuronal development: the sympathetic neuron model. *Cell Death Differ.* 21(7):1025–1035. doi:10.1038/cdd.2014.47.
- Kumar RA, KaraMohamed S, Sudi J, Conrad DF, Brune C, Badner JA, Gilliam TC, Nowak NJ, Cook EH, Dobyns WB, et al. 2007. Recurrent 16p11.2 microdeletions in autism. *Human Molecular Genetics.* 17(4):628–638. doi:10.1093/hmg/ddm376.
- Kumar V, Zhang M-X, Swank MW, Kunz J, Wu G-Y. 2005. Regulation of dendritic morphogenesis by Ras-PI3K-Akt-mTOR and Ras-MAPK signaling pathways. *J Neurosci.* 25(49):11288–11299. doi:10.1523/JNEUROSCI.2284-05.2005.
- Kwan KY, Sestan N, Anton ES. 2012. Transcriptional co-regulation of neuronal migration and laminar identity in the neocortex. *Development.* 139(9):1535–1546. doi:10.1242/dev.069963.

- Kyriakis JM, App H, Zhang XF, Banerjee P, Brautigan DL, Rapp UR, Avruch J. 1992. Raf-1 activates MAP kinase-kinase. *Nature*. 358(6385):417–421. doi:10.1038/358417a0.
- Larsen DD, Wickersham IR, Callaway EM. 2007. Retrograde tracing with recombinant rabies virus reveals correlations between projection targets and dendritic architecture in layer 5 of mouse barrel cortex. *Front Neural Circuits*. 1:5. doi:10.3389/neuro.04.005.2007.
- Leal G, Bramham CR, Duarte CB. 2017. BDNF and Hippocampal Synaptic Plasticity. In: *Vitamins and Hormones*. Vol. 104. Elsevier. p. 153–195. [accessed 2018 Jul 13]. <http://linkinghub.elsevier.com/retrieve/pii/S008367291630053X>.
- Lee D a, Portnoy S, Hill P, Gillberg C, Patton M a. 2005. Psychological profile of children with Noonan syndrome. *Developmental medicine and child neurology*. 47(1): 35–38. doi:10.1017/S001216220500006X.
- Lee Y-S, Ehninger D, Zhou M, Oh J-Y, Kang M, Kwak C, Ryu H-H, Butz D, Araki T, Cai Y, et al. 2014. Mechanism and treatment for learning and memory deficits in mouse models of Noonan syndrome. *Nature Neuroscience*. 17(12):1736–1743. doi:10.1038/nn.3863.
- Leone DP, Heavner WE, Ferenczi EA, Dobрева G, Huguenard JR, Grosschedl R, McConnell SK. 2015. Satb2 Regulates the Differentiation of Both Callosal and Subcerebral Projection Neurons in the Developing Cerebral Cortex. *Cereb Cortex*. 25(10):3406–3419. doi:10.1093/cercor/bhu156.
- Leone DP, Srinivasan K, Chen B, Alcamo E, McConnell SK. 2008. The determination of projection neuron identity in the developing cerebral cortex. *Curr Opin Neurobiol*. 18(1):28–35. doi:10.1016/j.conb.2008.05.006.
- Ley R, Balmanno K, Hadfield K, Weston C, Cook SJ. 2003. Activation of the ERK1/2 Signaling Pathway Promotes Phosphorylation and Proteasome-dependent Degradation of the BH3-only Protein, Bim. *Journal of Biological Chemistry*. 278(21):18811–18816. doi:10.1074/jbc.M301010200.
- Li S, Mattar P, Dixit R, Lawn SO, Wilkinson G, Kinch C, Eisenstat D, Kurrasch DM, Chan JA, Schuurmans C. 2014. RAS/ERK Signaling Controls Proneural Genetic Programs in Cortical Development and Gliomagenesis. *Journal of Neuroscience*. 34(6):2169–2190. doi:10.1523/JNEUROSCI.4077-13.2014.
- Li W, Cui Y, Kushner SA, Brown RAM, Jentsch JD, Frankland PW, Cannon TD, Silva AJ. 2005. The HMG-CoA Reductase Inhibitor Lovastatin Reverses the Learning and Attention Deficits in a Mouse Model of Neurofibromatosis Type 1. *Current Biology*. 15(21):1961–1967. doi:10.1016/j.cub.2005.09.043.
- Liu W, Ye P, O’Kusky JR, D’Ercole AJ. 2009. Type 1 insulin-like growth factor receptor signaling is essential for the development of the hippocampal formation and dentate gyrus. *J Neurosci Res*. 87(13):2821–2832. doi:10.1002/jnr.22129.

Lonze BE, Riccio A, Cohen S, Ginty DD. 2002. Apoptosis, Axonal Growth Defects, and Degeneration of Peripheral Neurons in Mice Lacking CREB. *Neuron*. 34(3):371–385. doi: 10.1016/S0896-6273(02)00686-4.

Lowenstein EJ, Daly RJ, Batzer AG, Li W, Margolis B, Lammers R, Ullrich A, Skolnik EY, Bar-Sagi D, Schlessinger J. 1992. The SH2 and SH3 domain-containing protein GRB2 links receptor tyrosine kinases to ras signaling. *Cell*. 70(3):431–442.

Lunn JS, Fishwick KJ, Halley PA, Storey KG. 2007. A spatial and temporal map of FGF/Erk1/2 activity and response repertoires in the early chick embryo. *Dev Biol*. 302(2):536–552. doi: 10.1016/j.ydbio.2006.10.014.

Luo J-M, Cen L-P, Zhang X-M, Chiang SW-Y, Huang Y, Lin D, Fan Y-M, van Rooijen N, Lam DSC, Pang CP, et al. 2007. PI3K/akt, JAK/STAT and MEK/ERK pathway inhibition protects retinal ganglion cells via different mechanisms after optic nerve injury. *Eur J Neurosci*. 26(4):828–842. doi: 10.1111/j.1460-9568.2007.05718.x.

Madisen L, Zwingman TA, Sunkin SM, Oh SW, Zariwala HA, Gu H, Ng LL, Palmiter RD, Hawrylycz MJ, Jones AR, et al. 2010. A robust and high-throughput Cre reporting and characterization system for the whole mouse brain. *Nature Neuroscience*. 13(1):133–140. doi: 10.1038/nn.2467.

Maisonpierre PC, Belluscio L, Friedman B, Alderson RF, Wiegand SJ, Furth ME, Lindsay RM, Yancopoulos GD. 1990. NT-3, BDNF, and NGF in the developing rat nervous system: parallel as well as reciprocal patterns of expression. *Neuron*. 5(4):501–509.

Majdan M, Shatz CJ. 2006. Effects of visual experience on activity-dependent gene regulation in cortex. *Nat Neurosci*. 9(5):650–659. doi: 10.1038/nn1674.

Margaret P Adam, Holly H Ardinger, Roberta A Pagon, Stephanie E Wallace, Lora JH Bean, Karen Stephens, Anne Amemiya, editors. 1993. *Gene Reviews*. Seattle (WA): University of Washington, Seattle.

Martinou I, Desagher S, Eskes R, Antonsson B, André E, Fakan S, Martinou JC. 1999. The release of cytochrome c from mitochondria during apoptosis of NGF-deprived sympathetic neurons is a reversible event. *J Cell Biol*. 144(5):883–889.

Mazzoni IE, Saïd FA, Aloyz R, Miller FD, Kaplan D. 1999. Ras regulates sympathetic neuron survival by suppressing the p53-mediated cell death pathway. *J Neurosci*. 19(22):9716–9727.

McCarthy MJ, Rubin LL, Philpott KL. 1997. Involvement of caspases in sympathetic neuron apoptosis. *J Cell Sci*. 110 (Pt 18):2165–2173.

McCubrey JA, Steelman LS, Chappell WH, Abrams SL, Wong EWT, Chang F, Lehmann B, Terrian DM, Milella M, Tafuri A, et al. 2007. Roles of the Raf/MEK/ERK pathway in cell growth, malignant transformation and drug resistance. *Biochimica et Biophysica Acta (BBA) - Molecular Cell Research*. 1773(8):1263–1284. doi: 10.1016/j.bbamcr.2006.10.001.

McKenna WL, Ortiz-Londono CF, Mathew TK, Hoang K, Katzman S, Chen B. 2015. Mutual regulation between *Satb2* and *Fezf2* promotes subcerebral projection neuron identity in the developing cerebral cortex. *Proc Natl Acad Sci USA*. 112(37):11702–11707. doi:10.1073/pnas.1504144112.

Mejias R, Adamczyk A, Anggono V, Niranjana T, Thomas GM, Sharma K, Skinner C, Schwartz CE, Stevenson RE, Fallin MD, et al. 2011. Gain-of-function glutamate receptor interacting protein 1 variants alter GluA2 recycling and surface distribution in patients with autism. *Proc Natl Acad Sci USA*. 108(12):4920–4925. doi:10.1073/pnas.1102233108.

Merline M, Kalil K. 1990. Cell death of corticospinal neurons is induced by axotomy before but not after innervation of spinal targets. *J Comp Neurol*. 296(3):506–516. doi:10.1002/cne.902960313.

Meyers EN, Lewandoski M, Martin GR. 1998. An *Fgf8* mutant allelic series generated by Cre- and Flp-mediated recombination. *Nat Genet*. 18(2):136–141. doi:10.1038/ng0298-136.

Minichiello L. 2009. TrkB signalling pathways in LTP and learning. *Nature Reviews Neuroscience*. 10(12):850–860. doi:10.1038/nrn2738.

Mitchell DJ, Blasler KR, Jeffery ED, Ross MW, Pullikuth AK, Suo D, Park J, Smiley WR, Lo KW-H, Shabanowitz J, et al. 2012. Trk activation of the ERK1/2 kinase pathway stimulates intermediate chain phosphorylation and recruits cytoplasmic dynein to signaling endosomes for retrograde axonal transport. *J Neurosci*. 32(44):15495–15510. doi:10.1523/JNEUROSCI.5599-11.2012.

Molnár Z, Cheung AFP. 2006. Towards the classification of subpopulations of layer V pyramidal projection neurons. *Neurosci Res*. 55(2):105–115. doi:10.1016/j.neures.2006.02.008.

Molyneaux BJ, Arlotta P, Menezes JRL, Macklis JD. 2007. Neuronal subtype specification in the cerebral cortex. *Nat Rev Neurosci*. 8(6):427–437. doi:10.1038/nrn2151.

Monje P, Hernández-Losa J, Lyons RJ, Castellone MD, Gutkind JS. 2005. Regulation of the transcriptional activity of c-Fos by ERK: A novel role for the prolyl isomerase Pin1. *Journal of Biological Chemistry*. 280(42):35081–35084. doi:10.1074/jbc.C500353200.

Morales B, Choi S-Y, Kirkwood A. 2002. Dark rearing alters the development of GABAergic transmission in visual cortex. *J Neurosci*. 22(18):8084–8090.

Newbern J, Zhong J, Wickramasinghe RS, Li X, Wu Y, Samuels I, Cherosky N, Karlo JC, O'Loughlin B, Wikenheiser J, et al. 2008. Mouse and human phenotypes indicate a critical conserved role for ERK2 signaling in neural crest development. *Proc Natl Acad Sci USA*. 105(44):17115–17120. doi:10.1073/pnas.0805239105.

Nikolaienko O, Eriksen MS, Patil S, Bito H, Bramham CR. 2017. Stimulus-evoked ERK-dependent phosphorylation of activity-regulated cytoskeleton-associated protein (Arc) regulates its neuronal subcellular localization. *Neuroscience*. 360:68–80. doi: 10.1016/j.neuroscience.2017.07.026.

Nowaczyk MJM, Thompson BA, Zeesman S, Moog U, Sanchez-Lara PA, Magoulas PL, Falk RE, Hoover-Fong JE, Batista DAS, Amudhavalli SM, et al. 2014. Deletion of *MAP2K2/MEK2*: a novel mechanism for a RASopathy?: *MAP2K2/MEK2* deletion. *Clinical Genetics*. 85(2):138–146. doi:10.1111/cge.12116.

Oberman L, Eldaief M, Fecteau S, Ifert-Miller F, Tormos JM, Pascual-Leone A. 2012. Abnormal modulation of corticospinal excitability in adults with Asperger's syndrome. *Eur J Neurosci*. 36(6):2782–2788. doi:10.1111/j.1460-9568.2012.08172.x.

O'Brien DE, Alter BJ, Satomoto M, Morgan CD, Davidson S, Vogt SK, Norman ME, Gereau GB, Demaro JA, Landreth GE, et al. 2015. ERK2 Alone Drives Inflammatory Pain But Cooperates with ERK1 in Sensory Neuron Survival. *J Neurosci*. 35(25):9491–9507. doi: 10.1523/JNEUROSCI.4404-14.2015.

Oliveira CS, Rigon AP, Leal RB, Rossi FM. 2008. The activation of ERK1/2 and p38 mitogen-activated protein kinases is dynamically regulated in the developing rat visual system. *International Journal of Developmental Neuroscience*. 26(3–4):355–362. doi: 10.1016/j.ijdevneu.2007.12.007.

Osterweil EK, Chuang S-C, Chubykin AA, Sidorov M, Bianchi R, Wong RKS, Bear MF. 2013. Lovastatin Corrects Excess Protein Synthesis and Prevents Epileptogenesis in a Mouse Model of Fragile X Syndrome. *Neuron*. 77(2):243–250. doi: 10.1016/j.neuron.2012.01.034.

O'Toole CM, Povey S, Hepburn P, Franks LM. 1983. Identity of some human bladder cancer cell lines. *Nature*. 301(5899):429–430.

Ozdinler PH, Macklis JD. 2006. IGF-I specifically enhances axon outgrowth of corticospinal motor neurons. *Nat Neurosci*. 9(11):1371–1381. doi:10.1038/nn1789.

Panja D, Dagyte G, Bidinosti M, Wibrand K, Kristiansen A-M, Sonenberg N, Bramham CR. 2009. Novel translational control in Arc-dependent long term potentiation consolidation in vivo. *J Biol Chem*. 284(46):31498–31511. doi: 10.1074/jbc.M109.056077.

Parada LF, Tabin CJ, Shih C, Weinberg RA. 1982. Human EJ bladder carcinoma oncogene is homologue of Harvey sarcoma virus ras gene. *Nature*. 297(5866):474–478.

Petrella LI, Cai Y, Sereno J V., Gonçalves SI, Silva AJ, Castelo-Branco M. 2016. Brain and behaviour phenotyping of a mouse model of neurofibromatosis type-1: an MRI/DTI study on social cognition. *Genes, Brain and Behavior*. 15(7):637–646. doi: 10.1111/gbb.12305.

Pfeiffer V, Götz R, Xiang C, Camarero G, Braun A, Zhang Y, Blum R, Heinsen H, Nieswandt B, Rapp UR. 2013. Ablation of BRAF impairs neuronal differentiation in the postnatal hippocampus and cerebellum. *PLoS ONE*. 8(3):e58259. doi: 10.1371/journal.pone.0058259.

Pillat MM, Lameu C, Trujillo CA, Glaser T, Cappellari AR, Negraes PD, Battastini AMO, Schwindt TT, Muotri AR, Ulrich H. 2016. Bradykinin promotes neuron-generating division of neural progenitor cells through ERK activation. *Journal of Cell Science*. 129(18):3437–3448. doi: 10.1242/jcs.192534.

Pinto D, Pagnamenta AT, Klei L, Anney R, Merico D, Regan R, Conroy J, Magalhaes TR, Correia C, Abrahams BS, et al. 2010. Functional impact of global rare copy number variation in autism spectrum disorders. *Nature*. 466(7304):368–372. doi: 10.1038/nature09146.

Plasschaert E, Eylen LV, Descheemaeker M-J, Noens I, Legius E, Steyaert J. 2015. Executive functioning deficits in children with neurofibromatosis type 1: The influence of intellectual and social functioning. *American Journal of Medical Genetics Part B: Neuropsychiatric Genetics*. 171(3):348–362. doi: 10.1002/ajmg.b.32414.

Poelmann RE, Gittenberger-de Groot AC. 1999. A subpopulation of apoptosis-prone cardiac neural crest cells targets to the venous pole: multiple functions in heart development? *Dev Biol*. 207(2):271–286. doi: 10.1006/dbio.1998.9166.

Polleux F, Snider W. 2010. Initiating and Growing an Axon. *Cold Spring Harb Perspect Biol*. 2(4). doi: 10.1101/cshperspect.a001925. [accessed 2018 Oct 16]. <https://www.ncbi.nlm.nih.gov/pmc/articles/PMC2845204/>.

Porcher C, Hatchett C, Longbottom RE, McAinch K, Sihra TS, Moss SJ, Thomson AM, Jovanovic JN. 2011. Positive feedback regulation between gamma-aminobutyric acid type A (GABA(A)) receptor signaling and brain-derived neurotrophic factor (BDNF) release in developing neurons. *J Biol Chem*. 286(24):21667–21677. doi: 10.1074/jbc.M110.201582.

Pouysségur J, Volmat V, Lenormand P. 2002. Fidelity and spatio-temporal control in MAP kinase (ERKs) signalling. *Biochemical Pharmacology*. 64(5–6):755–763. doi: 10.1016/S0006-2952(02)01135-8.

Pucilowska J, Puzerey PA, Karlo JC, Galan RF, Landreth GE. 2012. Disrupted ERK Signaling during Cortical Development Leads to Abnormal Progenitor Proliferation, Neuronal and Network Excitability and Behavior, Modeling Human Neuro-Cardio-Facial-Cutaneous and Related Syndromes. *Journal of Neuroscience*. 32(25):8663–8677. doi: 10.1523/JNEUROSCI.1107-12.2012.

Pucilowska J, Vithayathil J, Tavares EJ, Kelly C, Karlo JC, Landreth GE. 2015. The 16p11.2 Deletion Mouse Model of Autism Exhibits Altered Cortical Progenitor Proliferation and Brain Cytoarchitecture Linked to the ERK MAPK Pathway. *Journal of Neuroscience*. 35(7):3190–3200. doi: 10.1523/JNEUROSCI.4864-13.2015.

Purves D, editor. 2012. *Neuroscience*. 5th ed. Sunderland, Mass: Sinauer Associates.

- Qi H, Prabakaran S, Cantrelle F-X, Chambraud B, Gunawardena J, Lippens G, Landrieu I. 2016. Characterization of Neuronal Tau Protein as a Target of Extracellular Signal-regulated Kinase. *Journal of Biological Chemistry*. 291(14): 7742–7753. doi: 10.1074/jbc.M115.700914.
- Qian X, Riccio A, Zhang Y, Ginty DD. 1998. Identification and Characterization of Novel Substrates of Trk Receptors in Developing Neurons. *Neuron*. 21(5):1017–1029. doi: 10.1016/S0896-6273(00)80620-0.
- Qiu A, Mori S, Miller MI. 2015. Diffusion tensor imaging for understanding brain development in early life. *Annu Rev Psychol*. 66:853–876. doi: 10.1146/annurev-psych-010814-015340.
- Qui MS, Green SH. 1992. PC12 cell neuronal differentiation is associated with prolonged p21ras activity and consequent prolonged ERK activity. *Neuron*. 9(4):705–717.
- Ramkumar A, Jong BY, Ori-McKenney KM. 2018. ReMAPping the microtubule landscape: How phosphorylation dictates the activities of microtubule-associated proteins. *Dev Dyn*. 247(1):138–155. doi: 10.1002/dvdy.24599.
- Rao VR, Pintchovski SA, Chin J, Peebles CL, Mitra S, Finkbeiner S. 2006. AMPA receptors regulate transcription of the plasticity-related immediate-early gene *Arc*. *Nature Neuroscience*. 9(7):887–895. doi: 10.1038/nn1708.
- Rauen Katherine A. 2013. The RASopathies. *Annual Review of Genomics and Human Genetics*. 14(1):355–369. doi: 10.1146/annurev-genom-091212-153523.
- Rauen Katherine A. 2013. The RASopathies. *Annu Rev Genomics Hum Genet*. 14:355–369. doi: 10.1146/annurev-genom-091212-153523.The.
- Rauen KA. 2016. Cardiofaciocutaneous Syndrome. p. 20.
- Ray LB, Sturgill TW. 1987. Rapid stimulation by insulin of a serine/threonine kinase in 3T3-L1 adipocytes that phosphorylates microtubule-associated protein 2 in vitro. *Proceedings of the National Academy of Sciences*. 84(6):1502–1506. doi: 10.1073/pnas.84.6.1502.
- Reddy EP, Reynolds RK, Santos E, Barbacid M. 1982. A point mutation is responsible for the acquisition of transforming properties by the T24 human bladder carcinoma oncogene. *Nature*. 300(5888):149–152.
- Reichardt LF. 2006. Neurotrophin-regulated signalling pathways. *Philosophical Transactions of the Royal Society B: Biological Sciences*. 361(1473):1545–1564. doi: 10.1098/rstb.2006.1894.
- Riccio A, Ahn S, Davenport CM, Blendy JA, Ginty DD. 1999. Mediation by a CREB family transcription factor of NGF-dependent survival of sympathetic neurons. *Science*. 286(5448):2358–2361.
- Rossi J, Balthasar N, Olson D, Scott M, Berglund E, Lee CE, Choi MJ, Lauzon D, Lowell BB, Elmquist JK. 2011. Melanocortin-4 Receptors Expressed by Cholinergic

- Neurons Regulate Energy Balance and Glucose Homeostasis. *Cell Metabolism*. 13(2):195–204. doi:10.1016/j.cmet.2011.01.010.
- Rotwein P, Burgess SK, Milbrandt JD, Krause JE. 1988. Differential expression of insulin-like growth factor genes in rat central nervous system. *Proc Natl Acad Sci USA*. 85(1):265–269.
- Rubenstein JLR, Merzenich MM. 2003. Model of autism: increased ratio of excitation/inhibition in key neural systems. *Genes Brain Behav*. 2(5):255–267.
- Samuels IS, Saitta SC, Landreth GE. 2009. MAP'ing CNS Development and Cognition: An ERKsome Process. *Neuron*. 61(2):160–167. doi:10.1016/j.neuron.2009.01.001.
- Santos E, Martin-Zanca D, Reddy EP, Pierotti MA, Della Porta G, Barbacid M. 1984. Malignant activation of a K-ras oncogene in lung carcinoma but not in normal tissue of the same patient. *Science*. 223(4637):661–664.
- Santos E, Tronick SR, Aaronson SA, Pulciani S, Barbacid M. 1982. T24 human bladder carcinoma oncogene is an activated form of the normal human homologue of BALB- and Harvey-MSV transforming genes. *Nature*. 298(5872):343–347.
- Schreyer DJ, Jones EG. 1982. Growth and target finding by axons of the corticospinal tract in prenatal and postnatal rats. *Neuroscience*. 7(8):1837–1853.
- Scolnick EM, Papageorge AG, Shih TY. 1979. Guanine nucleotide-binding activity as an assay for src protein of rat-derived murine sarcoma viruses. *Proc Natl Acad Sci USA*. 76(10):5355–5359.
- Segarra J, Balenci L, Drenth T, Maina F, Lamballe F. 2006. Combined signaling through ERK, PI3K/AKT, and RAC1/p38 is required for met-triggered cortical neuron migration. *J Biol Chem*. 281(8):4771–4778. doi:10.1074/jbc.M508298200.
- Sheean ME, McShane E, Cheret C, Walcher J, Müller T, Wulf-Goldenberg A, Hoelper S, Garratt AN, Krüger M, Rajewsky K, et al. 2014. Activation of MAPK overrides the termination of myelin growth and replaces Nrg1/ErbB3 signals during Schwann cell development and myelination. *Genes Dev*. 28(3):290–303. doi:10.1101/gad.230045.113.
- Shepherd JD, Bear MF. 2011. New views of Arc, a master regulator of synaptic plasticity. *Nature Neuroscience*. 14(3):279–284. doi:10.1038/nn.2708.
- Shilyansky C, Lee YS, Silva AJ. 2010. Molecular and Cellular Mechanisms of Learning Disabilities: A Focus on NF1. *Annual Review of Neuroscience*. 33(1):221–243. doi:10.1146/annurev-neuro-060909-153215.
- Shinya M, Koshida S, Sawada A, Kuroiwa A, Takeda H. 2001. Fgf signalling through MAPK cascade is required for development of the subpallial telencephalon in zebrafish embryos. *Development*. 128(21):4153–4164.

Sohur US, Padmanabhan HK, Kotchetkov IS, Menezes JRL, Macklis JD. 2014. Feature article: Anatomic and molecular development of corticostriatal projection neurons in mice. *Cerebral Cortex*. 24(2):293–303. doi: 10.1093/cercor/bhs342.

Stevenson DA, Allen S, Tidyman WE, Carey JC, Viskochil DH, Stevens A, Hanson H, Sheng X, Thompson BA, Okumura MJ, et al. 2012. Peripheral muscle weakness in RASopathies. *Muscle Nerve*. 46(3):394–399. doi: 10.1002/mus.23324.

Steward O, Wallace CS, Lyford GL, Worley PF. 1998. Synaptic activation causes the mRNA for the IEG Arc to localize selectively near activated postsynaptic sites on dendrites. *Neuron*. 21(4):741–751.

Steward O, Worley PF. 2001. A cellular mechanism for targeting newly synthesized mRNAs to synaptic sites on dendrites. *Proc Natl Acad Sci USA*. 98(13):7062–7068. doi: 10.1073/pnas.131146398.

Stoner R, Chow ML, Boyle MP, Sunkin SM, Mouton PR, Roy S, Wynshaw-Boris A, Colamarino SA, Lein ES, Courchesne E. 2014. Patches of Disorganization in the Neocortex of Children with Autism. *New England Journal of Medicine*. 370(13):1209–1219. doi: 10.1056/NEJMoa1307491.

Supekar K, Uddin LQ, Khouzam A, Phillips J, Gaillard WD, Kenworthy LE, Yerys BE, Vaidya CJ, Menon V. 2013. Brain Hyperconnectivity in Children with Autism and its Links to Social Deficits. *Cell Reports*. 5(3):738–747. doi: 10.1016/j.celrep.2013.10.001.

Taparowsky E, Suard Y, Fasano O, Shimizu K, Goldfarb M, Wigler M. 1982. Activation of the T24 bladder carcinoma transforming gene is linked to a single amino acid change. *Nature*. 300(5894):762–765.

The UniProt Consortium. 2017. UniProt: the universal protein knowledgebase. *Nucleic Acids Research*. 45(D1):D158–D169. doi: 10.1093/nar/gkw1099.

Thomas GM, Haganir RL. 2004. MAPK cascade signalling and synaptic plasticity. *Nature Reviews Neuroscience*. 5(3):173–183. doi: 10.1038/nrn1346.

Thompson SJ, Sargsyan A, Lee S-A, Yuen JJ, Cai J, Smalling R, Ghyselink N, Mark M, Blaner WS, Graham TE. 2017. Hepatocytes Are the Principal Source of Circulating RBP4 in Mice. *Diabetes*. 66(1):58–63. doi: 10.2337/db16-0286.

Tidyman WE, Lee HS, Rauen KA. 2011. Skeletal muscle pathology in Costello and cardio-facio-cutaneous syndromes: developmental consequences of germline Ras/MAPK activation on myogenesis. *Am J Med Genet C Semin Med Genet*. 157C(2):104–114. doi: 10.1002/ajmg.c.30298.

Tidyman WE, Rauen KA. 2009. The RASopathies: developmental syndromes of Ras/MAPK pathway dysregulation. *Current Opinion in Genetics & Development*. 19(3):230–236. doi: 10.1016/j.gde.2009.04.001.

Tidyman WE, Rauen KA. 2016. Pathogenetics of the RASopathies. *Human Molecular Genetics*. 25(R2):R123–R132. doi: 10.1093/hmg/ddw191.

Timmusk T, Belluardo N, Persson H, Metsis M. 1994. Developmental regulation of brain-derived neurotrophic factor messenger RNAs transcribed from different promoters in the rat brain. *Neuroscience*. 60(2):287–291.

Tolbert DL, Der T. 1987. Redirected growth of pyramidal tract axons following neonatal pyramidotomy in cats. *J Comp Neurol*. 260(2):299–311. doi: 10.1002/cne.902600210.

Tomson SN, Schreiner MJ, Narayan M, Rosser T, Enrique N, Silva AJ, Allen GI, Bookheimer SY, Bearden CE. 2015a. Resting state functional MRI reveals abnormal network connectivity in neurofibromatosis 1. *Hum Brain Mapp*. 36(11):4566–4581. doi: 10.1002/hbm.22937.

Tomson SN, Schreiner MJ, Narayan M, Rosser T, Enrique N, Silva AJ, Allen GI, Bookheimer SY, Bearden CE. 2015b. Resting state functional MRI reveals abnormal network connectivity in neurofibromatosis 1. *Human Brain Mapping*. 36(11):4566–4581. doi: 10.1002/hbm.22937.

Toyoda R, Assimacopoulos S, Wilcoxon J, Taylor A, Feldman P, Suzuki-Hirano A, Shimogori T, Grove EA. 2010. FGF8 acts as a classic diffusible morphogen to pattern the neocortex. *Development*. 137(20):3439–3448. doi: 10.1242/dev.055392.

Traverse S, Gomez N, Paterson H, Marshall C, Cohen P. 1992. Sustained activation of the mitogen-activated protein (MAP) kinase cascade may be required for differentiation of PC12 cells. Comparison of the effects of nerve growth factor and epidermal growth factor. *Biochemical Journal*. 288(2):351–355. doi: 10.1042/bj2880351.

Tropea D, Kreiman G, Lyckman A, Mukherjee S, Yu H, Horng S, Sur M. 2006. Gene expression changes and molecular pathways mediating activity-dependent plasticity in visual cortex. *Nat Neurosci*. 9(5):660–668. doi: 10.1038/nn1689.

Ueno M, Fujita Y, Tanaka T, Nakamura Y, Kikuta J, Ishii M, Yamashita T. 2013. Layer V cortical neurons require microglial support for survival during postnatal development. *Nat Neurosci*. 16(5):543–551. doi: 10.1038/nn.3358.

Valiente M, Ciceri G, Rico B, Marín O. 2011. Focal Adhesion Kinase Modulates Radial Glia-Dependent Neuronal Migration through Connexin-26. *J Neurosci*. 31(32):11678–11691. doi: 10.1523/JNEUROSCI.2678-11.2011.

Vaudry D. 2002. Signaling Pathways for PC12 Cell Differentiation: Making the Right Connections. *Science*. 296(5573):1648–1649. doi: 10.1126/science.1071552.

Vetter IR. 2001. The Guanine Nucleotide-Binding Switch in Three Dimensions. *Science*. 294(5545):1299–1304. doi: 10.1126/science.1062023.

Wakamatsu Y, Mochii M, Vogel KS, Weston JA. 1998. Avian neural crest-derived neurogenic precursors undergo apoptosis on the lateral migration pathway. *Development*. 125(21):4205–4213.

Waltereit R, Dammermann B, Wulff P, Scafidi J, Staubli U, Kauselmann G, Bundman M, Kuhl D. 2001. Arg3.1/Arc mRNA induction by Ca²⁺ and cAMP requires protein kinase A and mitogen-activated protein kinase/extracellular regulated kinase activation. *J Neurosci.* 21(15):5484–5493.

Wang Y, Kim E, Wang X, Novitsch BG, Yoshikawa K, Chang L-S, Zhu Y. 2012. ERK Inhibition Rescues Defects in Fate Specification of Nf1-Deficient Neural Progenitors and Brain Abnormalities. *Cell.* 150(4):816–830. doi:10.1016/j.cell.2012.06.034.

Warne PH, Viciano PR, Downward J. 1993. Direct interaction of Ras and the amino-terminal region of Raf-1 in vitro. *Nature.* 364(6435):352–355. doi:10.1038/364352a0.

Weiss LA, Shen Y, Korn JM, Arking DE, Miller DT, Fossdal R, Saemundsen E, Stefansson H, Ferreira MAR, Green T, et al. 2008. Association between Microdeletion and Microduplication at 16p11.2 and Autism. *New England Journal of Medicine.* 358(7):667–675. doi:10.1056/NEJMoa075974.

Wiese S, Pei G, Karch C, Troppmair J, Holtmann B, Rapp UR, Sendtner M. 2001. Specific function of B-Raf in mediating survival of embryonic motoneurons and sensory neurons. *Nature Neuroscience.* 4(2):137–142. doi:10.1038/83960.

Willsey AJ, Sanders SJ, Li M, Dong S, Tebbenkamp AT, Muhle RA, Reilly SK, Lin L, Fertuzinhos S, Miller JA, et al. 2013. Coexpression Networks Implicate Human Midfetal Deep Cortical Projection Neurons in the Pathogenesis of Autism. *Cell.* 155(5):997–1007. doi:10.1016/j.cell.2013.10.020.

Wu S-X, Goebbels S, Nakamura Kouichi, Nakamura Kazuhiro, Kometani K, Minato N, Kaneko T, Nave K-A, Tamamaki N. 2005. Pyramidal neurons of upper cortical layers generated by NEX-positive progenitor cells in the subventricular zone. *Proc Natl Acad Sci USA.* 102(47):17172–17177. doi:10.1073/pnas.0508560102.

Xia Z, Dickens M, Raingeaud J I, Davis RJ, Greenberg ME. 1995. Opposing Effects of ERK and JNK-p38 MAP Kinases on Apoptosis. *Science.* 270(5240):1326–1331. doi:10.1126/science.270.5240.1326.

Xing L, Larsen RS, Bjorklund GR, Li X, Wu Y, Philpot BD, Snider WD, Newbern JM. 2016. Layer specific and general requirements for ERK/MAPK signaling in the developing neocortex. *eLife.* 5. doi:10.7554/eLife.11123. [accessed 2018 Jul 17]. <https://elifesciences.org/articles/11123>.

Xue M, Atallah BV, Scanziani M. 2014. Equalizing excitation-inhibition ratios across visual cortical neurons. *Nature.* 511(7511):596–600. doi:10.1038/nature13321.

Yang M, Wu M, Xia P, Wang C, Yan P, Gao Q, Liu J, Wang H, Duan X, Yang X. 2012. The role of microtubule-associated protein 1B in axonal growth and neuronal migration in the central nervous system. *Neural Regen Res.* 7(11):842–848. doi:10.3969/j.issn.1673-5374.2012.11.008.

Yates B, Braschi B, Gray KA, Seal RL, Tweedie S, Bruford EA. 2017. Genenames.org: the HGNC and VGNC resources in 2017. *Nucleic Acids Res.* 45(Database issue):D619–D625. doi:10.1093/nar/gkw1033.

York RD, Molliver DC, Grewal SS, Stenberg PE, McCleskey EW, Stork PJS. 2000. Role of Phosphoinositide 3-Kinase and Endocytosis in Nerve Growth Factor-Induced Extracellular Signal-Regulated Kinase Activation via Ras and Rap1. *Molecular and Cellular Biology*. 20(21):8069–8083. doi:10.1128/MCB.20.21.8069-8083.2000.

Zamboni S. L., Loenneker T, Boltshauser E, Martin E, Il'yasov KA. 2007. Contribution of diffusion tensor MR imaging in detecting cerebral microstructural changes in adults with neurofibromatosis type 1. *AJNR Am J Neuroradiol*. 28(4):773–776.

Zamboni S L, Loenneker T, Boltshauser E, Martin E, Il'yasov KA. 2007. Contribution of diffusion tensor MR imaging in detecting cerebral microstructural changes in adults with neurofibromatosis type 1. *AJNR American journal of neuroradiology*. 28(4): 773–776. doi:28/4/773 [pii].

Zhang L, Bartley CM, Gong X, Hsieh LS, Lin TV, Feliciano DM, Bordey A. 2014. MEK-ERK1/2-Dependent FLNA Overexpression Promotes Abnormal Dendritic Patterning in Tuberous Sclerosis Independent of mTOR. *Neuron*. 84(1):78–91. doi:10.1016/j.neuron.2014.09.009.

Zhang X, Tang N, Hadden TJ, Rishi AK. 2011. Akt, FoxO and regulation of apoptosis. *Biochimica et Biophysica Acta (BBA) - Molecular Cell Research*. 1813(11):1978–1986. doi:10.1016/j.bbamcr.2011.03.010.

Zhang XF, Settleman J, Kyriakis JM, Takeuchi-Suzuki E, Elledge SJ, Marshall MS, Bruder JT, Rapp UR, Avruch J. 1993. Normal and oncogenic p21ras proteins bind to the amino-terminal regulatory domain of c-Raf-1. *Nature*. 364(6435):308–313. doi:10.1038/364308a0.

Zhong J. 2016. RAS and downstream RAF-MEK and PI3K-AKT signaling in neuronal development, function and dysfunction. *Biol Chem*. 397(3):215–222. doi:10.1515/hsz-2015-0270.

Zhong J, Li X, McNamee C, Chen AP, Baccarini M, Snider WD. 2007. Raf kinase signaling functions in sensory neuron differentiation and axon growth in vivo. *Nat Neurosci*. 10(5):598–607. doi:10.1038/nn1898.

Zhou Y, Pernet V, Hauswirth WW, Di Polo A. 2005. Activation of the extracellular signal-regulated kinase 1/2 pathway by AAV gene transfer protects retinal ganglion cells in glaucoma. *Mol Ther*. 12(3):402–412. doi:10.1016/j.ymthe.2005.04.004.

APPENDIX A
CURRICULUM VITAE

George Reed Bjorklund

Arizona State University
School of Life Sciences
427 East Tyler Mall, LSE 317
Tempe, AZ 85287
gbjorklu@asu.edu

Permanent Address
4185 West Harrison Street
Chandler, AZ 85226
480-329-7174
reed.bjorklund@gmail.com

Education

Molecular and Cellular Biology PhD Arizona State University - Tempe, AZ	Expected completion Oct. 2018 Current Degree GPA – 3.94
Molecular and Cellular Biology MS Arizona State University - Tempe, AZ	Completed May 2015
Molecular Biosciences and Biotechnology Arizona State University - Tempe, AZ	Completed May 2011 Graduated <i>Magna cum Laude</i> Awarded Outstanding MBB Student of the Year 2010-2011
A.A.A.S. Computer Aided Drafting and Design Miller Institute/ITT Technical Institute	Completed Dec 1984

Experience

Graduate Research Assistant:

School of Life Sciences, ASU, Newbern Lab
Jan. 2014 - Present

- Developed a laboratory specific RNA isolation and enrichment protocol based on the "Ribotag" procedure to assess differential gene expression in RASopathy models.
- Performed protein expression analysis in embryonic, neo-natal, and mature models of neurodevelopmental disease using IHC and Western Blotting techniques.
- Performed axonal tract tracing experiments in models with neurodevelopmental disease to assess spinal cord innervation and axonal branching patterns in the forebrain, midbrain, hindbrain, and the spinal cord.
- Executed and maintained breeding programs for a variety of genetically modified mouse models used in developmental neuroscience research.
- Assisted in the start-up and operation of the laboratory as well as the continuing activities of the lab.

Center for Infectious Diseases and Vaccinology, Mason Lab
May 2011– Oct. 2014

- Continued working on the Ebola GP1 fusion protein by augmenting the expression cassette with an RNA silencing suppressor, p19, and a chaperone protein, calreticulin, to improve the plant-based production of human proteins of interest.
Patent issued: (WO2012145759) METHODS OF PROTEIN PRODUCTION AND COMPOSITIONS THEREOF
- Began a viral silencing project that would target individual transcription factors to abrogate or delay the cell death response caused by ER stress in plant cells while producing human proteins of interest.
- Taught and assisted intern students in laboratory protocol, safety, and procedures.
- Handled all laboratory purchasing and supply maintenance needs as well as the infrastructure of the laboratory to maintain a working environment.

Undergraduate Research Internship:

Center for Infectious Diseases and Vaccinology, Mason Lab
Dec. 2009 - May 2011

- Worked on the expression of Ebola coat protein/IgG fusion protein produced in plants to be used as vaccines against the Ebola virus.
- Learned and implemented various laboratory techniques used in recombinant DNA production and viral transfection of plants for protein production.

Teaching Assistant:

BIO 351: Developmental Biology Fall 2017

- Assisted in the lecture course teaching the principles of developmental biology, including the development of major organ systems and their cellular and molecular mechanisms.
- Held bi-weekly office hours to aid students in learning objectives. Proctored lecture exams. Assisted professors as needed with all aspects of course work.
- Graded quizzes and learning modules. Assisted in preparing and grading course exams.

BIO 201: Human Anatomy/Physiology I Fall 2015

- Taught the histology, location and general function of human anatomical structures using computer visualizations, human models, cadavers, and animal specimens.
- Created weekly quizzes, created and administered laboratory practical exams, and proctored lecture exams.
- Graded all quizzes, practical exams, and student experimental reports.

Animal Physiology Laboratory Fall 2014

- Taught experimental lab studies of the physiological mechanisms in animals and model systems.
- Taught basic scientific report writing and assessed student's reports.
- Created and administered weekly quizzes as well as the final exam for the course.

MIC 206: Microbiology Laboratory Fall 2011, Spring/Summer 2012, Summer 2013

- Taught laboratory principles and basic techniques for microbiology including culturing, staining, light microscopy, and species identification.
- Created and assessed weekly quizzes.
- Assessed student tests and written reports.

MBB 343: Genetic Engineering Fall 2012, Fall 2013

- Taught basic laboratory techniques and applications in molecular biology and genetic engineering.
- Prepped chemicals, organisms, and supplies used in all teaching labs for MBB 343.
- Aided and assessed students in scientific report writing.

MBB 247: Principles of Molecular and Cellular Biology II Spring 2012

- Taught basic laboratory techniques and applications used in molecular biology labs
- Aided and assessed students in scientific report writing.
- Administered and graded weekly quizzes.

General Manager/Owner

AZ-Tech Manufacturing Inc., Phoenix AZ

Mar 1993 - Mar 2005

- Started and incorporated an aerospace manufacturing facility in March of 1993. Operated until sale in March of 2005.
- Initiated and ran all aspects of the business including manufacturing engineering, quality control to ISO, AS, and customer specific specifications.
- Grew business from the ground-up to a multi-million-dollar entity employing up to 43 people running three shifts to service customers.
- Specialized in manufacturing complex aerospace hardware for OEMs such as Honeywell Aerospace, Allied Signal Aerospace, and TRW aerospace.
- Specialized in the manufacture of a variety of aerospace components used in aircraft, satellites, rockets, Space Shuttles, defense systems, and the International Space Station.

Previous work history can be provided upon request

Publications

Journal Articles:

Holter M*, **Bjorklund GR***, Nishimura K, Hewitt L, Nichols J, Shah S, Martinez J, Marsh S, Treiman D, Snider WD, Anderson T, Newbern JM. (2018) ERK/MAPK hyperactivation in embryonic GABAergic neurons reduces cortical Parvalbumin neuron number and increases cortical excitability. *In Preparation*

Bjorklund GR, Hewitt L, Moy S, Nikolova V, Nishimura K, Smith C, Xing L, Snider WD, Newbern JM. (2018) Hyperactivation of ERK/MAPK in cortical glutamatergic neurons results in projection axon deficits and aberrant motor learning in a layer autonomous manner *In Preparation*

Nichols J, **Bjorklund GR**, Newbern JM, Anderson T. "Parvalbumin Fast-Spiking Interneurons are Selectively Altered by Pediatric Traumatic Brain Injury". *The Journal of Physiology*. PMID:29333742 (2018).

Sinakevitch IT, **Bjorklund GR**, Newbern JM, Gerkin RC, and Smith BH. Comparative study of chemical neuroanatomy of the olfactory neuropil in mouse, honey bee and human. *Biological Cybernetics*. PMID:28852854 (2017).

Xing Lei, Rylan S. Larsen, **George Reed Bjorklund**, Xiaoyan Li, Yaohong Wu, Benjamin D. Philpot, William D. Snider, and Jason M. Newbern. "Layer Specific and General Requirements for ERK/MAPK Signaling in the Developing Neocortex." *ELife*. PMID:26848828 (2016).

Conference Abstracts and Poster Sessions:

Holter, M., **Bjorklund, G.**, Shah, S., Nishimura, K., Newbern, J. Constitutively active MEK1 signaling drives selective death of cortical parvalbumin-expressing GABAergic interneurons in mouse embryonic brain development. Abstract and poster session presented at: Neuroscience 2018. 48th annual conference of the Society for Neuroscience; 2018 Nov 3-7; San Diego, CA.

Bjorklund GR, Hewitt LT, Nishimura K, Newbern JM. Hyperactivation of ERK/MAPK leads to altered cortical projection neuron outgrowth, reduced activity dependent gene expression, and motor learning deficits. Abstract and poster session presented at: Neuroscience 2017. 47th annual conference of the Society for Neuroscience; 2017 Nov 11-15; Washington, D.C.

Holter M, **Bjorklund GR**, Shah SA, Nichols JD, Martinez JS, Anderson TR, Newbern JM. Functions of ERK/MAPK signaling in GABAergic neuron development and identity. Abstract and poster session presented at: Neuroscience 2017. 47th annual conference of the Society for Neuroscience; 2017 Nov 11-15; Washington, D.C.

Bjorklund GR, Hewitt LT, Xing L, Nikolova V, Moy SS, Snider WD, Newbern JM. ERK/MAPK hyperactivation leads to altered corticospinal neuron connectivity and motor learning deficits. Abstract and poster session presented at: Neuroscience 2016. 46th annual conference of the Society for Neuroscience; 2016 Nov 12-16; San Diego, CA.

Irina S, **Bjorklund GR**, Newbern JM, Smith BH. Comparative study of chemical neuroanatomy of the olfactory neuropil in mouse, honey bee and human. Paper and poster session presented at: Neural Coding 2016: 12th International Workshop, University of Cologne; 2016 Aug 29 – Sep 2; Cologne, Germany.

Bjorklund GR, Newbern JM. ERK/MAPK signaling is critical for corticospinal axon morphology. Poster session presented at: Barrow Neurological Institute 2016 Neuroscience Symposium; 7 Jan 2016; Phoenix, AZ.

Xing L, Larsen RS, **Bjorklund GR**, Li X, Wu Y, Philpot BD, Snider WD, Newbern JM. A bidirectional threshold of ERK/MAPK signaling regulates axonal outgrowth in developing corticospinal neurons. Abstract and poster session presented at: Neuroscience 2015. 45th annual conference of the Society for Neuroscience; 2015 Oct 17-21; Chicago, IL.

Moreno MA, Hewitt LT, **Bjorklund GR**, Daniels CW, Olive MF, Sanabria F, Marsh S, Treiman DM, Snider WD, Newbern JM. Hyperactivation of ERK1/2 signaling in developing GABAergic circuits reduces parvalbumin interneuron number and increases cortical excitability. Abstract and poster session presented at: Neuroscience 2015. 45th annual conference of the Society for Neuroscience; 2015 Oct 17-21; Chicago, IL.

Irina S, **Bjorklund GR**, Baluch DP, Newbern JM, Smith BH. Comparative study of chemical neuroanatomy of the olfactory neuropil in mouse, honey bee and human. Paper and poster session presented at: Olfaction 2015. Kavli Institute for Theoretical Physics Conference: Olfaction; 2015 Jul 7-10; Santa Barbara, CA.


Service:

- School of Life Sciences New Grad Mentor - Assisted new students in getting their bearings in SoLS. 2017-2018
- Ask a Biologist – Community outreach answering biological questions posed by pre-K-12 students and teachers. 2011 – 2018
- Invited speaker for the Molecular and Cellular Biology and Microbiology annual graduate student retreat. Oct. 2017
- Neuroscience and Molecular and Cellular Biology Program Representative for SoLS Septennial Review. Apr. 2017
- ASU Graduate and Professional Student Association - Volunteer for grant reviews and teacher awards reviews. Sept. 2015 - 2017
- Graduate Association of Interdisciplinary Neuroscience Students (GAINS) Community outreach volunteer. 2017
- Night of the Open Door – Volunteered, set-up, ran displays for the annual ASU open house. 2013, 2014, 2015
- Annual MCC Biotechnology Symposium – Panelist for College to University transfer forum. 2010, 2011, 2012, 2013

APPENDIX B

Parvalbumin fast-spiking interneurons are selectively
altered by pediatric traumatic brain injury

Parvalbumin fast-spiking interneurons are selectively altered by paediatric traumatic brain injury

Joshua Nichols^{1,2}, George Reed Bjorklund², Jason Newbern² and Trent Anderson¹ 

¹University of Arizona, College of Medicine – Phoenix, Phoenix, AZ, USA

²School of Life Sciences, Arizona State University, AZ, USA

Edited by: Ole Paulsen & Katalin Toth

Key points

- Traumatic brain injury (TBI) in children remains a leading cause of death and disability and it remains poorly understood why children have worse outcomes and longer recover times.
- TBI has shown to alter cortical excitability and inhibitory drive onto excitatory neurons, yet few studies have directly examined changes to cortical interneurons.
- This is addressed in the present study using a clinically relevant model of severe TBI (controlled cortical impact) in interneuron cell type specific Cre-dependent mice.
- Mice subjected to controlled cortical impact exhibit specific loss of parvalbumin (PV) but not somatostatin immunoreactivity and cell density in the peri-injury zone.
- PV interneurons are primarily of a fast-spiking (FS) phenotype that persisted in the peri-injury zone but received less frequent inhibitory and stronger excitatory post-synaptic currents.
- The targeted loss of PV-FS interneurons appears to be distinct from previous reports in adult mice suggesting that TBI-induced pathophysiology is dependent on the age at time of impact.

Abstract Paediatric traumatic brain injury (TBI) is a leading cause of death and disability in children. Traditionally, ongoing neurodevelopment and neuroplasticity have been considered to confer children with an advantage following TBI. However, recent findings indicate that the paediatric brain may be more sensitive to brain injury. Inhibitory interneurons are essential for proper cortical function and are implicated in the pathophysiology of TBI, yet few studies have directly investigated TBI-induced changes to interneurons themselves. Accordingly, in the present study, we examine how inhibitory neurons are altered following controlled cortical impact (CCI) in juvenile mice with targeted Cre-dependent fluorescence labelling of interneurons (*Vgat:Cre/Ai9* and *PV:Cre/Ai6*). Although CCI failed to alter the number of excitatory neurons or somatostatin-expressing interneurons in the peri-injury zone, it significantly decreased the density of parvalbumin (PV) immunoreactive cells by 71%. However, *PV:Cre/Ai6* mice subjected to CCI showed a lower extent of fluorescence labelled cell loss. PV interneurons are predominantly of a fast-spiking (FS) phenotype and, when recorded electrophysiologically from the peri-injury

Joshua Nichols studied how cortical neurons are altered after traumatic brain injury in the developing brain during his PhD at the University of Arizona and Arizona State University. This work led to the acceptance of a postdoctoral position at the Salk Institute, where he now investigates how cortical microcircuits process visual information. Addressing this phenomenon requires working at both the cellular and system-wide level to assess how populations of neurons co-operate to encode information. The combination of *in vivo* work with an analysis of synaptic connectivity and network dynamics *in vitro* aims to provide a more complete understanding of how neural circuits process information.

zone, exhibited intrinsic properties similar to those of control neurons. Synaptically, CCI induced a decrease in inhibitory drive onto FS interneurons combined with an increase in the strength of excitatory events. The results of the present study indicate that CCI induced both a loss of PV interneurons and an even greater loss of PV expression. This suggests caution is required when interpreting changes in PV immunoreactivity alone as direct evidence of interneuronal loss. Furthermore, in contrast to reports in adults, TBI in the paediatric brain selectively alters PV-FS interneurons, primarily resulting in a loss of interneuronal inhibition.

(Resubmitted 18 October 2017; accepted after revision 19 December 2017; first published online 15 January 2018)

Corresponding author T. Anderson: University of Arizona, College of Medicine – Phoenix, 425 N 5th St, Phoenix, AZ 85004, USA. Email: andersot@email.arizona.edu

Introduction

Children are one of the most at risk groups with respect to suffering a traumatic brain injury (TBI), with more than one in five children experiencing a TBI before reaching adulthood (Kraus *et al.* 1990; Bruns & Hauser, 2003). A TBI may range from mild to severe, although it will often lead to the development of lifelong cognitive and behavioural deficits (Caveness *et al.* 1979; Annegers *et al.* 1998; Barlow *et al.* 2000). Emerging evidence indicates that children have worse outcomes and take longer to recover than adults (Anderson & Moore, 1995; Schmidt *et al.* 2012; Cook *et al.* 2014). How TBI disrupts paediatric brain function and leads to the development of post-traumatic neurological disorders, such as post-traumatic epilepsy, remains unknown.

Disruption to cortical inhibition has been repeatedly implicated in the pathophysiology of numerous neurological disorders, including migraine (Palmer *et al.* 2000; Aurora *et al.* 2005), schizophrenia (Molloy *et al.* 2011; Lewis *et al.* 2012), epilepsy and seizures (Bromfield *et al.* 2006; Trevelyan & Schevon, 2013; Trevelyan *et al.* 2015), as well as the sequela that follow TBI. In adult animals, TBI has been shown to induce enhanced cortical excitability (Carron *et al.* 2016), as well as a loss of synaptic inhibition onto excitatory neurons and a decrease in expression of known markers for multiple subtypes of interneurons (Cantu *et al.* 2015). However, we have previously found that juvenile mice respond uniquely after TBI with a lack of generalized hyperexcitability (Goddeyne *et al.* 2015; Nichols *et al.* 2015) and the presence of unique synaptic bursts following more severe TBI (Nichols *et al.* 2015). This suggests the pathophysiology of TBI in juvenile animals is distinct, at least in part, from adults. In children, TBI has been shown to disrupt brain function and maturation via mechanisms distinct from adult TBI (Anderson & Moore, 1995; Schmidt *et al.* 2012; Cook *et al.* 2014). GABAergic neurons play a critical role in cortical development and disruption of the immature inhibitory circuit can have severe effects long into adulthood (Wang & Kriegstein, 2009; Judson *et al.* 2016). However, the precise nature of the changes to interneurons and the inhibitory circuit

induced by paediatric TBI is poorly understood. Even in the larger body of studies performed in adult animals, there is a paucity of direct examination of synaptic and cellular changes to cortical interneurons. In the present study, we directly examine how inhibitory interneurons in the cortex are altered in an animal model of paediatric TBI.

Cortical interneurons are a diverse population of cells with unique intrinsic and synaptic properties (Hensch, 2005; Yuste, 2005; Wonders & Anderson, 2006; Rudy *et al.* 2011). To examine for changes in the interneuron population, conventional approaches have often used cell type specific immunohistochemical markers. Parvalbumin (PV) and somatostatin (SST) immunohistochemical positive interneurons account for >70% of the interneuron population (Rudy *et al.* 2011) and have been implicated in the pathophysiology of TBI (Hunt *et al.* 2011; Cantu *et al.* 2015) and epilepsy (Caveness *et al.* 1979; Cossart *et al.* 2001; Jin *et al.* 2014). However, examination of immunohistochemical markers is unable to differentiate between a loss of immunoreactivity and overt cell death. Distinguishing between these two possibilities in interneurons is of particular importance to understanding the pathophysiology of TBI and potential interneuron targeted therapeutic interventions. Therefore, in the present study, we took advantage of the fact that almost all GABAergic interneurons selectively express the vesicular GABA transporter (VGAT) (McIntire *et al.* 1997; Chaudhry *et al.* 1998; Wojcik *et al.* 2006). We examined the outcome of TBI in transgenic animals that express Cre recombinase under the control of the *Vgat* promoter (*Vgat:Cre*) (Vong *et al.* 2011) and a Cre-dependent red fluorescent protein reporter (CAG-loxp-STOP-loxp-tdTomato; hereafter referred to as *Ai9*) (Madisen *et al.* 2010) to ubiquitously label GABAergic neurons. Furthermore, we similarly investigated interneuron subtype specific changes using transgenic mice with *PV:Cre*-dependent activation of a green fluorescent protein reporter (CAG-loxp-STOP-loxp-ZsGreen1). Consequently, because the fluorescent proteins are expressed under the control of the strong and ubiquitous CAG promoter, we were able to directly

determine whether TBI induces an actual loss of interneurons and also examine for functional changes to cortical inhibition.

Juvenile mice were subjected to controlled cortical impact (CCI), which has previously been shown to induce a clinical relevant injury that effectively models a severe TBI (Brody *et al.* 2007; Hunt *et al.* 2009; Nichols *et al.* 2015). Combined with whole-cell patch clamp and fluorescence immunohistochemical (IHC) approaches, we quantified CCI-induced changes to cortical interneurons. Although CCI did not induce a general interneuron loss, in the peri-injury zone, a significant reduction in the expression of PV immunoreactivity was observed in fluorescence labelled interneurons. By contrast to similar experiments conducted in adults, no accompanying loss of SST expression was observed (Cantu *et al.* 2015). PV positive interneurons are predominantly of a fast-spiking (FS) phenotype (Hu *et al.* 2014). Despite TBI-induced loss of PV interneurons, electrophysiological recordings confirmed the presence of FS interneurons with intrinsic properties similar to those of control neurons. However, there was a marked decrease in inhibitory synaptic drive onto FS interneurons with an accompanying increase in the strength of excitatory synaptic events. Our data indicate that, in contrast to previous reports in adult animals, CCI in juvenile mice preferentially alters PV-FS cortical interneurons.

Methods

Ethical approval

All laboratory and animal experiments were conducted in accordance with NIH guidelines, were approved by the University of Arizona Institutional Animal Care and Use Committee and conform to the principles and guidelines of *The Journal of Physiology* (Grundy, 2015). Genetically modified mouse lines were bred in-house from commercially available strain (Jackson Laboratories, Bar Harbor, ME, USA). Specifically, *Vgat:Cre* mice (B6J.129S6(FVB)-Slc32a1^{tm2(cre)Low/Mwarj}, #028862) have been characterized previously (Vong *et al.* 2011) and have Cre-recombinase directed to inhibitory GABAergic neurons. *Vgat:Cre* mice were bred with *Ai9* mice (Gt(ROSA)26Sor^{tm9(CAG-tdTomato)Hze}, #007909) allowing for the Cre-dependent expression of red-fluorescent protein (tdTomato) under the ubiquitous CAG promoter selectively in inhibitory GABAergic neurons. Similarly, *PV:Cre* mice (B6;129P2-Pvalb^{tm1(cre)Arhr/J}, #008069) selectively express Cre recombinase in PV-expressing neurons (Hippenmeyer *et al.* 2005) and were bred with *Ai6* mice (B6.Cg-GT(ROSA)26Sor^{tm6(CAG-ZsGreen1)Hze}, #007906) allowing for Cre-dependent expression of green-fluorescent protein

(ZsGreen1) under the CAG promoter selectively in PV neurons.

CCI

Juvenile mice, at post-natal day (P)22, were subjected to a severe CCI as described previously (Hunt *et al.* 2009; Nichols *et al.* 2015). Animal temperature was maintained for the duration of surgery and until mice were ambulatory post-surgery. The skull was exposed with a midline incision and a 5 mm craniotomy was made over the right somatosensory region (lateral to the sagittal suture between bregma and lambda). Precaution was taken during the craniotomy not to disturb the underlying dura. A frontoparietal CCI (3 mm diameter tip, 3.0 m s⁻¹, 2 mm depth, 500 ms in duration) was performed using an electromagnetic cortical impactor (Hatteras Instruments, Cary, NC, USA). After the impact, the removed bone flap was placed over the site of injury and sealed with dental cement. Control animals were naïve because previous reports have found that a craniotomy alone may be sufficient to cause an inflammatory response and/or induce brain injury (Olesen, 1987; Cole *et al.* 2010).

Preparation of brain slices

We have previously shown that all animals subjected to CCI develop *in vivo* epileptic activity by 14 days after injury and that this is an effective time-point for examining pathophysiological network changes after TBI (Nichols *et al.* 2015). Accordingly, to examine for CCI-induced changes to the inhibitory network, mice were deeply anaesthetized by inhalation of isoflurane and decapitated on post-injury day (PID) 14–19. The brain was rapidly removed and coronal slices (350 µm thick) prepared on a vibratome (VT 1200; Leica, Nussloch, Germany) as described previously (Anderson *et al.* 2010; Nichols *et al.* 2015). Slices were obtained from the somatosensory cortex at the site of injury in CCI animals or from the corresponding control cortex in control animals. The site of CCI was readily identifiable in whole brain and slices as indicated by significant cavitation and tissue loss (Fig. 1). Initial harvesting of brain slices was performed in an ice-cooled (4°C) carboxygenated (95% O₂, 5% CO₂) high sucrose solution containing (in mM): 234 sucrose, 11 glucose, 26 NaHCO₃, 2.5 KCl, 1.25 NaH₂PO₄H₂O, 10 MgSO₄7H₂O and 0.5 CaCl₂2H₂O. Slices were then incubated for 1 h at 32°C in carboxygenated artificial CSF (aCSF) containing (in mM): 126 NaCl, 26 NaHCO₃, 2.5 KCl, 10 Glucose, 1.25 Na₂H₂PO₄H₂O, 1 MgSO₄7H₂O and 2 CaCl₂H₂O (pH 7.4). Slices were then returned to room temperature before being individually moved to the recording chamber for whole-cell patch clamp recording.

In vitro electrophysiological recording

Coronal slices were prepared from CCI or control animals, placed in the recording chamber and submerged in flowing carboxygenated aCSF heated to 32°C. Submerged slices were first visualized under 4× brightfield for identification of layer V cortex. For slices from impacted mice, recordings were made in the peri-injury zone within 700 μm of the injury-induced cavitation. Recordings from control slices were made in the corresponding cortex to the peri-injury zone of CCI animals. Whole-cell recordings were obtained from FS interneurons using an upright microscope (Axioexaminer; Carl Zeiss, Thornwood, NY, USA) fitted with infrared differential interference contrast (DIC) optics. Fast-spiking neurons were distinguished based on their current clamp firing behaviour (Kawaguchi & Kubota, 1997). The electrode capacitance and bridge circuit were appropriately adjusted. The series resistance (R_s) of neurons chosen for analysis was <20% of membrane input resistance and monitored for stability. Membrane potential was not corrected for a calculated 10 mV liquid junction potential. A Multiclamp 700B patch clamp amplifier (Axon Instruments, Union City, CA, USA) was used for both current and voltage clamp mode. Recordings were obtained at 32°C using borosilicate glass microelectrodes (tip resistance, 2–5 MΩ). For recording of excitatory events, electrodes were filled with an intracellular solution containing (in mM): 135 KGluconate, 4 KCl, 2 NaCl, 10 Hepes, 4 EGTA, 4 Mg ATP and 0.3 Na Tris. With a calculated $E_{Cl} = -80$ mV and a holding potential of -70 mV, excitatory events were isolated as inward currents. Pharmacological isolation was avoided to prevent induced hyperexcitability that would interfere with baseline measurements of synaptic activity. For recording of inhibitory events, a high-chloride intracellular solution containing was used containing (in mM):

70 KGluconate, 70 KCl, 2 NaCl, 10 Hepes, 4 EGTA, 4 Mg ATP and 0.3 GTP. This internal solution has been used previously (Anderson *et al.* 2010; Nichols *et al.* 2015) and shown to facilitate the detection of inhibitory events. The calculated E_{Cl} was -16 mV, resulting in inward GABA_A currents at a holding potential of -70 mV. Inhibitory events were pharmacologically isolated by bath application of kynurenic acid (2 mM).

Whole-cell patch clamp analysis

Data analysis was performed using pCLAMP (Axon Instruments, Sunnyvale, CA, USA) Prism (GraphPad, La Jolla, CA, USA) and MiniAnalysis (Synaptosoft, Decatur, GA, USA). Data are reported as the mean ± SEM. For the detection of spontaneous events and parameters, automated threshold detection was employed using MiniAnalysis and detected events were subsequently manually verified. Decay time was calculated as time from peak to reach 37% of the peak amplitude. Input resistance was calculated from the steady-state voltage response to the input of a 1 s, -50 pA current step. Firing frequency was calculated by the number of spikes elicited per current step (-150 pA to 300 pA steps, 1 s duration). Resting membrane potential was measured prior to induced current steps. Action potentials were induced by intracellular current steps (2 nA, 0.5 ms), repeated 10 times and averaged prior to analysis. Rheobase was measured as the minimum 50 ms long current step that induced an action potential and was assessed with current delivered in $+5$ pA increments.

Immunohistochemistry

PID 14 mice and age-matched control animals were deeply anaesthetized and perfused transcardially with 4%

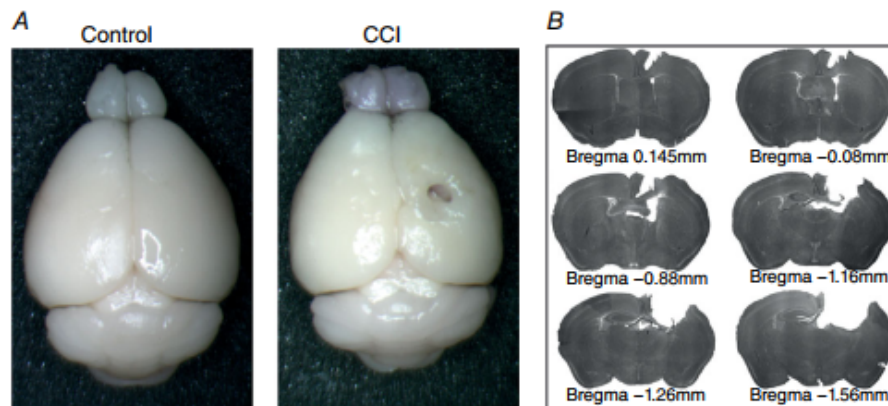


Figure 1. CCI induces marked tissue loss and cavitation at site of injury
A, example images of perfused control and CCI VGAT cre; Ai9 P36 mouse brains 14 days after injury. B, serial images of 60 μm slices showing extent of CCI induced injury. [Colour figure can be viewed at wileyonlinelibrary.com]

paraformaldehyde/PBS essentially as described previously (Xing *et al.* 2016). Immunohistochemistry was performed using 60 μm free-floating vibratome sections. Brain sections were collected in PBS, blocked with 5% normal serum in PBS with 0.1% Triton X-100 and incubated with primary antibodies in blocking solution for 24–48 h at 4°C. The primary antibodies used in the present study were: mouse anti-NeuN (dilution 1:1000; Chemicon, Temecula, CA, USA), goat anti-PV (dilution 1:1000; PVG213; Swant, Barron, WI, USA) and rabbit anti-SST-14 (dilution 1:1000; T4103; Peninsula Laboratories, Belmont, CA, USA). After rinsing, sections were then incubated with Alexa conjugated secondary antibodies (Invitrogen, Carlsbad, CA, USA) and 4',6-diamidino-2-phenylindole (DAPI) (dilution 1:2000; Roche, Basel, Switzerland) overnight at 4°C, rinsed three times in PBS, and mounted with Vectashield (Vector Laboratories, Inc., Burlingame, CA, USA). For biocytin filled neurons, sections were labelled with Alexa-488 conjugated streptavidin (dilution 1:1000; Jackson ImmunoResearch, West Grove, PA, USA) prior to rinsing and mounting.

Image acquisition and data analysis

Images were collected on a model SP5 (Leica) and a model 710 (Carl Zeiss) laser scanning confocal microscope using 10 \times or 20 \times objectives. Single fields were tiled together to generate high-resolution images of whole brain coronal sections. Images were corrected for brightness and contrast in Photoshop (Adobe Inc., San Jose, CA, USA). For the assessment of changes in neuron density, we defined a 350 μm wide region of interest (ROI) that extended across all cortical layers and was oriented perpendicular to the white matter. The ROI was positioned 3.15 mm lateral to midline on the injured hemisphere (i.e. over the lateral peri-injury site). For semi-automated assessment of *Vgat:Cre/Ai9*⁺ and NeuN⁺ cell density, single channel images from three separate sections were imported into ImageJ (NIH, Bethesda, MD, USA). Images were manually thresholded to optimize binary masking and the detection of immunofluorescent soma. To separate clearly overlapping soma, a watershed algorithm was applied. The analyse particle plugin was then employed using a minimal particle size of 70 pixels² ($\sim 50 \mu\text{m}^2$), which was chosen to enrich the detection of well labelled cell soma and to minimize counting cross-sectioned neuritis (Ippolito & Eroglu, 2010; Xing *et al.* 2016) (Ippolito & Eroglu, 2010; Xing *et al.* 2016). For the analysis of the less abundant PV- and SST-expressing neurons, area and number were manually determined in Photoshop. To determine density, the number of labelled neurons was recorded and divided by the area of tissue within the ROI. Density values were then averaged across three sections per animal. The results from this analysis were averaged using the data from at least three independent mice originating from

separate litters per condition. For sholl analysis, 100 μm wide regions, covering all cortical layers, were positioned serially beginning with the edge of the injury site. Data are reported as the mean \pm SEM. Statistical significance was tested with a one-way ANOVA with Tukey's multiple comparison test or Student's *t* test (paired or unpaired). $P < 0.05$ was considered statistically significant.

Results

To examine TBI-induced changes in the cortical inhibitory neuronal population, we performed unilateral CCI injuries on juvenile (P22) *Vgat:Cre/Ai9* mice. As previously described, animals were given 14 days to recover before further experimentation because this was the earliest time-point by which all juvenile animals subjected to CCI reliably showed spontaneous epileptic activity (Nichols *et al.* 2015). By PID 14, animals subjected to CCI showed marked cavitation and tissue loss at the site of injury (Fig. 1). Despite the significant tissue loss at the site of the CCI injury, no significant change in the thickness of the cortex was observed in the peri-injury zone (control: $1219.27 \pm 22.10 \mu\text{m}$; CCI: $1093.83 \pm 56.33 \mu\text{m}$) ($P = 0.13$) ($n = 3$).

Inhibitory interneuron (Ai9) cell density was unchanged after CCI

To quantify CCI-induced changes in different populations of cortical neurons, we performed IHC staining using the neuron specific marker NeuN or examined tdTomato labelled interneurons in transgenic mice (*Vgat:Cre/Ai9*). First, utilizing counts of the NeuN positive cells, we observed that CCI induced no significant change in neuronal density in the peri-injury zone (control: $2321.1 \pm 106 \text{ cells mm}^{-2}$; CCI: $2212.7 \pm 74 \text{ cells mm}^{-2}$) (Fig. 2) ($P = 0.15$). Next, we were able to directly examine for CCI-induced changes in the interneuron population by taking advantage of the select *Vgat:Cre*-dependent expression of tdTomato (Ai9) in interneurons. Similar to the NeuN findings, we observed no significant difference in tdTomato⁺ cell density between control and CCI mice (control: $471.7 \pm 29 \text{ cells mm}^{-2}$; CCI: $434.6 \pm 39 \text{ cells mm}^{-2}$) ($P = 0.49$) (Fig. 2). These experiments determined that, 14 days after a CCI in the juvenile brain, there is no significant change in the density of either total excitatory or inhibitory neurons within the peri-injury zone.

VGAT is reported to be expressed in 99% of all cortical interneurons (McIntire *et al.* 1997; Chaudhry *et al.* 1998; Vong *et al.* 2011) and the use of a *Vgat:Cre/Ai9* transgenic mouse allowed us to directly examine for changes in the global interneuron population without confounds related to alterations in the expression of typical

immunological targets. However, cortical interneurons are a mixed population of neurons with numerous subtypes and unique physiological roles (Gupta *et al.* 2000; Markram *et al.* 2004). One effective method for segregating interneurons subtypes is based on the gene expression pattern (Rudy *et al.* 2011). Specifically, in the cortex, the two most common interneuron subtypes express either PV (40–50%) or SST (~30%) (Markram *et al.* 2004, Rudy *et al.* 2011). Having established a lack of global cortical interneuron loss following CCI, we next investigated whether CCI induced changes in select interneuron subtypes by examining the expression of PV and SST.

Selective loss of PV expression following CCI

To examine for TBI-induced changes in PV expression, we used an immunohistochemical approach and again performed CCI in juvenile *Vgat:Cre/Ai9* mice. By contrast to tdTomato labelled interneurons where we observed no significant change, CCI induced a dramatic reduction in the number of cells that express PV (Fig. 3A). Specifically, CCI significantly reduced the density of neurons positively labelled by anti-PV antibody by >71% in the peri-injury zone (32.2 ± 5 cells mm^{-2}) compared to control (110.4 ± 5 cells mm^{-2}) ($P < 0.0001$) (Fig. 3A and B). Finally, to investigate whether the CCI-induced loss of PV expression was correlated with distance from the site of the injury, we examined the number of PV-expressing neurons within 100 μm ROIs (bins) extending even further

to 1 mm lateral from the edge of the injury. The loss of PV expression induced by CCI was significantly greater near (<300 μm) the injury site ($P < 0.05$) (Fig. 3B).

SST expression is not altered by CCI

Using an IHC approach, we examined for changes in SST expression in the peri-injury zone after CCI in juvenile *Vgat:Cre/Ai9* mice (Fig. 4A). By contrast to PV, we found that CCI induced no statistically significant difference in the density of SST⁺ neurons in the peri-injury zone compared to control animals (control: 108.3 ± 14 cells mm^{-2} ; CCI: 111.9 ± 11 cells mm^{-2}) ($P = 0.85$) (Fig. 4B). Similarly, no significant loss of SST positive neurons was observed across any 100 μm ROIs extending laterally from the site of injury ($P > 0.05$, one-way ANOVA). Taken together, these results show that, in juvenile mice, CCI does not induce a loss of SST-expression but, instead, selectively reduces PV-expression in the peri-injury zone.

PV interneuron (Ai6) cell density is decreased in the peri-injury zone

The observed decrease in PV expression may be solely the result of a loss of PV immunoreactivity or may reflect an actual loss of PV interneurons. To distinguish between these possibilities, we employed Cre-dependent genetic labelling of PV-expressing neurons with ZsGreen1

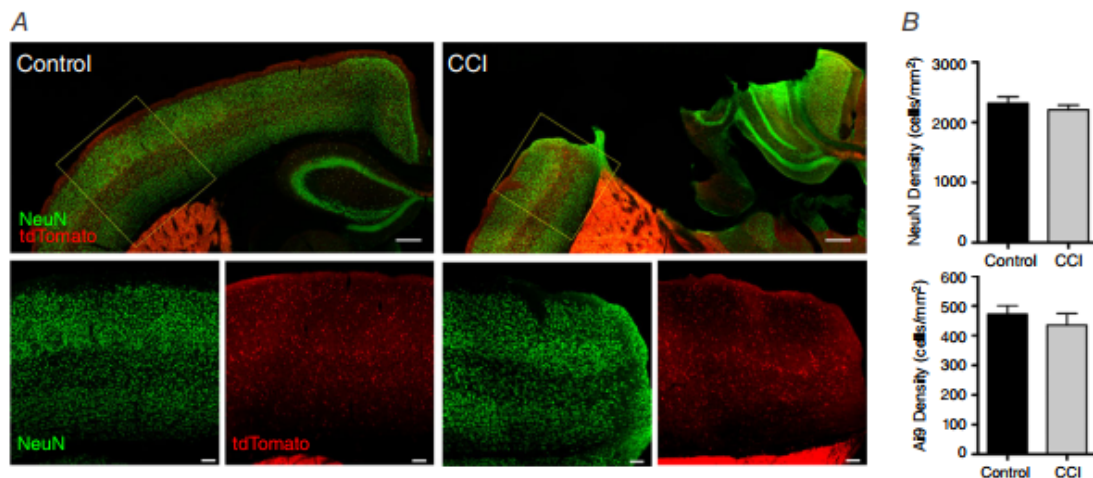


Figure 2. Ai9 cell density is not significantly changed in the peri-injury zone after CCI. *A*, top: NeuN (green) is qualitatively similar between control and CCI. Similarly, Ai9 (tdTomato) distribution is not altered after CCI. Bottom: higher magnification images taken from the peri-injury zone (yellow dotted box). Note the presence of total neurons (NeuN) and GABAergic neurons (Ai9) throughout this region. *B*, quantitative analysis shows that neither NeuN (top) or Ai9 cell density (bottom) are significantly reduced in CCI animals ($n = 3$ mice) compared to control ($n = 3$ mice) (NeuN: Control vs. CCI, $P = 0.15$; Ai9: Control vs. CCI, $P = 0.49$, unpaired Student's *t* test). Top: scale bar = 300 μm . Bottom: scale bar = 100 μm .

(*PV:Cre/Ai6*). PV expression rises postnally and is well established by the time of impact at P22 (de Lecea *et al.* 1995; Philpot *et al.* 1997; Erickson & Lewis, 2002), thereby indelibly labelling PV interneurons with ZsGreen1 (del Rio *et al.* 1994; Huang *et al.* 1999; Madisen *et al.* 2010). We were therefore able to fluorescence-label neurons that expressed PV at some point during development. Ongoing reporter gene expression was therefore independent of subsequent changes in PV promoter activity or immunoreactivity that might occur following CCI. One caveat to this approach is the potential labelling of ‘off-target’ cells, such as a few layer 5 excitatory neurons and SST neurons (Tanahira *et al.* 2009; Kobayashi & Hensch, 2013; Fujihara *et al.* 2015; Nassar *et al.* 2015) In line with these previous studies, we noted a significant fraction of ZsGreen1⁺

labelled cortical neurons in *PV:Cre/Ai6* mice do not express immunohistochemically significant levels of PV (Fig. 5).

In agreement with our IHC findings in *Vgat:Cre/Ai9* mice, TBI in *PV:Cre/Ai6* mice led to a 61% reduction in the density of cells labelled by PV IHC in the peri-injury zone (control: 157.14 ± 12.5 cells mm⁻²; CCI: 60.9 ± 7 cells mm⁻², $P < 0.001$). Interestingly, we found that the relative density of ZsGreen1⁺ (i.e. *PV:Cre* dependently labelled) cells was only reduced by 39% in the peri-injury zone compared to control mice (control: 248.7 ± 17 cells mm⁻²; CCI: 152.9 ± 21 cells mm⁻² CCI, $P < 0.01$) (Fig. 5A and B). Consistent with these results, the relative proportion of ZsGreen1⁺ cells that are also immunoreactive for PV [(PV+ and ZsGreen+)/Total

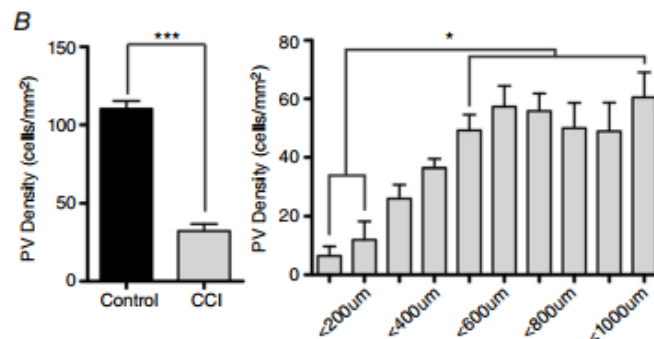
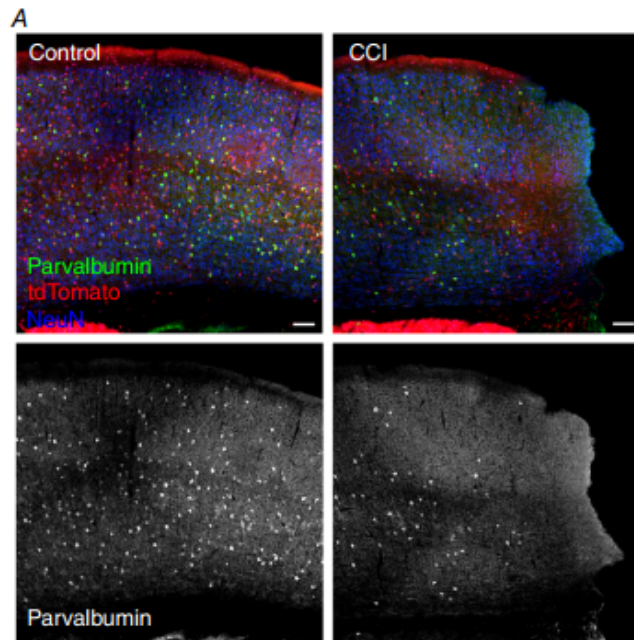


Figure 3. PV immunoreactivity is reduced after CCI
 A, peri-injury regions with PV in green, Ai9 in tdTomato and NeuN in blue. (Bottom) Monochrome image of immunostaining of PV shows loss of expression after injury. Scale bar = 100 μ m. B, left: quantification of PV density is significantly reduced after CCI ($n = 5$ mice per group, *** $P < 0.0001$, unpaired Student's t test). Right: distal analysis with 100 μ m wide columns was used to analyse changes in PV expression in relation to injury. Quantitatively, it shows that the loss of PV expression is greatest closest to the injury site ($n = 5$ mice, * $P < 0.05$, one-way ANOVA with a *post hoc* Tukey's test).

ZsGreen+] was significantly reduced by almost 34% in the peri-injury zone (control: $39.09 \pm 4.1\%$; CCI: $25.97 \pm 1.7\%$, $P < 0.0001$) (Fig. 5C). Overall, these data demonstrate that the global reduction of PV expression in the peri-injury zone is attributable to both the overt loss of a significant fraction of PV-expressing interneurons in addition to a reduction in PV expression in a subset of PV:Cre labelled neurons that persist following TBI.

Fast-spiking interneurons are not significantly altered following CCI

Subtypes of cortical interneurons can also be categorized by their electrophysiological patterns of action potential firing in response to sustained depolarizing current injection (Kawaguchi & Kubota, 1997; Markram *et al.* 2004; Uematsu *et al.* 2008; Rudy *et al.* 2011). PV

positive interneurons are predominantly of a FS electrophysiological phenotype (Galarreta & Hestrin, 1999) and are considered to play an important role in the maintenance of spike timing (Kinney *et al.* 2006; Orduz *et al.* 2013) and rhythmic firing (Orduz *et al.* 2013). Consequently, the select loss of PV expression following CCI led us to investigate whether the interneurons that persist in the peri-injury zone exhibit altered electrophysiological properties. We performed whole-cell patch clamp experiments in the peri-injury zone of coronal brain slices taken from *Vgat:Cre/Ai9* mice 14 days after CCI or in corresponding regions of un-injured control cortices. Neurons were first visually identified via DIC bright field imaging and confirmed to be tdTomato positive. Under current clamp, neurons were confirmed to have a FS phenotype based on the firing pattern induced by a series of intracellular current steps (-150 pA to 300 pA, 50 pA

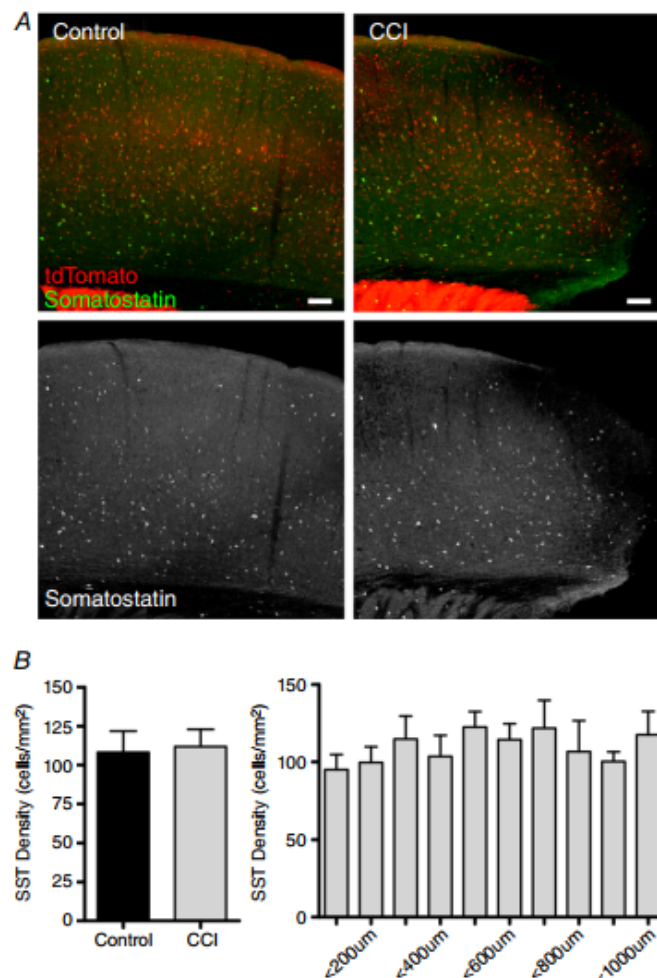


Figure 4. CCI does not alter the density of SST neurons in the cortex after CCI

A, top: control co-labelling of GABAergic neurons (tdTomato) and SST interneurons (green). Bottom: monochrome images of immunostaining of SST interneurons reveals no change in number after injury. Scale bar = $100 \mu\text{m}$. *B*, left: quantification of SST density is not significantly altered after CCI ($n = 3$ mice per group, $P = 0.63$, unpaired Student's *t* test. Right: distal analysis with $100 \mu\text{m}$ wide columns was used to analyse changes in SST expression in relation to injury. Quantitatively, it shows no loss of SST expression ranging from peri-injury zone to 1 mm lateral of injury site ($n = 5$ mice), one-way ANOVA with a *post hoc* Tukey's test.

steps, 1 s) (Fig. 6A) (Anderson *et al.* 2010; Hu *et al.* 2014). Following CCI, FS interneurons had a more depolarized resting membrane potential (-65.52 ± 1.1 mV) compared to control (-69.69 ± 1.6 mV) ($P < 0.05$). However, this was not accompanied by any significant difference in the input resistance (control: 150.42 ± 18.1 M Ω ; CCI: 156.46 ± 17.3 M Ω , $P = 0.82$) or average firing frequency across various current steps ($P > 0.05$, one-way ANOVA) (Fig. 6A). Similarly, compared with the control, no significant differences were observed in action potential height (control: 84.43 ± 4.1 mV; CCI: 83.20 ± 2.9 mV,

$P = 0.80$), threshold (control: -40.49 ± 0.9 mV; CCI: -41.33 ± 0.9 mV, $P = 0.76$) or half-width (control: 0.63 ± 0.1 ms; CCI: 0.87 ± 0.1 ms, $P = 0.07$) (Fig. 6B). Rheobase appeared decreased following CCI, although the change failed to reach significance (control: 152.5 ± 25 pA; CCI: 107.3 ± 18 pA, $P = 0.14$) (Fig. 6C). These findings confirmed that, although CCI induces a decrease in the immunohistochemical expression of PV, the FS interneurons that remain in the peri-injury zone possess similar intrinsic electrophysiological properties as control FS interneurons.

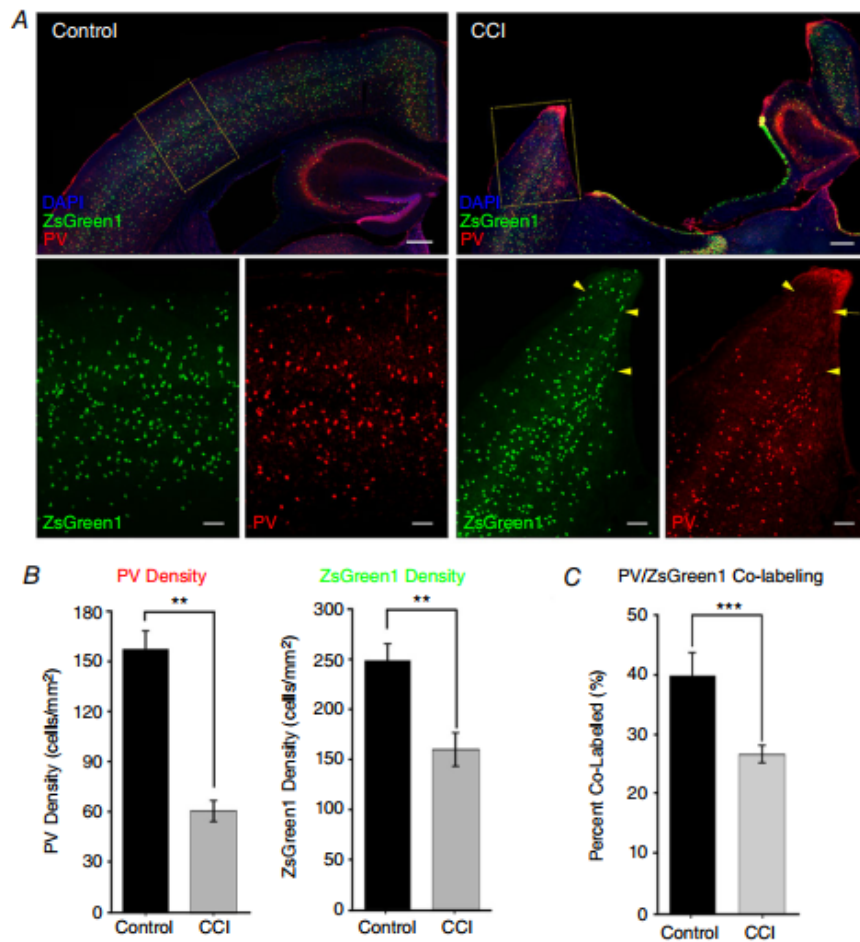


Figure 5. PV expression and cell density are decreased after CCI in the peri-injury zone
 A, representative images of ZsGreen1 expressing cells in PV:cre Ai6 mouse cortex from control or after CCI. Sections were counter-stained with DAPI (blue) and PV antibody (red). Higher magnification images from the region of the peri-injury zone (yellow box) are shown below. Note the presence of ZsGreen1 positive neurons in the peri-injury zone that are not co-immunoreactive with PV (yellow arrows). B, bar charts quantifying the statistically significant reduction in PV and ZsGreen1 density in the per-injury zone ($n = 4$ mice per group). C, the proportion of PV/ZsGreen1 co-labelled cells is significantly reduced in the peri-injury zone following CCI. ** $P < 0.01$, *** $P < 0.0001$ unpaired Student's t test). Top: scale bar = 300 μ m. Bottom: scale bar = 100 μ m.

CCI reduces inhibitory sIPSC frequency and increases synaptic kinetics

Next, we aimed to investigate whether synaptic neurotransmission onto FS interneurons was altered following CCI. We first examined for changes in inhibitory activity by recording spontaneous IPSCs (sIPSCs) in FS interneurons in the peri-injury zone 14 days after CCI or from corresponding cortical region in age-matched control animals. sIPSCs were pharmacologically isolated by bath application of the glutamate receptor antagonist kynurenic acid (2 mM). To increase the detection of inhibitory synaptic events, a modified internal solution ($E_{Cl^-} = -16$ mV) was used as described previously (Anderson *et al.* 2010). No significant change was observed in the amplitude (control = 23.10 ± 2.9 mV, CCI = 21.69 ± 1.9 mV) ($P = 0.68$) or charge (control = 77.43 ± 9.6 C, CCI = 91.84 ± 7.1 C) ($P = 0.23$) of sIPSCs. However, CCI significantly reduced the frequency of sIPSCs by >50% (control = 4.34 ± 0.8 Hz; CCI 1.96 ± 0.3 Hz) ($P = 0.004$) (Fig. 7A–D). CCI

also induced significant changes to the kinetics of sIPSC, as indicated by increases in both the rise (control = 2.56 ± 0.3 ms, CCI = 3.36 ± 0.2 ms) ($P < 0.05$) and decay (control = 3.32 ± 0.2 ms, CCI = 4.43 ± 0.4 ms) ($P < 0.05$) time (Fig. 7E–G). This suggests that CCI primarily induces a loss of inhibitory drive onto FS interneurons.

Excitatory synaptic strength increases after CCI

Finally, we examined for changes in excitatory input onto FS interneurons by recording spontaneous EPSCs (sEPSCs). For these experiments, a physiological internal was used ($E_{Cl^-} = -80$ mV) that allowed the detection of inward glutamatergic events isolated from outward GABAergic synaptic events. Excitatory activity was not pharmacologically isolated because blocking GABAergic activity may disinhibit the network and alter the ability to directly record CCI-induced changes. Again, whole-cell recording of sEPSCs in FS interneurons was performed in

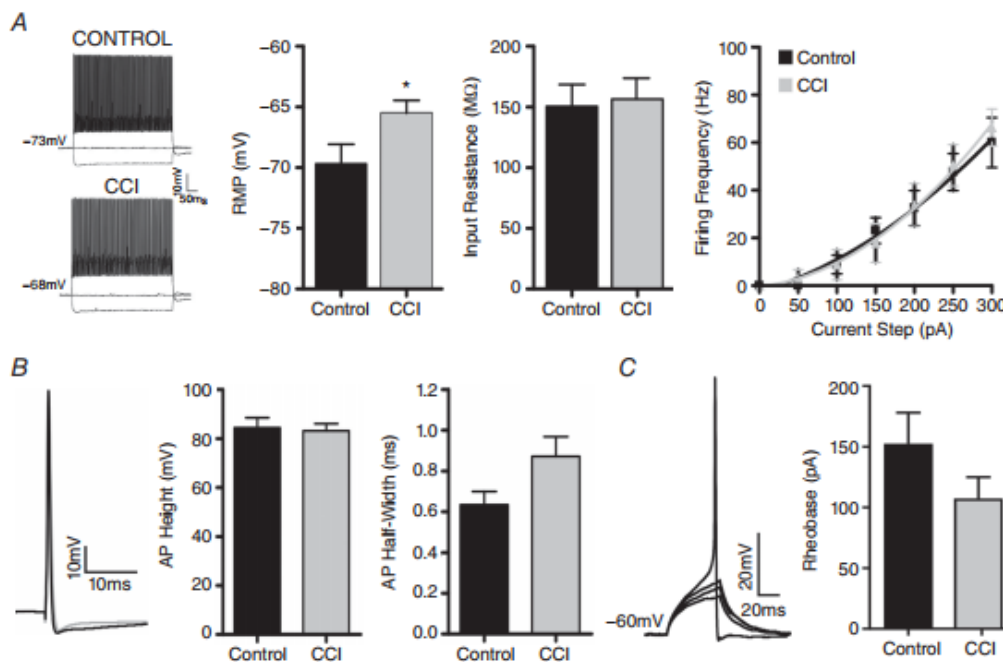


Figure 6. FS interneurons remain in the peri-injury zone following CCI

Whole-cell patch clamp recordings from FS neurons recorded from Vgat: Ai9 positive neurons from control ($n = 10$) or CCI ($n = 15$) mice. **A**, current clamp recordings of FS interneurons in response to intracellular current steps (-150 , 0 and 250 pA). Resting membrane potential of FS interneurons is more depolarized following CCI (* $P < 0.05$, unpaired Student's t test), whereas input resistance ($P > 0.05$, unpaired Student's t test) and firing frequency remain unchanged (curves fit with second-order polynomial, $R^2 = 0.990$ control, 0.997 CCI). **B**, examples of average single action potential (2 nA, 0.5 ms) from control (black) or CCI (grey) (left) and quantification of action potential height and half-width (right) ($P > 0.05$, unpaired Student's t test). **C**, example of a series of rheobase trial traces (left) and quantification (right) indicating no change between control and CCI ($P > 0.05$, unpaired Student's t test).

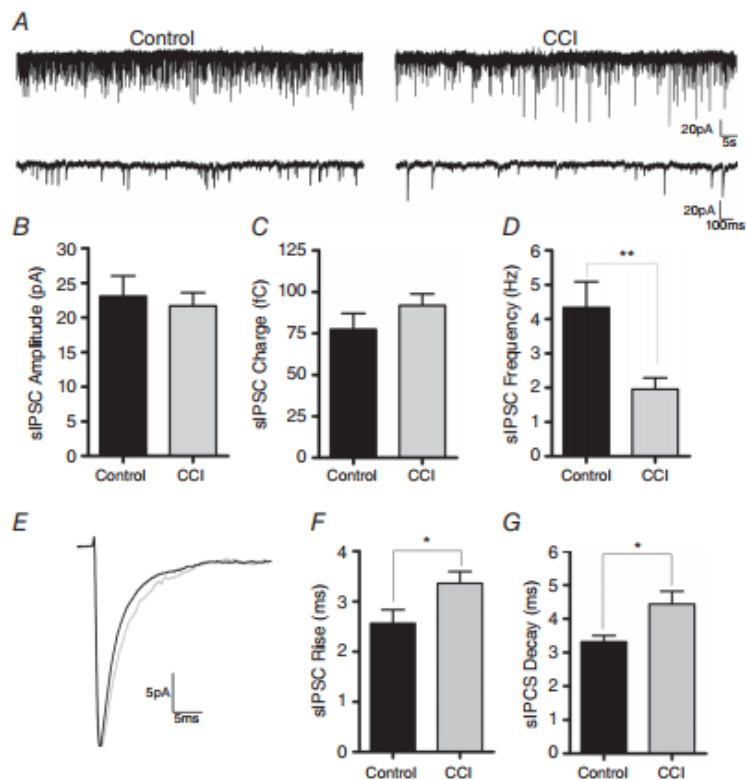
the peri-injury zone 14 days after CCI or in corresponding control animals. Analysis revealed a statistically significant increase in the amplitude (control = 14.33 ± 1.7 mV, CCI = 25.55 ± 2.5 mV) ($P < 0.001$) and charge (control = 32.92 ± 1.9 C, CCI = 61.98 ± 5.8 C) of sEPSCs following CCI compared to control ($P < 0.0001$) (Fig. 8A–C). However, in contrast to CCI-induced changes to sIPSCs, there was no change in sEPSC frequency (control = 8.34 ± 1.1 Hz, CCI = 9.16 ± 1.2 Hz) ($P = 0.61$), rise time (control = 3.04 ± 0.3 ms, CCI = 2.48 ± 0.2 ms) ($P = 0.20$) or decay time (control = 2.17 ± 0.2 , CCI = 2.47 ± 0.4) ($P = 0.50$) (Fig. 8D–G). This suggests that CCI primarily induces an increase in the strength of excitation onto FS interneurons.

Discussion

In the present study, we examined how cortical interneurons in juvenile animals are altered following TBI induced by CCI. To our knowledge, this is the first study to examine changes to the cortical interneuron network in a paediatric model of TBI. Using a combined IHC and electrophysiological approach in mice with targeted

Cre-dependent fluorescence labelled interneurons, we identified five key findings. First, as reported previously (Nichols *et al.* 2015), CCI induced significant tissue loss at the site of impact. However, within the surrounding peri-injury zone, there was no significant loss in the density of total neurons (NeuN) or inhibitory interneurons (tdTomato). Second, despite the lack of change in overall neuronal density, CCI induced a loss of immunoreactivity for the interneuron subtype specific marker PV but not SST. This is in contrast to TBI in adult mice where more global interneuron changes have been reported (Hunt *et al.* 2011; Cantu *et al.* 2015). Third, the loss of PV expression following CCI was accompanied, although to a lesser extent, by a decrease in the density of Cre-dependent fluorescence labelled PV interneurons (PV:Cre/Ai6). Fourth, despite the loss of PV immunoreactivity, a population of FS interneurons persisted in the peri-injury zone and had intrinsic electrophysiological parameters similar to control mice. Fifth, at a synaptic level, CCI decreased the frequency of inhibition at the same time as increasing the strength of excitation onto FS interneurons. These studies suggest that, in juvenile animals, PV-FS interneurons may be selectively vulnerable to the effects of CCI.

Figure 7. sIPSC frequency and kinetics are increased onto FS interneurons after CCI
 A, gap-free traces of sIPSCs recorded in voltage clamp from FS interneurons in control ($n = 10$) or after CCI ($n = 15$) ($V_{hold} = -70$ mV). B–C, bar graphs of average sIPSC properties indicating no significant change in sIPSC amplitude or charge following CCI. D, average sIPSC frequency was significantly reduced after injury (** $P < 0.01$, unpaired Student's *t* test). E, overlaid average sIPSC traces recorded in FS interneurons from control (black) or CCI (red). F–G, sIPSC rise and decay times are significantly increased after injury (* $P < 0.05$, unpaired Student's *t* test).



The pathogenesis of neurological symptoms associated with TBI remains poorly understood and even less is known about TBI in children and adolescents. A loss of inhibitory interneurons and inhibition has been repeatedly implicated in the pathophysiology of TBI and also in the development of subsequent neurological disorders, including post-traumatic epilepsy (Huusko & Pitkänen, 2014; Cantu *et al.* 2015). However, most studies have been conducted in adult animals and focused on the excitatory neuronal population, necessitating a direct examination of cortical interneurons in juvenile animals following TBI. Comparing mouse with human development is fraught with difficulty, although careful consideration was given to choice of the age of the mice at the time of the impact. At P22, the mouse is considered to be well within the 'paediatric' age range relevant to the present study (Ben-Ari, 2002; Vanhooren & Libert, 2013), whereas cortical interneurons are reaching maturity, are outside the period of maximum synaptogenesis, have inhibitory chloride potentials, and NMDA receptor insertion is nearing completion (Sutor & Luhmann, 1995). To investigate changes in the interneuron population, traditional approaches have utilized immunohistochemical labelling of neurochemical

markers including GAD65/67, as well as subtype specific markers (e.g. PV, SST, 5-HT3A, cholecystokinin). However, a major caveat to this approach is the inability to differentiate the reduced expression of these markers from actual neuronal loss. To overcome this, we took advantage of methods that Cre-dependently fluorescence label interneurons either ubiquitously (*Vgat:Cre/Ai9*) or subtype specifically (*PV:Cre/Ai6*). Accordingly, we were able to directly examine for loss of GABAergic neurons independent of changes in their immunoreactivity for select markers.

Traumatic brain injury selectively targets PV interneurons

As reported previously (Nichols *et al.* 2015), TBI in juvenile animals induced significant tissue loss and cavitation similar to that reported in adult animals (Hunt *et al.* 2009, 2011; Cantu *et al.* 2015). The cortical region most adjacent to the site of injury is considered to be a key component in the generation of epileptic activity and, in adult animals, it is a reported site of inhibitory dysfunction (Cantu *et al.* 2015). Despite the significant tissue loss at the site of injury, we observed no change in the density of excitatory (NeuN)

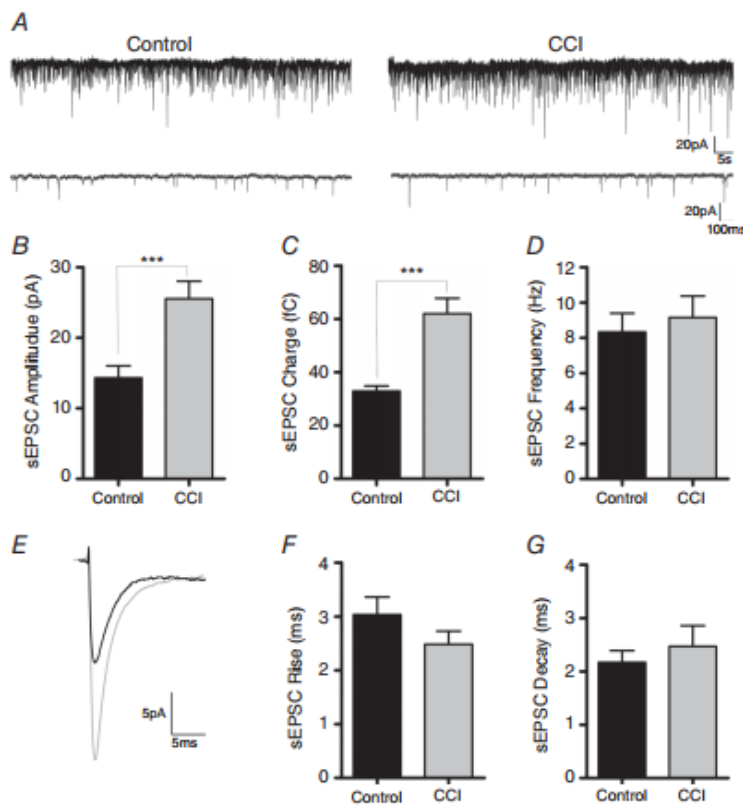


Figure 8. The strength of sEPSCs onto FS interneurons is increased after CCI. *A*, gap-free voltage clamp traces from FS interneurons recorded in control ($n = 13$) or after CCI ($n = 12$) ($V_{\text{hold}} = -70$ mV). *B–C*, bar graphs of average sEPSC properties indicating a significant increase in amplitude ($P < 0.001$) and charge ($P < 0.0001$) following CCI. *D*, average sEPSC frequency was not significantly reduced after injury. *E*, overlaid average sEPSC traces recorded in FS interneurons from control (black) or CCI (red). *F–G*, sEPSC kinetic properties (rise and decay times) are not significantly altered after injury. An unpaired Student's *t* test was used for all of the statistics.

neurons. At an inhibitory level, the *Vgat:Cre/Ai9* transgenic mouse approach allowed us to directly examine changes in the interneuron population. Similar to the excitatory population, no loss of inhibitory (tdTomato positive) neurons was observed in the peri-injury zone following CCI. This suggests that, 14–19 days after CCI, there is no significant cell death in either the excitatory or inhibitory peri-injury neuronal populations.

Inhibition in the cortex plays an essential role in regulating excitability and is governed by a broad group of interneurons with complex morphological, cellular, molecular and synaptic properties (Gupta *et al.* 2000; Markram *et al.* 2004; Rudy *et al.* 2011). In the present study, we tested how TBI alters the population of interneurons in juvenile mice by examining changes in the two most prominent interneuronal subtypes: PV and SST. PV and SST are independent neurochemical markers of cortical interneurons that display little overlap in expression and account for over 70% of the interneuron population (Kawaguchi & Kubota, 1997; Lee *et al.* 2010; Petilla Interneuron Nomenclature Group *et al.* 2008; Xu *et al.* 2010). We determined that TBI selectively reduces the expression of PV within the peri-injury zone without altering the expression of SST. This is in contrast to the more widespread changes in multiple interneuron subtypes reported in adult mice after CCI (Cantu *et al.* 2015). The selective loss of PV may therefore be a unique response to TBI in juvenile animals.

To determine whether the loss of PV expression was indicative of actual PV interneuron loss, we examined the effects of CCI on Cre-dependently labelled PV interneurons (*PV:Cre/Ai6*). PV mRNA can be detected starting in the second post-natal week (P8) and reaches near mature levels by P21 (de Lecea *et al.* 1995; Dong, 2008). As a result, PV interneurons are well and indelibly labelled by ZsGreen1 prior to the age (P22) that mice were subjected to CCI. The observed loss of density of ZsGreen1 positive neurons following CCI is therefore a clear indication of injury induced PV interneuron loss. Of note, the loss of PV density following CCI was substantially greater as indicated by IHC PV immunoreactivity (61%) then by Cre-dependent ZsGreen1 (39%) labelling. This suggests that, following TBI, some PV interneurons die, although a greater proportion only undergo phenotypic loss of PV immunoreactivity. This finding was validated by the electrophysiological determined presence of FS interneurons in the peri-injury (for further discussion, see below). This suggests caution is required with respect to the use and interpretation of IHC measures alone for indicating interneuron loss. Conversely, an important caveat to the use of the *PV:Cre*-dependent approach is indicated by the significant number of ZsGreen1⁺ cells that did not express detectable levels of PV (Fig. 5C). Off-target fluorescence labelling has been previously noted in *PV:Cre* mice (Tanahira *et al.* 2009; Kobayashi & Hensch,

2013; Fujihara *et al.* 2015; Nassar *et al.* 2015) and may be the result of a relatively reduced PV IHC detection efficacy or transient PV expression during development. Other independent IHC markers of PV interneurons (e.g. Kv3.1) (Chow *et al.* 1999; Yanagi *et al.* 2014) may yield a higher co-labelling efficiencies but, again, these are limited by distinguishing changes in expression over interneuron loss. In addition, the decrease in ZsGreen1 labelling following CCI was not detected using a GABAergic neuron-wide analysis approach (i.e. VGAT). This may reflect the increased detection sensitivity of our subtype specific targeted approach (i.e. *PV:Cre/Ai6*); however, subtle compensatory changes in other interneuron subtypes cannot be ruled out. The results of the present study clearly demonstrate reduced PV-Ai6 co-labelling after CCI, consistent with the loss of PV expression, although they also highlight the need for a combined IHC and genetic labelling approach to begin delineating TBI-induced changes with respect to the expression of interneuron markers and overt interneuron loss.

Synaptic input onto FS interneurons is disrupted by traumatic brain injury

PV neurons alone represent ~40% of GABAergic cortical interneurons and are predominantly of an FS phenotype (Kawaguchi & Kubota, 2002; Rudy *et al.* 2011). FS interneurons have unique properties, including sustained high frequency firing, which allows for electrophysiological identification (Connors & Gutnick, 1990; Cauli *et al.* 1997; Kawaguchi & Kubota, 1997; Gibson *et al.* 1999). PV-FS neurons has been shown to influence neuronal excitability (e.g. firing rate) and spike timing (Caillard *et al.* 2000; Schwaller *et al.* 2002; Orduz *et al.* 2013). However, the loss of PV expression in FS interneurons following CCI did not alter the majority of the intrinsic membrane properties we tested, including those known to be important to the pathophysiology of other neurological disorders (van Zundert *et al.* 2012; Prinz *et al.* 2013). The resting membrane potential of FS interneurons was more depolarized following CCI and this may contribute to the trend towards a reduced rheobase. However, this change in membrane potential did not translate into alterations in the input–output relationship of FS interneurons, as indicated by no significant difference in the firing frequency or action potential properties. This suggests that, although FS interneurons may lose their PV immunoreactivity, they are still present in the peri-injury zone and maintain a near ‘normal’ FS electrophysiological phenotype.

Beyond intrinsic excitability, regulation of calcium homeostasis by PV is considered to play an important role in synaptic neurotransmission (Kinney *et al.* 2006; Orduz *et al.* 2013). The loss of PV is predicted to disrupt inhibitory neurotransmission which is accordance with previous

work indicating inhibitory network dysfunction after brain injury (Hunt *et al.* 2011; Jin *et al.* 2011; Cantu *et al.* 2015; Nichols *et al.* 2015). Using an electrophysiological approach, we found that FS interneurons receive less frequent inhibition after CCI, indicative of a decrease in pre-synaptic release probability. We also observed an increased rise and decay time of inhibitory spontaneous synaptic events. Kinetic properties of synaptic events are often controlled by the specific expression of GABA receptor subunits that have been shown to be altered after TBI (Huusko & Pitkänen, 2014) and will be evaluated in future studies. Although the altered inhibitory synaptic kinetics may influence the synaptic integration window, this was not sufficient to increase synaptic charge and compensate for the >50% loss in inhibitory event frequency suggesting an overall loss of inhibitory drive onto FS interneurons.

On the excitatory side, the amplitude and charge transfer of sEPSCs onto FS interneurons was also increased after CCI, indicating increased excitatory synaptic strength. By contrast to the inhibitory changes, the frequency of sEPSC events was not significantly altered by CCI. The strengthening of excitatory events may also be a result of post-synaptic receptor changes, potentially driven by homeostatic mechanisms (Pozo & Goda, 2010; Turrigiano, 2012).

PV neurons preferentially synapse onto other PV and excitatory pyramidal neurons (Tamás *et al.* 1998; Gibson *et al.* 1999). The loss of PV interneurons makes it tempting to suggest that the reduced inhibitory input onto FS interneurons is the result of a loss of input from other PV interneurons. However, PV interneurons receive synaptic input from a wide array of interneuron subtypes and from various excitatory lamina and regions (Markram *et al.* 2004; Pfeffer *et al.* 2013; Pi *et al.* 2013; Jin *et al.* 2014). The recorded post-synaptic currents in FS interneurons in the present study are a compilation of these various inputs, foregoing the ability to discretely determine the subtype and/or source of these synaptic changes. Consequently, it remains possible that the reduced inhibitory synaptic activity following CCI is contributed to by alterations in other unstudied interneuron subtypes (e.g. 5-HT3A, VIP). In our previous work, we similarly found that excitatory pyramidal neurons in juvenile mice undergo unique changes following a TBI. By contrast to reports in adult mice (Cantu *et al.*, 2015), recordings from pyramidal neurons in juvenile mice revealed a lack of generalized hyperexcitability (Goddeyne *et al.* 2015; Nichols *et al.* 2015) and the presence of unique excitatory and inhibitory synaptic bursts following CCI (Nichols *et al.* 2015). These changes were evident at a time post-injury where epileptic activity was evident on EEG (i.e. by post-injury day 14) as examined in the present study. PV interneurons are considered as being important with respect to regulating the output of pyramidal neurons, gain control,

and contributing to network oscillations and synchrony (Bartos *et al.* 2007; Puig *et al.* 2008; Cardin *et al.* 2009; Wilson *et al.* 2012). Determining how the TBI-induced loss of PV expression and interneurons and associated TBI-induced synaptic changes contribute, or potentially even resist, synaptic bursting and network level excitability remains to be determined. Overall, the findings of the present study indicate that juvenile PV interneurons are particularly sensitive to brain injury and undergo unique changes following a TBI.

PV interneurons have been shown to play a crucial role in higher cognitive function (Schwaller *et al.* 2004; Sohal *et al.* 2009; Lewis *et al.* 2012; Ma & Prince, 2012). PV loss has been shown to increase seizure susceptibility (Schwaller *et al.* 2004) and induce behavioural deficits relevant to the core symptoms of autism (Wöhr *et al.* 2015) and is also implicated in the pathophysiology of schizophrenia (Sohal *et al.* 2009; Lewis *et al.* 2012) and epilepsy (Schwaller *et al.* 2004; Ma & Prince, 2012; Jin *et al.* 2014). Given that TBI is a known risk factor for both schizophrenia (Molloy *et al.* 2011), autism spectrum disorders (Wöhr *et al.* 2015) and epilepsy (Barlow *et al.* 2000; Hunt *et al.* 2009), the loss of PV expression following TBI may be a common denominator in the development of numerous neurological disorders. However, at present, it is unknown whether PV expression loss is an adaptive or maladaptive response to injury. Furthermore, it might be the case that PV loss serves in both capacities dependent on where an individual is along the time course of TBI and recovery. What is evident from these studies is that the response to TBI in juvenile brains appears to be distinct from that in adults. The alteration to PV-FS neurons after TBI may be critical to understanding how TBI in the paediatric brain may alter neurodevelopment and why children have worse outcomes and take longer to recover after brain injury.

References

- Anderson V & Moore C (1995). Age at injury as a predictor of outcome following pediatric head injury: a longitudinal perspective. *Child Neuropsychol* **1**, 187–202.
- Anderson TR, Huguenard JR & Prince DA (2010). Differential effects of Na⁺-K⁺ ATPase blockade on cortical layer V neurons. *J Physiol* **588**, 4401–4414.
- Annegers JF, Hauser WA, Coan SP & Rocca WA (1998). A population-based study of seizures after traumatic brain injuries. *N Engl J Med* **338**, 20–24.
- Aurora SK, Barrodale P, Chronicle EP & Mulleners WM (2005). Cortical inhibition is reduced in chronic and episodic migraine and demonstrates a spectrum of illness. *Headache* **45**, 546–552.
- Barlow KM, Spewart JJ & Minns RA (2000). Early posttraumatic seizures in non-accidental head injury: relation to outcome. *Dev Med Child Neurol* **42**, 591–594.

- Bartos M, Vida I & Jonas P (2007). Synaptic mechanisms of synchronized gamma oscillations in inhibitory interneuron networks. *Nat Rev Neurosci* **8**, 45–56.
- Ben-Ari Y (2002). Excitatory actions of gaba during development: the nature of the nurture. *Nat Rev Neurosci* **3**, 728–739.
- Brody DL, Mac Donald C, Kessens CC, Yuede C, Parsadarian M, Spinner M, Kim E, Schwetey KE, Holtzman DM & Bayly PV (2007). Electromagnetic controlled cortical impact device for precise, graded experimental traumatic brain injury. *J Neurotrauma* **24**, 657–673.
- Bromfield EB, Cavazos JE & Sirven JI (2006). An Introduction to Epilepsy. West Hartford (CT): American Epilepsy Society. Available from: <https://www.ncbi.nlm.nih.gov/books/NBK2508>.
- Bruns J & Hauser WA (2003). The epidemiology of traumatic brain injury: a review. *Epilepsia* **44**(Suppl 10), 2–10.
- Caillard O, Moreno H, Schwaller B, Llano I, Celio MR & Marty A (2000). Role of the calcium-binding protein parvalbumin in short-term synaptic plasticity. *Proc Natl Acad Sci USA* **97**, 13372–13377.
- Cantu D, Walker K, Andresen L, Taylor-Weiner A, Hampton D, Tesco G & Dulla CG (2015). Traumatic brain injury increases cortical glutamate network activity by compromising GABAergic control. *Cereb Cortex* **25**, 2306–2320.
- Cardin JA, Carlén M, Meletis K, Knoblich U, Zhang F, Deisseroth K, Tsai L-H & Moore CI (2009). Driving fast-spiking cells induces gamma rhythm and controls sensory responses. *Nature* **459**, 663–667.
- Carron SF, Alwis DS & Rajan R (2016). Traumatic brain injury and neuronal functionality changes in sensory cortex. *Front Syst Neurosci* **10**, 47.
- Cauli B, Audinat E, Lambolez B, Angulo MC, Ropert N, Tsuzuki K, Hestrin S & Rossier J (1997). Molecular and physiological diversity of cortical nonpyramidal cells. *J Neurosci Off J Soc Neurosci* **17**, 3894–3906.
- Caveness WF, Meirinsky AM, Rish BL, Mohr JP, Kistler JP, Dillon JD & Weiss GH (1979). The nature of posttraumatic epilepsy. *J Neurosurg* **50**, 545–553.
- Chaudhry FA, Reimer RJ, Bellocchio EE, Danbolt NC, Osen KK, Edwards RH & Storm-Mathisen J (1998). The vesicular GABA transporter, VGAT, localizes to synaptic vesicles in sets of glycinergic as well as GABAergic neurons. *J Neurosci Off J Soc Neurosci* **18**, 9733–9750.
- Chow A, Erisir A, Farb C, Nadal MS, Ozaita A, Lau D, Welker E & Rudy B (1999). K(+) channel expression distinguishes subpopulations of parvalbumin- and somatostatin-containing neocortical interneurons. *J Neurosci Off J Soc Neurosci* **19**, 9332–9345.
- Cole JT, Yarnell A, Kean WS, Gold E, Lewis B, Ren M, McMullen DC, Jacobowitz DM, Pollard HB, O'Neill JT, Grunberg NE, Dalgard CL, Frank JA & Watson WD (2010). Craniotomy: true sham for traumatic brain injury, or a sham of a sham? *J Neurotrauma* **28**, 359–369.
- Connors BW & Gutnick MJ (1990). Intrinsic firing patterns of diverse neocortical neurons. *Trends Neurosci* **13**, 99–104.
- Cook LG, Chapman SB, Elliott AC, Evenson NN & Vinton K (2014). Cognitive gains from gist reasoning training in adolescents with chronic-stage traumatic brain injury. *Front Neurol* **5**, 87.
- Cossart R, Dinocourt C, Hirsch JC, Merchan-Perez A, De Felipe J, Ben-Ari Y, Esclapez M & Bernard C (2001). Dendritic but not somatic GABAergic inhibition is decreased in experimental epilepsy. *Nat Neurosci* **4**, 52–62.
- Dong HW (2008). *The Allen Reference Atlas: A Digital Color Brain Atlas of the C57BL/6J Male Mouse*. Hoboken, NJ: John Wiley & Sons, Inc.
- Erickson SL & Lewis DA (2002). Postnatal development of parvalbumin- and GABA transporter-immunoreactive axon terminals in monkey prefrontal cortex. *J Comp Neurol* **448**, 186–202.
- Fujihara K, Miwa H, Kakizaki T, Kaneko R, Mikuni M, Tanahira C, Tamamaki N & Yanagawa Y (2015). Glutamate decarboxylase 67 deficiency in a subset of GABAergic neurons induces schizophrenia-related phenotypes. *Neuropsychopharmacol Off Publ Am Coll Neuropsychopharmacol* **40**, 2475–2486.
- Galarreta M & Hestrin S (1999). A network of fast-spiking cells in the neocortex connected by electrical synapses. *Nature* **402**, 72–75.
- Gibson JR, Beierlein M & Connors BW (1999). Two networks of electrically coupled inhibitory neurons in neocortex. *Nature* **402**, 75–79.
- Goddeyne C, Nichols J, Wu C & Anderson T (2015). Repetitive mild traumatic brain injury induces ventriculomegaly and cortical thinning in juvenile rats. *J Neurophysiol* **113**, 3268–3280.
- Grundy D (2015). Principles and standards for reporting animal experiments in The Journal of Physiology and Experimental Physiology. *J Physiol* **593**, 2547–2549.
- Gupta A, Wang Y & Markram H (2000). Organizing principles for a diversity of GABAergic interneurons and synapses in the neocortex. *Science* **287**, 273–278.
- Hensch TK (2005). Critical period plasticity in local cortical circuits. *Nat Rev Neurosci* **6**, 877–888.
- Hippenmeyer S, Vrieseling E, Sigrist M, Portmann T, Laengle C, Ladle DR & Arber S (2005). A developmental switch in the response of DRG neurons to ETS transcription factor signaling. *PLoS Biol* **3**, e159.
- Hu H, Gan J & Jonas P (2014). Fast-spiking, parvalbumin+ GABAergic interneurons: from cellular design to microcircuit function. *Science* **345**, 1255263.
- Huang ZJ, Kirkwood A, Pizzorusso T, Porciatti V, Morales B, Bear MF, Maffei L & Tonegawa S (1999). BDNF regulates the maturation of inhibition and the critical period of plasticity in mouse visual cortex. *Cell* **98**, 739–755.
- Hunt RF, Scheff SW & Smith BN (2009). Posttraumatic epilepsy after controlled cortical impact injury in mice. *Exp Neurol* **215**, 243–252.
- Hunt RF, Scheff SW & Smith BN (2011). Synaptic reorganization of inhibitory hilar interneuron circuitry after traumatic brain injury in mice. *J Neurosci Off J Soc Neurosci* **31**, 6880–6890.
- Huusko N & Pitkänen A (2014). Parvalbumin immunoreactivity and expression of GABA_A receptor subunits in the thalamus after experimental TBI. *Neuroscience* **267**, 30–45.
- Ippolito DM & Eroglu C (2010). Quantifying synapses: an immunocytochemistry-based assay to quantify synapse number. *J Vis Exp JoVE* **45**, 2270.

- Jin X, Huguenard JR & Prince DA (2011). Reorganization of inhibitory synaptic circuits in rodent chronically injured epileptogenic neocortex. *Cereb Cortex* **21**, 1094–1104.
- Jin X, Jiang K & Prince DA (2014). Excitatory and inhibitory synaptic connectivity to layer V fast-spiking interneurons in the freeze lesion model of cortical microgyria. *J Neurophysiol* **112**, 1703–1713.
- Judson MC, Wallace ML, Sidorov MS, Burette AC, Gu B, van Woerden GM, King IF, Han JE, Zylka MJ, Elgersma Y, *et al* (2016). GABAergic neuron-specific loss of Ube3a causes angelman syndrome-Like EEG abnormalities and enhances seizure susceptibility. *Neuron* **90**, 56–69.
- Kawaguchi Y & Kondo S (2002). Parvalbumin, somatostatin and cholecystokinin as chemical markers for specific GABAergic interneuron types in the rat frontal cortex. *J Neurocytol* **31**, 277–287.
- Kawaguchi Y & Kubota Y (1997). GABAergic cell subtypes and their synaptic connections in rat frontal cortex. *Cereb Cortex* **7**, 476–486.
- Kinney JW, Davis CN, Tabarean I, Conti B, Bartfai T & Behrens MM (2006). A specific role for NR2A-containing NMDA receptors in the maintenance of parvalbumin and GAD67 immunoreactivity in cultured interneurons. *J Neurosci Off J Soc Neurosci* **26**, 1604–1615.
- Kobayashi Y & Hensch TK (2013). Germline recombination by conditional gene targeting with Parvalbumin-Cre lines. *Front Neural Circuits* **7**, 168.
- Kraus JF, Rock A & Hemyari P (1990). Brain injuries among infants, children, adolescents, and young adults. *Am J Dis Child* **1960** **144**, 684–691.
- de Lecea L, del Río JA & Soriano E (1995). Developmental expression of parvalbumin mRNA in the cerebral cortex and hippocampus of the rat. *Brain Res Mol Brain Res* **32**, 1–13.
- Lee S, Hjerling-Leffler J, Zagha E, Fishell G & Rudy B (2010). The largest group of superficial neocortical GABAergic interneurons expresses ionotropic serotonin receptors. *J Neurosci* **30**, 16796–16808.
- Lewis DA, Curley AA, Glausier J & Volk DW (2012). Cortical parvalbumin interneurons and cognitive dysfunction in schizophrenia. *Trends Neurosci* **35**, 57–67.
- Ma Y & Prince DA (2012). Functional alterations in GABAergic fast-spiking interneurons in chronically injured epileptogenic neocortex. *Neurobiol Dis* **47**, 102–113.
- Madisen L, Zwingman TA, Sunkin SM, Oh SW, Zariwala HA, Gu H, Ng LL, Palmiter RD, Hawrylycz MJ, Jones AR, *et al* (2010). A robust and high-throughput Cre reporting and characterization system for the whole mouse brain. *Nat Neurosci* **13**, 133–140.
- Markram H, Toledo-Rodriguez M, Wang Y, Gupta A, Silberberg G & Wu C (2004). Interneurons of the neocortical inhibitory system. *Nat Rev Neurosci* **5**, 793–807.
- McIntire SL, Reimer RJ, Schuske K, Edwards RH & Jorgensen EM (1997). Identification and characterization of the vesicular GABA transporter. *Nature* **389**, 870–876.
- Molloy C, Conroy RM, Cotter DR & Cannon M (2011). Is traumatic brain injury a risk factor for schizophrenia? A meta-analysis of case-controlled population-based studies. *Schizophr Bull* **37**, 1104–1110.
- Nassar M, Simonnet J, Lofredi R, Cohen I, Savary E, Yanagawa Y, Miles R & Fricker D (2015). Diversity and overlap of parvalbumin and somatostatin expressing interneurons in mouse presubiculum. *Front Neural Circuits* **9**, 20.
- Nichols J, Perez R, Wu C, Adelson PD & Anderson T (2015). Traumatic brain injury induces rapid enhancement of cortical excitability in juvenile rats. *CNS Neurosci Ther* **21**, 193–203.
- Olesen SP (1987). Leakiness of rat brain microvessels to fluorescent probes following craniotomy. *Acta Physiol Scand* **130**, 63–68.
- Orduz D, Bischoff DP, Schwaller B, Schiffmann SN & Gall D (2013). Parvalbumin tunes spike-timing and efferent short-term plasticity in striatal fast spiking interneurons. *J Physiol* **591**, 3215–3232.
- Palmer JE, Chronicle EP, Rolan P & Mulleners WM (2000). Cortical hyperexcitability is cortical under-inhibition: evidence from a novel functional test of migraine patients. *Cephalalgia Int J Headache* **20**, 525–532.
- Petilla Interneuron Nomenclature Group, Ascoli GA, Alonso-Nanclares L, Anderson SA, Barrionuevo G, Benavides-Piccione R, Burkhalter A, Buzsáki G, Cauli B, Defelipe J, *et al* (2008). Petilla terminology: nomenclature of features of GABAergic interneurons of the cerebral cortex. *Nat Rev Neurosci* **9**, 557–568.
- Pfeffer CK, Xue M, He M, Huang ZJ & Scanziani M (2013). Inhibition of inhibition in visual cortex: the logic of connections between molecularly distinct interneurons. *Nat Neurosci* **16**, 1068–1076.
- Philpot BD, Lim JH & Brunjes PC (1997). Activity-dependent regulation of calcium-binding proteins in the developing rat olfactory bulb. *J Comp Neurol* **387**, 12–26.
- Pi H-J, Hangya B, Kvitsiani D, Sanders JL, Huang ZJ & Kepecs A (2013). Cortical interneurons that specialize in disinhibitory control. *Nature* **503**, 521–524.
- Pozo K & Goda Y (2010). Unraveling mechanisms of homeostatic synaptic plasticity. *Neuron* **66**, 337–351.
- Prinz A, Selesnew L-M, Liss B, Roeper J & Carlsson T (2013). Increased excitability in serotonin neurons in the dorsal raphe nucleus in the 6-OHDA mouse model of Parkinson's disease. *Exp Neurol* **248**, 236–245.
- Puig MV, Ushimaru M & Kawaguchi Y (2008). Two distinct activity patterns of fast-spiking interneurons during neocortical UP states. *Proc Natl Acad Sci USA* **105**, 8428–8433.
- del Río JA, de Lecea L, Ferrer I & Soriano E (1994). The development of parvalbumin-immunoreactivity in the neocortex of the mouse. *Brain Res Dev Brain Res* **81**, 247–259.
- Rudy B, Fishell G, Lee S & Hjerling-Leffler J (2011). Three groups of interneurons account for nearly 100% of neocortical GABAergic neurons. *Dev Neurobiol* **71**, 45–61.
- Schmidt AT, Hanten GR, Li X, Vasquez AC, Wilde EA, Chapman SB & Levin HS (2012). Decision making after pediatric traumatic brain injury: trajectory of recovery and relationship to age and gender. *Int J Dev Neurosci Off J Int Soc Dev Neurosci* **30**, 225–230.

- Schwaller B, Meyer M & Schiffmann S (2002). "New" functions for "old" proteins: the role of the calcium-binding proteins calbindin D-28k, calretinin and parvalbumin, in cerebellar physiology. Studies with knockout mice. *Cerebellum Lond Engl* **1**, 241–258.
- Schwaller B, Tetko IV, Tandon P, Silveira DC, Vreugdenhil M, Henzi T, Potier M-C, Celio MR & Villa AEP (2004). Parvalbumin deficiency affects network properties resulting in increased susceptibility to epileptic seizures. *Mol Cell Neurosci* **25**, 650–663.
- Sohal VS, Zhang F, Yizhar O & Deisseroth K (2009). Parvalbumin neurons and gamma rhythms enhance cortical circuit performance. *Nature* **459**, 698–702.
- Sutor B & Luhmann HJ (1995). Development of excitatory and inhibitory postsynaptic potentials in the rat neocortex. *Perspect Dev Neurobiol* **2**, 409–419.
- Tamás G, Somogyi P & Buhl EH (1998). Differentially interconnected networks of GABAergic interneurons in the visual cortex of the cat. *J Neurosci Off J Soc Neurosci* **18**, 4255–4270.
- Tanahira C, Higo S, Watanabe K, Tomioka R, Ebihara S, Kaneko T & Tamamaki N (2009). Parvalbumin neurons in the forebrain as revealed by parvalbumin-Cre transgenic mice. *Neurosci Res* **63**, 213–223.
- Trevelyan AJ & Schevon CA (2013). How inhibition influences seizure propagation. *Neuropharmacology* **69**, 45–54.
- Trevelyan AJ, Muldoon SF, Merricks EM, Racca C & Staley KJ (2015). The role of inhibition in epileptic networks. *J Clin Neurophysiol Off Publ Am Electroencephalogr Soc* **32**, 227–234.
- Turrigiano G (2012). Homeostatic synaptic plasticity: local and global mechanisms for stabilizing neuronal function. *Cold Spring Harb Perspect Biol* **4**, a005736.
- Uematsu M, Hirai Y, Karube F, Ebihara S, Kato M, Abe K, Obata K, Yoshida S, Hirabayashi M, Yanagawa Y, et al (2008). Quantitative chemical composition of cortical GABAergic neurons revealed in transgenic venus-expressing rats. *Cereb Cortex* **18**, 315–330.
- Vanhooren V & Libert C (2013). The mouse as a model organism in aging research: usefulness, pitfalls and possibilities. *Ageing Res Rev* **12**, 8–21.
- Vong L, Ye C, Yang Z, Choi B, Chua S & Lowell BB (2011). Leptin action on GABAergic neurons prevents obesity and reduces inhibitory tone to POMC neurons. *Neuron* **71**, 142–154.
- Wang DD & Kriegstein AR (2009). Defining the role of GABA in cortical development. *J Physiol* **587**, 1873–1879.
- Wilson NR, Runyan CA, Wang FL & Sur M (2012). Division and subtraction by distinct cortical inhibitory networks in vivo. *Nature* **488**, 343–348.
- Wöhr M, Orduz D, Gregory P, Moreno H, Khan U, Vörckel KJ, Wolfer DP, Welzl H, Gall D, Schiffmann SN & Schwaller B (2015). Lack of parvalbumin in mice leads to behavioral deficits relevant to all human autism core symptoms and related neural morphofunctional abnormalities. *Transl Psychiatry* **5**, e525.
- Wojcik SM, Katsurabayashi S, Guillemin I, Friauf E, Rosenmund C, Brose N & Rhee J-S (2006). A shared vesicular carrier allows synaptic corelease of GABA and glycine. *Neuron* **50**, 575–587.
- Wonders CP & Anderson SA (2006). The origin and specification of cortical interneurons. *Nat Rev Neurosci* **7**, 687–696.
- Xing L, Larsen RS, Bjorklund GR, Li X, Wu Y, Philpot BD, Snider WD & Newbern JM (2016). Layer specific and general requirements for ERK/MAPK signaling in the developing neocortex. *ELife* **5**, e11123.
- Xu X, Roby KD & Callaway EM (2010). Immunochemical characterization of inhibitory mouse cortical neurons: three chemically distinct classes of inhibitory cells. *J Comp Neurol* **518**, 389–404.
- Yanagi M, Joho RH, Southcott SA, Shukla AA, Ghose S & Tamminga CA (2014). Kv3.1-containing K⁺ channels are reduced in untreated schizophrenia and normalized with antipsychotic drugs. *Mol Psychiatry* **19**, 573–579.
- Yuste R (2005). Origin and classification of neocortical interneurons. *Neuron* **48**, 524–527.
- van Zundert B, Izaurieta P, Fritz E & Alvarez FJ (2012). Early pathogenesis in the adult-onset neurodegenerative disease amyotrophic lateral sclerosis. *J Cell Biochem* **113**, 3301–3312.

Additional information

Competing interests

The authors declare that they have no competing interests.

Author contributions

JNi, JNe and TA all contributed to the conception and design of experiments. All authors contributed to the data analysis, as well as to its interpretation and the writing of the manuscript. TA and JNe contributed financial support for materials and staffing. JNi performed all of the experimental procedures and collected data. GRB contributed to the immunohistochemical processing, imaging and analysis. All authors approved the final version of the manuscript submitted for publication.

Funding

TA is supported by R01-NS087031, R01-NS097537 and R21-EB020767 from the NIH and IOS-1353804 from the NSF. JNe is supported by R00-NS07661 and R01-NS097537.

Acknowledgements

We thank Dr David Adelson for scientific discussions and providing research equipment, as well as Mario Moreno and Johan Martinez from the Newbern laboratory for their technical assistance.

APPENDIX C
Animal Subjects

Research involving the use of animals conducted under the auspices of Arizona State University is reviewed by the University Institutional Animal Care & Use Committee (IACUC, approval #17-1521R), Institutional Biosafety Committee (IBC, approval #16-696), and in compliance with federal regulations. Documents containing any data collection from animal research require that applications be submitted to the University Animal Care & Use Committee for approval. For further information, contact the IACUC secretary in the IACUC Office at 480-965-4387 or visit <https://www.researchintegrity.asu.edu/animals>.

Appendix D

Table 2

Table 2

Gene Symbol	Fold-Change (Mut vs. Ctl)	p-value (Mut vs. Ctl)	Fold-Change (Mut vs. Ctl) (Description)	Gene Name
Neurotrophins and growth factors				
<i>Ntf3</i>	-1.0051	0.9550	Mut down vs Ctl	neurotrophin 3
<i>Ntf5</i>	1.0771	0.4970	Mut up vs Ctl	neurotrophin 5
<i>Bdnf</i>	1.0773	0.3826	Mut up vs Ctl	brain derived neurotrophic factor
<i>Ngf</i>	1.3762	0.0202	Mut up vs Ctl	nerve growth factor
<i>Egf</i>	1.0485	0.2787	Mut up vs Ctl	epidermal growth factor
<i>Fgf1</i>	-1.0805	0.1479	Mut down vs Ctl	fibroblast growth factor 1
<i>Fgf8</i>	1.0268	0.2164	Mut up vs Ctl	fibroblast growth factor 8
Neurotrophin receptors				
<i>Ngfr</i>	1.0629	0.3378	Mut up vs Ctl	nerve growth factor receptor (TNFR superfamily, member 16)
<i>Ntrk1</i>	1.0872	0.4857	Mut up vs Ctl	neurotrophic tyrosine kinase, receptor, type 1
<i>Ntrk2</i>	1.0020	0.9480	Mut up vs Ctl	neurotrophic tyrosine kinase, receptor, type 2
<i>Ntrk3</i>	-1.0812	0.0777	Mut down vs Ctl	neurotrophic tyrosine kinase, receptor, type 3
<i>Egfr</i>	-1.0495	0.4289	Mut down vs Ctl	epidermal growth factor receptor
<i>Fgfr1</i>	1.0260	0.3259	Mut up vs Ctl	fibroblast growth factor receptor 1
<i>Fgfr2</i>	-1.0840	0.1611	Mut down vs Ctl	fibroblast growth factor receptor
Ionotropic glutamate receptor subunits (AMPArs, NMDARs, KainateRs)				
<i>Gria1</i>	1.0266	0.5541	Mut up vs Ctl	glutamate receptor, ionotropic, AMPA1
<i>Gria2</i>	-1.0454	0.0961	Mut down vs Ctl	glutamate receptor, ionotropic, AMPA2
<i>Gria3</i>	-1.0276	0.2202	Mut down vs Ctl	glutamate receptor, ionotropic, AMPA3
<i>Gria4</i>	-1.1496	0.0015	Mut down vs Ctl	glutamate receptor, ionotropic, AMPA4
<i>Grid1</i>	1.0426	0.4885	Mut up vs Ctl	glutamate receptor, ionotropic, delta 1
<i>Grid2</i>	1.0586	0.4474	Mut up vs Ctl	glutamate receptor, ionotropic, delta 2
<i>Grik1</i>	1.0099	0.8779	Mut up vs Ctl	glutamate receptor, ionotropic, kainate 1
<i>Grik2</i>	1.0444	0.4132	Mut up vs Ctl	glutamate receptor, ionotropic, kainate 2 (beta 2)
<i>Grik3</i>	-1.0411	0.7017	Mut down vs Ctl	glutamate receptor, ionotropic, kainate 3
<i>Grik4</i>	-1.2210	0.0318	Mut down vs Ctl	glutamate receptor, ionotropic, kainate 4
<i>Grik5</i>	-1.0454	0.4093	Mut down vs Ctl	glutamate receptor, ionotropic, kainate 5 (gamma 2)
<i>Grin1</i>	1.0051	0.9682	Mut up vs Ctl	glutamate receptor, ionotropic, NMDA1 (zeta 1)
<i>Grin1</i>	-1.0321	0.4421	Mut down vs Ctl	glutamate receptor, ionotropic, NMDA1 (zeta 1)
<i>Grin2a</i>	-1.1401	0.0948	Mut down vs Ctl	glutamate receptor, ionotropic, NMDA2A (epsilon 1)
<i>Grin2b</i>	-1.0189	0.5716	Mut down vs Ctl	glutamate receptor, ionotropic, NMDA2B (epsilon 2)
<i>Grin2b</i>	-1.0806	0.6816	Mut down vs Ctl	glutamate receptor, ionotropic, NMDA2B (epsilon 2)
<i>Grin2c</i>	1.1999	0.1812	Mut up vs Ctl	glutamate receptor, ionotropic, NMDA2C (epsilon 3)
<i>Grin2c</i>	1.0105	0.8669	Mut up vs Ctl	glutamate receptor, ionotropic, NMDA2C (epsilon 3)
<i>Grin2d</i>	1.0443	0.1135	Mut up vs Ctl	glutamate receptor, ionotropic, NMDA2D (epsilon 4)
<i>Grin2d</i>	1.0393	0.6052	Mut up vs Ctl	glutamate receptor, ionotropic, NMDA2D (epsilon 4)
<i>Grin3a</i>	1.1201	0.1397	Mut up vs Ctl	glutamate receptor ionotropic, NMDA3A
<i>Grin3b</i>	1.1243	0.0786	Mut up vs Ctl	glutamate receptor, ionotropic, NMDA3B
Metabotropic glutamate receptors (MGLURs)				
<i>Grm1</i>	1.1858	0.0822	Mut up vs Ctl	glutamate receptor, metabotropic 1
<i>Grm2</i>	-1.0565	0.5959	Mut down vs Ctl	glutamate receptor, metabotropic 2
<i>Grm3</i>	-1.1767	0.0287	Mut down vs Ctl	glutamate receptor, metabotropic 3
<i>Grm4</i>	-1.1794	0.0469	Mut down vs Ctl	glutamate receptor, metabotropic 4
<i>Grm5</i>	1.0417	0.0875	Mut up vs Ctl	glutamate receptor, metabotropic 5
<i>Grm6</i>	1.0437	0.3602	Mut up vs Ctl	glutamate receptor, metabotropic 6
<i>Grm7</i>	1.0819	0.0353	Mut up vs Ctl	glutamate receptor, metabotropic 7
<i>Grm8</i>	1.2054	0.0925	Mut up vs Ctl	glutamate receptor, metabotropic 8